Novel strategies for targeting botulinum neurotoxin-based therapeutics to neuronal populations involved in pain sensation

Thesis submitted for the degree

of

Doctor of Philosophy

by

Marc Nugent, B.A.

Supervised by

Prof. J. Oliver Dolly

Co-supervised by

Dr. Jiafu Wang and Dr. Gary Lawrence

School of Biotechnology

Dublin City University Ireland

June 2017

Declaration

I hereby certify that this material, which I now submit for assessment on the programme of study leading to the award of Doctor of Philosophy is entirely my own work, that I have exercised reasonable care to ensure that the work is original, and does not to the best of my knowledge breach any law of copyright, and has not been taken from the work of others save and to the extent that such work has been cited and acknowledged within the text of my work.

Signed: ID No: 12110892

Date:

Acknowledgments

I would like to express my deep and sincere gratitude to my supervisor, Professor J. Oliver Dolly, who never ceased to inspire, support and provide assistance when it was needed most. The opportunities that you afforded me, together with your encouragement, guidance and unparalleled commitment are things for which I am exceptionally fortunate and, forever, grateful.

I want to especially thank my co-supervisors Dr. Jiafu Wang and Dr. Gary Lawrence for their ongoing support, critical thinking and their constructive interpretations of my results. I want also to offer my heartfelt thanks to all my colleagues Dr. Tomas Zurawski and Ms. Sharon Whyte in particular for their constant discussion, inspiration, practical help and friendship.

I am indebted to Prof. Joan Geoghegan of Trinity College Dublin, who provided both reagents and, more importantly, made time to discuss with me the development of an approach which was instrumental in the success of this project. Also, Prof. Bazbek Davletov of the University of Sheffield, who facilitated me spending time in his lab to overcome technical issues which I was at one time encountering.

A very special thanks to Helen and Pat McGonagle, who were at all times extremely supportive, generous and thoughtful, and to my parents, who always believed in me and gave me the confidence to believe I could do this.

Most importantly, my partner Peggy-Ann, without whom none of this would have ever been possible. You were there for every high and every low, and your unwavering kindness and understanding has made the last few years that bit easier. I can now finally start trying to make it all up to you… something I know I'll never truly be able to do.

Finally, I want to thank The Irish Research Council, who together with Dr. Maurice Treacy of Powerscourt Lifescience Consulting, LLC funded my research project as part of an IRCSET Enterprise partnership scheme.

Abbreviations used

$(His)_6$, polyhistidine purification tag

^{125}I, ^{125}I-iodine

AP, alkaline phosphatase

BCA, bicinchoninic acid protein assay

BoNT, botulinum neurotoxin

BoNT/A, botulinum neurotoxin serotype A

bp, base pairs

BSA, bovine serum albumin

CGNs, cerebellar granule neurons

CGRP, calcitonin gene-related peptide

CNS, central nervous system

DCU, Dublin City University

DD, double-digest

DkTx, double-knot toxin

DMEM, Dulbecco's modified Eagle's medium

DNA, deoxyribonucleic acid

DPM, disintegrations per minute

DRGs, dorsal root ganglion neurons

EC_{50}, half maximal effective concentration

EDTA, ethylenediaminetetraacetic acid

EGF, epidermal-growth factor

EGFR, epidermal-growth factor receptor

ERK 1/2, extracellular regulated kinases 1 and 2

Fab, fragment antigen-binding

FBS, fetal bovine serum

Fc, fragment crystallizable domain of immunoglobulin G

GFP, green-fluorescent protein

Gp64, glycoprotein 64

GST, glutathione-S-transferase

HBSS, hanks balanced salt solution

H_C, acceptor binding domain

HC, heavy chain

H_N, translocation domain

ICC, immuno-cytochemistry

ICK, inhibitory-cysteine knot

IgG, immunoglobulin G

IMAC, immobilized metal affinity chromatography

IPTG, isopropyl β-D-1-thiogalactopyranoside

K_D, equilibrium dissociation constant

kbp, kilobase pairs

LC, light chain

MCS, multiple cloning site

MOI, multiplicity of infection

M_r, molecular mass relative to $\frac{1}{12}$ the mass of a carbon 12 atom

n.s., non-significant

Native-PAGE, non-denaturing polyacrylamide gel electrophoresis

NGF, nerve growth factor

OD_{600}, absorbance at a wavelength of 600 nm

$P2X_3$, Purinergic receptor 3

PBS, phosphate buffered saline

PCR, polymerase chain reaction

PG4, tetraethylene glycol

PMSF, phenylmethylsulfonyl fluoride

PNS, peripheral nervous system

PVDF, polyvinylidene fluoride

rA, recombinant botulinum neurotoxin A

rA_{W985L}, recombinant botulinum neurotoxin A containing mutation W985L

rFC, rabbit immunoglobulin G Fc domain

RFP, red-fluorescent protein

RPM, rotations per minute

RPMI-1640, Roswell Park Memorial Institute 1640 medium

RT, room-temperature

S.E.M, standard error of the mean

ScFv, single-chain variable fragment

SD, single-digest

SDS-PAGE, sodium dodecyl sulfate polyacrylamide gel electrophoresis

Skp, seventeen-kilodalton protein

SNAP-25, synaptosomal-associated protein of Mr = 25 k

SNAP-$25_{/A}$, BoNT/A-truncated synaptosomal-associated protein of Mr = 25 k

SNARE, soluble N-ethylmaleimide-sensitive factor attachment protein receptor

SP, substance P

SpA, *Staphylococcus aureus* Protein A

SpA-B, *Staphylococcus aureus* Protein A domain B

SpA-B_{mut}, *Staphylococcus aureus* Protein A domain B mutant (D36A, D37A)

ßME, beta-mercaptoethanol

ßNGF, nerve-growth factor homodimer

TAMRA, carboxytetramethylrhodamine flurophore

TF, trigger-factor

TGNs, trigeminal ganglion neurons

TK, thymidine kinase

Trans-UV, ultra-violet light transilluminator

TrkA, tropomyosin-related kinase A

TRPV1, transient receptor potential vanilloid 1

Trx, thioredoxin tag

VAMP, vesicle-associated membrane protein

Publications and presentations

Papers

1. Jiafu Wang, Jianghui Meng, Marc Nugent, Minhong Tang and J. Oliver Dolly. Neuronal entry and high neurotoxicity of botulinum neurotoxin A require its N-terminal binding sub-domain. (Wang et al., 2017b).
2. Marc Nugent, Jiafu Wang, Gary Lawrence, Tom Zurawski, Joan Geoghegan and J. Oliver Dolly. Novel conjugate of an IgG binding domain and a derivative of botulinum neurotoxin A productively targets SNARE-cleaving protease into TrkA expressing cells following coupling to pertinent IgG or a Fc-βNGF fusion. (Bioconjugate Chemistry, under review).

Presentations

1. Marc Nugent, Tom Zurawski, Ahmed Al-Sabi and J. Oliver Dolly. Successful generation of functional double-knot toxin, a potent agonist of transient receptor potential vanilloid 1, as a possible targeting ligand for sensory neurons. Neuroscience Ireland Biennial Conference 2015, 1st-2nd September, 2015.

Table of Contents

Results

List of Figures

Chapter 1

Chapter 2

Chapter 3

Chapter 4

Chapter 5

List of Tables

Chapter 1

Chapter 2

Abstract

Thesis title: Novel strategies for targeting botulinum neurotoxin-based therapeutics to neuronal populations involved in pain sensation

Author: Marc Nugent

Botulinum neurotoxin serotype A (BoNT/A) is a bacterial di-chain protein containing a protease light-chain which cleaves synaptosomal-associated protein of M_r = 25 k (SNAP-25), a protein essential for neuronal exocytosis; this produces prolonged, but ultimately reversible, abolishment of neurotransmitter release. The retargeting of a BoNT/A-derivative to sensory neurons involved in heightened pain sensation is a potential therapeutic strategy for the treatment chronic pain. The development of such a therapeutic is, however, a complex multi-step process dependent on the identification of suitable cell-surface target receptors, functional expression of appropriate targeting ligands, and the employment of an effective means of conjugating the latter to a binding domain-deficient BoNT/A core-therapeutic.

An extensive literature research was conducted which identified both transient receptor potential vallinoid 1 (TRPV1) and tyrosine kinase A (TrkA) as promising target candidates and, furthermore, a spider-venom peptide (double-knot toxin) and nerve-growth factor (NGF) as respective means by which to target them. Two published approaches for the conjugation of targeting ligands to the core-therapeutic were initially assessed: conventional protein fusion and “protein stapling” technology. Comprehensive investigation of these strategies highlighted relative advantages and deficiencies; hence, an additional novel method was developed, based on the binding of *S. aureus* protein A to immunoglobulin G (IgG) antibodies.

This latter strategy was optimized to provide a means to couple the core-therapeutic to either antibodies raised against TrkA, or a recombinantly expressed fusion of NGF and fragment crystallizable (Fc) of rabbit IgG. These approaches both culminated in detectable delivery of the protease into target cells, demonstrating the versatility of this innovative technology. However, NGF produced considerably more efficient protease delivery than its IgG counterpart, thereby, highlighting that for effective toxin retargeting the biological activity of the employed ligand is paramount. Consequently, NGF-mediated targeting via TrkA represents a potentially viable strategy for the intracellular delivery of engineered BoNT/A-based pain therapeutics.

Chapter 1. General introduction

1.1 Botulinum neurotoxin as a potential therapeutic for chronic pain

1.1.1 Nociception, pain and chronic pain

Pain has been defined as a "complex constellation of unpleasant sensory, emotional and cognitive experiences provoked by real or perceived tissue damage and manifested by certain autonomic, psychological, and behavioural reactions" (Terman, 2003). The complexity of this definition mirrors the actual intricacy of pain sensation; it is highly subjective, involving interplay and communication between the peripheral nervous system (PNS) and central nervous system (CNS).

Physiological pain sensation is instigated by a process termed nociception that involves specialized high-threshold sensory neurons within the PNS known as nociceptors. These are primarily non-myelinated C-fibre neurons or thinly myelinated Aδ-fibres expressing a plethora of surface receptors and channels that sense noxious stimuli which signal actual or potential tissue damage. Noxious heat, cold or the release of inflammatory mediators such as cytokines, growth factors or proteases following tissue insult, activate specific receptors on the nociceptors, which participate in the generation of an action potential (transduction); the latter is transmitted along the nerve fibre by voltage-gated ion channels (conduction). This signal is relayed from the peripheral neurons to second order neurons in the spinal cord (transmission) which processes and propagates the signal to the appropriate regions of the brain, where the message is interpreted (modulation) and may lead to the sensation of pain (Dubin and Patapoutian, 2010).

The system described above affords an extraordinary evolutionary advantage, enabling rapid response to damaging or dangerous stimuli and, thus, supports the preservation of homeostasis. However, advantages conferred by sensation of acute pain are nullified if the sensation of pain no longer signals information regarding preventable tissue damage. Chronic pain is defined as pain lasting longer than 6 months, which extends far beyond the benefit of acute pain sensation associated with the initial injury (Treede et al., 2015). This definition can be further sub-divided into chronic inflammatory and neuropathic pain (Xu and Yaksh, 2011). The inflammatory variety occurs as a result of the aberrant release of inflammatory mediators, resulting in long-lasting and increased pain sensation (Huang et al., 2006). Neuropathic pain involves the sensitization of sensory neurons, due to an injury-induced increase in the surface expression of channels involved in nociceptive

transduction, conduction and transmission; resulting in lower thresholds to noxious stimuli (hyperalgesia) or painful interpretation of innocuous stimuli (allodynia) (Bridges et al., 2001).

Chronic pain represents a major challenge for both patients and healthcare providers. Estimates of its prevalence vary wildly, but it is generally accepted that as many as 20% of European adults suffer from the condition (Breivik et al., 2006). In the Irish context, its incidence has been estimated as high as a staggering 35.5% of the population (Raftery et al., 2011). It has been estimated that in 2008 its overall cost to the Irish exchequer was €5.34 billion or 2.86% of GDP, with the average cost in Ireland per patient standing at €5,665 per annum (Raftery et al., 2012). Current treatments for the disorder rely heavily on short-acting non-steroidal anti-inflammatory drugs, which often have serious side effects. This restricts most patients to on-going pain management with often inadequate analgesics or highly addictive opioid drugs (Rosenblatt and Catlin, 2012). There is, therefore, a severe unmet need for effective, long-acting and non-addictive therapeutics for chronic pain.

1.1.2 SNARE complex-mediated Ca^{2+}-dependent exocytosis

Soluble *N*-ethylmaleimide-sensitive factor attachment protein receptor (SNARE) proteins are essential constituents of the membrane fusion apparatus, responsible for regulated fusion of intracellular vesicles with the cell membrane. In neurons, the respective SNAREs are: synaptosomal-associated protein of relative molecular mass (M_r) of 25 k (SNAP-25), tethered to the plasma membrane via several cysteine-linked palmitoyl chains, and, syntaxin 1 and vesicle-associated membrane protein (VAMP) which are anchored on the plasma and vesicle membranes, respectively. Formation of a neuronal SNARE complex involves the assembly of a parallel four-α-helical bundle. The nascent complex initially links the vesicle and cell membranes prior to a Ca^{2+}-dependent fusion event, resulting in the exocytosis of the vesicle contents (Südhof and Rizo, 2011). The core SNARE complex consists of one α-helix respectively from syntaxin-1 and VAMP, with an additional two helices contributed by SNAP-25 (Sutton et al., 1998). Assembly of SNARE complexes requires exquisite regulation to prevent spontaneous membrane fusion. To this end, vesicle-bound synaptotagmin serves as a Ca^{2+} sensor, with an additional role in early docking of synaptic vesicles to the presynaptic membrane via interaction with SNAP-25. Upon binding Ca^{2+}, synaptotagmin instigates the fusion of

vesicles with the presynaptic membrane, resulting in exocytosis (Fig. 1.1) [reviewed by (Chapman, 2008)].

The stimulated exocytosis of pain signalling neurotransmitters from nociceptors is mediated by such Ca^{2+} dependent SNARE complex formation (Meng et al., 2007). Moreover, the insertion of nociceptive transducers into the membrane of nociceptors has been demonstrated to utilize these same SNAREs (Meng et al., 2016). Consequently, inhibition of such mechanisms has considerable potential in a novel therapeutic approach for chronic pain. To this end, neuronal proteolytic toxins known as botulinum neurotoxins (BoNTs) are of particular significance, due to their ability to specifically, but reversibly, cleave SNARE proteins, perturbing the formation of the SNARE complex and, consequently, inhibiting exocytosis.

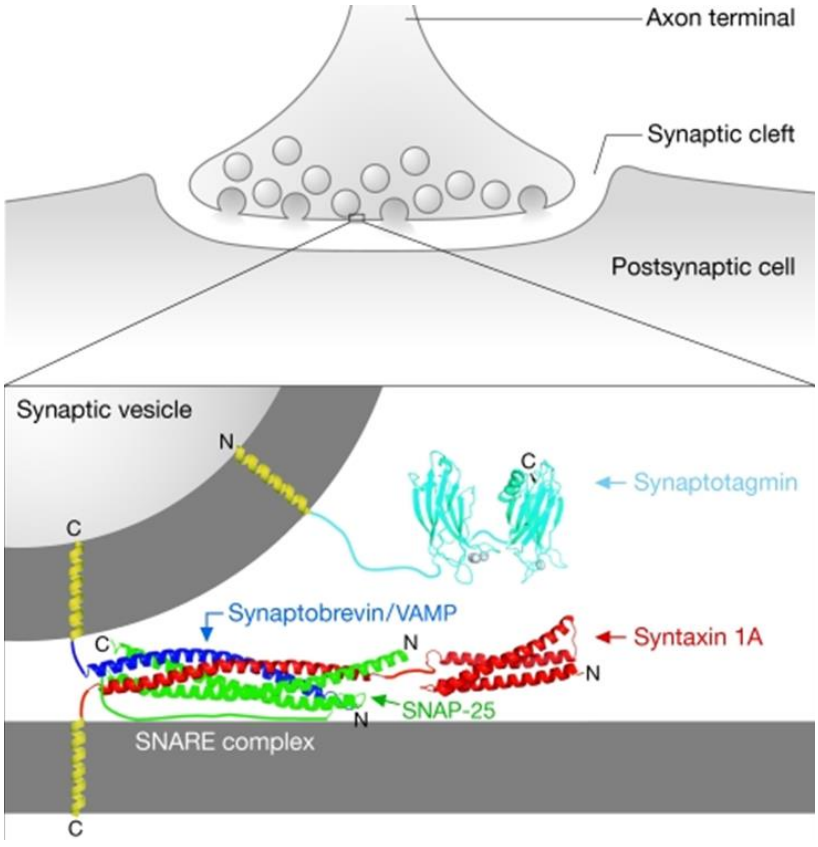

Figure 1. 1 SNARE complex-mediated Ca^{2+}-dependent exocytosis
The core SNARE complex is formed by four α-helices, to which VAMP (dark-blue) and syntaxin (red) contribute one each to the exocytotic vesicle and the cell membrane, respectively, with the additional two provided by cell membrane localized SNAP-25 (green). Vesicle-bound synaptotagmin (light-blue) functions as a Ca^{2+} sensor, and upon binding the latter instigates SNARE zipping, resulting in vesicle-membrane fusion and the consequent exocytosis of vesicle cargo. Schematic adapted from (Carr and Munson, 2007).

1.1.3 Structure and mechanism of action of botulinum neurotoxins (BoNTs)

BoNTs are a group of homologous 150 k di-chain proteins consisting of 7 confirmed serotypes (A-G), with a controversial 8th serotype (H) recently reported (Dover et al., 2013). BoNTs contain 4 structural domains (individually colored in Fig. 1.2), which mediate distinct steps in the multi-step intoxication of neurons (Fig. 1.3). This process culminates in the cytosolic delivery of a zinc dependent proteolytic light-chain (LC = ~50 k), that selectively cleaves at least one of the aforementioned SNARE proteins involved in Ca^{2+}-dependent exocytosis of neurotransmitters. The LC from each BoNT serotype uses binding sites remote from its active protease site to recognize distinct regions on SNAREs; these exosites dictate both which SNARE is cleaved by each serotype and the position of the scissile bond (Breidenbach and Brunger, 2004) (Table 1.1).

The LC is linked by a disulphide bond to a heavy chain (HC = ~100 k). The C terminus of the HC (H_C) consists of two binding sub-domains: H_{CN} and H_{CC} (both ~25 k each). The H_{CC} binds the toxin to acceptors composed of Gt1b and Gd1a gangliosides, and ectopic domains of synaptic vesicle proteins (Table 1.1). Binding of both together is necessary for effective endocytosis of the toxin with the binding to gangliosides serving as an initial step, anchoring the toxin at the cell membrane. The exposure of the luminal domains of synaptic vesicle proteins, following neuronal exocytosis, facilitates the high-affinity binding of the toxin to these acceptors; the toxin is then internalized into the cell during endocytic recycling (Dong et al., 2006). The exact functional role of the H_{CN} subdomain has not yet been fully elucidated, despite it being highly-conserved between all BoNT serotypes (Lacy and Stevens, 1999). It has, however, been shown to interact with phosphatidylinositol phosphates in the mammalian cell membrane, and on this basis has been predicted to contribute to toxin binding. It has also been suggested that this binding may assist in the correct orientation of the toxin within endosomes, a prerequisite for effective translocation (Muraro et al., 2009).

The N terminus of the HC is referred to as the translocation domain (H_N = ~50 k), because it is thought to be responsible for the translocation of the LC across the limiting membrane of the endocytic vesicle into the neuronal cytosol, following binding and internalization of the toxin (Fischer et al., 2012). The precise mechanism by which the H_N orchestrates translocation of the LC remains somewhat enigmatic, although the acidification of the endosome is an essential pre-requisite (Fischer et al., 2008), as translocation is prevented

by inhibitors of the vesicular proton pump or other chemicals that attenuate endosome acidification (Azarnia Tehran et al., 2015). A decrease in endosomal pH below pH 5.5 causes the alpha helices of the H_N to undergo conformational change and penetrate the endosomal membrane; creating a channel through which a partially unfolded LC can travel. The disulfide bond linking the LC, is then cleaved by vesicle bound thioredoxin reductase, releasing the protease into the cytoplasm (Pirazzini et al., 2016). There is no inherent pH sensor on BoNT, it has instead been suggested that protonation of carboxylate residues in the HC precedes H_N channel formation and this, potentially, serves a role in coordinating efficient translocation in response to endosomal acidification (Pirazzini et al., 2013).

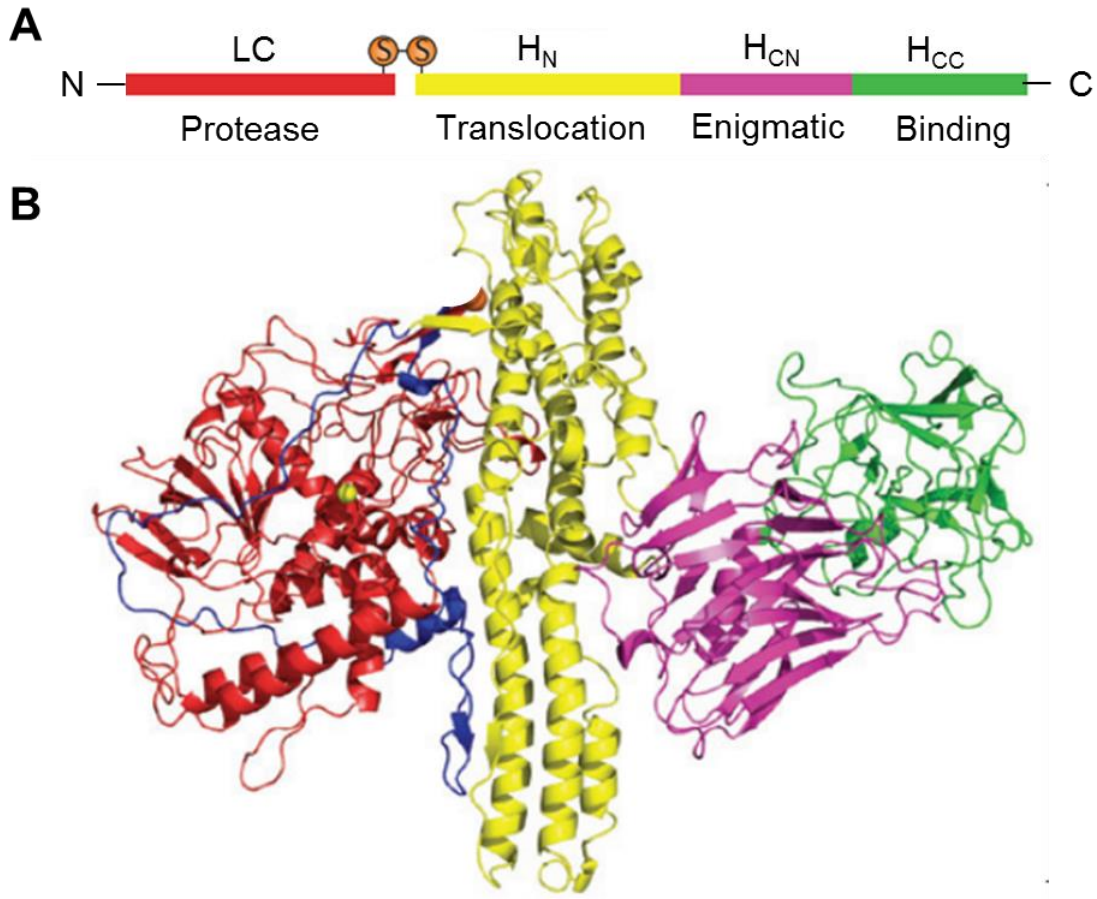

Figure 1. 2 BoNT structure

(A) Schematic representation and (B) crystal structure of BoNT/A (PDBcode; 3BTA). The same color scheme applies to both (**A**) and (**B**). The LC protease, H_N translocation, the enigmatic H_{CN} and the H_{CC} receptor binding domains are colored red, yellow, purple and green, respectively. Crystal structure in (**B**) taken from (Rossetto et al., 2014).

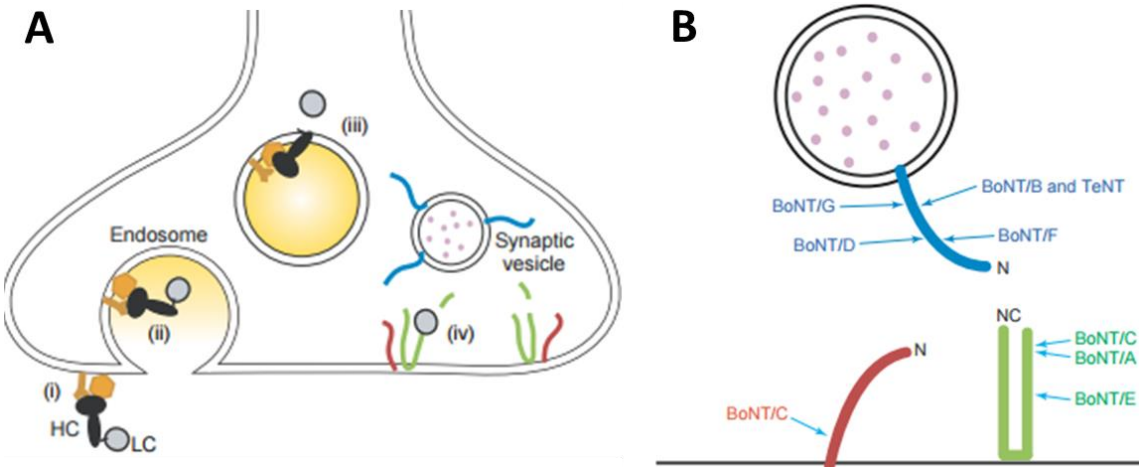

Figure 1. 3 Inhibitory action of BoNTs on transmitter release

(**A**) Four steps are involved in the neuronal intoxication by BoNTs: (i) the BoNT heavy chain (HC, black) orchestrate dual-binding on the cell-surface through an initial interaction with gangliosides (orange), followed by binding to glycoprotein receptors (orange); (ii) acceptors-mediated internalization by endocytosis; (iii) translocation of light chain LC (grey) to the cytosol mediated by the H_N translocation domain following acidification of the endosome and (iv) Proteolytic LCs cleave their respective SNARE substrates; VAMP (blue), syntaxin (red) and SNAP-25 (green). (**B**) The SNARE substrate cleavage sites of each BoNT serotype. Schematic adapted from (Breidenbach and Brunger, 2005).

Table 1. 1 BoNTs and their respective cleavage substrates

BoNT serotype	Intracellular target protein	Cleavage sites in human	Protein acceptor
/A	SNAP-25	EANQ^{197}RATK	Synaptic vesicle 2 & fibroblast growth factor receptor 3
/B	VAMP 1/2	GASQ^{76}FETS	Synaptotagmin II & I
/C	SNAP-25 Syntaxin I	ANQR^{198}ATKM DTKK^{254}AVKY	Unknown
/D	VAMP 1/2	RDQK^{61}LSELD	Synaptic vesicle 2
/E	SNAP-25	QIDR^{180}IMEK	Synaptic vesicle 2
/F	VAMP 1/2	ERDQ^{60}KLSE for I ERDQ^{58}KLSE for II	Synaptic vesicle 2
/G	VAMP 1/2	ETSA^{83}AKLK for I ETSA^{81}AKLK for II	Synaptotagmin II & III

1.1.4 Potential of BoNT/A as a novel pain therapeutic

BoNT/A preferentially targets cholinergic neurons of the neuromuscular junction through binding of a ganglioside (GT1b) plus synaptic vesicle 2 (SV2) (Stenmark et al., 2008), with another co-acceptor, fibroblast growth factor receptor 3 (FGFR3) recently reported (Jacky et al., 2013). BoNT/A then acts through cleavage of SNAP-25, a SNARE indispensable in the stimulated exocytosis of acetylcholine, the neurotransmitter which stimulates muscle contraction (Lebeda et al., 2008). BoNTs have long been exploited therapeutically to treat a broad range of disorders by inhibiting over-active muscles and glands (Bigalke et al., 1985). There are several BoNT-based therapeutics available, probably the most well-known of which is BOTOX® (Allergan Inc., California), which contains BoNT/A as its active component in a complex with accessory proteins.

BOTOX® or BoNT/A have shown potential in the treatment of >100 human conditions (Münchau and Bhatia, 2000, Mahajan and Brubaker, 2007, Luvisetto et al., 2015), and the therapeutic use of botulinum neurotoxins (BoNTs) represents an emerging treatment for chronic pain as, significantly, BoNT activity is not restricted to cholinergic neurons. The internalization of toxin into other nerve cell types, albeit requiring higher concentrations, also results in SNARE cleavage and inhibition of transmitter release (Meng et al., 2014). It was observed that following administration of BOTOX® for cosmetic purposes, patients reported a reduction in the incidence, duration and severity of migraine (Silberstein et al., 2000). Furthermore, after a number of supportive clinical trials, the FDA approved BOTOX® for the treatment of chronic migraines in 2010. Although it has yet to be fully deciphered how BOTOX® or its active component BoNT/A acts to alleviate migraine, experimental evidence from *in-vitro* experiments suggests it could result from a dual effect upon nociceptors. Firstly, BoNT/A inhibits release of neurotransmitters and peptides involved in pain transmission (Durham et al., 2004, Meng et al., 2009) and, secondly, cleavage of SNAREs reduces the surface expression of channels and receptors which function as nociceptive transducers (Morenilla-Palao et al., 2004, Meng et al., 2016). These suggested applications are supported by pain studies in animal models (Cui et al., 2004, Aoki, 2005).

The above-noted dual action has potential as a proficient means by which to attenuate sensation of pain. Furthermore, BoNT/A has a long duration of action, with a single-treatment capable of inhibiting neurotransmitter release for up to 6 months in the human

facial area (Flynn, 2010). As a well-tolerated protein-based therapeutic, BoNT/A could conceivably confer significant personal and economic benefits as a non-addictive, efficient, long-lasting and sorely needed alternative treatment for chronic pain.

Despite the therapeutic value of BoNT/A, its inhibition of acetylcholine release remains a concern for many applications due to the risk of neuromuscular weakness (Pappert and Germanson, 2008). The exceptional potency of BoNTs limits dosage and, thus, the therapeutic window. In order to capitalize upon the effectiveness of BoNTs, the toxins must be redesigned in such a way as to retain the desirable high efficiency ablation of SNARE complex formation, while preferentially retargeting of BoNT/A away from cholinergic neurons, and towards the pain-sensing peripheral nociceptive neurons. It is fortuitous, therefore, that BoNTs and BoNT/A in particular, are well characterized proteins which have been the subject of intense investigation since 1822, when Justinus Kerner first alluded to potential therapeutic uses of this "sausage poison" (Erbguth, 2004). Since then, the depth of research and continued interest in BoNTs is demonstrated by "botulinum toxin" producing 17,448 unique results on PubMed (as of November 2016).

The extensive research into BoNTs has involved attempts to fully characterize the functional role of each domain which has, consequently, highlighted the modular nature of the toxin. Each domain is for the most part structurally-and functionally-distinct; this characteristic allows engineering at the genetic level to manipulate the protein domains for defined functional outcomes and, most interestingly, the creation of BoNT chimeras (Wang et al., 2008). The development of novel chimeras, which substitute the receptor binding domain of BoNT/A with an appropriate targeting peptide could, in theory, target BoNT/A away from the cholinergic neurons and, instead, redirect its SNARE protease into nociceptors. The principle of BoNT retargeting to normally refractory cells has been previously established (Chaddock et al., 2000a), demonstrating the feasibility of such an approach. A novel nociceptor-targeted BoNT/A chimera could afford significant potential as an innovative treatment of chronic pain, by greatly reducing the prospect for motor deficits and, thus, increasing the therapeutic window.

1.2 Nociceptor selective cell-surface proteins

1.2.1 Literature review to identify putative nociceptor targets

For identifying putative novel targets for a novel nociceptor selective BoNT/A-based therapeutic, an exhaustive literature research was conducted to categorize protein receptors or channels which are expressed on the surface of peripheral nociceptors. The criteria were then refined to isolate candidates which are unique to such nociceptive neurons, and absent from peripheral motor neurons or sensory neurons responsible for non-noxious sensation. The nociceptive roles of the resultant candidates were then assessed to ensure they represent viable targets for a chronic pain therapeutic, based on the criteria that they (i) function in the transduction or conduction of painful stimulus and (ii) their surface expression is up-regulated during incidences of chronic pain.

It had to be determined that the refined list of putative targets were also compatible with the requirements of a BoNT therapeutic, namely that they undergo ligand-induced endocytosis, to elicit internalization of the toxin, and then enter endocytic acidifying vesicles. Acidification of the endocytic vesicle is paramount, as once the toxin is successfully internalized, the LC must be translocated across the limiting membrane into the cytoplasm in order to cleave its SNARE substrate, for which vesicle acidification is a critical step (Fischer et al., 2008). The summary of findings from the described literature review are outlined in Table 1.2.

The literature review identified 28 proteins which fulfilled aspects of the prescribed criteria; however, only 9 satisfied the aforementioned requisites: Acid Sensing Ion Channel 3 (ASIC3), Voltage-gated Sodium Channels 1.7 and 1.8 (Nav 1.7 and 1.8), MAS-related G-protein coupled receptor D (MrgD), Purinergic receptors 2 and 3 ($P2X_2$ and $P2X_3$), Tropomyosin kinase A (TrkA), Transient receptor potential ankyrin 1 (TRPA1) and Transient receptor potential vallinoid 1 (TRPV1). The targeting of a BoNT/A based therapeutic to the above channels/receptors, would require conjugation of a toxin-based core-therapeutic to a pertinent ligand, capable of binding and inducing internalization of its defined target. To this end, the 9 potential target candidates were subjected to a final screening, which involved further appraisal of the available literature, to determine if suitable targeting ligands could be identified for each respective candidate. This resulted in the ultimate refinement of the list to 2 targets: TRPV1 and TrkA.

Table 1. 2 Candidate nociceptor selective cell-surface targets

Nociceptor expressed receptor	Nociceptor selective	Function in nociception	Expression upregulated	Ligand induced endocytosis	References
ASIC3	√	√	√	√	(Deval et al., 2008)
TRESK	X	√	√	?	(Wood, 2010)
TREK-1	X	√	?	√	(Noël et al., 2009)
TRAAK	X	√	?	?	(Hur et al., 2009)
KNCQ	X	√	√	√	(Passmore et al., 2003)
mGluRs	X	√	√	√	(Yogeeswari et al., 2009, Blackshaw et al., 2011)
MrgD	√	√	√	√	(Rau et al., 2009, Honda et al., 2012)
MrgX1	√	√	√	X	(Solinski et al., 2010, Sikand et al., 2011)
MrgX2	√	√	√	X	(Yang et al., 2005)
MrgX3	√	√	?	?	(Kaisho et al., 2005)
Nav 1.7 and 1.8	√	√	√	√	(Fang et al., 2005, Chahine and O'Leary, 2014)
Neuropeptide Y receptors	X	√	√	√	(Walker et al., 1988)
N-type Ca^{2+} Channels	X	√	√	√	(Saegusa et al., 2001)
P2X2	√	√	√	√	(Staikopoulos et al., 2007)
P2X3	√	√	√	√	(Staikopoulos et al., 2007, Stanchev et al., 2009)
P75	X	√	√	√	(Bronfman et al., 2003)
PAR2	X	√	√	√	(Noorbakhsh et al., 2003)
TrkA	√	√	√	√	(Fang et al., 2005, Kumar and Mahal, 2012)
TRPA-1	√	√	√	√	(Eid et al., 2008, Schmidt et al., 2009)
TRPC1	X	√	?	√	(Remillard and Yuan, 2006)
TRPC3	X	√	?	√	(Kunert-Keil et al., 2006)
TRPC5	X	√	√	√	(Zimmermann et al., 2011)
TRPC6	X	√	√	√	(Guilbert et al., 2008)
TRPM8	X	√	√	√	(de la Peña et al., 2005, Bautista et al., 2007)

TRPV1	√	√	√	√	(Michael et al., 1997, Bohlen et al., 2010, Julius, 2013)
TRPV2	X	√	√	√	(Tamura et al., 2005)
TRPV4	X	√	√	√	(Wegierski et al., 2006)
T-Type Ca2+ Channels	X	√	√	√	(Jagodic et al., 2008)

√ = Confirmed; X = negative; ? = not known or disputed

1.2.2 TRPV1 as a nociceptor target for a BoNT/A-based pain therapeutic

TRPV1 is tetrameric, non-selective cation channel, with each subunit consisting of 6 transmembrane α-helices (Fig. 1.4). It is a key component in the transduction and modulation of nociceptive signaling, and in the PNS is almost exclusively expressed in sub-populations of non-myelinated C-fibre and thinly-myelinated Aδ-fibre nociceptors (Mitchell et al., 2010). TRPV1 has been shown in several studies to be up-regulated during chronic pain (Kim et al., 2014) and a contributor to the pathophysiology of migraine (Meents et al., 2010). TRPV1 was originally known as the "capsaicin receptor" (Schumacher, 2010). Capsaicin, the main pungent ingredient in 'hot' chilli peppers, has long been known to elicit a sensation of burning pain; however, since the cloning of TRPV1 (Michael et al., 1997) a multi-faceted and integral role of TRPV1 in nociceptive transduction has been deciphered.

TRPV1 acts as a molecular sensor of noxious heat and a polymodal integrator of painful stimuli, placing it in a central role in the pathophysiology of pain (Wang and Woolf, 2005). TRPV1 responds directly to huge variety of exogenous and endogenous physical and chemical stimuli, including capsaicin, heat >42°C, H^+, ATP, and certain spider venoms (Winter et al., 2013). In response to such stimulus, the TRPV1 channel pore opens, with the resultant influx of Ca^{2+} producing localized depolarization, leading to the generation of an action potential (Takayama et al., 2015). The gating of TRPV1 is, however, far from simplistic. There is an enormous degree of molecular interplay; for example, a certain stimulus might lower the overall threshold of TRPV1 for activation by a secondary stimulus that may, previously, have been innocuous (Julius, 2013). In terms of the pain response of a patient, this manifests as a heightened pain response to noxious stimulus (hyperalgesia) or a painful response to what is normally an innocuous stimulus

(allodynia). Allodynia and hyperalgesia have been described as the cornerstones of neuropathic pain (Bridges et al., 2001).

TRPV1 is expressed on the surface of peptidergic nociceptors which release, SNARE-dependently, pain-eliciting inflammatory neuropeptides calcitonin gene-related product (CGRP) and substance P (SP) (Meng et al., 2009). In addition to the transduction of nociceptive signals, the influx of Ca^{2+} following TRPV1 activation induces the exocytosis of CGRP and SP, which subsequently interact with adjacent immune cells such as basophils and mast cells, stimulating them to release an "inflammatory soup". The latter contains a plethora of noxious compounds which further activates the already sensitized TRPV1 channel, resulting in additional amplification of the nociceptive signal (Julius, 2013) (Fig. 1.5).

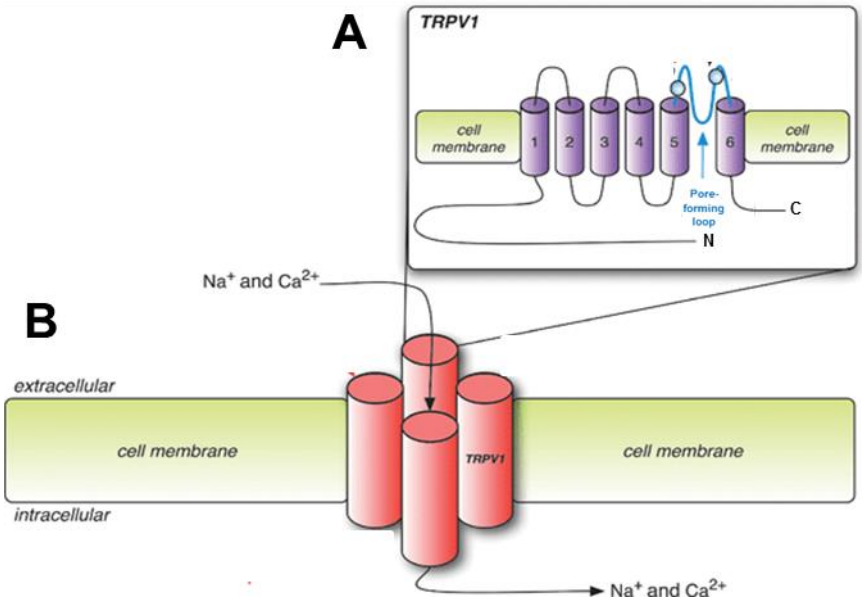

Figure 1. 4 Structure of TRPV1
(A) Individual TRPV1 subunit showing the 6 transmembrane α-helices depicted in purple. The pore-forming region occurs between the 5th and 6th α-helix. **(B)** Tetrameric structure of TRPV1 consisting of 4 identical subunits, which functions as a non-selective cation channel, depicted by the arrow indicating Na^+ and Ca^{2+} travelling through the channel. Figure adapted from (Conway, 2008).

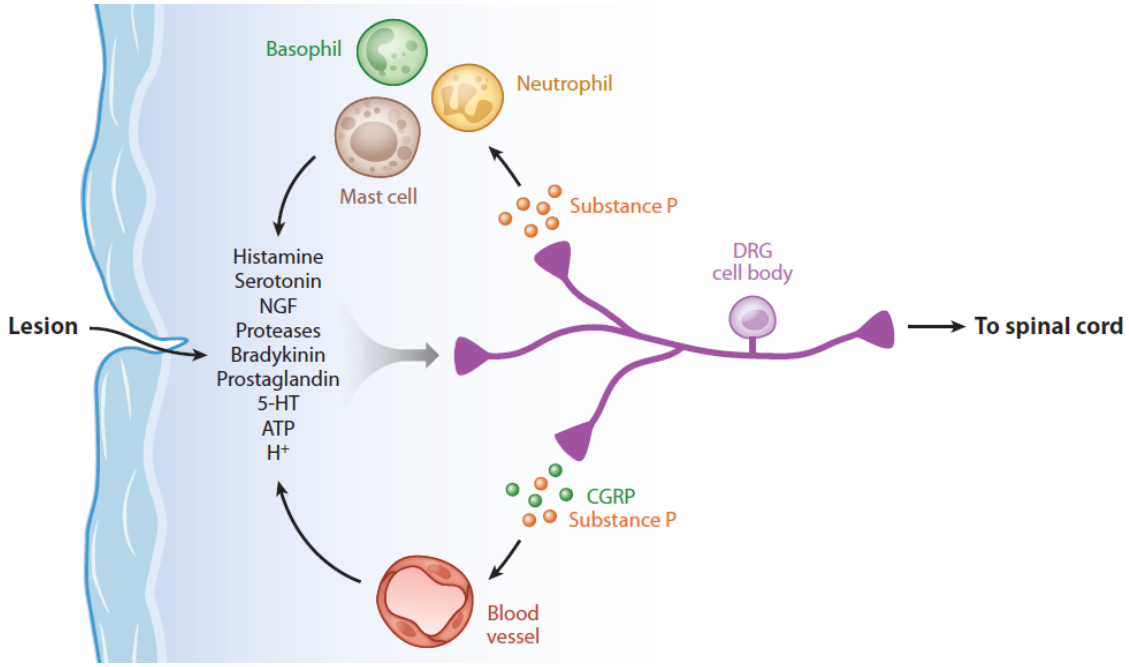

Figure 1. 5 Amplification of nociceptive signalling in the PNS

The nociceptor is depicted in purple; TRPV1 is expressed at the nerve terminal and along the fiber (not shown). Tissue injury activates TRPV1 stimulating the release of SP and CGRP, which interact with immune cells to stimulate the release of "inflammatory soup" containing histamines, proteases etc. These then further act upon TRPV1 causing an amplification cycle. The noxious stimulus is transmitted down the nerve fiber to the spinal cord, where it is relayed to the CNS, inducing a pain response. Diagram taken from (Julius, 2013).

Although TRPV1 has a primary role in pain transduction, somewhat paradoxically, agonists of the channel have long been appreciated for their analgesic properties. As early as 4000 BC, the therapeutic benefit of chili peppers was realized by the ancient Aztecs; it was used as a treatment for toothache and other such inflammatory conditions (Schumacher, 2010). Separated geographically and temporally, the ancient Romans used the resin from the cactus *Euphorbia resinifera* to treat arthritic pain; this resin is now known to contain resinferatoxin, an ultra-potent analogue of capsaicin (Schumacher, 2010). One way in which these ancient analgesics functioned was by exploiting one of the inherent characteristics of TRPV1: it undergoes agonist-induced internalization. The result of which is a reduction in the levels of TRPV1 on the cell surface, rendering the nociceptors less-responsive to noxious stimulus. Significantly, TRPV1 endocytic vesicles undergo acidification (Sanz-Salvador et al., 2012). Thus, in principle, a novel BoNT-based derivative which contains an agonistic TRPV1 targeting moiety could serve as an effective means by which to productively deliver the SNARE-cleaving protease into peripheral nociceptors.

1.2.3 TrkA as a nociceptor target for a BoNT/A-derived pain therapeutic

TrkA is the high-affinity receptor for nerve-growth factor (NGF) (Wiesmann et al., 1999). It is a canonical receptor tyrosine kinase, which exists as a monomer on the cell surface of certain sensory neurons and some sympathetic neurons in both the PNS and CNS (Fig. 1.6 A). Biologically active NGF occurs as a homodimer (βNGF), with each of its subunits capable of binding to the immunoglobulin like domain of TrkA monomers and, thus, induce dimerization of adjacent receptors and transphosphorylation of their intracellular tyrosine kinase sites (Grimes et al., 1996) (Fig. 1.6 B); stimulating internalization of the complex into endosomes which undergo subsequent acidification (Diering et al., 2013). βNGF-TrkA signalling mediates neurotrophic effects during development by initiating multiple intracellular signalling cascades involving mitogen-activated protein kinases, protein kinase B and protein kinase C. The activations of these proteins initially promote neuronal survival and differentiation, which are indispensable for the maturation of sensory neurons (Lindsay, 1996). However, upon reaching adulthood, peripheral expression of TrkA is restricted to TRPV1 expressing small-diameter peptidergic C-fibre nociceptors (Averill et al., 1995), where TrkA signalling transitions from a role in neuronal survival to also promoting whole organism survival through mediation of nociceptive function (Kumar and Mahal, 2012). As such, either sequestering NGF (Kan et al., 2016), or antagonizing TrkA with small molecules (Watson et al., 2008) has emerged as a therapeutic strategy for pain management.

TrkA activation recruits numerous downstream effectors, including phosphatidylinositol 3-kinase (PI3K), which subsequently phosphorylates TRPV1; this sensitizes the channel (Bonnington and McNaughton, 2003) and increases its trafficking and membrane insertion (Huang et al., 2006). Significantly, the up-regulation of TRPV1 surface expression occurs via SNARE-mediated exocytosis (Morenilla-Palao et al., 2004), which can be reduced by BoNT/A truncation of SNAP-25 (Meng et al., 2016). TrkA activation also upregulates the expression of both CGRP and SP (Lindsay and Harmar, 1989), the SNARE-dependent exocytosis of which serves to incite further release of NGF from adjacent immune cells (Aloe et al., 1992, Ye et al., 2011); this rapidly elevates the surface expression of TrkA (McKelvey et al., 2013), thereby, producing a self-perpetuating nociceptive positive-feedback loop (Kumar and Mahal, 2012). A TrkA targeted BoNT/A-derived therapeutic could, therefore, serve as an additional approach by which to productively target peripheral nociceptors for analgesic benefit.

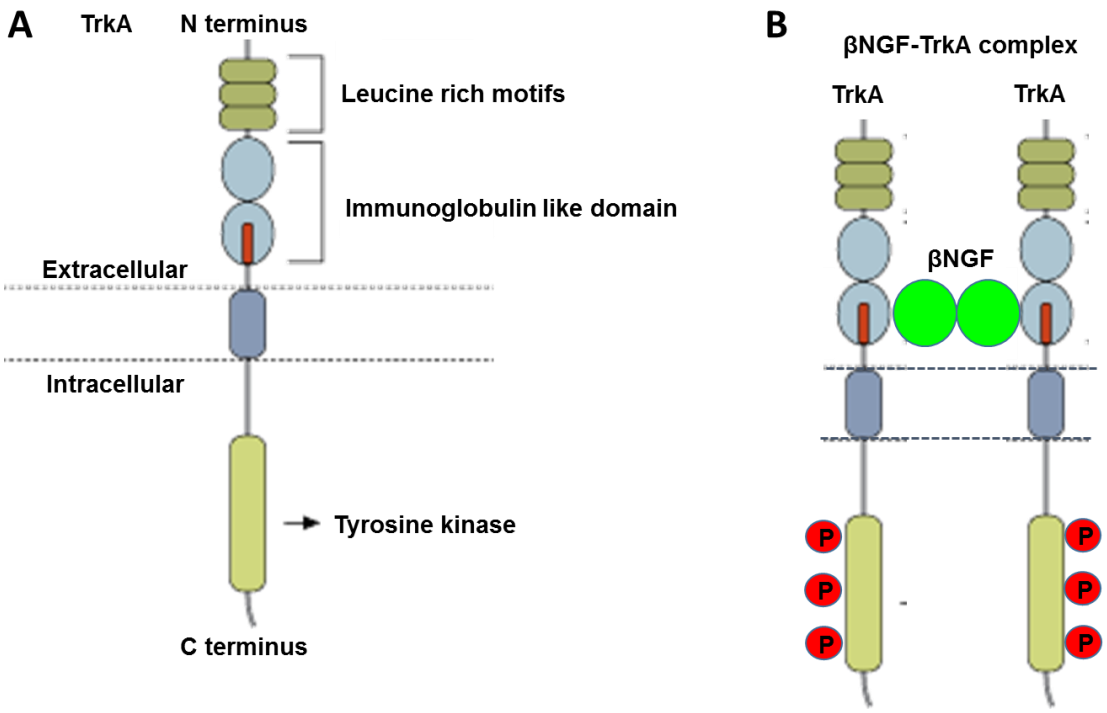

Figure 1. 6 TrkA structure and activation

(**A**) Schematic of the TrkA monomer indicating the intracellular tyrosine kinase, the extracellular immunoglobulin like domain which serves as the binding site for βNGF and the leucine rich motif which stabilizes the association with βNGF. (**B**) The binding of the βNGF homodimer to two adjacent TrkA receptors induces their dimerization, resulting in phosphorylation of the intracellular tyrosine kinases, which subsequently phosphorylates downstream effectors such as mitogen-activated protein kinases, protein kinase B and protein kinase C.

1.3 Previous approaches to retargeting the BoNT protease

The retargeting of BoNT to specific cell types had been previously achieved by a variety of methods. The first published accounts of which involved preparation of BoNT/A derivatives lacking the H_C following digestion of full-length toxin with trypsin protease. These binding domain deficient toxins were then purified and subsequently chemically conjugated to NGF (Chaddock et al., 2000a), wheat germ agglutinin (Chaddock et al., 2000b) and a lectin from *Erythrina cristagalli* (Duggan et al., 2002). Although a degree of protease delivery into cultured cells was achieved for each of these ligands, trypsin removal of the H_{CC} from BoNT confers an inherent risk of both off-target proteolytic degradation, or incomplete digestion leading to a heterogeneous product (Shone et al., 1985). Furthermore, chemical conjugation can lead to inactivation of either the BoNT or ligand components due to over-derivatization, and was reported to produce conjugation efficiency of only 12-16% (Chaddock et al., 2000b, Duggan et al., 2002).

The recombinant expression of BoNT derivatives which had been manipulated genetically to substitute the H_C with targeting ligands, provided an advance on the chemical conjugation of ligands to trypsin treated BoNT toxins. Genetic fusion was employed for targeting moieties such as epidermal-growth factor (EGF) (Foster et al., 2006, Fonfria et al., 2016), growth-hormone releasing hormone (Somm et al., 2012) and single-chain antibodies (Ma et al., 2014). These fused ligands successfully delivered the SNARE protease into cultured cells *in vitro*, and in the case of growth-hormone releasing hormone, the rat pituitary gland *in vivo*. In addition to BoNT retargeting, genetic manipulation has been utilized to make composite BoNT toxins such as a LC/E-BoNT/A tri-chain, in which the SNARE protease of BoNT/E was fused to full-length BoNT/A to confer two SNAP-25 cleaving enzymes (Wang et al., 2017a). Also a functional hybrid of LC/A and full-length tetanus toxin has been published, capable of delivering the LC/A protease into neurons susceptible to tetanus, but refractory to BoNT (Wang et al., 2012). However, genetic fusion presents its own limitations due to an inherent difficulty in expressing the resultant chimeras in soluble form (Wang et al., 2011, Wang et al., 2012), as well as issues regarding the functionality of both the BoNT and targeting ligand components (Arsenault et al., 2013).

To address the above-mentioned concerns with both chemical and genetic linkage of BoNT to ligands, a protein-mediated coupling strategy termed protein stapling has been developed (Ferrari et al., 2012) (detailed in Chapter 4). This approach was successful in the high-efficiency conjugation of a BoNT/A derivative devoid of the H_C to a panel of 9 targeting ligands, with each capable of mediating detectable delivery of the SNAP-25 protease into neuroendocrine tumour cells (Arsenault et al., 2013). Although the above approaches demonstrated the feasibility of developing a nociceptor-specific BoNT/A-based therapeutic, the diversity in targeting moieties employed, as well as the multifariousness of the conjugation protocols utilized, meant that there was no defined effective strategy for the conjugation of BoNT to targeting ligands.

1.4 Project aims and objectives

The principle project objective was the development of a novel means by which to productively deliver the LC/A protease into either TRPV1 or TrkA expressing cells, through specific targeting of the latter proteins. Achievement of this could, potentially, contribute to the future development of a novel targeted BoNT/A-based pain therapeutic.

TRPV1 and TrkA were selected due to their PNS expression being constrained to peptidergic nociceptors which utilize SNAP-25, their respective endocytosis in response to ligand binding, and the subsequent acidification of the resultant endosomes, characteristics considered indispensable for the delivery of the SNARE protease.

The contribution of the H_{CN} sub-domain to BoNT neuronal binding being unsubstantiated, consequently, presented an additional facet of the toxins functionality which merited investigation. The inclusion of the H_{CN} in a nociceptor-targeted BoNT chimera would permit elucidation of its contribution to neuronal intoxication (see Chapter 3). Furthermore, although the published examples of BoNT retargeting demonstrated the feasibility of the endeavor, there existed an innate divergence in the ligand conjugation approaches. A secondary aim of the project was, therefore, an appraisal of the previously-employed fusion and protein stapling conjugation strategies, to identify their respective advantages and shortcomings (see Chapter 3 and 4). The independent evaluation of these approaches, supported the design and development of an optimized and innovative technology, applicable to the conjugation of BoNT to diverse ligands. This novel strategy facilitated the specific targeting of a nociceptive transducing receptor by two distinct approaches, both of which culminated in the delivery of the SNARE-cleaving LC/A protease into pertinent cells (see Chapter 5).

Chapter 2. Materials and methods

2.1 Materials

2.1.1 Plasmid vectors

The bacterial expression vectors pET32b and pGEX-KG were, respectively, purchased from Merck Millipore or kindly provided by Dr. Gopal of the Adyar Cancer Institute, India. The *Staphylococcus aureus* Protein A immunoglobulin G antibody binding domain B (SpA-B) in the pGEX-KG vector was provided by Prof. Joan Geoghegan of Trinity College, Dublin. The pACYC duet vector for co-expression of seventeen kilodalton protein (Skp) and trigger-factor (TF) protein chaperones (Lamppa et al., 2013), was generously provided by Prof. Karl Griswold of Dartmouth College, USA.

pIRES2-EGFP and pIRES2-DsRed2 mammalian expression vectors were provided by my co-supervisor, Dr. Jiafu Wang, Dublin City University (DCU), and the TRPV1 gene in the pcDNA3.1 vector gifted by Prof. David Julius of the University of California, USA.

2.1.2 Synthetic deoxyribonucleic acid

Synthetic deoxyribonucleic acid (DNA) with codon optimization for the bacterial expression of double-knot toxin (DkTx), and the insect cell expression of human NGF and rabbit immunoglobulin gamma chain C (rFc), was supplied by Life Technologies.

2.1.3 Molecular biology reagents

Polymerase chain reaction (PCR) reagents, benzonase® nuclease and thrombin were purchased from Merck Millipore. TOP10™ and Origami B™ *E. coli*, TOPO™ gateway cloning vectors and the Baculodirect™ insect cell expression system were purchased from Biosciences, a distributor for Life Technologies. Kits for DNA isolation and purification were purchased from Qiagen. Oligonucleotides for the PCR manipulation of DNA were from Eurofins Genomics. Restriction endonucleases, DNA ligase, DNA kilobase pair (kbp) size standards, DNA sample buffer and SHuffle® *E. coli* were purchased from Brennan & Company, a distributor of New England Biolabs. Glutathione agarose, Talon® resin and HisTrap Excel™ columns were purchased from Sigma Aldrich, a supplier for GE Healthcare.

2.1.4 Synthetic syntaxin peptide

A synthetic peptide encompassing residues 201-245 of rat syntaxin, labelled on the C-terminus with N-terminal carboxytetramethylrhodamine (TAMRA) fluorophore was purchased from either Biomatik (USA) or Peptide Synthetics (UK).

2.1.5 Mammalian cell lines

HEK-293, SH-SY5Y, F11 and PC-12 cells were purchased from ATCC.

2.1.6 Animals

Sprague Dawley rats were purchased from Envigo (formerly Harlan), and bred in an approved Bio-resources Unit in DCU. The experiments, maintenance and care of the rodents complied with the European Communities (Amendment of Cruelty to Animals Act 1876) Regulations 2002 and 2005. Experimental procedures had been approved by the Research Ethics Committee of DCU, and licenced by the Irish Health Products Regulatory Authority.

2.1.7 Cell culture and related reagents

Dulbecco's modified Eagle's medium (DMEM), Roswell Park Memorial Institute 1640 medium (RPMI-1640), fetal bovine serum (FBS), horse serum, trypan blue, Dulbecco's phosphate buffered saline (PBS), penicillin/streptomycin antibiotics, L-glutamine, Cytosine-β-D-arabinofuranoside, dispase II, collagenase I, poly-L-lysine and laminin were purchased from Sigma. TransIT®-LT1 Transfection Reagent was bought from Mirus Bio. Mouse nerve growth factor (NGF-2.5S) and capsaicin were supplied by Alomone. I-PER® lysis reagent, Sf-900™ and Sf-900II™ insect cell media, AlamarBLUE™ and Fluo-4 AM were provided by Biosciences, a distributor for Life Technologies. Tissue culture flasks and plates were from Sarstedt.

2.1.8 Western-blotting and immuno-cytochemical reagents

Polyvinylidene fluoride (PVDF) membrane, nitrocellulose membrane, Precision Plus protein™ molecular mass standards and Bio-Rad protein assay reagents were purchased from Fannin, a distributor of Bio-Rad. Immobilon™ enhanced chemiluminescent luminol (ECL) substrate and Hoescht stain were obtained from Merck Millipore. NuPAGE™ and

BOLT™ polyacrylamide gels were purchased from Biosciences, a distributor of Life Technologies. Vector Laboratories provided VECTASHIELD Mounting medium.

2.1.9 Antibodies used

Table 2. 1 List of primary antibodies

Antibody target (catalogue number)	Raised in species (immunogen epitope)	Vendor	Dilution / concentration used	
			Western blotting	Immuno-fluorescence
α-Tubulin (T9026)	Mouse (purified α-Tubulin)	Sigma Aldrich	1 : 1000	Not tested
ß-Tubulin III (T8578)	Mouse (residues 436-450)	Sigma Aldrich	1 µg/ml	Not tested
TrkA (ANT-018)	Rabbit (TrkA, residues 342-356)	Alomone	1 : 500	1 : 50
Erk 1/2 (ab17942)	Rabbit, (ERK residues 317-339)	Abcam	1 : 1,000	Not-tested
BoNT LC/A	Rabbit (residues not defined)	Allergan. Inc.	1 : 1,000	Not-tested
Nerve-growth factor (AN-240)	Rabbit (purified NGF-2.5 S)	Alomone	1 : 200	Not-tested
Poly-histidine [$(His)_6$] (OB05)	Mouse, $(His)_6$	Merck Millipore	1 µg/ml	4 µg/ml
p-Erk 1/2 (ab4819)	Rabbit, [ERK 1(pT202/pY204) and ERK 2 (pT185/pY187)]	Abcam	1 : 1,000	Not-tested
SNAP-25 (SMI-81)	Mouse (N-terminus of SNAP-25)	Abcam	1 : 3,000	Not-tested

SNAP-25$_{/A}$	Rabbit (SNAP-25 residues 190-197)	Allergan. Inc.	1: 1,000	Not-tested
TRPV1	Rabbit (human TRPV1, residues 606-621)	Produced in-house	1 µg/ml	5 µg/ml
VAMP 1/2/3 (104 011)	Mouse (purified VAMP 1)	Synaptic systems	1 : 1,000	Not-tested

Rabbit non-immune immunoglobulin G (IgG) was purchased from Sigma; anti-species secondary antibodies conjugated to horseradish peroxidase (used at 1:5,000) or to either Alexa-Fluor® 488 or Alexa-Fluor® 590 fluorescent probes (used at 1:3,000) were obtained from Jackson Immuno-Research or Life technologies, respectively.

2.1.10 Other reagents

Sodium ^{125}I-iodine (Specific activity: ~17 Ci/mg, radioactive concentration: 103.23 mCi/ml, quantity: 3 mCi) was purchased from Perkin Elmer. All other reagents and chemicals were purchased from Sigma Aldrich.

2.1.11 Suppliers

Suppliers' addresses are listed in the Appendix.

2.2 Generation of constructs for expression of recombinant proteins

2.2.1 DNA isolation and purification

Plasmid DNA was isolated using either QIAprep® Mini, Midi or Maxi Kits according to the manufacturer's instructions, typically producing purified DNA with yields of 1 µg/µl in a final volume of 50, 500 and 1,000 µl, respectively.

2.2.2 Polymerase chain reaction

PCR amplification was performed in a DNA thermal cycler (Applied Biosystems). Reactions were typically carried out in 50 µl volumes using KOD Hot Start DNA polymerase. Plasmid DNA (10 ng) was used as template for PCR, with DNA primers, deoxynucleotide triphosphates and $MgSO_4$ added to final concentrations of 0.3 µM, 0.2 mM and 1.5 mM, respectively.

Initial denaturation was performed at 95°C (2 min) followed by 30-35 cycles of denaturation (20 s) at 95°C, 10 s annealing (temperature dependent on primer used) and extension at 70°C for 20 s/kb. PCR products were purified using QIAquick® PCR purification kit and the final DNA yields quantified by absorbance at 260/280 nm using a spectrophotometer (Nanodrop™ 1000).

Site-directed mutagenesis was carried out using the Quikchange™ method, with the PCR performed as above. Purified PCR produces were subsequently incubated with 1 U Dpn1 restriction endonuclease at 37°C for 60 min to digest methylated parental template DNA.

2.2.3 Restriction endonuclease digest of DNA and agarose electrophoresis

Isolated plasmid DNA or purified PCR products were subjected to either single or double restriction endonuclease digest, according to the protocol prescribed by New England Biolabs. Agarose gels were prepared by dissolving 1-2% agarose in boiling Tris-acetate-ethylenediaminetetraacetic acid (EDTA) buffer (40 mM Tris, 20 mM acetic acid and 1 mM EDTA), with ethidium bromide added to a final concentration of 0.5 μg/mL. The gels were subsequently cooled to 65°C and cast in mini trays, with combs inserted to produce wells for sample loading.

Digested DNA was combined with DNA sample loading buffer, added to wells, subjected to electrophoresis at 90 V in Tris-acetate-EDTA buffer and imaged by exposure to transilluminator ultra-violet (Trans-UV) light using G: BOX Chemi-16 gel documentation system (Syngene). In instances where the digested DNA was to be utilized for cloning, the DNA was isolated from the gel and subsequently purified using the QIAquick® gel extraction kit, according to the manufacturer's instructions.

2.2.4 DNA ligation and bacterial transformation

DNA fragments (plasmid vector DNA or PCR products) restriction digested to generate compatible 5' and 3' ends and gel purified (see 2.2.3) were ligated using T4 DNA ligase. Typically, digested plasmid vector and PCR products were combined in a 1:3 respective molar ratio overnight at 22°C with 1 U T4 DNA ligase, in a final volume of 20 μl.

E. coli strains (TOP10™, BL21, Origami B™ or SHuffle®) were made chemically competent as described (Hanahan et al., 1991) and subsequently transformed with the ligated vectors by the heat-shock method (Froger and Hall, 2007). The bacteria were then

spread on Luria broth (LB) agar containing an appropriate antibiotic to select for positive transformants, and incubated overnight at 37°C. The DNA inserts in plasmid vectors isolated from individual clones was assessed by size analysis of the base pairs (bp) excised following restriction digest, prior to confirmation of sequence fidelity by DNA sequencing.

2.2.5 Constructs generated for bacterial expression of recombinant proteins

Table 2. 2 List of constructs for recombinant bacterial expression

Construct No.	Expression vector	DNA insert encoding (amino acid residues)	Restriction endonuclease sites		Vector notes
			5'	3'	
1	pET32b	BoNT/$A_{(1-1092)}$	SacI	XhoI	The vector encodes an in-frame 5' fusion with folding chaperones, purification tags and protease susceptible sites. See Figure 2.1.
2	pET32b	BoNT/$A_{(1-1092)}$-linker[1]-DkTx$_{(1-79)}$	SacI	XhoI	" "
3	pET32b	DkTx$_{(1-79)}$	SacI	XhoI	" "
4	pET32b	BoNT/$A_{(1-878)}$-SNAP-25$_{(1-206)}$	MscI	XhoI	" "
5	pET32b	VAMP 2$_{(25-84)}$–linker[2]-DkTx$_{(1-79)}$	MscI	XhoI	" "
6	pET32b	BoNT/$A_{(1-1092)}$-H_{CC}/B$_{(1081-1291)}$	MscI	XhoI	As above + H_{CC}/B contains mutations (K1192E, Q1200K)

7	pET32b	BoNT/$A_{(1-1092)}$-$H_{CC}/B_{(1081-1291)}$-linker[1]-$DkTx_{(1-79)}$	MscI	XhoI	As above + H_{CC}/B contains mutations (K1192E, Q1200K)
8	pGEX-KG	BoNT/$A_{(1-878)}$-SNAP-$25_{(1-206)}$	XmaI	XhoI	The vector encodes an in-frame 5' fusion with glutathione-S-transferase purification tag and a thrombin protease susceptible site. See Figure 2.2.
9	pGEX-KG	VAMP $2_{(25-84)}$–linker[1]-$DkTx_{(1-79)}$	XmaI	XhoI	" "
10	pGEX-KG	VAMP $2_{(25-84)}$–linker[1]-epidermal growth $factor_{(1-53)}$	XmaI	XhoI	" "
11	pGEX-KG	BoNT/$A_{(1-878)}$-linker[1]-SpA-$B_{(1-58)}$	XmaI	XhoI	As above + SpA-B contains mutations (D36A, D37A)

Linker[1] = 10 alternating glycine-serine amino acid residues
Linker[2] = 27 alternating glycine-serine amino acid residues

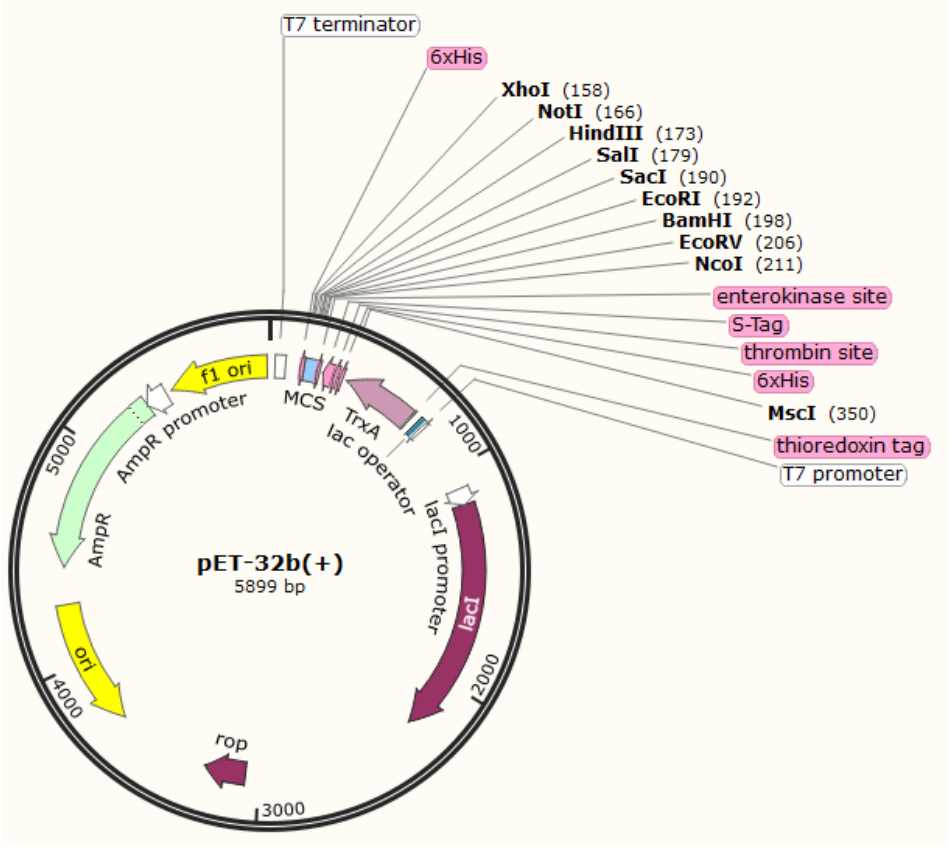

Figure 2. 1 Schematic of pET32b bacterial expression vector
Adapted from (Liu and Yang, 2012), prepared using SnapGene software.

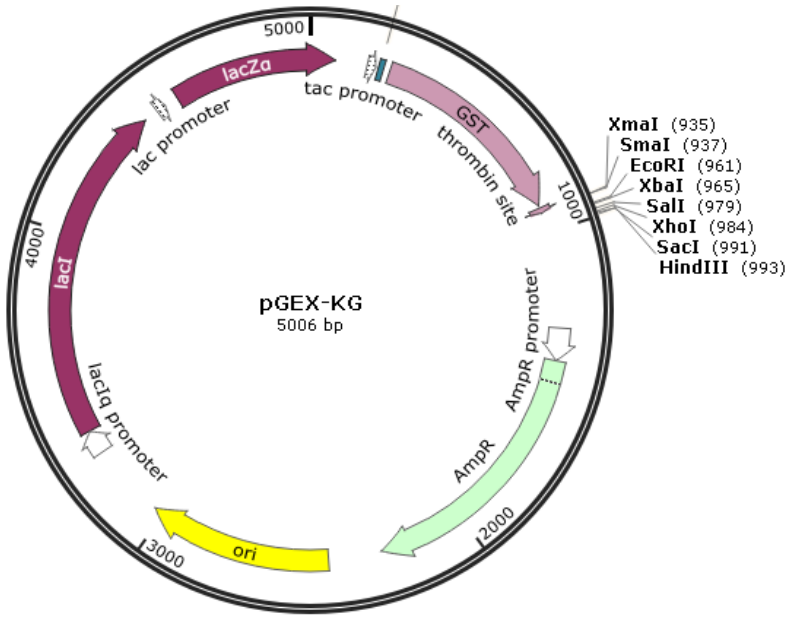

Figure 2. 2 Schematic of pGEX-KG bacterial expression vector
Adapted from (Hakes and Dixon, 1992), prepared using SnapGene software.

2.2.6 Generation of recombinant baculovirus stocks for protein expression in insect cells

Recombinant DNA encoding the full-length of human NGF was designed with a direct 3' fusion of nucleotides encoding residues 102-324 of rFc, with a subsequent 3' sequence encoding a thrombin protease cleavage site and a polyhistidine [$(His)_6$] purification tag. The resultant gene (NGF-rFc-thrombin-His_6) was synthesised with codon optimization for insect cell expression. The full-length gene, or a fragment encoding only NGF was inserted into pENTR-D/TOPO™ Gateway vectors by the prescribed method. These Gateway cloning vectors were subsequently recombined with Baculodirect™ DNA; recombinant baculovirus stocks were generated according to the manufacturer protocol.

The titre of each baculovirus was determined by a standard plaque assay. Briefly, 10-fold dilutions of the viral stocks were prepared in 1 ml of Sf900II™ medium before applying to Sf9 insect cells seeded at 8 x 10^5 cells/well in 6-well plates. The cells were incubated for 1 hour at 27.5°C, the medium was then removed and the cells were overlaid with agarose diluted to a final concentration of 4% in Sf900™ medium. The cells were then incubated for 6 days at 27.5°C until plaques were well formed. The viral titre was calculated as plaque forming units per ml (pfu/ml), determined by the formula: pfu/ml = pfu / dilution factor × ml of inoculum.

2.3 Expression and purification of recombinant proteins

2.3.1 Bacterial expression of recombinant proteins by auto-induction, and preparation of culture lysate

This was performed in ZYP-500 auto-induction medium, as previously defined (Studier, 2005), supplemented with appropriate antibiotics to select for the relevant expression construct. The medium was inoculated 1:500 with an overnight starter culture of transformed bacteria, grown at 37°C with shaking at 220 rotations per minute (RPM) for 8 hours, then at 22°C overnight, following which the cells were collected by centrifugation at 5,000 x g for 30 minutes at 4°C. The resultant cell pellet was lysed by resuspension in 1 ml of "bacteria lysis buffer" (150 mM NaCl, 20 mM HEPES, pH 8.0) per g of cell pellet, followed by benzonase® at 500 U/L of culture, with lysozyme added to a final concentration of 2 mg/ml. The mixture was shaken at room temperature (RT) for 40 minutes followed by freezing at -20°C and thawing at 22°C, repeated three times.

The soluble fraction of the lysate was subsequently isolated by centrifugation at 14,000 x g for 30 minutes at 4°C, and stored at -20°C until purification (see 2.3.3 and 2.3.4).

2.3.2 Induction of bacterial expression of recombinant proteins by isopropyl β-D-1-thiogalactopyranoside

Luria broth medium was supplemented with selective antibiotics, inoculated 1:500 with an overnight starter culture of transformed bacteria and grown at 37°C with shaking at 220 RPM until an absorbance of 0.6 - 0.8 at a wavelength of 600 nm (OD_{600}) was reached. Expression was induced by addition of 0.1 mM isopropyl β-D-1-thiogalactopyranoside (IPTG), lowering the temperature to 22°C and incubation overnight. The subsequent cell harvesting, lysis and clarification was performed as described (see 2.3.1).

2.3.3 Immobilized metal affinity chromatography of recombinant proteins expressed in bacteria

Recombinant proteins fused with a $(His)_6$ tag were purified from the soluble fraction of prepared cell lysates (see 2.3.1) by immobilized metal affinity chromatography (IMAC), after incubation with 1 ml bed volume of Talon® resin per 100 ml of lysate, initially by batch binding with agitation for 1 hour at 4°C, this was followed by binding in a 25 ml column at RT, with the flow-rate determined by gravity. The resin was washed with 2 column volumes of "IMAC wash buffer" (150 mM NaCl, 20 mM HEPES, 5 mM imidazole, pH 8.0), following which the protein was eluted in 1 ml fractions with "IMAC elution buffer" (500 mM imidazole, 150 mM NaCl, 20 mM HEPES, pH 8.0). The total protein of each eluted fraction was measured by the Bio-Rad protein assay, and the three with the highest content were buffer exchanged into "protein storage buffer" (150 mM NaCl, 20 mM HEPES, pH 7.4) using PD-10 gel filtration columns. The protein yield following buffer exchange was determined by bicinchoninic acid (BCA) protein assay against standards of bovine serum albumin (BSA).

2.3.4 Affinity chromatography of recombinant proteins expressed in bacteria

Recombinant proteins fused with a glutathione-S-transferase (GST) tag were purified from the soluble fraction of prepared cell lysates (see 2.3.1) by affinity chromatography following incubation with 1 ml bed volume of glutathione agarose per 100 ml of lysate, initially by batch binding overnight with agitation at 4°C, followed by binding in a 25 ml column at RT. The agarose was initially washed with 2 column volumes of protein storage

buffer (150 mM NaCl, 20 mM HEPES, pH 7.4), following which it was resuspended in a volume of the latter buffer equal to its bed volume. The bound recombinant proteins were released from the agarose immobilized GST by incubation with thrombin protease (2 U/per ml of agarose) for 40 minutes at 22°C. Activity of thrombin was then quenched by adding of phenylmethane sulfonyl fluoride (PMSF) to a final concentration of 1 mM. Eluates containing the purified proteins were then separated from the agarose by centrifugation using SigmaPrep™ filtration spin columns, and the protein yield was determined by BCA protein assay against BSA standards.

2.3.5 Baculovirus-mediated expression of recombinant proteins in Sf9 insect cells

Sf9 insect cells were cultured in Sf900II™ medium at 27.5°C either adherent in T-75 flasks or in shake flasks with rotation at 130 RPM. Recombinant expression in Sf9 insect was induced by the inoculation of the culture with medium containing baculovirus. The volume of inoculum was determined by the desired multiplicity of infection (MOI), as indicated in the figure legends, and was calculated according to the formula: Inoculum required = MOI (pfu/cell) × number of cells / viral titre (pfu/ml). The cells were then incubated for up to 96 hours at 27.5°C prior to harvesting of the supernatant.

The optimal protocol for baculovirus-mediated recombinant expression of NGF containing fusion proteins involved seeding Sf9 cells in log-phase growth at $2.5x10^6$ cells/ml in Sf900II™ medium, in a total volume of 500 ml. Cells were infected with low-passage recombinant baculovirus at a MOI of 0.05 and incubated for 96 hours at 27.5°C, with shaking at 130 RPM. Intact cells and cellular debris were subsequently cleared from the cell supernatant by centrifugation at 5,000 x g for 30 minutes at 4°C, followed directly by IMAC purification (see 2.3.6).

2.3.6 Fast protein liquid chromatography of $(His)_6$-tagged proteins from insect cell supernatant by IMAC

The clarified Sf9 supernatant containing recombinant homo-dimerized NGF (ßNGF) fused to rFc and a $(His)_6$ tag (see 2.3.5) was purified by IMAC on a ÄKTA explorer (GE Healthcare) fast protein liquid chromatography (FPLC) system using a 1 ml HisTrap Excel™ column. The supernatant was applied to the column at a flow-rate of 1 ml/min overnight at RT, in a recirculating loop. The column was then washed with 20 column volumes (100 mM sodium phosphate, pH 7.4) and the protein eluted in 1 ml fractions

(500 mM imidazole, 100 mM sodium phosphate, pH 7.4). The protein contents of the eluted fractions were subsequently precipitated by the addition of ammonium sulfate to 80% saturation, following which the protein pellets were isolated and reconstituted into 200 µl of protein storage buffer (150 mM NaCl, 20 mM HEPES, pH 7.4).

2.4 Sodium dodecyl sulfate polyacrylamide gel electrophoresis, protein staining and Western-blotting

2.4.1 Sodium dodecyl sulfate polyacrylamide gel electrophoresis

Protein samples were mixed with "SDS sample buffer" (final concentration: 62.5 mM Tris-HCl pH 6.8, 2.5 % SDS, 10% glycerol, 0.002% bromophenol blue) and heated at 95°C for 5 minutes. In instances where it was necessary to reduce disulfide bonds, beta-mercaptoethanol (ßME) was freshly added to a final concentration of 2.5%. Prepared samples were loaded onto self-cast or precast NuPAGE™ sodium dodecyl sulfate polyacrylamide gels (SDS-PAGE) between 8 and 15%. Electrophoresis was run at 180 volts at 4°C using MOPs running buffer (250 mM MOPS, 250 mM Tris, 5 mM EDTA, 0.1% SDS) until proteins were separated according to their molecular masses, indicated by pre-stained protein markers.

2.4.2 Protein staining

Protein staining was performed by incubation of SDS-PAGE gels for 10 minutes in "Coomassie stain" (40% methanol, 10% acetic acid, 0.1% Coomassie) heated to ~60°C. The gel was then removed, rinsed and incubated with deionized H_2O with gentle agitation at RT. The H_2O was replenished continuously until the background staining on the gel was sufficiently diminished and protein bands became distinct; digitised gel images were recorded using G: BOX Chemi-16 gel documentation system (Syngene).

2.4.3 Western-blotting

Proteins to be subjected to Western-blotting were resolved by SDS-PAGE, then electrophoretically transferred to PVDF membrane by the semi-dry method, using a Pierce™ power blotter (Thermofisher) according to the prescribed protocol. Non-specific binding to membranes was inhibited by incubation for 30 minutes in "TBS" (10 mM Tris-HCl, 100 mM NaCl, pH 7.4) containing 5% (w/v) BSA. The membrane was then probed with pertinent primary antibodies diluted in the same buffer for either 1 hour at RT or

overnight at 4°C, washed three times with gentle agitation for 10 min in TBS buffer; bound antibody was detected by incubation with anti-species specific antibody conjugated to horseradish peroxidase (HRP). Following additional wash steps, the membrane was exposed to ECL, which reacts with HRP to release a fluorescent signal; this was recorded as a digitised image using G: BOX Chemi-16 gel documentation system (Syngene).

2.4.4 Densitometric quantification and statistical analysis

Densitometric analysis of digitised images following either Coomassie staining or Western-blotting was performed using ImageJ software, with the resultant data normalized as indicated in figure legends. Data collated from several independent experiments were processed using Excel and graphs generated by GraphPad Prism 6.0; each point represents the means ± S.E.M.; student's unpaired t-test was used to evaluate significance of changes observed.

2.5 Conversion of purified single-chain BoNT/A derivatives to di-chain isoform, and confirmation of proteolytic activity towards a recombinant SNAP-25 substrate

2.5.1 Thrombin-mediated creation of di-chain forms of purified BoNT/A derivatives

The recombinant BoNT/A derivatives outlined in Table 2.2, were expressed, purified as detailed in section 2.3 and isolated as single-chain proteins. These each contained an inter-chain thrombin protease cleavage site engineered between the LC and HC, as previously described (Wang et al., 2011), facilitating conversion to disulfide bonded di-chain. Typically, thrombin protease was added directly to the sample of purified protein (1 U/mg of protein), and incubated for 1 hour at 22°C, with the thrombin subsequently inactivated by addition of PMSF to a final concentration of 1 mM. To visualize the conversion of the proteins to active di-chain form and the presence of an inter-chain disulfide bond, an aliquot of the sample was subjected to SDS-PAGE in both the presence and absence of reductant, followed by Coomassie staining.

2.5.2 *In vitro* protease cleavage of recombinant SNARE fragment substrate

The proteolytic activities of di-chain BoNT/A derivatives were assessed using an established *in vitro* SNAP-25 cleavage assay (Wang et al., 2012). Briefly, toxin samples

were diluted appropriately into the assay buffer (20 mM HEPES, 100 mM NaCl, 10 µM $ZnCl_2$, 5 mM dithiothreitol, 10 µg/ml BSA, pH 7.4) and a recombinant SNAP-25 fragment substrate (residues 134-206) C-terminally fused to green fluorescent protein (GFP), was added to a final concentration of 0.5 mg/ml and incubated at 37°C for 30 minutes. To determine the % of SNAP-25 cleavage, the samples were resolved on SDS-PAGE, Coomassie stained, imaged and subjected to densitometric analysis using ImageJ software.

2.6 Culture of mammalian cells and transient transfection

2.6.1 Storage and maintenance of mammalian cell lines

Low passage aliquots of the cell lines listed in Table 2.3 were stored in the defined medium, supplemented with 10% dimethyl sulfoxide and submerged in liquid nitrogen. Once thawed, the cells were maintained in T-75 tissue culture flasks at 37°C, 5% CO_2 in 15 ml of culture medium. When the cells reached ~90% confluency, typically every 4 days, the medium was decanted, the cells were washed with PBS and detached from the flasks by the addition of 3 ml of trpysin-EDTA and incubation for 3 minutes at RT, subsequently quenched by the addition of 12 ml of medium pre-warmed to 37°C. The cell suspension was collected, subjected to centrifugation for 3 minutes at 170 x g, and the resultant cell pellet resuspended in 10 ml of fresh medium. For maintenance of cells, a 1:5 dilution was then made into a fresh T-75 flask, and the cell passage number increased by 1. Cells were never maintained in excess of 20 such passages. For cell-based assays, the resuspended cells were counted using a haemocytometer (Sigma-Aldrich), with trypan blue exclusion used to determine cell viability (Strober, 2001). The cells were then seeded into tissue culture plates or dishes, as indicated in the figure legends.

Table 2. 3 Mammalian cell lines cultured

Cell line name	Species	Origin	Tissue derived	Culture medium
HEK-293	Human	Embryonic	Kidney	DMEM supplemented with 10% FBS, 20 mM glutamine and 1% penicillin/streptomycin antibiotics

SH-SY5Y	Human	Neuroblastoma	Bone marrow	" "
F11	Rat/mouse hybrid fusion	Neuroblastoma / embryonic	Dorsal root ganglion	" "
PC-12	Rat	Neuroblastoma / embryonic	Adrenal medulla	RPMI-1640 supplemented with 10% horse serum, 5% FBS, 20 mM glutamine and 1% penicillin/streptomycin antibiotics

2.6.2 Constructs generated for exogenous protein over-expression in mammalian cell-lines

The constructs listed in Table 2.4 were generated as outlined in section 2.2

Table 2. 4 List of constructs for recombinant mammalian protein expression

Construct no.	Vector	DNA insert encoding residues	Restriction endonuclease sites		Vector notes
			5'	3'	
1	pIRES2-EGFP	SNAP-25$_{(1-206)}$	XhoI	SacI	Vector encodes GFP reporter which is independently co-expressed with inserted genes
2	pIRES2-EGFP	Human TRPV1$_{(1-839)}$	NheI	EcoRI	" "
3	pIRES2-DsRed	Human TRPV1$_{(1-839)}$	NheI	EcoRI	Vector encodes *Discosoma* sp. red fluorescent protein

					(DsRed) reporter which is independently co-expressed with inserted genes
4	pcDNA3.1	Human $TRPV1_{(1-839)}$	NheI	EcoRI	N/A

2.6.3 Transient transfection of mammalian cell lines

Unless otherwise stated, HEK-293, SH-SY5Y or F11 cells were seeded at $1x10^5$ cells/well in a 12-well plate (3.8 cm^2/well), and transient transfection with the constructs listed in Table 2.3 was performed using TransIT®-LT1 Transfection Reagent, according to the manufacturer protocol. All assays were performed 48 hours post-transfection.

2.6.4 Culturing of rat trigeminal ganglion neurons

Trigeminal ganglion neurons (TGNs) were dissected from 1-5 day old neonatal rat pups; dissociated and cultured as previously described (Malin et al., 2007). Briefly, the TGNs were dissected and stored temporarily in ice-cold DMEM, following which they were pelleted by configuration at 170 x g for 5 minutes, and the tissue was chopped into small pieces and incubated at 37°C for 25 minutes in Hanks Balanced Salt Solution [HBSS (137 mM NaCl, 5.4 mM KCl, 0.25 mM Na_2HPO_4, 0.1 g glucose, 0.44 mM KH_2PO_4, 1.3 mM $CaCl_2$, 1 mM $MgSO_4$, 4.2 mM $NaHCO_3$, pH 7.0)] with dispase II and colleganse I diluted to final concentrations of 2.4 U/ml and 1 mg/ml, respectively. The suspension was gently triturated through a 10 ml serological pipette, before the addition of DNase I to a final concentration of 1 mg/ml and incubation at 37°C for 15 minutes. The cells were subjected to centrifugation at 170 x g for 5 minutes, the resultant pellet was resuspended and washed three times in DMEM containing 10% FBS (v/v). Cells were seeded at ~$3x10^6$ cells/well onto poly-L-lysine (0.1 mg/ml) and laminin (20 µg/ml) coated 24-well plates (1.9 cm^2/well) in DMEM supplemented with 10% FBS and 50 ng/ml 2.5S NGF. After 24 hours incubation at 37°C, 5% CO_2, and every other day thereafter, the culture supernatant was replaced with medium containing an antimitotic agent, Ara-C, diluted to a final

concentration of 10µM. The cultures were maintained as described for a minimum of 7 days *in vitro* prior to cell treatment.

2.7 Immuno-cytochemical staining, microscopy and recording of images

Immuno-cytochemical (ICC) staining was performed on cultured cells seeded at $3x10^4$ cells/well on poly-L-lysine coated 16 mm coverslips in 24-well plates,. Cells were washed three times in PBS warmed to 37°C, then fixed by the addition of formaldehyde to a final concentration 4% and incubated for 20 minutes at RT. The cells were then washed with PBS three times; at this point, cells were either left un-permeabilized or subjected to permeabilization by 20 minutes of treatment with 0.2% Triton X-100 in PBS. To prevent non-specific binding of antibodies, cells were incubated for 1 hour with either 10% goat or donkey serum diluted in PBS. Primary antibodies were applied in the same solution and left overnight at 4ºC; after extensive washing, fluorophore-conjugated secondary antibodies were added for 1 hour at room temperature. The cells were subjected to a final series of washings in PBS, prior to rinsing in deionized H_2O and mounting onto microscope slides with VECTASHIELD Hardset Mounting medium.

Immuno-fluorescent micrographs were taken with an inverted fluorescence microscope (Olympus IX71) equipped with a CCD camera or an inverted Zeiss confocal microscope (LSM 710) and analysed using Image-Pro Plus 5.1 or Zen Pro 2008, respectively. The omission of primary antibody gave the background of secondary antibody binding; the signal intensity above this was taken as positive reactivity.

Live cultured cells were imaged with the inverted fluorescence microscope (Olympus IX71), following pre-incubation for 15 minutes at 37°C with Hoescht nuclear stain diluted into the culture medium to a final concentration of 1 µg/ml; images were processed and analysed using Image-Pro Plus 5.1 software.

2.8 Functional characterization of TRPV1 transiently-expressed in HEK-293 cells

2.8.1 Electrophysiological recordings of cation influx in response to TRPV1 activation

HEK-293 cells, either untransfected or transiently-transfected with pIRES2-EGFP-TRPV1, were seeded onto poly-L-lysine coated 33mm coverslips at $5x10^3$ cells/coverslip and subjected to patch clamp recordings, using defined extracellular and recording solutions (Bohlen et al., 2010). Transfected HEK-293 cells exhibiting GFP fluorescence were assumed to be TRPV1-positive and selected for patching; subsequent perfusion of capsaicin to a final concentration of 1 µM confirmed a functional response elicited by TRPV1. The resultant influx Na^+ was recorded by whole-cell recording, using a patch clamp system [EPC1 amplifier and controlled by HEKA pulse (HEKA Elektronik, Lambrecht, Germany)]. Cells presenting a strong inward current were washed to remove capsaicin and the extracellular solution was perfused with chimeric fusion proteins containing DkTx, as indicated in the figure legends. The experiment was then repeated with untransfected HEK-293 cells as a negative control. The described electrophysiological recordings were performed in collaboration with Dr. Ahmed Alsabi, DCU.

2.8.2 Intracellular Ca^{2+} imaging following activation of TRPV1: acquisition of confocal images and data analysis

HEK-293 cells transiently-transfected with pcDNA3.1-TRPV1 were plated onto 35 mm dishes coated with poly-L-Lysine at a density of $3x10^5$ and loaded with 5 µM Fluo-4 AM in DMEM for 30 minutes at RT. Cells were then washed three times in HBSS, and placed on an inverted Zeiss confocal microscope (LSM 710) and regions of interest selected which contained a high-proportion of cells exhibiting a healthy morphology. An argon laser was used to excite the fluorophore at 488 nm, and the baseline fluorescence was recorded for ~20s, following which the cells were exposed to either capsaicin or DkTx fusion proteins diluted in HBSS to a final concentration of 1 µM and 5 µM, respectively. A timed series of images were taken over 120s, with images of fluorescent signals grabbed every ~2 s. The intensity of fluorescence emission at 505–530 nm was analysed offline on a cell-by-cell basis using Zeiss software (Zen Pro 2008).

2.9 Investigation of the biological activities of recombinant growth-factor fusions

2.9.1 Dose-dependent survival of serum-starved PC-12 cells in response to recombinant NGF fusions

The assay was designed based on a published protocol (Gazzano-Santoro et al., 1999); briefly, PC-12 cells were seeded at $4x10^4$ per well in a 24-well plate in serum-free medium, and incubated for 48 hours at 37°C, 5% CO_2 with either 2.5S NGF or purified rFc-ßNGF-$(His)_6$ as indicated in the figure legend. AlamarBLUE™, a cell-permeable compound which produces fluorescent metabolites, was added to each well and incubated for a further 24 hours. Fluorescence was measured using a Tecan Safire II plate reader (excitation 570 nm, emission 585 nm).

2.9.2 Phosphorylation of extracellular signal regulated kinases 1/2 in cells exposed to recombinant growth-factor fusions

This assay was performed as described (Lu et al., 2014); briefly, either PC-12 or SH-SY5Y cells were seeded $4x10^4$ per well in a 24-well plate and cultured in serum-free medium overnight. Recombinant growth factors were diluted, as indicated in the figure legends, into serum-free DMEM and added to the cultured cells for up to 1 hour, prior to preparation of cell lysates. Western-blotting was subsequently performed to detect phosphorylation of extracellular signal regulated kinases 1/2 (ERK 1/2).

2.10 Conjugation of BoNT/A-based core-therapeutics to targeting ligands

2.10.1 SNARE-mediated protein stapling

Protein stapling reactions were performed as previously published (Ferrari et al., 2012). Briefly, recombinant proteins containing C-terminal fusions of either full-length SNAP-25 or VAMP $2_{(25-84)}$ were combined with TAMRA-labelled synthetic peptide based on $syntaxin_{(201-245)}$, in a respective molar ratio of 5:7:7 in stapling buffer" (100 mM NaCl, 20 mM HEPES, 0.8% n-octyl-β-D-glucopyranoside, pH 7.4) for one hour at RT. The efficiency of protein conjugation was determined by densitometric analysis of the observed size-shift on Coomassie stained SDS-PAGE.

A variation of protein stapling using the pull-down format was performed by immobilization of GST tagged protein fusions containing either SNAP-25 or VAMP $2_{(25-84)}$ on glutathione agarose, subsequently incubated with their corresponding stapling partners for 1 hour at RT in stapling buffer. The agarose was then washed extensively with the same buffer and the presence of both SNAP-25 and VAMP 2 confirmed by SDS-PAGE followed with either Coomassie staining or Western-blotting.

2.10.2 Conjugation of SpA-B containing fusions to either rabbit immunoglobulin G antibodies or rFc-ßNGF-$(His)_6$

The chimeric protein fusion encoded by construct number 11 of Table 2.2 was recombinantly expressed and immobilized on glutathione agarose, as described in section 2.3.4. Typically, 10 µg of protein was immobilized on 10 µl of agarose and incubated for 1 hour at 4°C with either 1 ml of rabbit serum, 3-fold molar excess of rabbit immunoglobulin G (IgG) antibodies diluted in 200 µl PBS (137 mM NaCl, 10 mM phosphate, 2.7 mM KCl, pH 8.3) or 200 µl of purified rFc-ßNGF-$(His)_6$ in protein storage buffer. The agarose was washed extensively with PBS to remove excess unbound protein, and the coupled complexes were then released from agarose by incubation with 1 U thrombin for 40 minutes at RT; separation of the agarose and eluate was achieved by centrifugation with SigmaPrep™ filtration spin columns.

The binding of proteins to SpA-B containing fusion proteins was investigated by SDS-PAGE followed either by Coomassie staining or Western-blotting, with the antibodies indicated in the figure legends. Dot-blotting analysis was also performed by applying 2 µl of 10-fold dilutions of the conjugated proteins directly to nitrocellulose membrane, blocking in TBS containing 5% (w/v) BSA and then probing the membrane with an anti-rabbit IgG antibody conjugated to HRP for 1 hour at RT. Following additional wash steps, the membrane was exposed to ECL, and a digitised image of the fluorescent signals were recorded using G: BOX Chemi-16 gel documentation system (Syngene).

2.11 Treatment of cultured cells with recombinant BoNT/A derivatives and monitoring of SNAP-25 cleavage

2.11.1 Toxin incubation, cell lysis, SDS-PAGE and immunoblotting

Cultured rat TGNs were prepared as outlined in section 2.6.4. The mammalian cell lines listed in Table. 2.3 and cultured as described in 2.6.1, were typically seeded at $2x10^6$ cells/well in a 24-well plate and allowed to attach. Cells, were untreated or treated with either targeted or untargeted purified BoNT/A derivatives, diluted directly into the culture medium at the concentrations specified in figure legends. The cells were incubated at 37°C, 5% CO_2 for 42-48 hours, after which the medium was removed and the cells were washed with 2 x 1 of ml chilled PBS. Cell lysates were prepared by the addition of 100 µl of SDS sample buffer directly to the cell monolayer, vigorous mixing and subsequent harvesting by aspiration. The lysates were then subjected to SDS-PAGE, followed by Western-blotting using antibodies which detect cleaved SNAP-25.

2.11.2 Quantification of SNAP-25 cleavage

After development with ECL, digital images of chemiluminescent signals were obtained using the G BOX Chemi-16 gel documentation system, and intensities of each lane quantified with ImageJ software. For determination of the fraction of SNAP-25 cleaved, the ratios were calculated against a requisite internal standard (i.e. a cytoskeleton protein) to normalize any variation in loading between wells. Treated samples were expressed relative to those for non-toxin treated controls. Data were processed using Excel and graphs generated using GraphPad Prism 6.0 software; each point represents the mean ± S.E.M, from several independent experiments.

2.11.3 Binding of an anti-TrkA IgG conjugated-BoNT/A derivative to PC-12 lysate

PC-12 lysate (2 µg in 2 µl) was applied directly to nitrocellulose membrane and incubated for 5 minutes at RT; further binding to the membrane was then prevented by blocking in TBS containing 5% (w/v) BSA for 30 minutes at RT. A BoNT/A derivative (5 ng) either conjugated to anti-TrkA IgG (see 2.10.2) or an unconjugated control, was applied directly to the lysate and incubated for 10 minutes at RT. The membrane was then washed extensively with TBS to remove unbound protein, and probed with an anti-LC/A antibody for 1 hour at RT. The membrane was subjected to additional washing prior to incubation

with an anti-species IgG antibody conjugated to HRP for 1 hour at RT. Following a final set of wash steps, the membrane was exposed to ECL, and digitised images of the fluorescent signals were recorded using G: BOX Chemi-16 gel documentation system (Syngene).

2.12 Radio-iodination of BoNT/A derivatives and their binding to rat cultured cerebellum granule neurons

2.12.1 Radio-labelling of BoNTs with ^{125}I-iodine

Recombinant wild-type BoNT/A or its mutated derivatives as indicated in the results section, were labelled with sodium ^{125}I-iodine (^{125}I) by a previously-described chloramine-T method (Williams et al., 1983). Briefly, each BoNT (40 µg in 40 µl) was added to 1 mCi (10 µl) of carrier free ^{125}I and derivatisation initiated by adding chloramine-T (5 µl of 2 mM, yielding a final concentration of 0.22 mM). The reaction was quenched after 40s by addition of an excess of L-tyrosine (25 µl of 1 mg/ml in 0.1 M sodium phosphate buffer pH 7.4 containing 150 mM NaCl). Free ^{125}I and tyrosine were separated from the ^{125}I-labelled toxin by gel filtration, using a PD-10 column equilibrated with the latter buffer, with an aliquot subsequently taken to determine the specific radioactivity. This was calculated by counting γ-emission with a γ-counter (LKB, 1275, minigamma counter), the counts per minute (CPM) were then converted to disintegrations per minute (DPM) based on a pre-determined counter efficiency of 58%. The DPM in the aliquot was then extrapolated to determine total amount of isotope (Ci) associated with toxin (mmol). Radio-labelled toxins were stored at 4°C in the presence of gelatin to a final concentration of 0.25% (w/v).

2.12.2 Saturatable binding of ^{125}I-BoNTs to rat cerebellum granule neurons and quantification of γ-emission

Rat cultured cerebellum granule neurons (CGNs) prepared as previously described (Meng et al., 2007) by Dr. Jiafu Wang and cultured for a minimum of 10 days *in vitro*, were suspended in PBS and the total cell protein content was determined by BCA protein assay. Aliquots (50-150 µg) were supplemented with BSA to a final concentration of 1 mg/ml and incubated with increasing concentrations of each ^{125}I-labelled toxin for 1 hour at 4°C, or together with its unlabelled counterpart at ≤100-fold molar excess over the highest

concentration of ^{125}I-toxin used. Binding was terminated by centrifugation (9,000 x g for 2 min) and resuspension in ice-cold PBS, after which pellets were washed two further times as described prior to γ-counting (LKB, 1275, minigamma counter). A scatchard plot was constructed by calculating the ratio of bound toxin to unbound toxin at each concentration, with the equilibrium disassociation constant (K_D) subsequently determined by calculating the negative reciprocal of the resultant slope. The capacity of increasing concentrations of unlabelled BoNT/A (0-1 µM) to compete with 1 nM ^{125}I-BoNT/A for CGN binding sites was performed as above. Data were processed using Excel and graphs generated using GraphPad Prism 6.0 software; each point represents the mean ± S.E.M, from several independent experiments.

Chapter 3. Chimeric fusion of a TRPV1-activating spider-venom peptide with a binding domain-deficient BoNT/A core-therapeutic: a novel retargeting strategy

3.1 Overview

As presented in the General Introduction, TRPV1 is a polymodal integrator of noxious stimuli, highly selective for peptidergic nociceptors which exhibit SNARE-dependent release of pain-eliciting neuropeptides and inflammatory mediators (Wang and Woolf, 2005). In response to agonist binding, TRPV1 undergoes ligand-induced endocytosis into vesicles which undergo acidification (Sanz-Salvador et al., 2012). This is a requisite for toxin internalization and the subsequent cytosolic delivery of its LC/A protease. TRPV1, thus, serves as a model candidate for the generation of novel retargeted BoNT/A-based anti-nociceptives.

With TRPV1 established as an initial receptor candidate, the next consideration was designing a means by which to target it. Preliminary ideas included the chemical conjugation of BoNT/A to a commercially-available TRPV1 antibody, or generation of BoNT/A fused to a single-chain variable fragment (ScFv) antibody targeting TRPV1; the latter approach had already achieved some targeting of BoNT/A to another protein, $P2X_3$ (Ma et al., 2014). However, chemical linkage of BoNT/A has been reported as inefficient, and implicated in a reduction in activity (Band et al., 2010). Furthermore, as an antibody-mediated approach only offered limited success, it was deemed imperative to adopt a more innovative and ambitious targeting strategy.

My literature research for target candidates and their ligands had unearthed a remarkable TRPV1 agonist, Double-Knot Toxin (DkTx) isolated from the venom of the Malaysian Earth Tiger tarantula (Bohlen et al., 2010). This was recognised as a significant opportunity, the potential of which could be further exploited through development of an original targeting approach: generation of a BoNT/A-spider venom chimera. Consequently, a novel BoNT/A based fusion protein was generated, in which the H_{CC}/A binding domain was deleted and replaced with DkTx to yield LC.H_N.H_{CN}/A-DkTx. The H_{CN} sub-domain was retained, in contrast to the majority of other BoNT-retargeting strategies (see section 1.3), as it was hypothesised that greater fidelity to both native toxin structure and membrane interactions (Muraro et al., 2009) could potentially increase neuronal delivery of LC.H_N.H_{CN}/A-DkTx.

DkTx is a ‘short’ peptide of 79 residues, arranged in two tandemly repeated structural motifs termed inhibitory cystine knot (ICK), each characterized by 3 stabilizing disulphide bonds; the first 2 are involved in the creation of a loop, which is then threaded by a third disulphide creating the ‘knot’(Craik et al., 2001). This conformation confers incredible stability, serving as a model platform, exploited ubiquitously in nature and in an enormously diverse range of bioactive peptides (Herzig and King, 2015). DkTx is however, unique, as its 2 tandemly repeated ICK units are structurally and functionally autonomous, but act synergistically as a single polypeptide (Bohlen et al., 2010).

DkTx is an irreversible agonist of TRPV1 which binds to the pore region locking this channel in an open conformation. The two independent knots of DkTx confer an antibody-like bivalency, enabling the toxin to bind two sites simultaneously within a single TRPV1 channel (Fig. 3.1 A and B). This bivalency is the basis of the irreversible nature of DkTx, as the disassociation constant is such that by the time one knot has disassociated, the other has reattached, and vice a versa. Recombinantly expressed DkTx possesses a half maximal effective concentration (EC_{50}) of 144 nM (Bohlen et al., 2010) which, when combined with its well defined selectivity for TRPV1, provided a promising means for retargeting BoNT/A to TRPV1 expressing neurons. The specificity and high-avidity of the binding of DkTx to TRPV1 was recently underscored by its utilization in two separate publications in a single issue of Nature (Erhu et al., 2013, Maofu et al., 2013), with DkTx playing an integral role in revealing the full crystal structure of TRPV1; which hitherto had been unachievable (Moiseenkova-Bell and Wensel, 2009).

The expression of soluble and functional ICK toxins is notoriously difficult (Kurokawa et al., 2001, Schmoldt et al., 2005, Sermadiras et al., 2013), considerably more so for a toxin such as DkTx which has two ICK motifs (Klint et al., 2013). DkTx contains 6 separate disulfide bonds, which could afford the theoretical formation of ~280,000 different disulfide bond isomers (Klint et al., 2013). Additionally, the generation of chimeric fusion proteins can have unpredictable effects on the functionality of the constituent protein domains. In anticipation of this, and supplementary to the generation of the LC.H_N.H_{CN}/A-DkTx chimera, it was deemed pertinent to additionally express recombinant DkTx without fusion to BoNT/A domains. This would expedite optimization of parameters for recombinant expression and purification of functional DkTx and, subsequently, enable evaluation of the consequence of additional polypeptide cargo on the biological activity of DkTx.

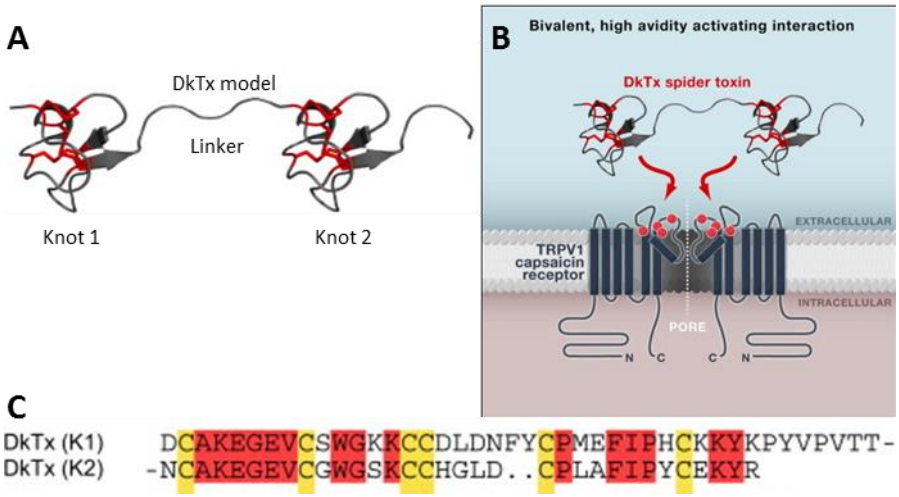

Figure 3. 1 DkTx structure and its interaction with TRPV1
(A) Representation of the structure of DkTx, showing the tandemly-repeated ICK motif (knot 1 and knot 2), separated by a linker (Julius, 2013). (**B)** Schematic showing the interaction of DkTx with the pore region of TRPV1; each knot is capable of binding a separate region within the channel. (**C)** Sequence alignment of the two knots of DkTx; yellow depicts cystine residues highly conserved in all ICKs while red shows residues which appear in both knots. Adapted from (Bohlen et al., 2010).

To ascertain the contribution of DkTx to the targeting of LC.H_N.H_{CN}/A-DkTx, an untargeted control protein was generated (LC.H_N.H_{CN}/A) and investigated in parallel. The presence of the H_{CN}/A sub-domain afforded an opportunity to investigate its contribution to neuronal binding. In light of interesting findings in this regards, a series of radio-ligand binding assays were performed with ^{125}I labelled native BoNT/A, BoNT/$A_{\Delta HCN}$ in which the H_{CN} was deleted, and BoNT/$A_{W985L,}$ containing a single point mutation in the H_{CN} sub-domain. The binding of these labelled BoNT/A derivatives to CGNs provided insight into the involvement of the H_{CN} sub-domain in both toxin binding and, significantly, internalization.

3.2 Results

3.2.1 Design and cloning of expression constructs encoding the first generation of chimeric fusion proteins

The inherent difficulty frequently encountered in the recombinant expression of functional disulfide bond containing proteins as mentioned above, emphasized that the initial cloning strategy was paramount for the successful expression of DkTx fusion proteins. To this end, the pET32b expression vector was selected, as insertion of recombinant genes into its multiple cloning site (MCS) produces in-frame fusion with

thioredoxin (Trx) tag. The Trx-tag is a 12 k cytoplasmic *E. coli* protein, widely utilized as a solubility enhancer when co-expressed as a fusion to recombinant proteins, especially with short peptides (Yasukawa et al., 1995). Trx tag also possesses intrinsic oxido-reductase activity which can promote the formation of disulfide bonds through thio-disulfide exchange (Young et al., 2012). As the Trx-tag does not exhibit any inherent affinity properties, the pET32b vector also confers fusion to both $(His)_6$ and S-Tag, enabling purification by immobilized metal affinity chromatography (IMAC) or antibody affinity chromatography, respectively.

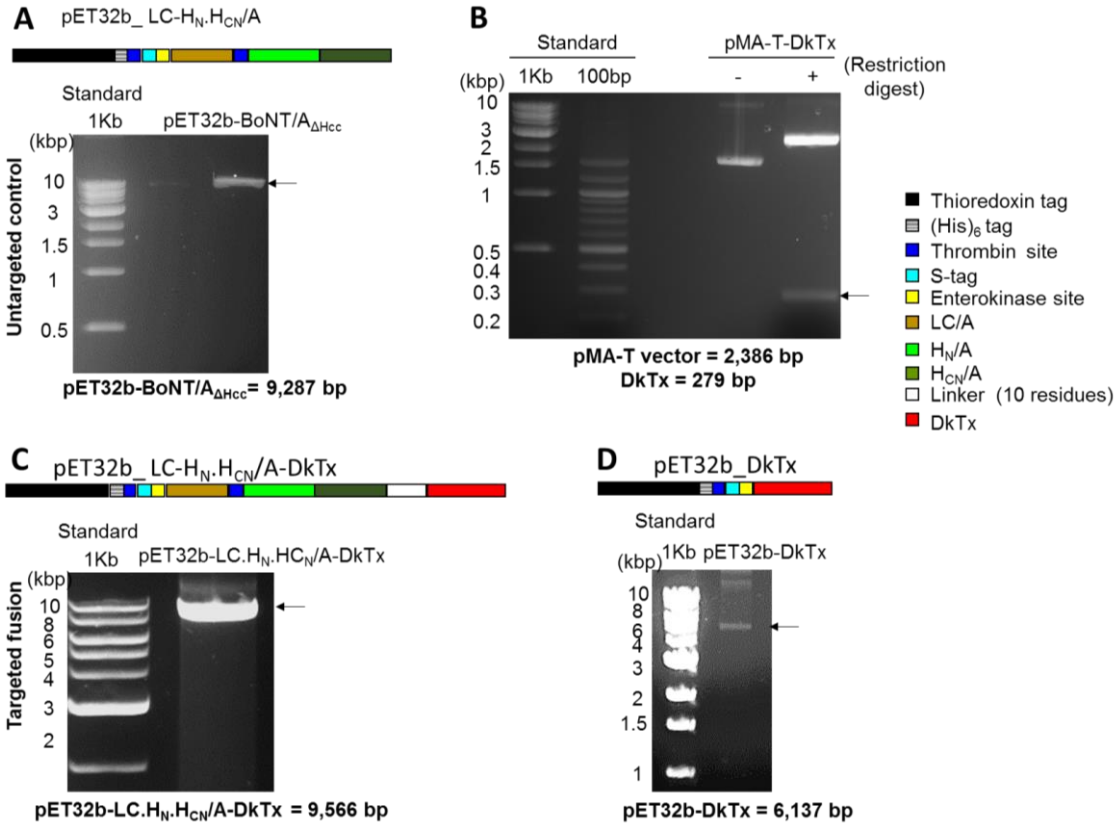

Figure 3. 2 Cloning of expression constructs encoding the first generation of fusion proteins
(A) Restriction digest of the depicted vector (SacI enzyme) was resolved by agarose gel electrophoresis and visualized by trans-UV. Arrow indicates the predicted plasmid size, as detailed below the gel. **B)** DNA for DkTx was commercially synthesized and provided in the pMA-T vector, that was subsequently restriction digested (SacI and XhoI enzymes), resolved by agarose gel electrophoresis and visualized by trans-UV. Arrow indicates the excised DkTx gene. (**C-D)** Performed as described in (**A**).

A construct containing a mutated version of BoNT/A, in which nucleotides encoding the acceptor binding sub-domain (H_{CC}/A) had been deleted, was provided by my co-supervisor Dr. Jiafu Wang. The resultant gene LC.H_N.H_{CN}/A was subcloned into the pET32b expression vector (Fig. 3.2 A), producing Trx-$(His)_6$-S-Tag-LC.H_N.H_{CN}/A to act as an untargeted control. In the next instance, the DNA for DkTx was synthesised, codon

optimised for bacterial expression and provided in the pMA-T vector (Fig. 3.2 B); such codon optimisation has been reported to support soluble and functional expression of non-prokaryotic proteins in bacterial expression systems (Burgess-Brown et al., 2008). The DkTx gene was subsequently subcloned either as a 3' fusion to LC.H_N.H_{CN}/A to encode Trx-$(His)_6$-S-Tag-LC.H_N.H_{CN}/A-DkTx (Fig. 3.2 C) or directly into the MCS of pET32b to encode Trx-$(His)_6$-S-Tag-DkTx (Fig. 3.2 D).

3.2.2 Recombinant expression and IMAC purification of the first generation of fusion proteins

In addition to the critical nature of the DkTx construct design, the selection of an appropriate bacterial expression system was of equivalent significance. The standard *E. coli* expression strains possess a reductive cytoplasm adversative to disulfide bond formation (Kong and Guo, 2014). The Origami B™ *E. coli* strain contains mutations in both the thioredoxin reductase (trxB) and glutathione reductase (gor) genes (Seras-Franzoso et al., 2012), creating an oxidizing cytoplasmic environment more conducive to disulfide bond formation. Hence, this has been widely affirmed to enhance functional expression of disulfide bond containing proteins (Berkmen, 2012). The Origami B™ strain is known to be particularly successful in the expression of disulfide containing protein when used in conjunction with the pET32b expression vector (Stewart et al., 1998). Thus, the combination of both the pET32b vector and the Origami B™ expression strain increased the probability of obtaining soluble and functional DkTx fusion proteins.

Trx-$(His)_6$-S-Tag-LC.H_N.H_{CN}/A-DkTx and Trx-S-Tag-$(His)_6$-DkTx were expressed in *E. coli* by auto-induction and purified from the resultant lysates by IMAC. Subsequent analysis of the respective purifications was performed by SDS-PAGE followed by Coomassie staining which visualized predominant bands at the predicted respective M_r of 145 k and 27 k (Fig. 3.3 A and B), as determined by a semi-log plot. The untargeted control protein, Trx-$(His)_6$-S-Tag-LC.H_N.H_{CN}/A, was expressed and purified independently by Dr. Matthew King.

The design of the first generation fusion proteins was such that successive cleavage with thrombin and enterokinase proteases was expected to remove the Trx-$(His)_6$ and S-Tags, respectively. The enterokinase cleavage of Trx-$(His)_6$-S-Tag-LC.H_N.H_{CN}/A-DkTx proved ineffective, failing to produce the expected size shift on SDS-PAGE, and resulted in the degradation of the protein, evident by the appearance of multiple protein bands at

higher concentrations of enterokinase (Fig. 3.3 C, left panel). Thrombin cleavage proved efficient in removing the N-terminal Trx tag (Fig. 3.3 C, right panel), and simultaneously cleaved the protease site between LC/A and H_N/A, converting the single-chain purified protein to disulfide bond linked di-chain (Fig. 3.3 D). Although the S-Tag was retained in the purified proteins due to the inefficiency of the requisite enterokinase cleavage, as it was not utilized for any further purpose and to simplify descriptions, the tag is omitted from future protein names.

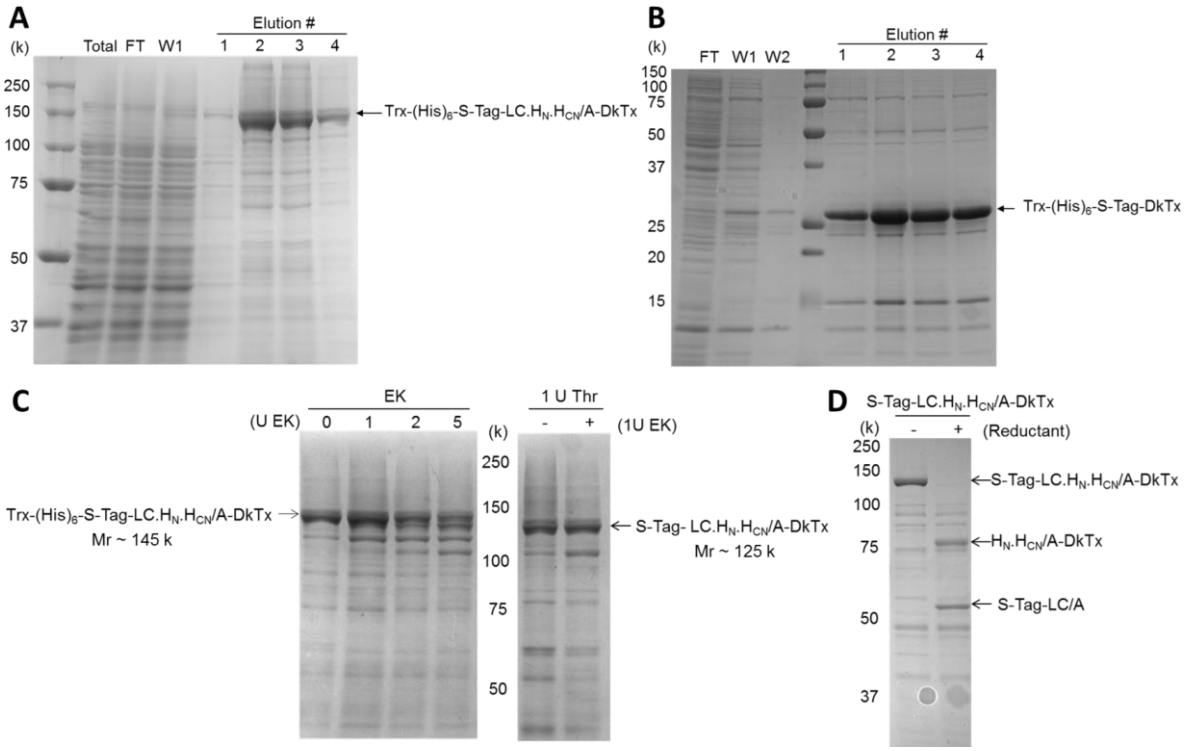

Figure 3. 3 Recombinant expression and IMAC purification of the first generation of fusion proteins

(A) SDS-PAGE followed by Coomassie staining confirmed the expression and IMAC purification of Trx-$(His)_6$-S-Tag-LC.H_N.H_{CN}/A-DkTx at the predicted M_r of 145 k. (**B)** SDS-PAGE followed by Coomassie staining, demonstrated the expression and IMAC purification of Trx-$(His)_6$-S-Tag-DkTx at the predicted M_r of 27 k. (**C)** Coomassie stained SDS-PAGE of Trx-$(His)_6$-S-Tag-LC.H_N.H_{CN}/A-DkT treated with either enterokinase (EK) or thrombin (Thr) proteases. Treatment with enterokinase resulted in degradation of the protein (left panel), while thrombin cleavage produced a 20 k size shift corresponding to Trx-$(His)_6$ removal (right panel). (**D)** Thrombin treated S-Tag-LC.H_N.H_{CN}/A-DkTx was resolved on SDS-PAGE in non-reducing and reducing conditions (+2.5% ßME) and subjected to Coomassie staining.

3.2.3 SNARE protease activities of both LC.H_N.H_{CN}/A-DkTx and the untargeted control were comparable to that of wild-type BoNT/A

The protease activity of both LC.H_N.H_{CN}/A and LC.H_N.H_{CN}/A-DkTx was assessed by an established *in vitro* protease cleavage assay (Wang et al., 2012), confirming the successful conversion of both proteins to di-chain following thrombin cleavage. The protease

activities of the respective proteins were shown to be comparable, and corresponded to the cleavage efficiency of native BoNT/A (Fig. 3.4). This provided confirmation that neither the genetic manipulation of the BoNT/A domains, retention of the S-Tag nor the inclusion of a DkTx fusion impacted upon the LC/A protease.

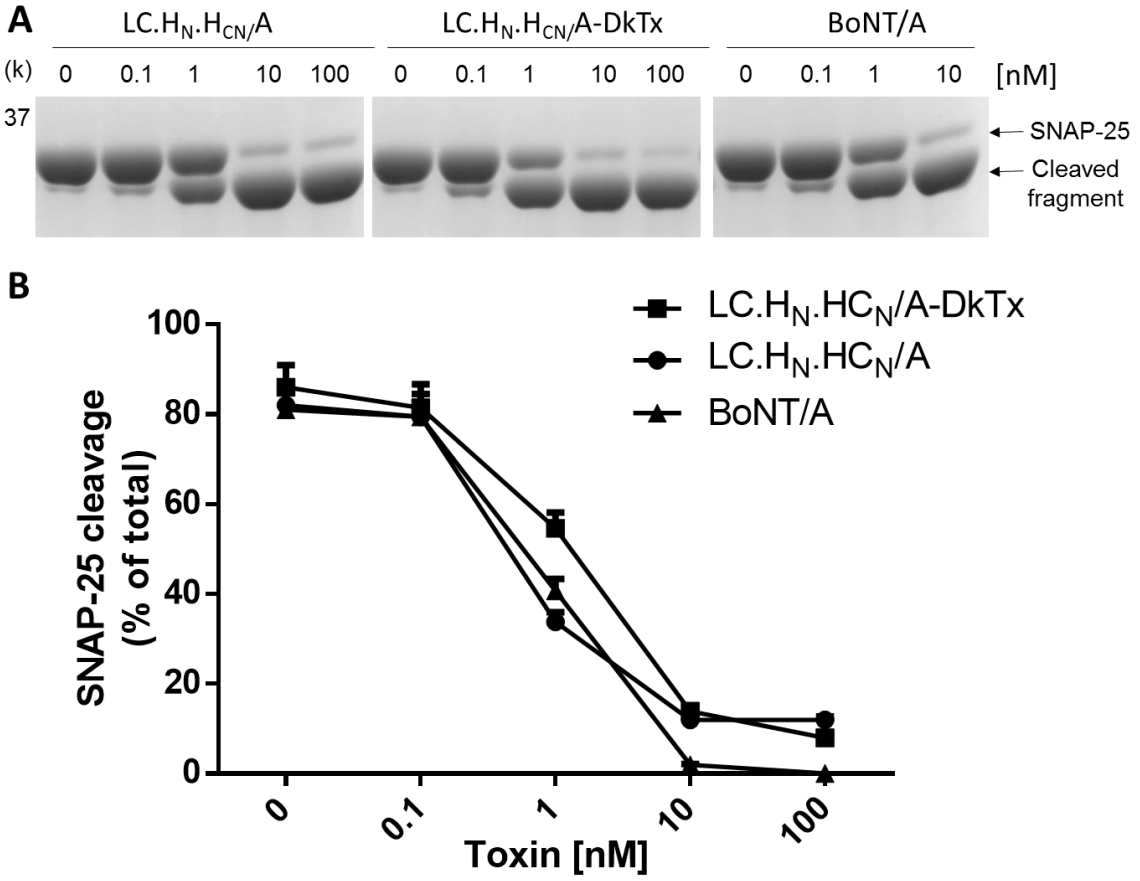

Figure 3. 4 *In vitro* cleavage of a recombinant SNAP-25 fragment substrate by LC.H$_N$.H$_{CN}$/A-DkTx, the untargeted control or recombinant wild-type BoNT/A

(A). *In-vitro* SNAP-25 cleavage assay was performed with 0.1 – 100 nM LC.H$_N$.H$_{CN}$/A or LC.H$_N$.H$_{CN}$/A-DkTx, and 0.1 – 10 nM BoNT/A. Cleavage of the SNAP-25 fragment substrate was visualized by Coomassie staining of SDS-PAGE. (**B**) Densitometric analysis of data from (**A**) performed with ImageJ software to determine percentage of SNAP-25 cleaved at each respective concentration, Data plotted are means ± S.E.M; n=3.

3.2.4 Endogenous and exogenous expression of TRPV1 and SNAP-25 in cultured cell lines

Functional characterization of DkTx, and the subsequent assessment of its ability to mediate delivery of the LC protease into cells, required co-expression of both the TRPV1 target and the SNAP-25 substrate. Rat TGN and dorsal root ganglion (DRG) primary neurons express TRPV1 and SNAP-25 (Winter, 2005, Meng et al., 2016). However, the valuable and finite supply of rats from which to harvest these neurons, coupled with

difficulties with both dissection and culturing encouraged the screening for TRPV1 and SNAP-25 expression in available HEK-293, F11 and SH-SY5Y cell lines (Fig. 3.5 A).

The F11 cell line was of particular interest, as these are derived from DRG and reported to express TRPV1 (Goswami et al., 2010). However, following immuno-blotting of the cell lysates with antibodies against either TRPV1 or SNAP-25, no endogenous expression of TRPV1 could be detected, although SNAP-25 could be readily seen in both F11 and SH-SY5Y cell lysates (Fig. 3.5 A). As the initial focus was establishing the functionality of DkTx, and no cell line endogenously expressed TRPV1, mammalian expression vectors were constructed to facilitate its exogenous expression by transient transfection. To this end only HEK-293 cells were found to be capable of expressing TRPV1 following transfection; TRPV1 could not be detected in the other cell lines (Fig. 3.5 A). HEK-293 cells were found to produce functional TRPV1 channels, sufficient to facilitate assessment of the biological activity of the DkTx fusion (see 3.2.5).

However, TRPV1 expression in HEK-293 cells corresponded with morphological changes, reduced cell proliferation and an overall reduction in cell viability when compared to untransfected controls; this prevented the development of a cell line stably expressing TRPV1. The cytotoxicity of TRPV1 expression was hypothesised to be due to increased entry of Ca^{2+} into cells, in keeping with previous observations (Thomas et al., 2007). The subcloning of TRPV1 into pIRES2-GFP and pIRES2-dsRED expression vectors, in addition to conferring the respective co-expression of either green-fluorescent protein (GFP) or red-fluorescent protein (RFP) reporters to aid selection of TRPV1 positive cells, reduced the overall level of TRPV1 expression (Fig. 3.5B). Consequently, this appeared to increase the tolerance of HEK-293 cells to TRPV1 expression; however, attempts at developing a stable cell line still proved unsuccessful, as no cells survived the selection process. The cell-surface localization of TRPV1 in HEK-293 cells transfected with pIRES2-GFP-TRPV1 was confirmed by ICC staining of non-permeabilized cells; imaged by Z-stack confocal microscopy (Fig. 3.5 C).

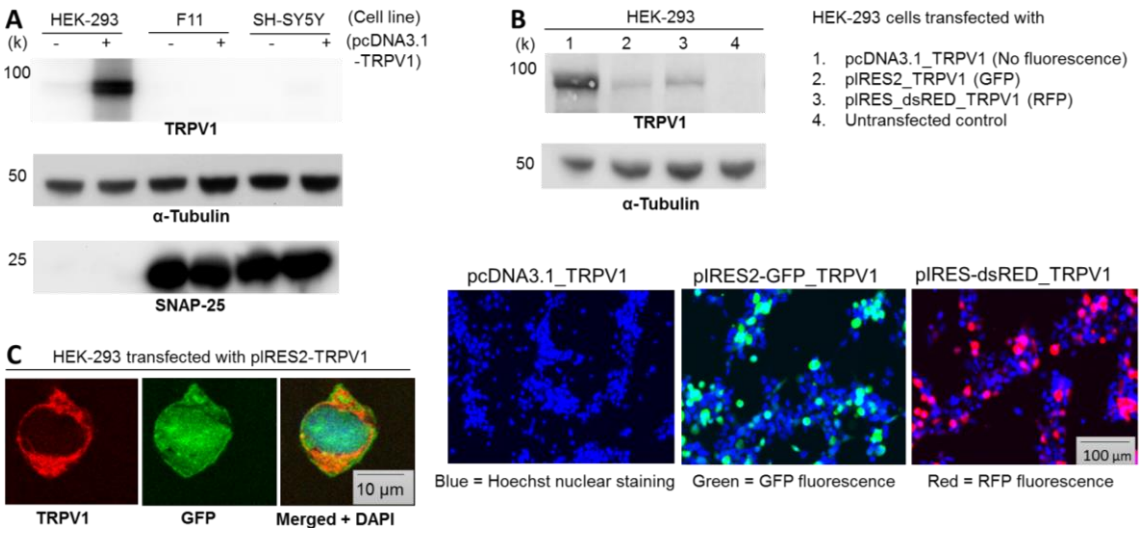

Figure 3. 5 Analysis of endogenous and exogenous TRPV1 expression in cultured cell lines
(A) HEK-293, F11 or SH-SY5Y cells were either untreated, or transfected with pcDNA3.1_TRPV1 and subjected to Western-blotting with antibodies against TRPV1 and SNAP-25, with α-Tubulin serving as a loading control. (**B)** HEK-293 cells were transiently transfected with one of the three indicated expression vectors, lysed and subjected to Western-blotting with antibodies against TRPV1 or α-Tubulin. Fluorescence microscopy was performed prior to lysis to visualize GFP and RFP reporters, with Hoechst stain used to produce nuclear staining. (**C)** HEK-293 cells were transfected with pIRES2-GFP-TRPV1 and subjected to ICC using an anti-TRPV1 antibody, followed by a second antibody conjugated Alexa Fluor® 590 fluorescent probe, subsequently imaged by Z-stack confocal microscopy.

3.2.5 Recombinantly-expressed Trx-$(His)_6$-DkTx is biologically active

The retargeting of LC.H_N.H_{CN}/A-DkTx to TRPV1 expressing cells could only be achieved if DkTx is functionally active. In order to establish if the pET32b vector/Origami B™ *E. coli* combination was capable of producing biologically active DkTx, a series of functional assays were performed using Trx-$(His)_6$-DkTx. This protein was selected over LC.H_N.H_{CN}/A-DkTx as its smaller mass facilitated production of greater protein yields, more conducive to the micro molar concentrations required for DkTx functional assays (Bohlen et al., 2010). The Trx and $(His)_6$ tags were not removed due to problems with the protease cleavage as previously detailed (Fig. 3.3 C). Moreover, the preservation of the protein tags on DkTx was hypothesised to be advantageous, as it would demonstrate that the protein was capable of interacting with TRPV1 despite an encumbered N-terminus and would, thus, be representative of the LC.H_N.H_{CN}/A-DkTx fusion.

The retention of the $(His)_6$ tag also presented further opportunity, as in the absence of an antibody specific for DkTx, an anti-$(His)_6$ antibody could be used for detection of Trx-$(His)_6$-DkTx. The binding of the latter to either wild-type HEK-293 cells or those

transiently-expressing TRPV1 was evaluated by ICC staining using antibodies against either TRPV1 or $(His)_6$. The co-localization of $(His)_6$ and TRPV1 specific signals confirmed successful and selective association of Trx-$(His)_6$-DkTx with TRPV1 expressing cells (Fig. 3.6 A).

With the binding of DkTx to TRPV1-positive cells established, the next step was to determine if it was capable of activating the channel. To this end, voltage-clamp recordings were performed on HEK-293 transfected with pIRES2-GFP-TRPV1 (Fig. 3.6 B). The presence of a functional TRPV1 channel in GFP-positive cells was confirmed by exposure to 1 µM capsaicin as previously published (Neelands et al., 2005); following washout of capsaicin, the current amplitude was returned to baseline. The cells were subsequently exposed to 1.3 µM of Trx-$(His)_6$-DkTx; this produced an inward current comparable to that of capsaicin but which was still present after washing, demonstrating the irreversible binding of DkTx to the channel (Bohlen et al., 2010).

TRPV1 is a non-selective cation channel but has a high propensity for Ca^{2+}. Hence, the detection of an increase in intracellular Ca^{2+} levels is a well-established functional assay for its activation (Tóth et al., 2004, Meng et al., 2016). HEK-293 cells expressing TRPV1 were loaded with Fluo-4-AM, a Ca^{2+} specific green fluorescent indicator, and baseline fluorescence was established. Following exposure to 1 µM capsaicin but not to the wash buffer, the fluorescence level was increased in a proportion of cells, surmised to be TRPV1 positive. Once the controls had been established, the experiment was repeated with 5 µM Trx-$(His)_6$-DkTx, using fresh cells, which responded with a comparable increase in fluorescence as that elicited by capsaicin (Fig. 3.6 C). A secondary effect was observed following treatment with either capsaicin or Trx-$(His)_6$-DkTx; the responsive cells underwent morphological changes and ultimately detached from the culture dish, corroborating previous observations that rapid TRPV1-mediated Ca^{2+} influx can induce cell death (Puntambekar et al., 2004, Thomas et al., 2007). The experiment was subsequently repeated with wild-type HEK-293 cells, with no cells responding to either capsaicin or Trx-$(His)_6$-DkTx (Fig. 3.6 D); confirming that the increase in intracellular Ca^{2+} levels was a specific response to TRPV1 activation.

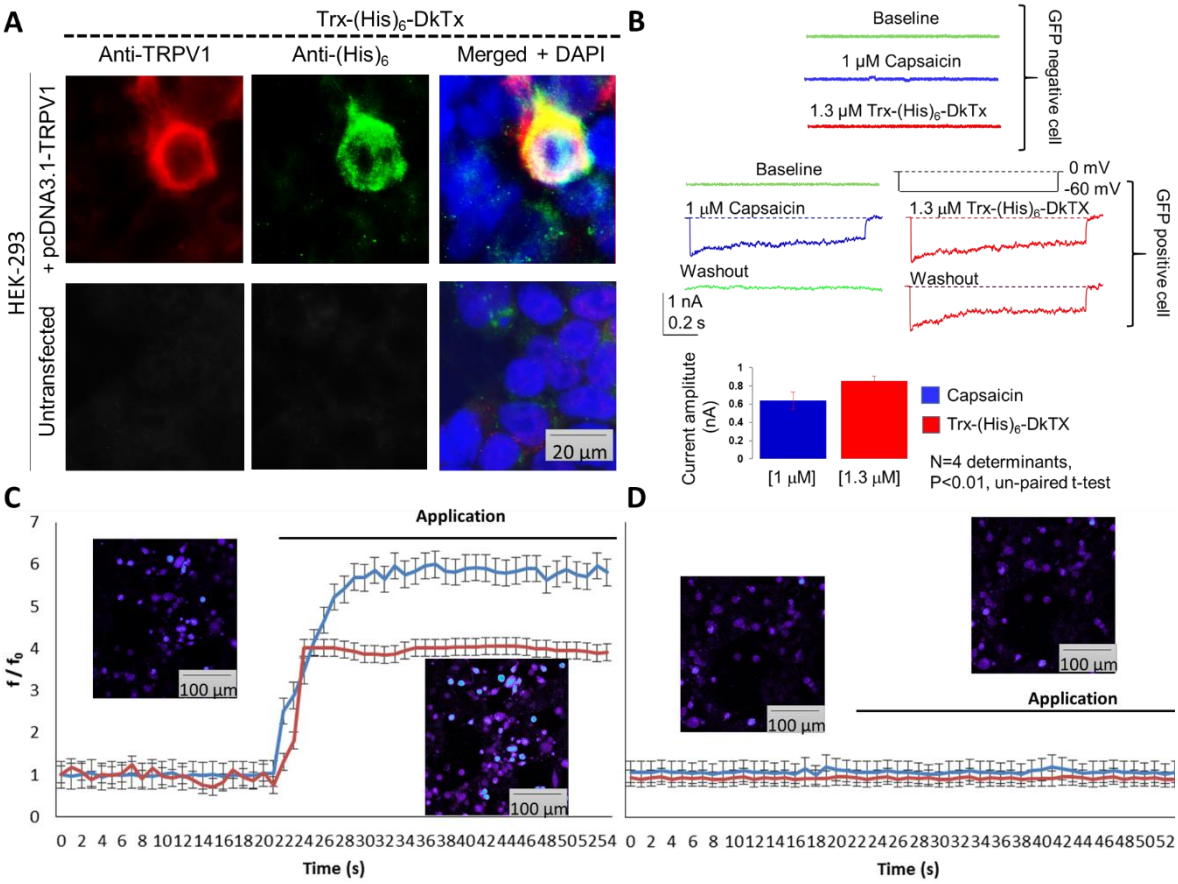

Figure 3. 6 Trx-(His)$_6$-DkTx binds and activates TRPV1 exogenously-expressed in HEK-293 cells
(A) HEK-293 cells either wild-type, or transfected with pcDNA3.1-TRPV1 were treated with 1 µM Trx-(His)$_6$-DkTx diluted directly into the culture medium, incubated for 5 minutes at 37°C, washed extensively and fixed by treatment with 4% formaldehyde solution. ICC staining was subsequently performed using antibodies specific for either (His)$_6$ or TRPV1 followed by secondary antibodies conjugated to either Alexa-Fluor® 488 or Alexa-Fluor® 590 fluorescent probes, nuclear staining by DAPI is shown in blue. Image chosen is representative (n=10). **(B)** HEK-293 cells transfected with pIRES2-GFP-TRPV1 were seeded onto coverslips, GFP positive cells presumed to be TRPV1-expressing were selected and patched. The perfusion of 1 µM capsaicin diluted in the extracellular solution induced an inward current, confirming the presence of functional TRPV1 channels, with currents returning to baseline following washout. Trx-(His)$_6$-DkTx was subsequently applied by perfusion to a final concentration of 1.3 µM and elicited an inward current, which persisted after washing. The current amplitude from responsive cells treated with either 1 µM capsaicin or 1.3µM Trx-(His)$_6$-DkTx (each N=4) was subjected to statistical analysis and compared by un-paired student t-test; $P < 0.01$. (**C)** HEK-293 cells transfected with pcDNA3.1-TRPV1 were loaded with Fluo-4-AM Ca^{2+} indicator and fluorescent signal measured following laser excitation at 488 nm was taken as baseline fluorescence (f_0). Subsequent washing with HBSS failed to provoke an increase in fluorescent signal, whereas application of either 1 µM capsaicin (blue line) or 5 µM Trx-(His)$_6$-DkTx (red line) diluted in the latter buffer produced rapid increases in intracellular fluorescence (f). Inset images are fluorescence signals prior to and after the application of Trx-(His)$_6$-DkTx. Values are the mean ± S.D.; n=8 from individual cells, normalized against baseline fluorescence. (**D)** Performed as in (**C**) using untransfected wild-type HEK-293 cells.

3.2.6 TRPV1 and SNAP-25 can be co-expressed in HEK-293 cells following transient co-transfection

The combination of pET32b and Origami B™ *E. coli* shown to competently produce functional DkTx sustained the supposition that DkTx might be adept at targeting LC.H_N.HC_N/A to TRPV1 expressing cells. However, assessment of LC.H_N.HC_N/A-DkTx retargeting required cellular co-expression of TRPV1 as the target of DkTx, and SNAP-25 as the substrate of LC/A to give a detectable readout. The lack of endogenous TRPV1 expression in available cell lines which expressed SNAP-25 presented a difficulty, further compounded by the inability to over-express TRPV1 in these same cells (Fig. 3.5 A). Significantly, the exogenous expression of SNAP-25 in HEK-293 cells had been previously employed as a means of evaluating delivery of biotinylated BoNT/A, targeted to avidin-conjugated low-density lipoprotein receptor (Yeh et al., 2011).

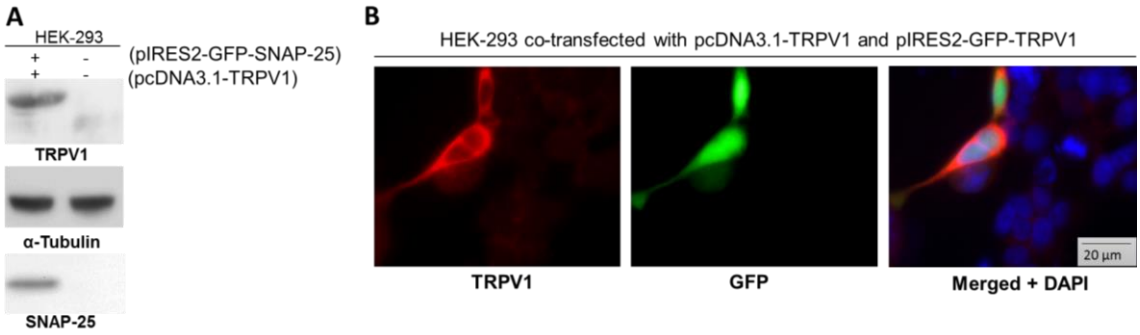

Figure 3. 7 Exogenous co-expression of both TRPV1 and SNAP-25 in HEK-293 cells following transient transfection

(A) HEK-293 cells transiently co-transfected with 1 µg of pcDNA3.1_TRPV1 and 0.25 µg of pIRES2-GFP-SNAP-25 combined in the same transfection reagent complex, were incubated for 48 hours. Cell lysates were prepared and subjected to Western-blotting with antibodies against TRPV1, α-Tubulin or SNAP-25. (**B)** HEK-293 cells were co-transfected as described in (**A**). ICC staining was performed using an anti-TRPV1 antibody with a secondary antibody conjugated to an Alexa-Fluor® 590 fluorescent probe used to detect binding, with subsequent image acquisition performed by fluorescence microscopy. GFP fluorescence was conferred by pIRES2-GFP-SNAP-25. Image chosen is representative (n=10).

This prompted the development of a novel system for the initial appraisal of LC.H_N.H_{CN}/A-DkTx targeting, in which both TRPV1 and SNAP-25 were co-expressed in HEK-293 cells by co-transfection with pcDNA3.1-TRPV1 and pIRES2-GFP-SNAP-25. Co-transfection of plasmids has been demonstrated to produce high efficiency co-expression in positively transfected cells, with low incidence of separate expression (Xie et al., 2011). The presence of both TRPV1 and SNAP-25 in HEK-293 cells was subsequently confirmed by Western-blotting (Fig. 3.7 A), and the co-expression of these proteins in positively-transfected cells was determined by a combination of ICC staining

and fluorescence microscopy (Fig. 3.7 B), with less than 10% of transfected cells demonstrating singular expression.

3.2.7 HEK-293 cells co-expressing TRPV1 and SNAP-25 are an ineffective system for the evaluation of DkTx-mediated delivery of the SNARE protease

HEK-293 cells co-expressing TRPV1 and SNAP-25 (see 3.2.6), were treated with 1-25 nM of either LC.H_N.H_{CN}/A-DkTx or untargeted control for 48 hours prior to lysis, with subsequent Western-blotting performed with anti-TRPV1 or anti-SNAP-25 antibodies. This analysis established that both TRPV1 and SNAP-25 are expressed, and confirmed the presence of SNAP-25 cleavage (Fig. 3.8 A). The levels of cleaved SNAP-25 were, however, comparable between both toxins at each concentration (Fig. 3.8 B).

The previously described compromise of HEK-293 cell viability being associated with TRPV1 expression was hypothesised to have rendered the cells more permeable to toxin, resulting in non-specific entry of both LC.H_N.H_{CN}/A and LC.H_N.H_{CN}/A-DkTx. In addition, the relative levels of both TRPV1 and SNAP-25 expression in individual cells could not be ascertained, with an inevitable differential existing between each cell (Xie et al., 2011). Further to this, as expression of both TRPV1 and SNAP-25 in HEK-293 cells is artificial, the cellular dynamics cannot be anticipated. The culmination of these deficiencies rendered the initial targeting results inconclusive.

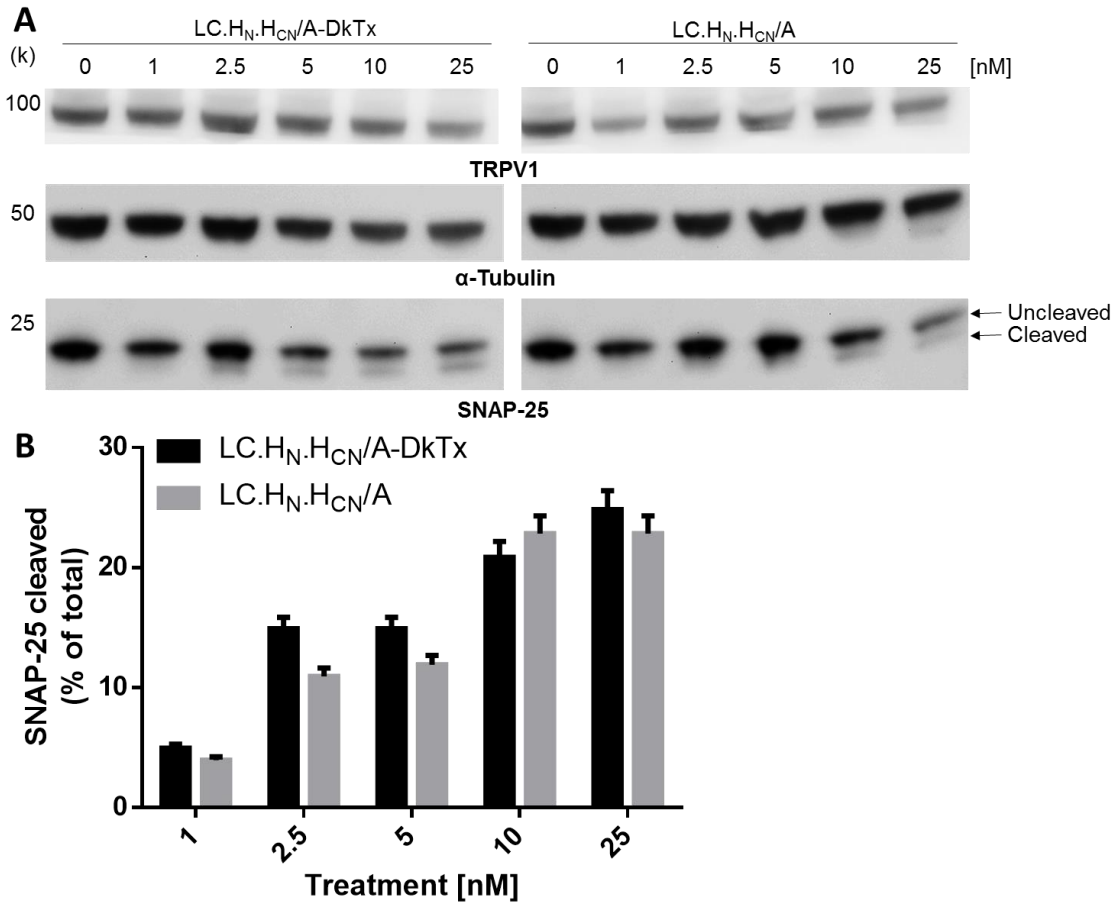

Figure 3. 8 SNAP-25 cleavage in HEK-293 cells co-expressing TRPV1 and SNAP-25 treated with LC.H_N.H_{CN}/A-DkTx or untargeted control

(A) HEK-293 cells, co-transfected with pcDNA3.1-TRPV1 and pIRES2-GFP-SNAP-25 were treated with LC.H_N.H_{CN}/A-DkTx or LC.H_N.H_{CN}/A for 48 hours prior to lysis. The lysates were then subjected to SDS-PAGE followed by Western-blotting with antibodies against TRPV1, α-Tubulin or SNAP-25. (**B)** Cleaved SNAP-25 as a percentage of total SNAP-25 was determined by densitometric analysis using ImageJ software. Data plotted are means ± S.E.M; n =3.

3.2.8 LC.H_N.H_{CN}/A binds and intoxicates TGNs comparable to LC.H_N.H_{CN}/A-DkTx but less efficiently than native BoNT/A

The inadequacy of HEK-293 cells co-expressing TRPV1 and SNAP-25, as a system for preliminary evaluation of LC.H_N.H_{CN}/A-DkTx targeting, compelled the immediate use of cultured neurons. TGNs were selected due to their expression of both TRPV1 and SNAP-25 (Meng et al., 2016). In addition, they represent an established model for sensory neurons with a well-defined physiological role in pain sensation (Durham et al., 2004), which have previously been employed for the development of BoNT/A-based anti-hyperalgesics (Meng et al., 2007, Meng et al., 2009).

TGNs were harvested from neonatal rats and cultured as previously described (Malin et al., 2007) and subsequently treated with LC.H_N.H_{CN}/A-DkTx or LC.H_N.H_{CN}/A as

indicated, or 1 nM of wild-type BoNT/A (Fig. 3.9 A). The relative association of LC.H_N.H_{CN}/A-DkTx or LC.H_N.H_{CN}/A with TGNs was determined by Western-blotting using an anti-LC/A antibody, capable of detecting LC/A of both toxins at comparable levels at least at higher doses (300 and 100 nM). Additionally, there was no significant difference in SNAP-25 cleavage observed between either toxins at any concentration (Fig. 3.9 B), with ~20% cleavage observed in cells treated with 300 nM of either LC.H_N.H_{CN}/A-DkTx or LC.H_N.H_{CN}/A.

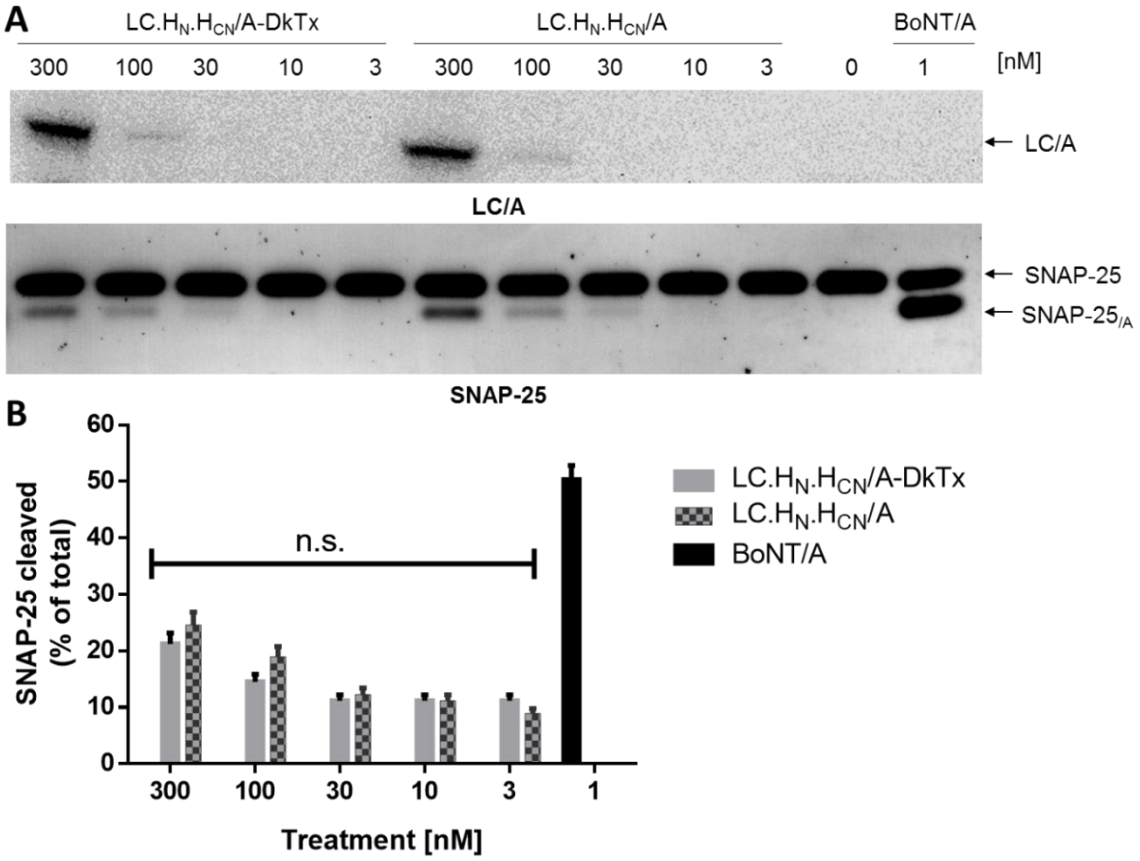

Figure 3. 9 SNAP-25 cleavage levels in TGNs following treatment with LC.H_N.H_{CN}/A-DkTx, untargeted control or wild-type BoNT/A

(A) TGNs treated with 300 – 3 nM of LC.H_N.H_{CN}/A-DkTx or LC.H_N.H_{CN}/A, or 1 nM of BoNT/A were incubated for 24 hours, prior to washing and preparation of cell lysates, which were subjected to Western-blotting using antibodies against LC/A or SNAP-25. (**B)** Cleaved SNAP-25 as a percentage of total was determined by densitometric analysis, using ImageJ software. Data plotted are means ± S.E.M; n=3 from independent experiments. Statistical analysis performed by unpaired student t-test; n.s. = not significant, $p>0.05$.

Treatment of TGNs with 1 nM of full-length BoNT/A, containing an intact receptor binding domain, produced ~50% cleavage of SNAP-25. This emphasised that neither LC.H_N.H_{CN}/A-DkTx nor LC.H_N.H_{CN}/A was capable of mediating efficient delivery of the protease relative to native BoNT/A. Interestingly, the ability of higher concentrations of

LC.H_N.H_{CN}/A to bind to TGNs and cleave SNAP-25, led to the supposition that the H_{CN}/A domain was potentially mediating low-affinity binding to the cell membrane, in keeping with previous observations (Muraro et al., 2009). This proposed interaction was postulated to be promoting pervasion of the untargeted control into cells and, thus, masking any low-efficiency targeting being conferred by DkTx.

3.2.9 Comparison of the binding of ^{125}I-labelled BoNT/A or BoNT/A$_{\Delta HCN}$ to cerebellar granular neurons

To ascertain the contribution of H_{CN}/A to the cellular interaction and intoxication of LC.H_N.H_{CN}/A, the nucleotides encoding the H_{CN} (residues I874-Q1091) were deleted from a previously described BoNT/A gene construct (Wang et al., 2011). The subsequent protein (rAΔH_{CN}), along with full-length BoNT/A (rA), were recombinantly expressed and purified by Dr. Jiafu Wang, who additionally performed the genetic deletion.

The rA and rAΔH_{CN} proteins were radiolabelled with ^{125}I to high-specific activity (~920 and ~840 Ci/mmol, respectively) by an established protocol, based on the chloramine-T method (Williams et al., 1983). The saturatable binding of ^{125}I-rA to rat cultured CGNs was investigated (Fig. 3.10 A) by incubation of cells with increasing concentrations, in both the presence and absence of 1 µM of an unlabelled single-chain mutant of protease-inactive BoNT/A (Wang et al., 2011). Scatchard analysis of the binding data confirmed that ^{125}I-rA binds to CGNs with high-affinity (K_D = 0.46 ± 0.03 nM) (Fig. 3.10 B). Additionally, unlabelled BoNT/A dose-dependently competed the binding of ^{125}I-rA with an IC_{50} ~ 9 nM. (Fig. 3.10 C). Significantly, measurement of the interaction of ^{125}I-rAΔH_{CN} with CGNs (Fig. 3.10 D), revealed no saturatable high-affinity binding. Thus, it can be deduced that the H_{CN} sub-domain contributes to the neuronal binding of BoNT/A.

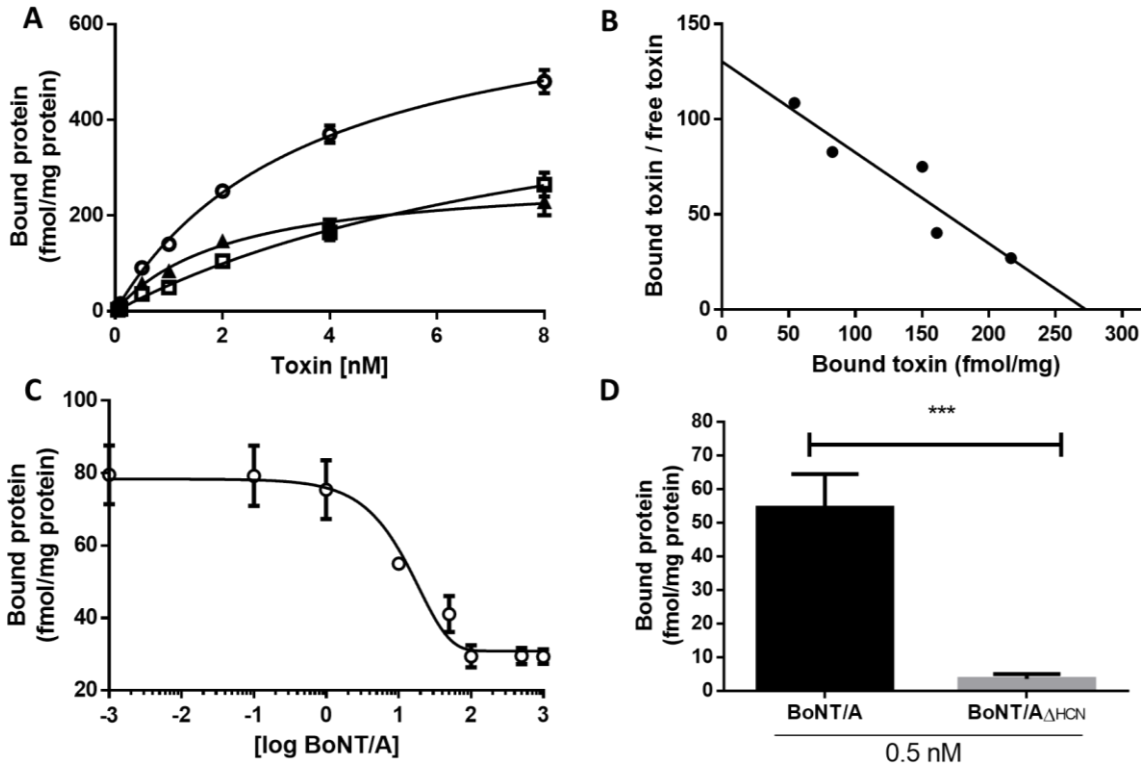

Figure 3. 10 Binding of ^{125}I-labelled BoNT/A or BoNT/AΔH_{CN} to CGNs
(A) CGNs were incubated with increasing concentrations of ^{125}I-rA alone (○) or in the presence of 1 µM unlabelled BoNT/A (□) for 1h at 4°C before three washes. The radioactive content of the pellet was measured using a γ counter. Subtracting non-saturatable binding (□) from the total binding (○) yielded the saturatable binding (Δ). Data are mean ± S.E.M from two independent experiments performed in duplicates. (**B)** Scatchard plot showing the saturatable binding of ^{125}I-rA to CGNs, K_D = 0.46 nM. (**C)** Binding of 1 nM ^{125}I-BoNT/A to CGNs in the presence of increasing concentrations of unlabelled BoNT/A was performed as in (**A**). (**D)** Binding of rAΔH_{CN} performed as in (**A**); deletion of H_{CN} from BoNT/A greatly reduced its binding to CGNs. Data plotted are means ± S.E.M from two independent experiments performed in duplicates. Statistical analysis carried out by unpaired student t-test, ***P < 0.001.

3.2.10 Tryptophan 985 in the H_{CN} of BoNT/A contributes to the delivery of the SNARE protease into cultured CGNs without influencing the initial binding

As a direct contribution of the H_{CN} to neuronal binding of BoNT/A was now established, it was pertinent to examine residues potentially involved. The crystal structure of a BoNT mosaic serotype C/D in complex with tetraethylene glycol (PG4) has been solved (Zhang et al., 2013). PG4 is a moiety typical of the hydrophobic fatty acid tails of phospholipids and, as such, has been taken to mimic the cell membrane. The aforementioned crystal structure enabled the identification of several residues of the H_{CN} which seemingly interact with PG4.

To investigate their functional role, 8 of the putative PG4 binding residues in H_{CN}/A were individually altered by site-directed mutagenesis, and the 8 resultant proteins

recombinantly expressed and purified. Their subsequent functional characterization identified one mutation (W985L), as having a direct role in neuronal intoxication, as the consequent protein (rA_{W985L}) exhibited a 10-fold decrease in intra-neuronal SNAP-25 cleavage compared to wild-type BoNT/A (Fig 3.11 A), without loss of LC protease activity (Fig. 3.11 B). This work was performed Dr. Jiafu Wang. In order to ascertain if rA_{W985L} exhibited reduced binding to neuronal cells, the protein was labelled with ^{125}I to a specific activity of ~740 Ci/mmol, and binding to CGNs performed as previously described. Significantly, ^{125}I- rA_{W985L} exhibited high-affinity (K_D = 0.47 ± 0.01 nM) saturatable binding (Fig. 3.11 C and D), nearly identical to that of native ^{125}I-rA (Fig. 3.10 B). Hence, the H_{CN}/A sub-domain is involved not only in initial binding, but also contributes to the productive internalization of BoNT/A.

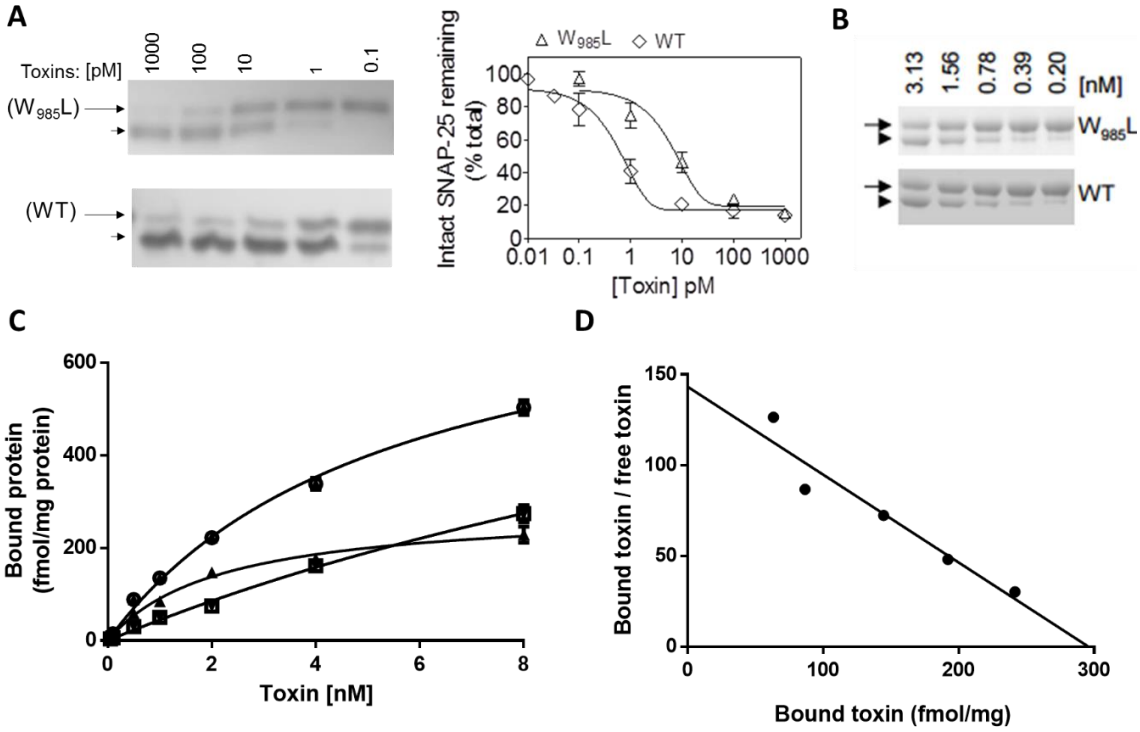

Figure 3. 11 Mutation of W985L in BoNT/A H_{CN} decreases cleavage of SNAP-25 in cultured CGNs without a reduction in initial cell binding

(A) CGNs treated with increasing concentrations of either rA or rA_{W985L} were cultured for 24 hours at 37°C prior to washing and preparation of cell lysates. These were subjected to SDS-PAGE followed by Western-blotting with an anti-SNAP-25 antibody. The arrow and arrowhead indicate intact and cleaved SNAP-25, respectively. Data plotted are mean ± S.E.M, n=3. (**B**) A representative Coomassie stained SDS-PAGE gel showing BoNT/A WT and $W_{985}L$ mutant have similar protease activities in cleaving GST-SNAP-$25C_{73}$-$(His)_6$ substrate. The arrow and arrowhead indicate intact and cleaved substrate, respectively. Experiments in (**A**) and (**B**) were carried out by Dr. Jiafu Wang. (**C**) Binding of ^{125}I-BoNT/A($W_{985}L$) to CGNs was performed as in Fig. 3.10 (**A**). Subtracting non-saturatable binding in the presence of 1 µM unlabelled rA($W_{985}L$) SC (○) from the total binding (□) yielded the saturatable binding (Δ). Data are mean ± S.E.M from two independent experiments performed in duplicates. (**D**) Scatchard plot showing the saturatable binding of ^{125}I-rA_{W985L} to CGNs, giving a K_D = 0.47 nM.

3.2.11 Cloning, bacterial expression and abortive purification of second generation fusion proteins

This confirmation that H_{CN}/A sub-domain directly contributes to both toxin binding and productive internalization, although a significant finding, was not of direct benefit to the targeting of LC.H_N.H_{CN}/A-DkTx to TRPV1. In an attempt to reduce the H_{CN}-mediated binding of the untargeted control, whilst simultaneously increasing the targeting capacity of DkTx and preserving H_{CN}-mediated internalization, an innovative approach was adopted. This involved development of a second generation of fusion constructs (Fig. 3.12 A). These constructs encoded the C-terminal receptor binding sub-domain of BoNT/B (H_{CC}/B), attached to the C-terminus of H_{CN}/A. The residues (K1192E, Q1200K) responsible for binding to the BoNT/B synaptotagmin II acceptor (Rummel et al., 2007), were mutated to generate a binding deficient-mutant domain (H_{CC}/B_{mut}). The receptor binding domain of BoNT/B was chosen on account of the critical residues for synaptotagmin II binding being published, with the comparable residues for BoNT/A SV2 binding not becoming available (Benoit et al., 2014, Strotmeier et al., 2014) till after this work. The cloning of these constructs is detailed in Fig. 3.12 B.

The rationale behind this approach was two-fold: firstly, the new untargeted control (LC.H_N.H_{CN}/A-H_{CC}/B_{mut}) would no longer have the H_{CN}/A domain free on the C-terminus which could, conceivably, have been promoting interaction with the cell membrane. Secondly, the H_{CC}/B_{mut} sub-domain should not be able to bind the synaptotagmin II protein receptor, but would still confer binding to GD1a and GT1b gangliosides (Atassi et al., 2014). It was hypothesised that this would enable the DkTx targeted toxin (LC.H_N.H_{CN}/A-H_{CC}/B_{mut}-DkTx) to more closely mirror the dual receptor binding strategy of native toxin (Berntsson et al., 2013) which, in tandem with the H_{CN}, could potentially increase the delivery of protease into TRPV1-expressing cells. The presence of H_{CC}/B_{mut} sub-domain would also confer ganglioside binding to the untargeted control, perceived as an opportunity to investigate the contribution of dual receptor binding to BoNT neuronal delivery when targeting to an exogenous protein receptor.

In addition, the cloning strategy was improved and simplified, with the constructs encoding the second generation fusion proteins redesigned to allow simultaneous single step removal of all protein tags, and concurrent di-chain formation following treatment with thrombin protease. The second fusions were expressed in Origami B *E. coli*, however

neither LC.H_N.H_{CN}/A-H_{CC}/B_{mut}-DkTx nor LC.H_N.H_{CN}/A-H_{CC}/B_{mut} could be purified from the resultant bacterial lysates (Fig. 3.12 C), despite several attempts at optimization.

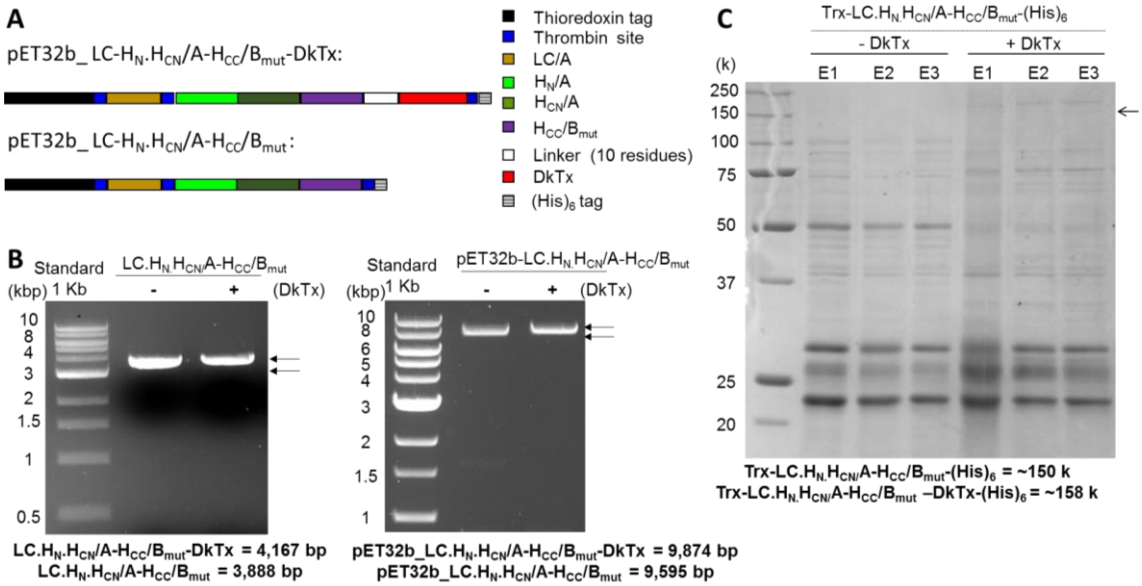

Figure 3. 12 Design, cloning of expression constructs and attempted purification of the second generation of fusion proteins

(A) Graphic depiction of the constructs designed for bacterial expression of a second generation of fusion proteins. (**B)** DNA sequences encoding either LC.H_N.H_{CN}/A-H_{CC}/B_{mut} or LC.H_N.H_{CN}/A-H_{CC}/B_{mut}-DkTx were amplified by PCR with appropriate 5' and 3' restriction sites to allow insertion into pET32b expression vector (left panel). The resultant pET32b vectors containing either of the inserted genes (right panel) were subjected to restriction enzyme digest (XhoI enzyme), resolved by agarose gel electrophoresis and visualized by trans-UV. Arrows indicate the predicted sizes as detailed below the gels. (**C)** Coomassie stained SDS-PAGE confirmed that neither LC.H_N.H_{CN}/A-H_{CC}/B_{mut}-$(His)_6$ nor LC.H_N.H_{CN}/A-H_{CC}/B_{mut}-DkTx-$(His)_6$ could be purified by IMAC following recombinant expression. E1, E2 and E3 correspond to IMAC eluted fractions; arrow indicates the approximate predicted molecular masses of the two proteins.

3.3 Discussion

The previously adopted methods for retargeting of BoNTs primarily involved chemical conjugation of pertinent targeting ligands to BoNT/A (Chaddock et al., 2000a, Chaddock et al., 2000b, Mustafa et al., 2013), a process which can be difficult to control and often produces heterogeneous products (Foster et al., 2006). The use of a fusion approach, as outlined in this Chapter, is fairly unique; the only previously published accounts of such a strategy involved targeting of BoNT/C (Foster et al., 2006) or BoNT/A (Fonfria et al., 2016) via fusion of epidermal-growth factor (EGF). The EGF protein however, unlike DkTx, is amenable to bacterial expression even as a fusion protein (Ishikawa et al., 2001, Abdull Razis et al., 2008).

This Chapter describes the first instance in which the soluble and functional bacterial cytoplasmic expression of DkTx has been achieved, with previous recombinant expression of DkTx entailing secretion to the *E. coli* periplasm (Klint et al., 2013) or resorting to oxidative refolding from inclusion bodies (Bohlen et al., 2010, Bae et al., 2012). Furthermore, this is the first successful functional expression of DkTx as a constituent of a fusion protein. The combination of pET32b vector in conjunction with the Origami B™ *E. coli* expression strain has, therefore, been validated as a system for generation of functionally-active disulfide bond stabilized targeting ligands. The successful expression and purification of soluble Trx-$(His)_6$-LC.H_N.H_{CN}/A-DkTx can also be achieved with this vector/expression strain combination.

The exogenous expression of TRPV1 in HEK-293 cells resulted in the surface expression of functional capsaicin-responsive channels, in accord with previous work (Erhu et al., 2013, Julius, 2013, Maofu et al., 2013). Although this system facilitated confirmation of Trx-$(His)_6$-DkTx biological activity, the co-expression of SNAP-25 in these same cells was ultimately inadequate as a means of assessing $(His)_6$-LC.H_N.H_{CN}/A-DkTx retargeting. This emphasised that evaluation of forthcoming retargeting strategies would have to be restricted to validated and established model systems. The subsequent finding that both LC.H_N.H_{CN}/A-DkTx and LC.H_N.H_{CN}/A produced comparable binding and equivalent SNAP-25 cleavage in cultured TGNs, implied that the H_{CN}/A of the untargeted control was capable of binding to the neuronal membrane. This was an obvious disadvantage in terms of DkTx-mediated retargeting but was, paradoxically, also fortuitous as it prompted further investigation of the contribution of the H_{CN} sub-domain to BoNT/A neuronal intoxication. The subsequent comparison of the binding of both rA and rAΔH_{CN} to CGNs, following their labelling with ^{125}I, confirmed that the H_{CN} performs an integral role in the initial binding of BoNT/A to neuronal cells. Furthermore, identification of W985 in H_{CN} being an important contributor to productive internalization represents a significant advance towards deciphering the membrane interactions which support neuronal delivery of BoNT/A.

The established contribution of the H_{CN}/A to neuronal binding was theorized to have promoted the binding of the untargeted control and, thus, to have negated detection of any DkTx-mediated targeting. Unfortunately, the subsequent attempt at mitigating binding of LC.H_N.H_{CN}/A to cells, by the innovative approach of creating a novel full-length LC.H_N.H_{CN}/A-H_{CC}/B_{mut} chimera, proved unsuccessful. The difficulty in purifying

the latter has previously been experienced in the expression of other BoNT chimeras (Wang et al., 2011, Wang et al., 2012), highlighting that despite their modular nature and general tolerance of genetic manipulation, certain combinations are destabilizing to the overall protein structure.

A significant limitation in the interpretation of DkTx-mediated targeting was the inability to confirm the biological activity of DkTx when expressed as a fusion to LC.H_N.H_{CN}/A, due to the µM concentrations required for the established DkTx functional assays (Bohlen et al., 2010). Significantly, this highlighted that despite the specificity and high-avidity binding of DkTx to TRPV1, its reported EC_{50} of 144 nM (Bohlen et al., 2010) was a concentration at which the untargeted control was shown to bind cells, and induce SNAP-25 cleavage. The aforementioned publications on BoNT/A retargeting had utilized targeting ligands of far higher affinity, exemplified by EGF possessing an EC_{50} of 2 nM (Neelam et al., 1998). The recognition and appreciation of the need for not only a specific but, also, a high-affinity targeting ligand underscored that DkTx was potentially inadequate for retargeting of BoNT/A.

The culmination of concerns and complications with the initial fusion strategy, fortuitously coincided with the publication of an innovative protein coupling technology, termed protein stapling (Ferrari et al., 2012). Protein stapling had proven successful in the coupling of a BoNT/A-based therapeutic to a diverse range of recombinant targeting peptides; these displayed limited abilities to deliver the LC/A protease into neuronal cell lines (Arsenault et al., 2013). This technology provided not only a potential solution to encountered difficulties, but also presented an opportunity to concurrently evaluate a published BoNT/A conjugation/retargeting strategy. This gainful combination prompted the immediate adoption of the approach, the implementation and successful application of which, is described in Chapter 4.

Chapter 4. Evaluation of a protein stapling strategy and its applicability to DkTx-mediated targeting of the BoNT/A core-therapeutic

4.1 Overview

The difficulty in assessing the adequate delivery of LC.H_N.H_{CN}/A-DkTx fusion into TGNs was postulated to be multi-faceted. An initial consideration was that the DkTx ligand was non-functional when fused to the BoNT/A domains, exasperated by the inability to confirm interaction of the fusion with TRPV1 due to the µM concentrations of DkTx required for functional analysis. Additionally, the established contribution of H_{CN}/A to neuronal binding and internalization was suggested to promote interaction of the untargeted LC.H_N.H_{CN}/A control with the TGN membrane which could mask any targeting being conferred by the DkTx targeted molecule. Consequently, the initial fusion strategy was considered ineffectual as a means of conjugating DkTx to BoNT/A, necessitating a new approach.

The use of an innovative conjugation technology termed 'protein stapling', based on the assembly of the neuronal SNARE complex, had proven successful as a means of coupling LC.H_N/A to a selection of neuropeptide and growth-factor targeting ligands and delivering the LC/A protease into neuroblastoma cell-lines, albeit to a limited extent (Arsenault et al., 2013). Protein stapling exploits the high-efficiency formation of SNARE complex, and involves the tagging of protein components with respective fragments of the SNARE complex constituents (SNAP-25, VAMP 2 and syntaxin); when combined, these assemble as a conjugated complex of extraordinary chemical and thermal stability. Application of 'stapling' to BoNT/A retargeting entailed the bacterial expression of LC.H_N/A fused to full-length SNAP-25 and pertinent ligands fused to VAMP $2_{(25\text{-}84)}$, with a peptide based on $\text{syntaxin}_{(201\text{-}245)}$ synthesised commercially (Fig. 4.1). The combination of these components in a molar ratio of 5:7:7, for 60 minutes at room temperature incorporated <90% of LC.H_N/A-SNAP-25 into a stapled SDS-resistant supra-molecular entity, which could only be disassociated following exposure to temperatures exceeding 95°C (Darios et al., 2010).

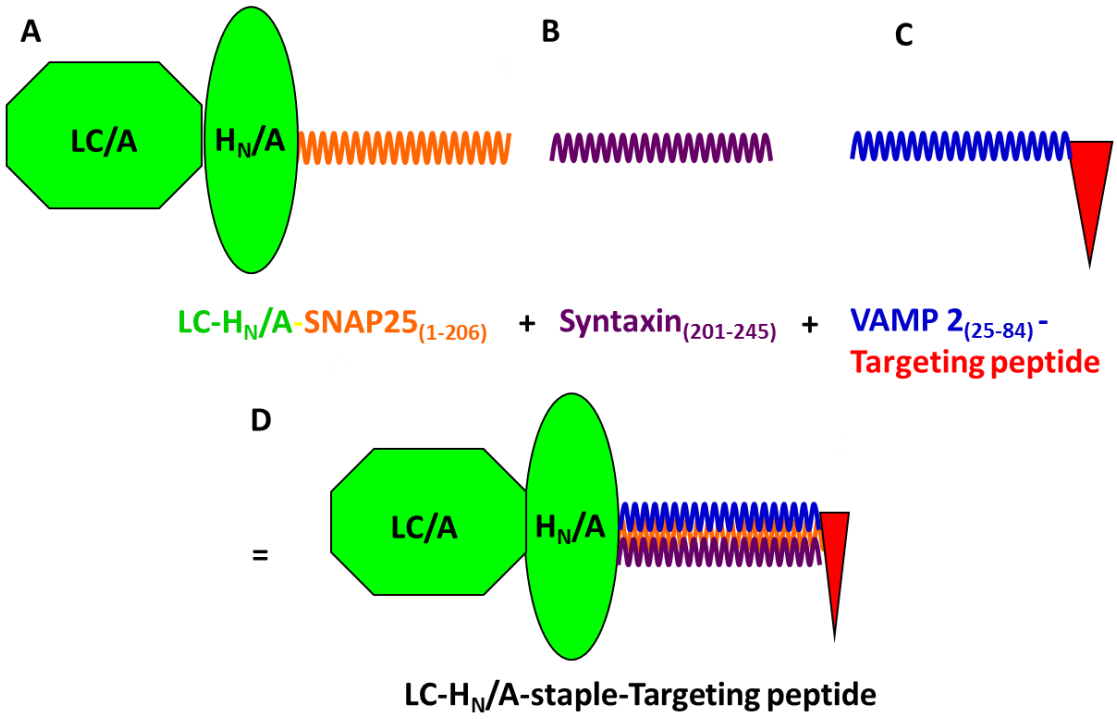

Figure 4. 1 Illustration of the protein stapling strategy
(A) LC.H_N/A genetically fused on its C terminus to full-length SNAP-25. **(B)** Synthetic peptide based upon syntaxin residues 201-245. **(C)** A targeting ligand genetically fused on either its N or C terminus to VAMP 2 fragment (residues 25-84). **(D)** Combining the three components produces a highly stable complex. Figure adapted from (Darios et al., 2010).

The conjugation of DkTx to LC.H_N/A by this strategy was perceived as affording multiple advantages. In the first instance, the independent expression of LC.H_N/A-SNAP-25 and VAMP 2-DkTx would enable the functional optimization and characterization of the two proteins prior to stapling. Significantly, the singular expression of VAMP 2-DkTx should enable the production of sufficient protein yields to facilitate confirmation of its interaction with TRPV1, prior to coupling to LC.H_N/A-SNAP-25. Furthermore, LC.H_N/A-SNAP-25 lacking any stapled ligand was considered an ideal untargeted control, particularly as the membrane binding H_{CN}/A sub-domain was omitted. Although the requirement of the H_{CN}/A for efficient neuronal delivery of native BoNT/A was confirmed (see Chapter 3), its inclusion in retargeted BoNT/A variants could potentially be a disadvantage, for reasons described above. On the other hand, the previous success of BoNT retargeting approaches which employed only the LC and H_N, implied that the entire H_C was dispensable when targeting via exogenous ligands.

The protein stapling strategy had been utilized for the successful conjugation of the core-therapeutic to a panel of 9 targeting ligands (Arsenault et al., 2013), in addition to the

reassembly of full-length BoNT/A from two SNARE-tagged components (Darios et al., 2010). This approach, therefore, permitted a more expeditious screening of ligands than would be achievable by protein fusion. Furthermore, the fusion strategy is hindered by the uni-directional nature of protein translation, obliging putative ligands to a constrained N-terminus, due to the requisite fusion to the C-terminus of H_N/A. The protein stapling technology however, affords flexibility, permitting either N terminal or C terminal tagging with VAMP 2 (Arsenault et al., 2013). A necessity to examine more ligands than DkTx was apparent, due to the latent risk of investing in a solitary targeting moiety.

In order to comprehensively evaluate protein stapling-mediated targeting, a proven ligand, VAMP 2-EGF, was generated in parallel with VAMP 2-DkTx. Treatment of neuroblastoma cells with 10 nM LC.H_N/A-stapled-EGF had been shown to produce a significant increase in SNAP-25 cleavage over that of the untargeted LC.H_N/A-SNAP-25 control (Arsenault et al., 2013). VAMP 2-EGF would, thus, serve as a positive control for both the stapling conjugation reaction and the subsequent cellular targeting. This should aid the accurate interpretation of VAMP 2-DkTx targeting results, while permitting a concurrent appraisal of the published findings.

4.2 Results

4.2.1 Cloning, expression and purification of Trx-$(His)_6$ tagged LC.H_N/A-SNAP-25 and VAMP 2-DkTx

The original publications (Darios et al., 2010, Ferrari et al., 2012, Arsenault et al., 2013, Ferrari et al., 2013) employed the pGEX-KG expression vector for all stapling constructs, with subsequent affinity purification of the recombinantly expressed components via the vector encoded GST. Due to my previous success attained with the pET32b vector, in particular the functional expression of a DkTx fusion, and in order to expedite construct generation by making use of available reagents, the stapling constructs were cloned into pET32b as detailed in Fig. 4.2 A. The cloning strategy was designed in conjunction with Dr. Matthew King, who additionally generated the pET32b-LC.H_N/A-SNAP-25 construct.

VAMP 2-DkTx DNA was generated by PCR amplification of the ligated genes encoding human VAMP $2_{(25-84)}$ and DkTx, with an intervening sequence encoding 27 alternating

glycine-serine residues. The linker length was adopted on the hypothesis that a relatively long intervening sequence between VAMP 2 and DkTx would confer greater flexibility, supporting the ability of both "knots" of DkTx to interact with TRPV1. Insertion of the resultant DNA followed by a $(His)_6$ purification tag into the pET32b vector created a 5' in-frame fusion with the advantageous Trx tag (detailed in Chapter 3) generating pET32b-Trx-$(His)_6$-VAMP 2-DkTx (Fig. 4.2 B).

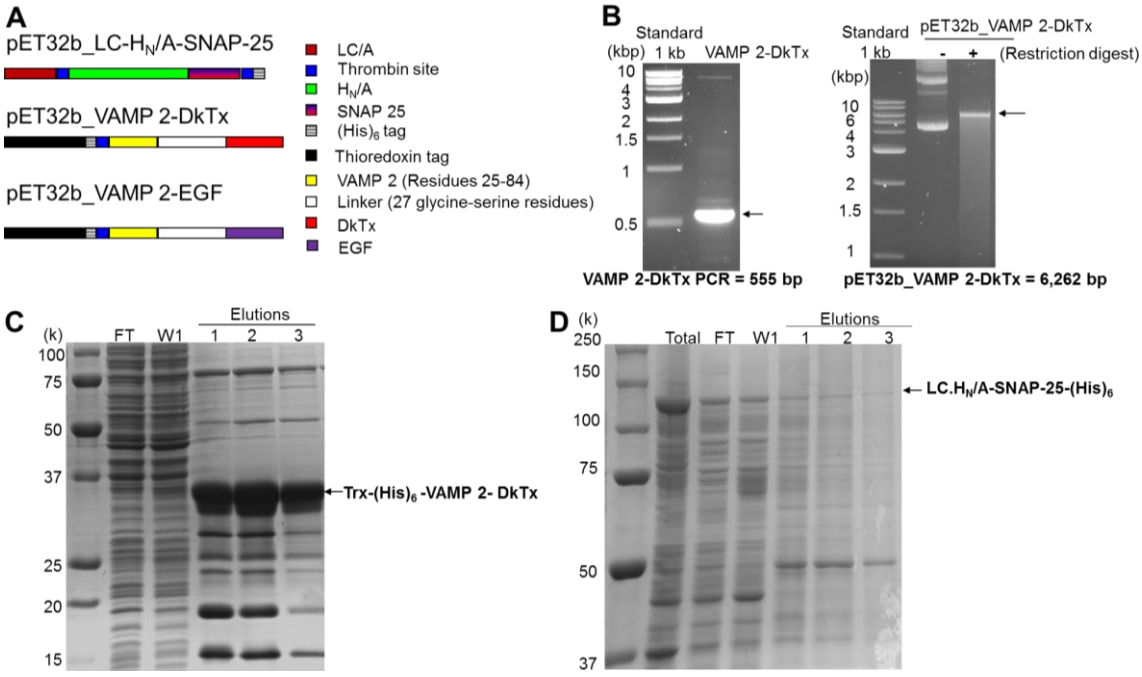

Figure 4. 2 Cloning, expression and purification of the first generation of stapling components
(A) Illustration of the first generation stapling constructs. **(B)** VAMP 2-DkTx gene was amplified by PCR to incorporate appropriate restriction enzyme sites for insertion into the pET32b vector. The resultant pET32b_VAMP 2-DkTx vector subjected to restriction digest (XhoI), resolved by agarose gel electrophoresis and visualized by trans-UV. Arrows indicates the predicted DNA sizes. (**C)** SDS-PAGE followed by Coomassie staining confirmed expression and IMAC purification of Trx-$(His)_6$-VAMP 2-DkTx at the predicted M_r of 35 k. Abbreviations: IMAC flow-through (FT); IMAC wash (W1). **(D)** SDS-PAGE followed by Coomassie staining revealed expression of $(His)_6$-LC.H$_N$/A_SNAP-25 at the expected M_r of 125 k, but the resultant protein could not be purified by IMAC.

Recombinant expression of both Trx-$(His)_6$-VAMP 2-DkTx and LC.H$_N$/A-SNAP-25-$(His)_6$ was performed in Origami B™ *E. coli* by auto-induction. IMAC purification of Trx-$(His)_6$-VAMP 2-DkTx gave yields of ~3 mg/L, as determined by BCA protein assay. The Coomassie staining of IMAC fractions subjected to SDS-PAGE detected a predominant protein band at the predicted M_r of 27k, as determined by semi-log plot (Fig. 4.2 C). In contrast, the IMAC purification of LC.H$_N$/A-SNAP-25-$(His)_6$ proved ineffectual, although Coomassie staining of SDS-PAGE gels detected a strong protein

band in the bacterial lysate, corresponding to the predicted M_r of 125 k (Fig. 4.2 D); the resultant protein being almost entirely insoluble, with the tiny soluble proportion failing to bind the IMAC resin.

4.2.2 GST-fusion tag increases the solubility of LC.H_N/A-SNAP-25 and facilitates its purification by affinity chromatography

The inability to express and purify soluble LC.H_N/A-SNAP-25-$(His)_6$ was jarringly analogous to issues formerly encountered with LC.H_N.H_{CN}/A.H_{CC}/B_{mut}. However, as soluble expression of LC.H_N/A-SNAP-25 had been achieved when fused with a GST purification tag (Ferrari et al., 2012), it was evident that the latter was functioning as an enhancer of solubility, in keeping with previous observations (Costa et al., 2014). This compelled an overhaul of the cloning strategy, with reversion to the established approach (Ferrari et al., 2013). LC.H_N/A-SNAP-25 DNA was amplified by PCR with appropriate restriction sites to permit insertion into the pGEX-KG expression vector. The induction of recombinant genes into the MCS of pGEX-KG generated an in-frame 5' fusion nucleotides encoding a 25 k GST purification tag, with an intervening thrombin protease cleavage site (Fig 4.3 A). The location of this protease site is particularly advantageous, as it facilitates thrombin-mediated release of recombinant proteins from GST following affinity purification, with the GST tag remaining immobilized on the glutathione affinity agarose.

The resultant protein, GST-LC.H_N/A-SNAP-25, was recombinantly expressed in BL21 (DE3) *E. coli* by IPTG induction, following which the clarified bacterial lysate was incubated with affinity resin. Analysis by Coomassie staining of SDS-PAGE gels indicated significant binding of GST-LC.H_N/A-SNAP-25 to the resin, validating the contribution of GST to increased solubility (Fig. 4.3 B). The subsequent incubation with thrombin protease released LC.H_N/A-SNAP-25 from the agarose associated GST tag, resulting in the predicted 25 k decrease in molecular mass (Fig. 4.3 B). In addition, treatment with thrombin simultaneously cleaved at the internal protease site between the LC/A and H_N/A, converting the protein from single-chain into di-chain isoform (Fig. 4.3 B), with a protein yield of ~1 mg/L determined by BCA protein assay. Utilization of the pGEX-KG expression vector for expression of LC.H_N/A-SNAP-25 was, therefore, a significant advancement on the previously employed strategy, enhancing the soluble

expression and providing a single-step approach to liberate the protein from the associated purification tag, as well as to convert it to the di-chain form.

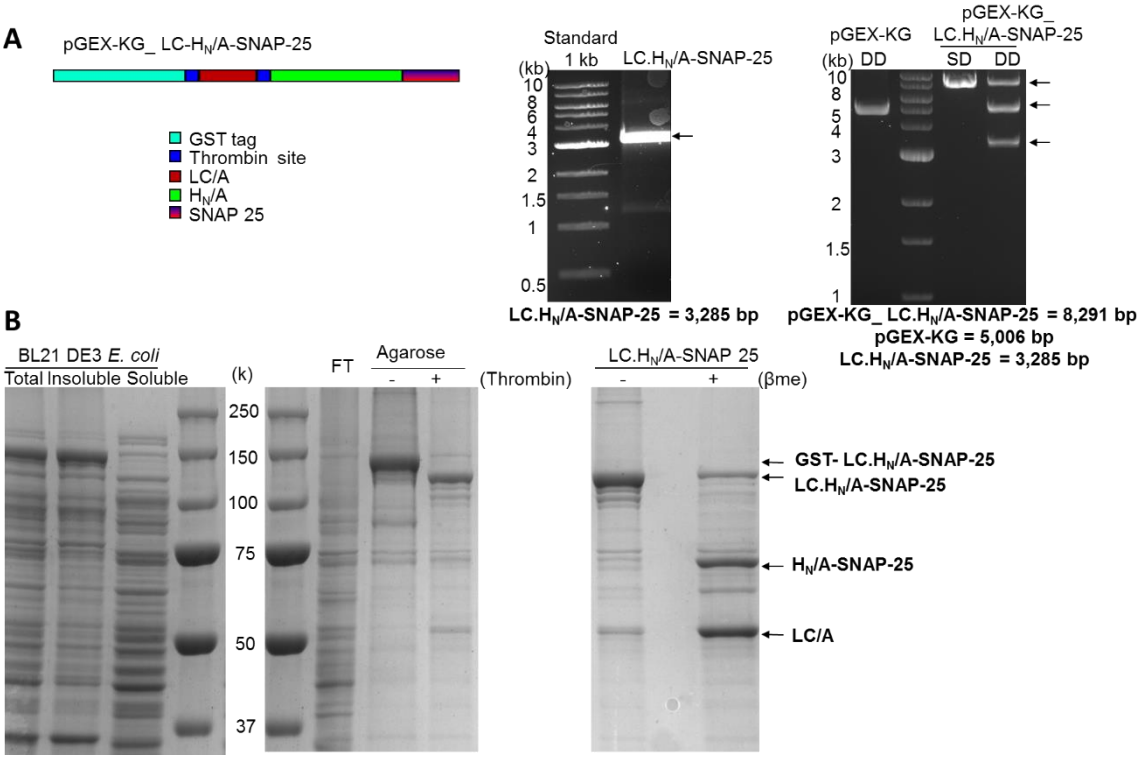

Figure 4. 3 Design, cloning and purification of second generation of LC.H$_N$/A-SNAP-25
(A) LC.H$_N$/A-SNAP-25 gene was generated by PCR amplification with appropriate restriction enzyme sites for insertion into pGEX-KG vector (left panel). The resultant pGEX-KG-LC.H$_N$/A-SNAP-25 vector (right panel) was subjected to restriction enzyme single digest with XhoI (SD) or double digest with XmaI and XhoI (DD), resolved by agarose gel electrophoresis and visualized by trans-UV. Arrows indicated the predicted DNA sizes, as detailed below the gels. **(B)** SDS-PAGE followed by Coomassie staining, confirmed expression and affinity purification of GST-LC.H$_N$/A-SNAP-25; subsequent treatment with thrombin protease released di-chain LC.H$_N$/A-SNAP-25. The addition of ßME (2.5%) to a purified sample disassociated the disulfide linked LC and HC fragments.

4.2.3 SNARE-protease efficiency of LC.H$_N$/A-SNAP-25 is comparable to that of wild-type recombinant BoNT/A

The protease activity of LC.H$_N$/A-SNAP-25 was assessed by a standard *in vitro* protease cleavage assay (Wang et al., 2012) and shown to correspond to the level of cleavage efficiency by wild-type BoNT/A (Fig. 4.4 A and B). This established that neither the presence of GST adjacent to LC/A prior to removal by thrombin cleavage nor the retention of the C-terminal fusion of SNAP-25 impeded the folding or activity of LC/A. Furthermore, the thrombin mediated conversion of LC.H$_N$/A-SNAP-25 to active di-chain was confirmed.

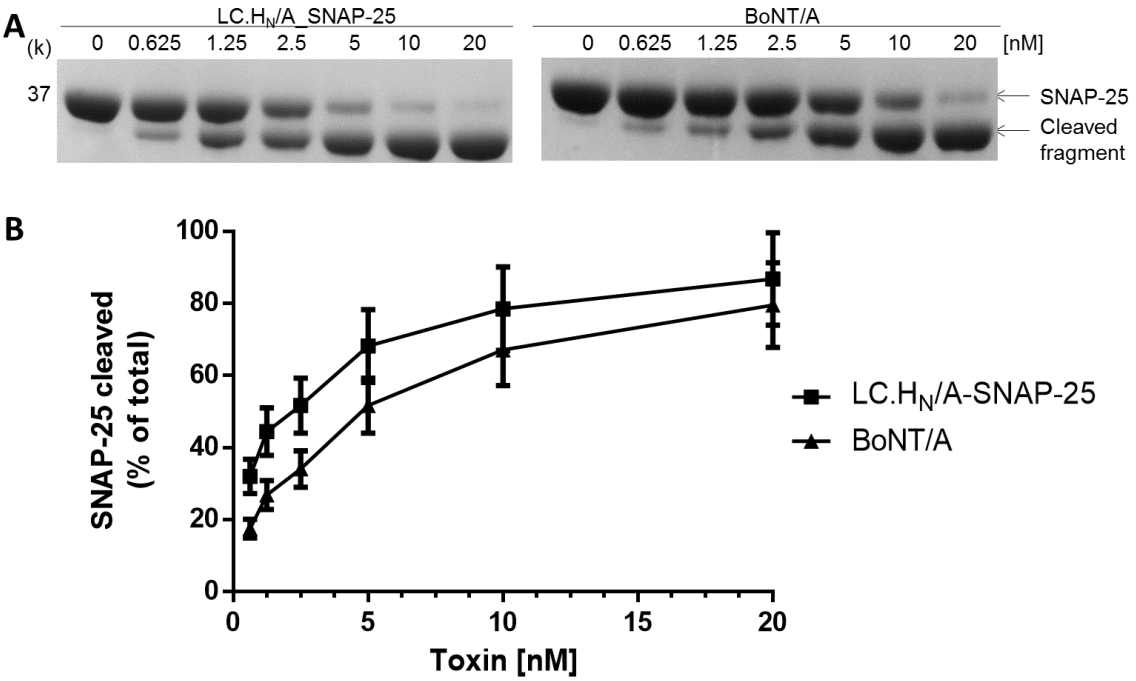

Figure 4. 4 *In vitro* cleavage of recombinant SNAP-25 fragment substrate by LC.H$_N$/A-SNAP-25 or full-length BoNT/A

(A) GFP-SNAP-25$_{(134-206)}$ incubated with the indicated concentration of LC.H$_N$/A-SNAP-25 or BoNT/A, was subjected to SDS-PAGE followed by Coomassie staining. (**B)** Densitometric analysis data from (**A**) performed with ImageJ software to determine % cleavage at each concentration. Data plotted are means ± S.E.M; n=3.

4.2.4 Trx-(His)$_6$-VAMP 2-DkTx undergoes rapid degradation at room temperature

IMAC purification of Trx-(His)$_6$-VAMP 2-DkTx, although producing a high yield, was deemed of inadequate purity for any downstream stapling reaction, as a significant number of co-purified unidentified protein bands were detected (Fig. 4.2 C). A devised solution of performing ion-exchange chromatography to increase the purity of the sample could not be undertaken, as it materialized that following purification Trx-(His)$_6$-VAMP 2-DkTx was highly unstable at room temperature, with the protein rapidly degrading (Fig. 4.5 A).

A review of the literature implicated the adopted 27 residue linker as the instigator of Trx-(His)$_6$-VAMP 2-DkTx degradation, as overly-long linker sequences have been previously demonstrated to induce protein instability (Prescott et al., 1999). To address this the linker sequence was shortened to 10 residues, with the resultant protein expressed and purified as previously described. This significantly increased the temperature tolerance and stability of Trx-(His)$_6$-VAMP 2-DkTx but, ultimately, failed to entirely stabilize the protein (Fig. 4.5 A and B).

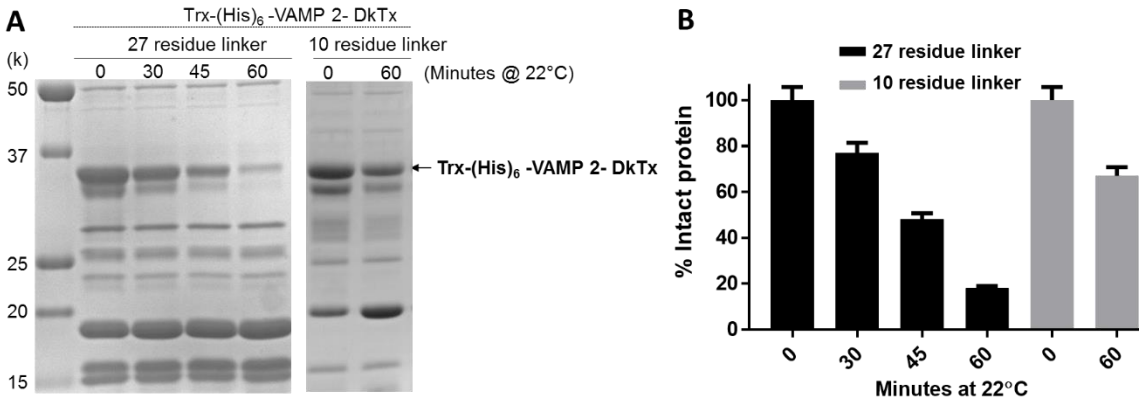

Figure 4. 5 Analysis of the temperature stability of Trx-(His)$_6$-VAMP 2-DkTx
(A) Trx-(His)$_6$-VAMP 2-DkTx samples containing a 27 or 10 residue linker were incubated for up to 1 hour at 22°C prior to being subjected to SDS-PAGE followed by coomassie staining. (**B)** Densitometric analysis of the data from (**A**). Data plotted are means ± S.E.M; n=3.

4.2.5 Fusion of GST to VAMP 2-DkTx significantly improves the purity and stability of the purified protein

The instability of VAMP 2-DkTx was irreconcilable with both stapling to LC.H$_N$/A-SNAP-25 or any preceding functional assays, thereby, rendering the protein ineffectual. As the former issues with expression and purification of soluble LC.H$_N$/A-SNAP-25 had been overcome through utilization of the pGEX-KG vector and its associated GST purification tag, this encouraged the immediate adoption of this cloning strategy for both VAMP 2-DkTx and VAMP 2-EGF.

The pGEX-KG constructs were designed and cloned as depicted in Fig. 4.6 A and B. Recombinant expression of both GST-VAMP 2-DkTx and GST-VAMP 2-EGF was performed in BL21 (DE3) *E. coli*, the expression strain previously employed in the generation of protein stapling ligands (Arsenault et al., 2013), thus, ensuring rigorous adherence to the established protocols. As with the purification of LC.H$_N$/A-SNAP-25 following GST affinity purification, treatment with thrombin released VAMP 2-DkTx from the affinity resin by orchestrating cleavage of the associated 25 k GST tag. The resultant purified protein was visualized by Coomassie staining of SDS-PAGE gels at the predicted M$_r$ of 16 k (Fig. 4.6 C), with a protein yield of ~3 mg/L, as determined by BCA protein assay. Employment of GST purification for VAMP 2-DkTx, rectified the previous concern regarding protein purity and, most significantly, the purified VAMP 2-DkTx remained stable (Fig. 4.6 D). On account of the comparable sizes of both the genes and resultant DkTx and EGF proteins, the data for cloning and expression of both VAMP 2-DkTx and VAMP 2-EGF were almost identical; thus, only the data relating to VAMP 2-

DkTx are presented, but fully representative of the corresponding findings for VAMP 2-EGF.

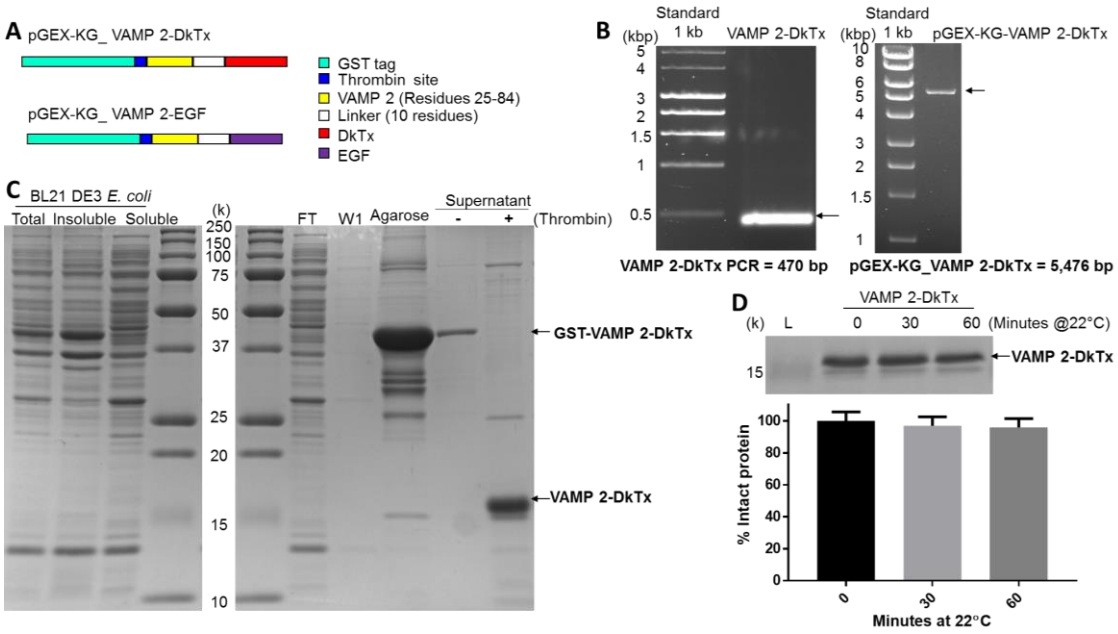

Figure 4. 6 Design, cloning, expression, affinity purification and stability analysis of the second generation of VAMP 2-DkTx

(A) Illustration of the second generation VAMP 2-DkTx and VAMP 2-EGF constructs. **(B)** PCR amplification was used to generate the VAMP 2-DkTx with appropriate restriction enzyme sites to enable insertion into pGEX-KG vector (left panel). The resultant pGEX-KG_VAMP 2-DkTx vector (right panel) was subjected to restriction digest (XhoI), agarose gel-electrophoresis and visualized by trans-UV. Arrows indicated the predicted DNA sizes, as detailed below the gels. The gels presented are representative of the parallel cloning of pGEX-KG_VAMP 2-EGF. **(C)** Coomassie staining of SDS-PAGE gels confirmed expression and affinity purification of GST-VAMP 2-DkTx. Cleavage with thrombin protease released VAMP 2-DkTx from the 25 k GST tag, which remained associated with the glutathione agarose. The gel is representative of the parallel expression and purification of GST-VAMP 2-EGF. **(D)** VAMP 2-DkTx incubated at 22°C for up to 1 hour was resolved on SDS-PAGE, Coomassie stained and subjected to densitometric analysis. Data plotted are means ± S.E.M; n=3.

4.2.6 Initial combination of the stapling components did not produce the predicted SDS-resistant conjugated complex

The protein stapling reaction, as previously outlined, is based upon the formation of the highly stable SNARE complex and, thus, involves combining full-length SNAP-25 with the minimal contributing domains of both VAMP $2_{(25\text{-}84)}$ and syntaxin $_{(202\text{-}247)}$, in a respective molar ratio of 5:7:7 for 1 hour at room temperature. The predicted result is high efficiency formation of an exceptionally stable SDS-resistant complex (Arsenault et al., 2013). With the aforementioned purification and stability issues relating to the recombinant LC.H_N/A-SNAP-25 and the VAMP 2 tagged ligands successfully resolved, it was possible to progress to protein conjugation. The 45 residue syntaxin peptide, with

an N-terminal TAMRA flurophore as published (Arsenault et al., 2013), was synthesised commercially by Biomatik to 90% purity, indicated in the companies quality control data-sheet. The initial stapling reaction was performed with the VAMP 2-EGF control, the resultant formation of LC.H_N/A-staple-EGF was anticipated to produce protein bands on Coomassie stained SDS-PAGE at M_r of ~145 k in non-reducing conditions (Fig. 4.7 A), and at ~95 k following reductant-induced dissociation of the LC/A (Fig. 4.7 B). In addition, the incorporation of the TAMRA-labelled syntaxin into the complex was expected to result in a fluorescent signal at the above molecular masses following exposure of the gel to Trans-UV. These expected observations could not be detected with either VAMP 2-EGF or VAMP 2-DkTx, despite multiple attempts at optimization. This indicated that either coupling was not occurring, or that the coupled complex was being formed but was stable when run on SDS-PAGE, in contradiction of the published work (Arsenault et al., 2013). These findings highlighted that additional issues prevailed with either the conjugation protocol or the proteins stapling components.

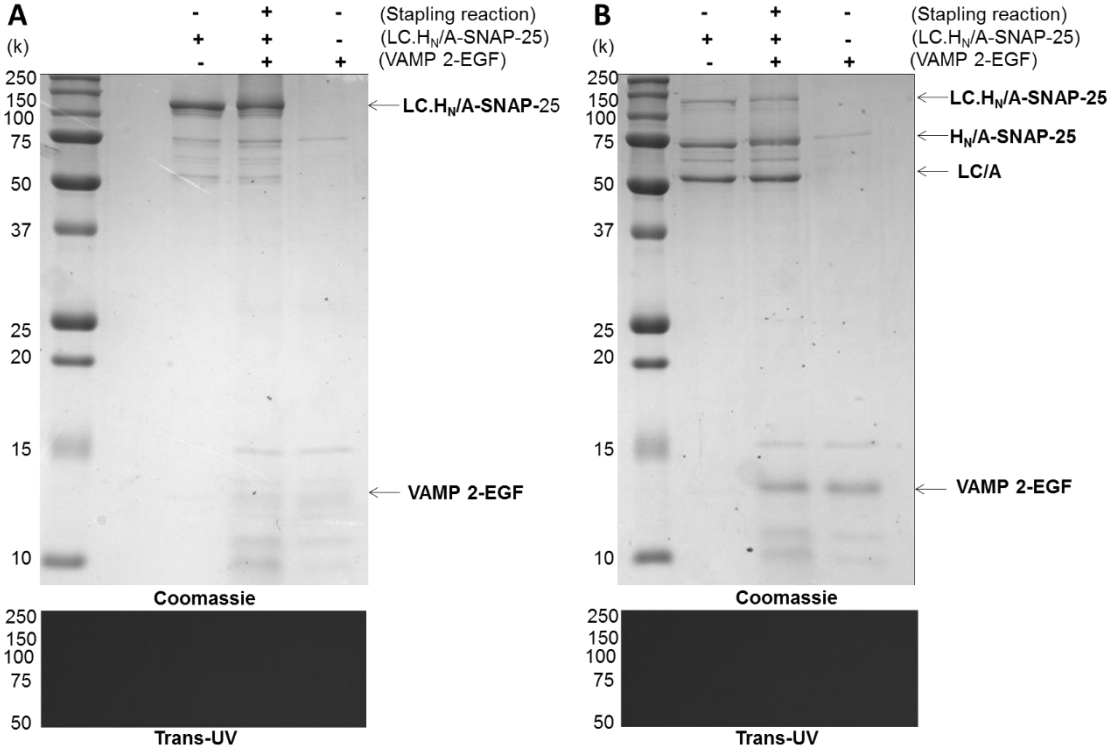

Figure 4. 7 Initial stapling of VAMP 2-EGF and LC.H_N/A-SNAP-25 proved unsuccessful
(A) LC.H_N/A-SNAP-25, VAMP 2-EGF and synthetic syntaxin peptide were combined at a respective 5:5:7 molar ratio and incubated for 1 hour at room temperature. The samples were then subjected to SDS-PAGE followed by Coomassie staining and subsequently exposed to Trans-UV to visualize TAMRA labelled syntaxin. **(B)** Samples from (**A**) were combined with ßME (2.5%) and subjected to SDS-PAGE, followed by Coomassie staining. Note, VAMP 2-EGF exhibits stronger protein staining in the presence of reductant.

4.2.7 LC.H_N/A-SNAP-25 and VAMP 2-EGF bind with low efficiency in the absence of syntaxin

As both LC.H_N/A-SNAP-25 and VAMP 2-EGF/VAMP 2-DkTx were now cloned, expressed and purified exactly as published, it stood to reason that they should be capable of interacting and, thus, implicated the commercially-synthesised syntaxin peptide as the "weak link". In order to confirm the competency of VAMP 2 and SNAP-25, a set of experiments were performed based on the established pull-down of SNARE complex components by immobilized cognate constituents (Söllner et al., 1993, Shen et al., 2007). To this end, either GST-VAMP 2-EGF or GST-LC.H_N/A-SNAP-25 was immobilized on glutathione agarose, and ability to pull-down their respective purified stapling partner from solution was assessed (Fig. 4.8 A and B, respectively). The pull down of LC.H_N/A-SNAP-25 by agarose immobilized GST-VAMP 2-EGF was detected by Western-blotting, using an anti-SNAP-25 antibody (Fig. 4.8 A), confirming that the SNAP-25 and VAMP 2 constituents of the respective proteins were capable of interacting. This was further validated by the converse pull-down, in which agarose immobilized GST-LC.H_N/A-SNAP-25 successfully pulled down VAMP 2-EGF, on this occasion detectable by Coomassie staining and further confirmed by Western-blotting using an antibody which detects VAMP 2. Significantly, the inclusion of the syntaxin peptide in the reaction did not increase the pull-down efficiency of VAMP 2-EGF (Fig. 4.8 B). The pull-down experiments validated that the recombinant stapling proteins were capable of interacting, and that their binding was independent of syntaxin, with inclusion of the latter failing to increase the pull-down efficiency or confer SDS resistance to the resultant complex.

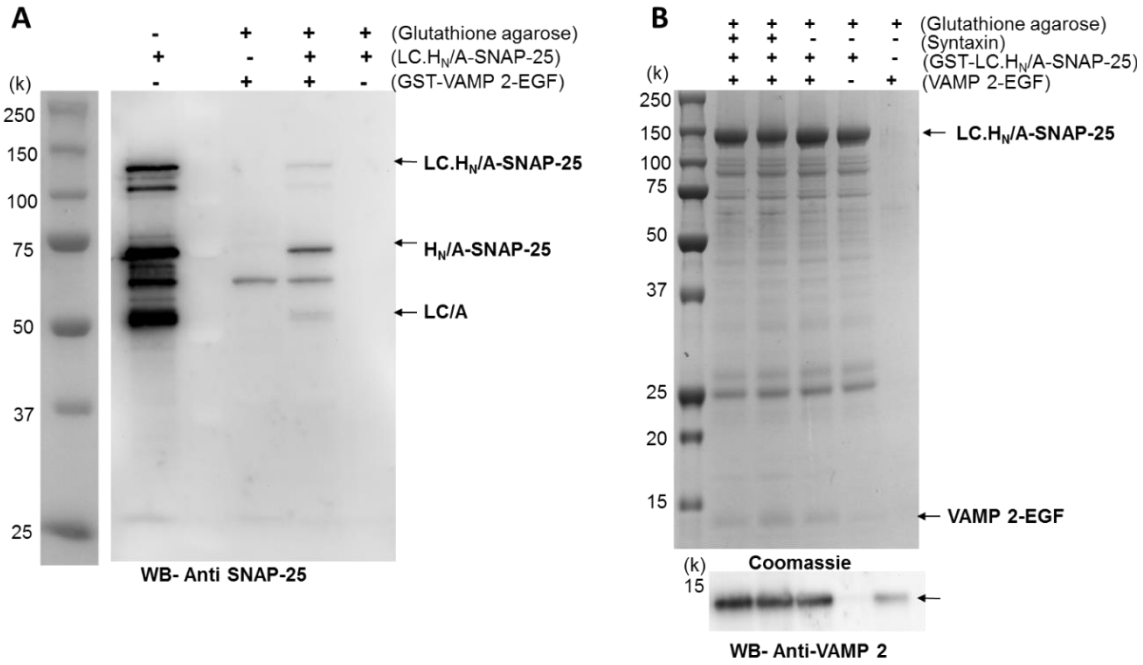

Figure 4. 8 Pull-down of stapling components by their immobilized counterparts
(A) Western-blotting using an anti-SNAP-25 antibody confirmed agarose immobilized GST-VAMP 2-EGF binds to purified LC.H_N/A-SNAP-25 following 60-minute incubation. **(B)** Coomassie staining of SDS-PAGE verified the binding of agarose immobilized GST-LC.H_N/A-SNAP-25 to purified VAMP 2-EGF, further confirmed by Western-blotting using an anti-VAMP 2 antibody.

4.2.8 The oxidation of the commercial syntaxin peptide rendered it ineffectual for SNARE complex formation/stabilization

To identify and resolve the prevailing issue with either the protein stapling components or protocol, training was arranged at the laboratory of Prof. Davletov in the University of Sheffield. This involved the interchange of reagents from the ICNT and from Prof. Davletovs lab, and detailed instruction on all aspects of the protocol. The critical sequences of the protein components were confirmed as identical, and the stapling reaction protocols when compared and contrasted were found to be synonymous, indicating that a lack of complex formation was due to one of the three stapling constituents.

The sequential interchange of the latter determined that both LC.H_N/A-SNAP-25 and VAMP 2-EGF were capable of forming an SDS resistant stable complex with their respective counterparts provided by Prof. Davletov (Fig. 4.9 A and B), corroborating the results from the pull-down experiments. When an aliquot of syntaxin provided by Prof. Davletov was employed in the stapling reaction, it resulted in the high-efficiency formation of an SDS resistant ‘stapled’ complex, producing both the expected size shift on Coomassie staining SDS-PAGE, and corresponding fluorescence from incorporation

of the TAMRA flurophore into the complex (Fig 4.9 A and B). In contrast, the commercial syntaxin peptide purchased from Biomatik was unable to support complex formation. The datasheet for the syntaxin peptide synthesized for Prof. Davletov was acquired, and an identical order placed using the same company (Peptide Synthetics UK).

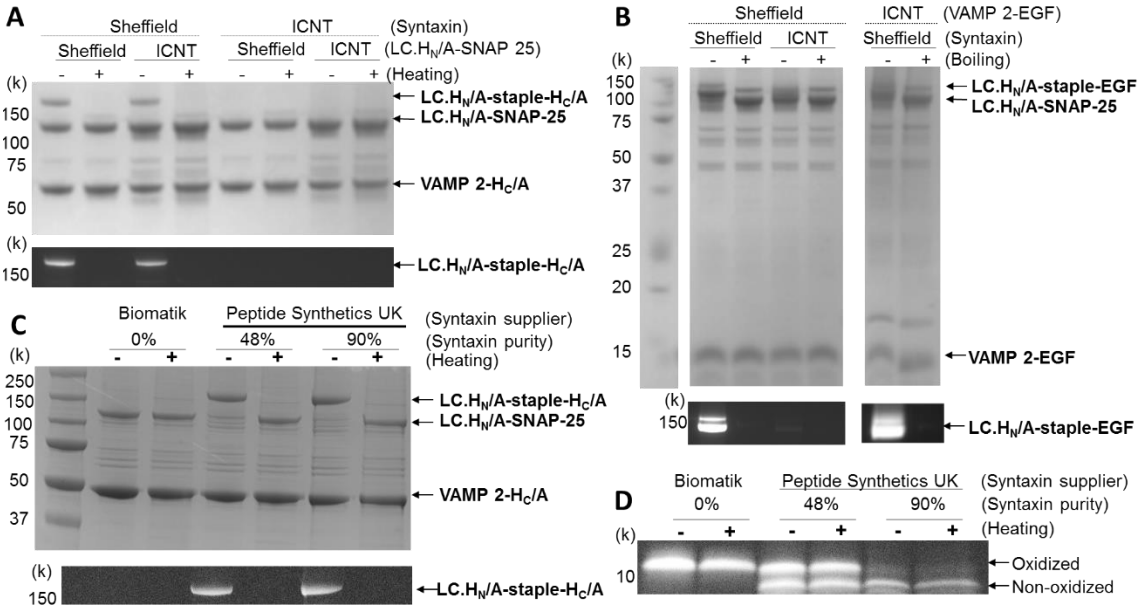

Figure 4. 9 Inter-exchange of stapling components from ICNT and the University of Sheffield
(A) LC.H_N/A-SNAP-25 either from the ICNT or from the lab of Prof. Davletov, University of Sheffield was combined with VAMP 2 fused to the receptor binding domain of BoNT/A (VAMP 2-H_C/A) and a syntaxin peptide (Sheffield) at a respective molar ratio of 5:7:7 for 1 hour at room temperature. Heating of the sample to ~95°C was used to disassociate the SDS resistant complex prior to resolution by SDS-PAGE followed by Coomassie staining. The fluorescence conferred by the TAMRA labelled syntaxin was visualized by trans-UV. **(B)** Performed as in (**A**) using LC.H_N/A-SNAP-25 from the ICNT, and VAMP 2-EGF samples either from ICNT or Sheffield. **(C)** Performed as in (**A**) using syntaxin peptides as indicated. **(D)** The three samples of commercial syntaxin were subjected to SDS-PAGE and exposed to trans-UV to visualize the TAMRA flurophore. Note, the levels of sequence oxidation altered the migration rate of the peptide.

The replacement syntaxin peptide was supplied by Peptide Synthetics UK in two forms of purity, 48% and 90%, dependent on the synthesis protocol employed, with the degree of purity corresponding to the level of sequence oxidation. The company reported that the latter was exacerbated by the presence of the TAMRA flurophore, which contains a conjugative phenyl character, promoting oxidation of syntaxin methionine residues. The differential between the 48% and 90% purity syntaxin peptides did not impede complex formation, with both producing comparable levels of SDS-resistant stapled product. In contrast, no complex formation was detected with the original syntaxin peptide supplied by Biomatik, denoted as 0% purity (Fig. 4.9 C). When the syntaxin peptides were analyzed by SDS-PAGE, the level of peptide oxidation was shown to produce a

differential migration pattern, with the oxidized form migrating slower than the non-oxidized form (Fig. 4.9 D). The syntaxin peptide originally supplied by Biomatik was determined to be fully oxidized (0% purity), when compared with the 48% and 90% purity samples supplied by Peptide Synthetics UK.

4.2.9 Use of high-purity syntaxin produced SDS-resistant conjugation of VAMP 2-EGF or VAMP 2-DkTx to LC.H_N/A-SNAP-25

The ability to effectively recapitulate the protein stapling technology finally allowed progression to retargeting assessment. Stapling of both VAMP 2-DkTx (Fig. 4.10 A) and VAMP 2-EGF (Fig. 4.10 B), was performed as previously described. In both cases SDS-resistant complex formation was affirmed, and could be detected by both Coomassie staining of SDS-PAGE gels and through visualization of the incorporated TAMRA-labelled syntaxin. Efficiency of the stapling reaction was found to vary between VAMP 2-EGF and VAMP 2-DkTx, determined by densitometric analysis, to be ~80% and ~30%, respectively (Fig. 4.10 C). Furthermore, it was observed that stapling of VAMP 2-DkTx resulted in the production of aggregates which failed to enter the gel (Fig. 4.10 B). Precipitation of LC.H_N/A-staple-DkTx was not observed in the complex solution following centrifugation, with the aggregation only detected when samples were run on SDS-PAGE.

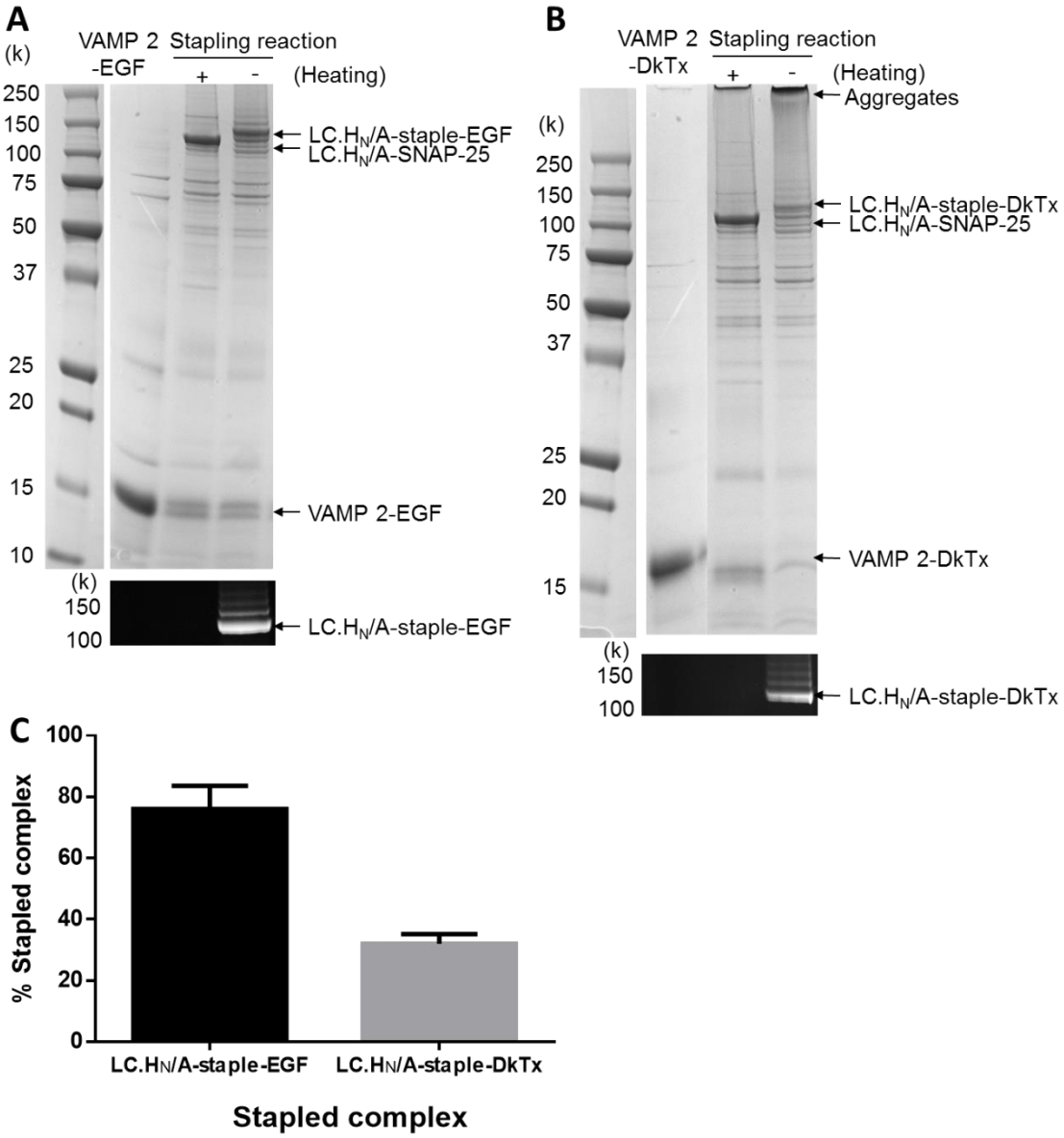

Figure 4. 10 Conjugation of either VAMP 2-EGF or VAMP 2-DkTx to LC.H$_N$/A-SNAP-25
(A) Complex formation following combination of LC.H$_N$/A-SNAP-25, VAMP 2-EGF and syntaxin in a respective 5:7:7 molar ration, was visualized by Coomassie staining of SDS-PAGE and Trans-UV. Heating of the samples to 95°C for 5 minutes was used to disassociate the SDS-resistant complexes. **(B)** Stapling reaction performed as in (**A**), except substituting VAMP 2-DkTx in the place of VAMP 2-EGF. **(C)** % complex formation was determined by densitometric analysis of the Coomassie stained SDS-PAGE gels. Data plotted are means ± S.E.M; n=3.

4.2.10 Treatment of serum-starved SH-SY5Y cells with VAMP 2-EGF induces ERK 1/2 phosphorylation

The ability to confirm the functional activity of uncoupled VAMP 2-tagged ligands was considered one of the principle advantages of the protein stapling. Thus, prior to assessment of LC.H$_N$/A-staple-EGF targeting of SH-SY5Y neuroblastoma cells, it was pertinent to first confirm that VAMP 2-EGF was capable of interacting with the EGF receptor (EGFR). Expression of EGFR in SH-SY5Y cells has been established (Lu et al.,

2014), and binding of EGF induces intracellular signalling events which include the phosphorylation of extracellular receptor kinase 1 and 2 (ERK 1/2) (Lu et al., 2014). Functionality of VAMP 2-EGF was consequently assessed by a qualitative but sensitive phosphorylation assay which involved serum-starving SH-SY5Y overnight to reduce background phosphorylation; this was followed by a 5 minute exposure to increasing concentrations of VAMP 2-EGF prior to preparation of cell lysates. Western-blotting using antibodies against either the phosphorylated or non-phosphorylated isoforms of ERK 1/2, demonstrated that VAMP 2-EGF treatment induced ERK 1/2 phosphorylation, with no response detected in the untreated control (Fig. 4.11 A). The increase in signal for p-ERK 1/2 corresponded to a dose-dependent reduction in signal for the unphosphorylated species, with blotting using an anti-SNAP-25 antibody confirming comparable loading between all conditions.

In a further attempt to confirm VAMP 2-EGF activity, SH-SY5Y cells were treated with up to 300 nM VAMP 2-EGF for 42 hours in an attempt to induce cell differentiation. Disappointingly, there were no morphological changes detectable when compared to the untreated control (Fig. 4.11 B), corroborating previous observations that it is challenging to induce SH-SY5Y differentiation via EGFR (Tyson et al., 2003).

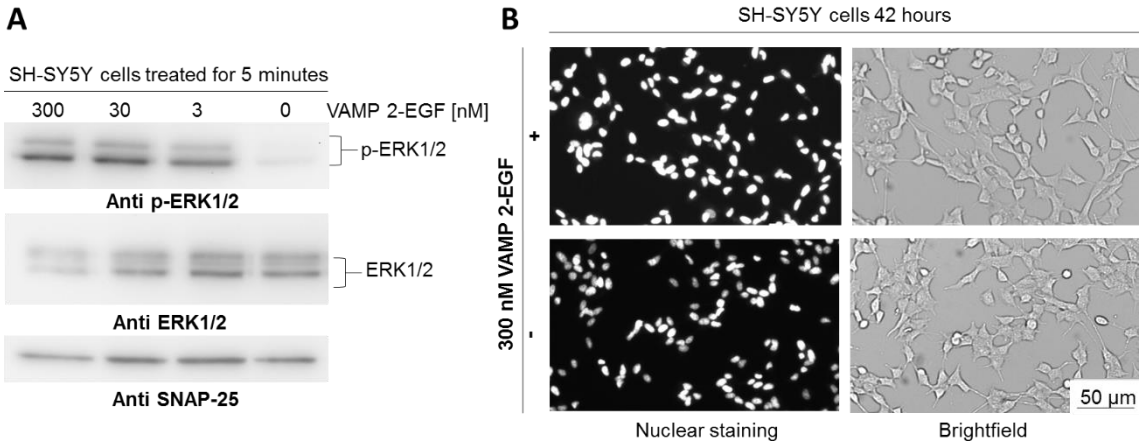

Figure 4. 11 Functional interaction between VAMP 2-EGF and SH-SY5Y cells
(A) SH-SY5Y cells, serum-starved overnight prior to 5 minute treatment with increasing concentrations of VAMP 2-EGF were lysed and subjected to Western-blotting using antibodies against ERK1/2, -p-ERK 1/2 and SNAP-25. Increase in p-ERK 1/2 signal correlates with a decrease in the detection of the non-phosphorylated isoform. **(B)** SH-SY5Y cells either untreated, or treated with VAMP 2-EGF diluted into the culture medium to a final concentration of 300 nM, were incubated for 42 hours at 37°C, 5% CO_2. Cells were incubated with Hoechst nuclear stain prior to image acquisition.

4.2.11 LC.H_N/A-staple-EGF increases cleavage of SNAP-25 in SH-SY5Y cells relative to the untargeted control, but the increment is lost at concentrations which exceed 10 nM

To ascertain if the stapling technology represented a viable strategy for adapting to both DkTx and potential future targeting ligands, it was deemed appropriate to first recapitulate the targeting of LC.H_N/A-staple-EGF reported by others (Arsenault et al., 2013). LC.H_N/A-staple-EGF complex was prepared as previously described (Fig. 4.10 A), producing a coupling efficiency of ~80% (Fig. 4.10 C). The original publication on LC.H_N/A-staple-EGF targeting employed a fixed toxin concentration of 10 nM (Arsenault et al., 2013). To investigate if targeting of LC.H_N/A-staple-EGF could be detected at a lower concentration, and conversely to determine if there was any significant uptake of untargeted control at higher doses, SH-SY5Y cells were treated with 1, 10 and 100 nM of either LC.H_N/A-staple-EGF or LC.H_N/A-SNAP-25 untargeted control for 42 hours prior to lysis. Western-blotting of the resultant cell lysates with an antibody which detects both cleaved and uncleaved SNAP-25 confirmed truncation of SNAP-25 in cells treated with 10 nM of LC.H_N/A-stapled-EGF, but not with 10 nM of untargeted LC.H_N/A-SNAP-25 (Fig. 4.12 A). This successful recapitulation of the published result (Arsenault et al., 2013), confirmed that protein stapling could be utilized for ligand-mediated delivery of LC/A into pertinent cells. There was, however, comparable SNAP-25 cleavage detected for both the EGF targeted and untargeted LC.H_N/A-SNAP-25 control at 100 nM treatment concentration and, thus, highlighted a significant limitation of the strategy. The subsequent reprobing of the blot with an antibody against LC/A cleaved SNAP-25 (SNAP-$25_{/A}$), which is far more sensitive in the detection of the cleaved isoform, confirmed increased truncation of SNAP-25 in cells treated with both 1 nM and 10 nM of LC.H_N/A-stapled-EGF, but again could not discern any difference at the higher treatment dose of 100 nM. Furthermore, this sensitive antibody was able to detect a minute level cleavage of SNAP-25 in cells treated with 10 nM untargeted LC.H_N/A-SNAP-25 (Fig. 4.12 B).

The succeeding treatment of SH-SY5Y cells with a narrower dose range of either LC.H_N/A-staple-EGF or LC.H_N/A-SNAP-25 (Fig. 4.12 C), and subsequent Western-blotting performed with the sensitive anti-SNAP-$25_{/A}$ antibody, confirmed the presence of cleaved SNAP-25 in cells treated with untargeted LC.H_N/A-SNAP-25 at concentrations as low as 2.5 nM. It was evident following densitometric analysis that

LC.H_N/A-stapled-EGF produced greater levels of truncated SNAP-25 (Fig. 4.12 D), confirming that LC/A was being retargeted, albeit to limited extent, into SH-SY5Y cells through the EGF targeting peptide. However, the delivery of the "untargeted" LC.H_N/A-SNAP-25 into SH-SY5Y cells was a grave concern, as it demonstrated that the protein stapling retargeting strategy was not as refined as anticipated.

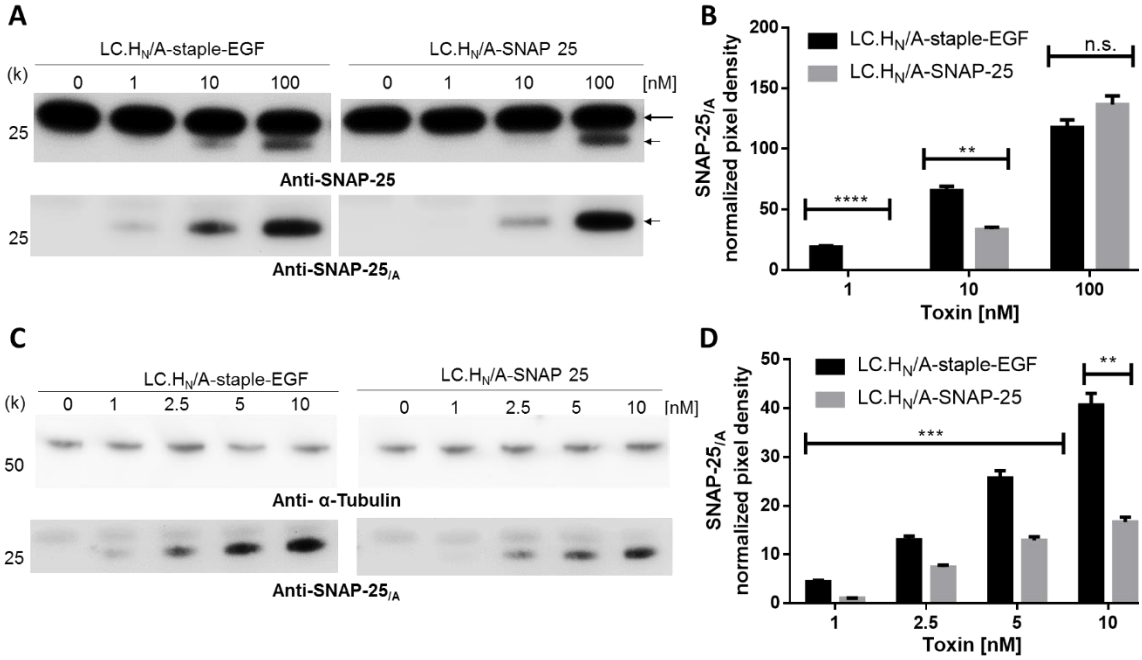

Figure 4. 12 SNAP-25 cleavage in SH-SY5Y cells following treatment with LC.H_N/A-staple-EGF or untargeted control

(A) SHSY-5Y cells treated with the indicated concentrations of either LC.H_N/A-staple-EGF or LC.H_N/A-SNAP-25 were incubated for 42 hours, prior to washing and preparation of cells lysates; these were subjected to Western-blotting using an antibody which detects both cleaved (arrowhead) and uncleaved (arrow) isoforms of SNAP-25 or the only the cleaved isoform (SNAP-$25_{/A}$). **(B)** Data from (**A**), normalized against levels of total SNAP-25 was subjected to densitometric analysis using ImageJ software. Data plotted are means ± S.E.M; n=3 from three independent experiments, statistical analysis carried out by unpaired student t-test, ** $p < 0.01$, **** $p < 0.0001$, n.s., $p > 0.05$. **(C)** SH-SY5Y cells were treated as described in (**A**), and subjected to Western-blotting using antibodies against either α-Tubulin or cleaved SNAP-$25_{/A}$. A high exposure of the resultant blot was taken to permit detection of SNAP-$25_{/A}$ in LC.H_N/A-SNAP-25 treated samples. **(D)** Data from (**C**) was subjected to densitometric analysis. Data plotted are means ± S.E.M; n=3, normalized against the α-Tubulin loading control; statistical analysis was performed by unpaired student t-test, ** $p < 0.01$, *** $p < 0.001$.

4.2.12 VAMP 2-DkTx is non-functional and does not interact with TRPV1

In advance of the assessment of LC.H_N/A-staple-DkTx retargeting, it was essential to first confirm the functional activity of the DkTx ligand. This was particularly pertinent in light of the findings that 100 nM untargeted LC.H_N/A-SNAP-25 was capable of inducing significant SNAP-25 cleavage in SH-SY5Y cells, a concentration below the published 144 nM EC_{50} of DkTx (Bohlen et al., 2010). An additional consideration was that the

previously attained DkTx functionality, described in the Chapter 3, had been achieved through use of the pET32b expression vector and the associated Trx fusion tag. This system was regrettably incompatible with the VAMP 2-DkTx protein as detailed in Fig. 4.5, necessitating utilization of an expression strategy less conducive to the disulfide bond formation. The functional assessment of VAMP 2-DkTx was performed by both Ca^{2+} influx measurement (Fig 4.13 A) and electrophysiology recordings (Fig. 4.13 B and C) using HEK-293 cells transiently-expressing TRPV1. The presence of functional TRPV1 channels on the HEK-293 cells was confirmed in both cases by exposure to the TRPV1 agonist, capsaicin. Subsequent treatment with up to 5 µM VAMP 2-DkTx failed to illicit any functional response, signifying that VAMP 2-DkTx was inactive and incapable of interacting with TRPV1.

Notwithstanding the inability to demonstrate functional activity of VAMP 2-DkTx, availability of LC.H_N/A-staple-DkTx warranted assessment of its ability to target to TRPV1 expressing TGNs (Meng et al., 2016). Furthermore, this would ascertain if the observed penetration of untargeted LC.H_N/A-SNAP-25 into SH-SY5Y cells would be reprised in cultured sensory neurons. An additional constraint on LC.H_N/A-staple-DkTx, was the observation that following stapling, the resultant complex appeared to produce aggregates when run on SDS-PAGE (Fig. 4.10 A). Cultured TGNs were treated with 1, 10 and 100 nM of either LC.H_N/A-staple-DkTx or LC.H_N/A-SNAP-25 for 42 hours prior to lysis. Subsequent Western-blotting of the resultant neuronal lysates using the anti-SNAP-$25_{/A}$ antibody detected comparable SNAP-25 cleavage between both toxins at each respective concentration (Fig. 4.13 D), indicating the formation of LC.H_N/A-staple-DkTx aggregates did not effect its delivery into neurons. The lack of targeting effect was of more pressing concern, as it confirmed the inactivity of the DkTx targeting ligand and, furthermore, highlighted that LC.H_N/A-SNAP-25 was as adept at infiltrating cultured TGNs as it was SH-SY5Y cells.

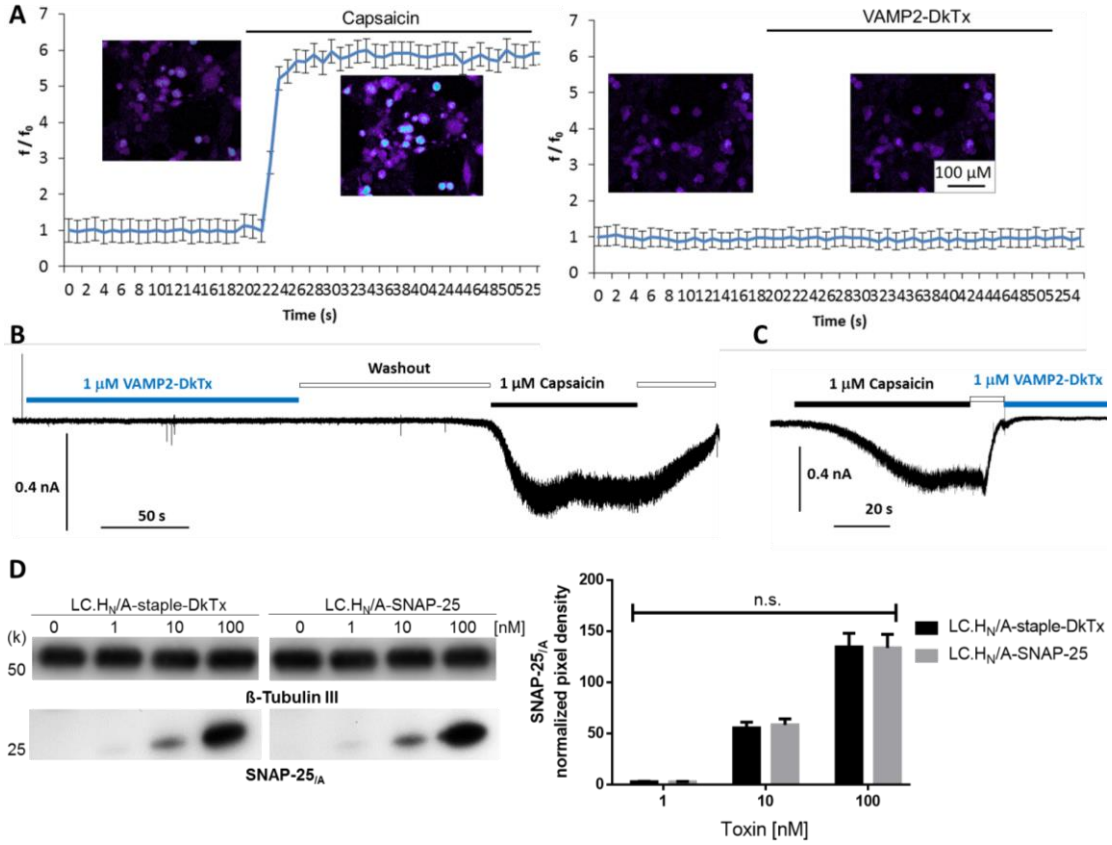

Figure 4. 13 Functional assessment of VAMP 2-DkTx in HEK-293 cells transiently-expressing TRPV1: SNAP-25 cleavage by conjugate or control protein in cultured TGNs

(A) HEK-293 cells transiently-expressing TRPV1 were loaded with Fluo-4-AM Ca^{2+} indicator and measurement of fluorescent signal following laser excitation at 488 nm was used to determine baseline fluorescence (f_0). Washing with either HBSS or treatment with 5 µM VAMP 2-DkTx diluted in the latter buffer failed to provoke an increase in fluorescence, whereas exposure to 1 µM capsaicin diluted in HBSS produced an increase in intracellular fluorescence (f). Values are the mean ± S.D.; n=8 from individual cells, normalized against baseline fluorescence. Inset images are fluorescence signal prior to, and after the application of either capsaicin or VAMP 2-DkTx, as indicated. **(B)** HEK-293 cells transiently-transfected with pIRES2-GFP-TRPV1 were seeded onto coverslips, GFP-positive cells were presumed to be TRPV1 expressing, selected and patched. The perfusion of VAMP 2-DkTx to a final concentration of 1 µM in the extracellular solution failed to induce an inward current. The cells were washed and capsaicin was subsequently perfused to a final concentration of 1 µM; this elicited an inward current, confirming the presence of functional TRPV1 channels. **(C)** Performed as in (**B**), but with the presence of functional TRPV1 channels confirmed prior to VAMP 2-DkTx application. **(D)** TGNs cells were treated as indicated for 42 hours, lysed, and subjected to Western-blotting using antibodies against $SNAP\text{-}25_{/A}$ or ß-Tubulin III. The subsequent densitometric analysis was performed with ImageJ software. Data plotted are means ± S.E.M, normalized against ß-Tubulin III as a loading control. Statistical analysis was performed by unpaired student t-test, n.s. = $p > 0.05$; n=3 from three independent experiments.

4.2.13 Employment of SHuffle® *E. coli* expression strain, and co-expression of chaperone proteins is ineffective at increasing VAMP 2-DkTx functionality

As the previous tactic of expressing functional DkTx through fusion to Trx could not be employed, with the recombinant approach seemingly restricted to the prescribed pGEX-KG strategy, an additional methodology for maximizing disulfide bond formation was

required. A comprehensive review of the literature identified a novel *E. coli* expression strain based on BL21 (DE3) termed SHuffle®. This *E. coli* strain possesses all of the advantageous characteristics of the previously employed Origami B™ strain (Seras-Franzoso et al., 2012), but in addition to the trxB and gor mutations which create a more oxidizing bacterial cytoplasm, the SHuffle® strains contains an additional mutation which results in the cytoplasmic expression of Disulfide bond C. The latter is a prokaryotic disulfide bond isomerase usually expressed in the *E. coli* periplasm (Lobstein et al., 2012), which has an integral role in orchestrating correct disulfide bond formation through isomerization of mis-oxidized proteins to their native states (Kurokawa et al., 2001). In addition, employment of the SHuffle® strain, in conjunction with the exogenous co-expression of seventeen kilodalton protein (Skp) and trigger-factor (TF) chaperones had been shown to significantly enhance the functional cytoplasmic expression of complex disulfide bond stabilized proteins (Lamppa et al., 2013). The pACYC duet vector for co-expression of Skp and TF was obtained from the original authors and subjected to restriction enzyme linearization to confirm the predicted molecular size (Fig. 4.14 A). SHuffle® *E. coli* were subsequently transformed with either pGEX-KG-VAMP 2-DkTx only, or co-transformed with both pACYC-Skp_TF and pGEX-KG-VAMP 2-DkTx. The recombinant expression from the respective transformants was induced by IPTG overnight at 22°C, following which the bacterial lysates were subjected to SDS-PAGE followed by Coomassie staining, this confirmed the co-expression of both Skp and TF in the pertinent bacteria, which significantly enhance the solubility of VAMP 2-DkTx in SHuffle® (Fig. 4.14 B). Unfortunately, following GST affinity purification and subsequent removal of the GST tag by thrombin cleavage, VAMP 2-DkTx expressed in SHuffle® in the absence of Skp and TF became almost entirely insoluble (Fig. 4.14 C). Conversely, although the co-expression of TF and Skp enhanced the solubility of VAMP 2-DkTx, the Skp chaperone remained associated with VAMP 2-DkTx and was co-purified following release from the agarose immobilized GST tag (Fig. 4.14 C). Consequently, the SHuffle® *E. coli* strain, even with the co-expression of chaperone proteins, was deemed inadequate for functional expression of VAMP 2-DkTx

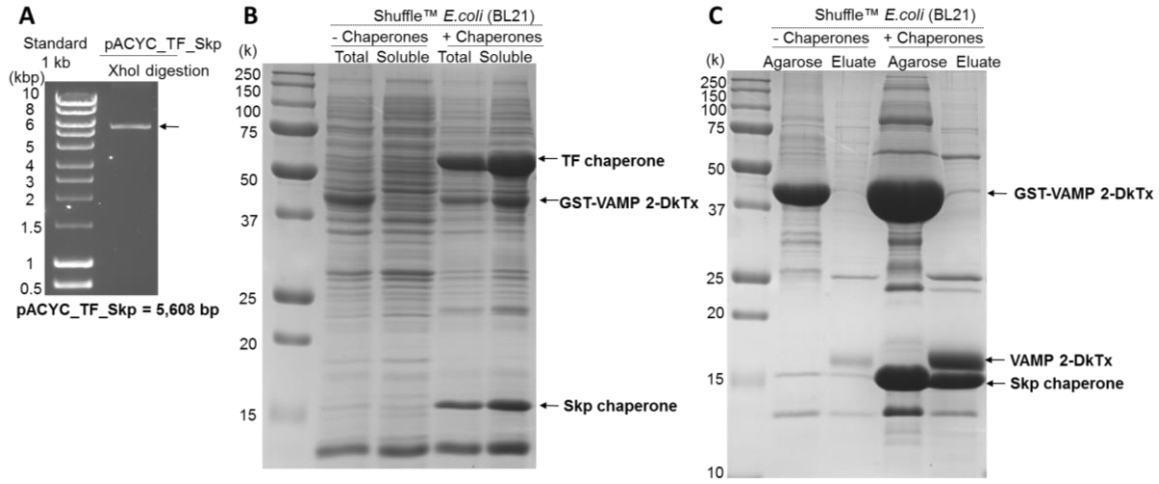

Figure 4. 14 Expression of VAMP 2-DkTx in SHuffle™ *E. coli* with or without co-expressed chaperone proteins, and purification by affinity chromatography

(A) pACYC_TF_Skp was subjected to restriction digest (XhoI enzyme), resolved by agarose gel-electrophoresis and visualized by trans-UV. **(B)** SHuffle® *E. coli*, were transformed with either pGEX-KG-VAMP 2-DkTx, or pGEX-KG-VAMP 2-DkTx and pACYC_TF_Skp (+ chaperones). The recombinant expression of the proteins was induced overnight at 22°C via IPTG. The total and soluble fractions of the resultant lysates were subjected to SDS-PAGE followed by Coomassie staining. **(C)** The soluble lysates from (**B**) were incubated with glutathione agarose, washed extensively and treated with thrombin protease to release VAMP 2-DkTx. The agarose prior to thrombin treatment, or the eluate following treatment, were subjected to SDS-PAGE followed by Coomassie staining.

4.3 Discussion

The ability to productively deliver the LC.H_N/A-stapled-EGF into cultured SH-SY5Y cells, corroborates the published work, and validates protein stapling as an effective conjugation strategy, applicable to BoNT retargeting. The increased delivery of LC.H_N/A-stapled-EGF into cultured cells was however marginal, with detection restricted to a narrow window of low nM concentrations (1-10 nM) and requiring a 42 hour incubation (Arsenault et al., 2013). This highlighted that the EGF targeting ligand was inefficient at mediating delivery of the SNARE protease. Furthermore, the detected SNAP-25 cleavage elicited by untargeted LC.H_N/A-SNAP-25 was an obvious concern, suggesting that even when lacking the H_C, the retained H_N domain is capable of binding to the cell membrane. This observation is supported by recent findings that the isolated H_N/A domain is capable of associating with the plasma membrane (Ayyar et al., 2015, Ayyar and Atassi, 2016).

The capacity of untargeted LC.H_N/A-SNAP-25 to intoxicate cells, coupled with the poor efficiency of EGF in delivering the stapled complex, explained the employment of a fixed toxin concentration of 10 nM by the original authors. This validated the supposition that DkTx, with an EC_{50} of 144 nM, was unlikely to mediate a detectable increase in protease

delivery over the untargeted control. In addition, the culmination of difficulties in expressing function VAMP 2-DkTx indicated that obtaining testable material in a reasonable time-frame was unlikely.

The protein stapling strategy is an impressive conjugation technology, notwithstanding the extensive troubleshooting that was required for its successful implementation. Although capable of mediating a degree of cellular targeting it did not confer the envisaged ligand flexibility; this was highlighted by the challenge in obtaining stable and functional VAMP 2-DkTx. Identification and application of suitable targeting moieties is an appreciated constraint in developing retargeted BoNT molecules (Masuyer et al., 2014); therefore, an innovative approach was required which would permit the screening of diverse, high-affinity ligands. To this end, a novel coupling strategy was designed and developed based on the binding of *Staphylococcus aureus* protein A (SpA) to immunoglobulin G (IgG) antibodies; the design and application of this progressive approach is detailed in Chapter 5.

Chapter 5. A conjugate of an IgG binding domain and BoNT/A core-therapeutic targets TrkA-expressing cells following coupling to anti-TrkA IgG or a Fc-ßNGF fusion

5.1 Introduction

The retargeting of BoNT/A derivatives by previous strategies, including protein stapling, largely employed mammalian growth-factors (Chaddock et al., 2000a, Foster et al., 2006, Arsenault et al., 2013) which possess low nM or even pM affinity for their respective receptors. Hence, comparatively low-affinity ligands such as DkTx prove far more challenging. Although the stapling strategy afforded several advantages, and successfully targeted the core-therapeutic to SH-SY5Y cells following conjugation to VAMP 2-EGF, the detectable cleavage of SNAP-25 by the untargeted control revealed that more proficient ligands of even higher-affinity were required for effective targeting.

TrkA, the high-affinity receptor for NGF (Wiesmann et al., 1999), consequently came to the fore as a favourable target substitute to TRPV1, particularly as TrkA is co-expressed with the latter in peptidergic C-fibre nociceptors (Averill et al., 1995). Homodimerized NGF (ßNGF) possesses an EC_{50} of 0.1 nM (Mehta et al., 2012), and upon binding to TrkA induces internalization of the complex into signalling endosome which undergo acidification (Grimes et al., 1996). Consequently, ßNGF would be expected to be significantly more efficacious at delivering BoNT/A core-therapeutic than DkTx. Furthermore, the chemical conjugation of ßNGF to a binding domain deficient BoNT/A had been previously demonstrated to productively target TrkA expressing cells (Chaddock et al., 2000a), affording an opportunity to evaluate an additional ligand for BoNT retargeting. It was, however, deemed imperative for progression of the project to also develop an additional parallel approach for the targeting of TrkA. Significantly, the binding site of βNGF has been localized to the IgG like domain of TrkA (HoldenPaul et al., 1997), and IgG antibodies which bind this region have been shown to induce receptor crosslinking, resulting in its internalization (Clary et al., 1994). Accordingly, the conjugation of the BoNT/A core-therapeutic to a pertinent antibody was a promising alternative means of targeting TrkA.

Although the protein stapling presented ligand flexibility as an advantage, there was no provision for the conjugation to IgG. As demonstrated in Chapter 4, the approach was in fact quite restrictive, with any deviation from the prescribed protocol proving ineffective. Furthermore, the difficulty in achieving biologically-active VAMP 2-DkTx highlighted the inherent challenge in expressing complex eukaryotic targeting moieties in a bacterial system. Notwithstanding these deficiencies, the independent expression of the protein

stapling core-therapeutic and targeting ligands represented an advance on the initially employed fusion approach. In order to preserve this advantageous attribute, an innovative conjugation strategy was devised and developed based on the binding to IgG of *Staphylococcus aureus* virulence factor Protein A (SpA).

SpA consists of 5 highly modular IgG binding domains (A-E) (Moks et al., 1986), which bind to both the fragment crystallisable (Fc) and fragment antigen-binding (Fab) regions of IgG, with an overall K_D value of ~$5x10^{-9}$ M (Tsukamoto et al., 2014). Each IgG binding domain is thermodynamically autonomous (Deis et al., 2014), and capable of independently binding IgG with high efficiency and stability (Jansson et al., 1998). Accordingly, the incorporation of a SpA domain into a BoNT/A core-therapeutic was perceived as a new way to conjugate the latter to IgG. To this end, the IgG binding domain B of SpA (SpA-B), the best characterized (Deisenhofer, 1981) and most utilized of the domains (Lindborg et al., 2013), was selected and the residues responsible for the binding to IgG Fab (D36, 37), were mutated by site-directed mutagenesis (Fig. 5.1 A and B) (Kim et al., 2010). As the Fab region of IgG is responsible for recognition of the antibody epitope, precluding this interaction reduced the potential for hindrance of target binding by coupled IgG. The fusion of this SpA-B_{mut} domain onto the C-terminus of LC.H_N/A generated a new core-therapeutic (LC.H_N/A-SpA-B_{mut}) (Fig. 5.1 C and D).

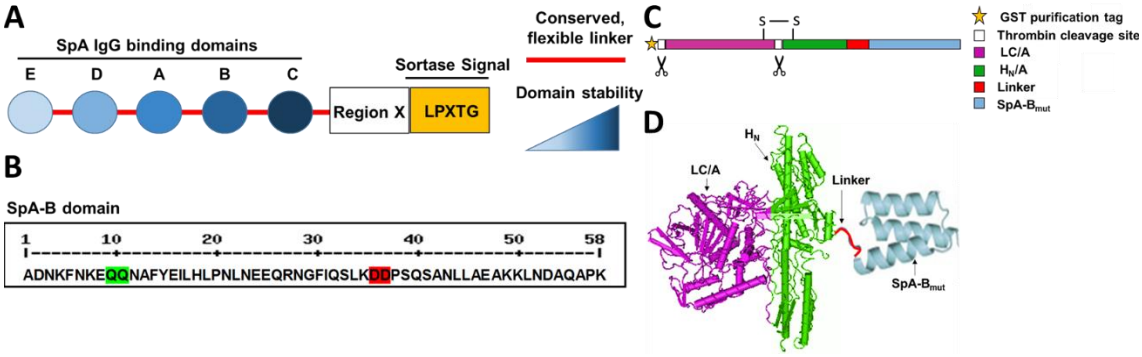

Figure 5. 1 Overview of LC.H_N/A-SpA-B_{mut} core-therapeutic
(**A**) Representation of the SpA protein, indicating the relative stability of 5 IgG binding domains, region X and the LPXTG sortase signal which are responsible for attachment to the bacterial cell wall. (**B**) Amino acid sequence of the SpA-B domain, residues involved in binding of Fc (Q9, 10) and IgG Fab (D36, 37) are highlighted in green and red, respectively. (**C**) Schematic of the novel LC.H_N/A-SpA-B_{mut} DNA cloned into pGEX-KG expression vector, indicating the thrombin protease sites, and the inter-chain disulfide bond. (**D**) Hypothetical structure of the resultant purified protein. Adapted and combined from the crystal structure of BoNT (Masuyer et al., 2015) and SpA-B (Sato et al., 2004).

LC.H_N/A-SpA-B_{mut} was designed to enable selective monovalent coupling to IgG Fc without any requirement for chemical modification and, consequently, permit the direct use of unadulterated commercial IgG targeting TrkA. As it was also desirable to target

this receptor via conjugation of the core-therapeutic to ßNGF, an innovative approach of tagging the latter with a single-chain of the fragment crystallisable domain of rabbit IgG (rFc) was developed. The NGF protein is expressed as an immature monomeric precursor containing an N-terminal pre-pro peptide, which orchestrates extensive post-translational modifications of the nascent protein (Seidah et al., 1996). Accordingly, the recombinant expression of functional NGF is difficult to achieve in bacterial systems (Kurokawa et al., 2001). However, baculovirus mediated expression of NGF in Sf9 insect cells results in the correct intracellular processing of NGF, and the secretion of biologically-active homodimeric ßNGF into the cell supernatant (Buxser et al., 1991). To this end, a recombinant baculovirus for insect cell expression of rFC-ßNGF was generated, with an incorporated C-terminal $(His)_6$ to facilitate subsequent IMAC purification (Fig. 5.2 A). The SpA-B_{mut} fusion strategy would, therefore, confer exceptional flexibility, providing a singular approach for the coupling of LC.H_N/A-SpA-B_{mut} to either anti-TrkA IgG or rFC-ßNGF (Fig. 5.2 B) and, thus, an opportunity to directly compare the targeting efficiencies via these diverse moieties.

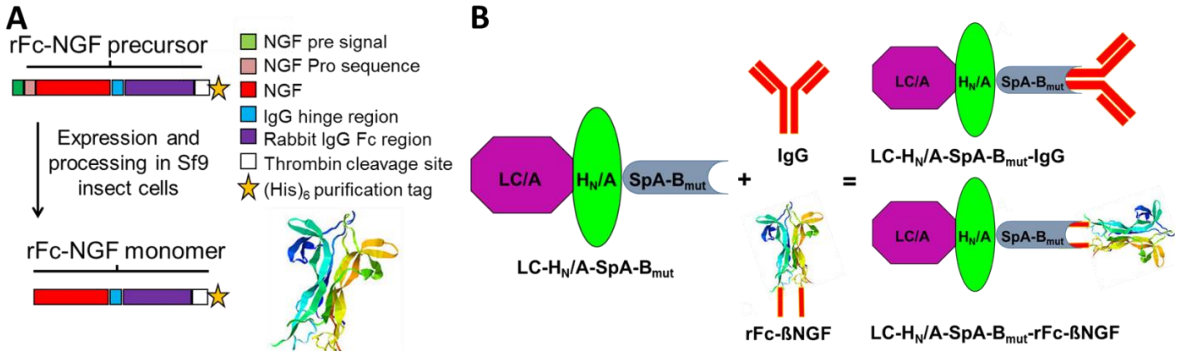

Figure 5. 2 Schematic of SpA-B_{mut} coupling strategy
(**A**) Illustration of the recombinant fusion protein rFc-NGF. Pre-ProNGF-rFc-$(His)_6$, when expressed in Sf9 insect cells undergoes intracellular processing, and enters the secretion pathway, removing the pre-pro signal and resulting in secretion of homo-dimerized rFc-ßNGF-$(His)_6$ into the Sf9 supernatant. A C-terminal $(His)_6$ enables IMAC purification, which is removed by thrombin cleavage. The crystal structure of ßNGF is shown, without fusion to rFc; adapted from (Wiesmann et al., 1999). (**B**). The affinity of SpA-B_{mut} for IgG Fc would facilitate coupling of LC.H_N/A-SpA-B_{mut} to either anti-TrkA IgG or rFc-ßNGF-$(His)_6$ without any requirement for chemical modification or crosslinking.

5.2 Results

5.2.1 Site-directed mutagenesis of SpA-B Fab binding sites and recombinant expression of GST-SpA-B_{mut}

The DNA encoding SpA-B in the pGEX-KG vector was provided by Prof. Joan Geoghegan (Trinity College Dublin) and the nucleotides encoding residues responsible

for IgG Fab interaction (D36, 37) were subsequently mutated to alanine by site-directed mutagenesis; this is an established substitution which abolishes binding to IgG Fab (Kim et al., 2010). The pGEX-KG vectors containing either SpA-B_{WT} or SpA-B_{mut} were linearized by single-site restriction digest prior to being subjected to agarose gel electrophoresis, this gave the predicted molecular size for both vectors (Fig. 5.3 A), with subsequent DNA sequencing performed to confirm successful sequence mutagenesis. The pGEX-KG-SpA-B_{mut} vector was transformed into BL21 (DE3) *E. coli*, and recombinant expression performed by IPTG induction. The resultant bacterial lysate was subjected to SDS-PAGE followed by Coomassie staining (Fig. 5.3 B), which confirmed a significant yield of soluble protein at ~33k, the predicted molecular mass of GST-SpA-B_{mut}. The latter was immobilized on glutathione agarose, with SpA-B_{mut} being released from the agarose-associated GST tag following incubation with thrombin protease. A final yield of ~3 mg/L was determined by BCA protein assay. The results described are representative of the parallel expression and purification of SpA-B_{WT}.

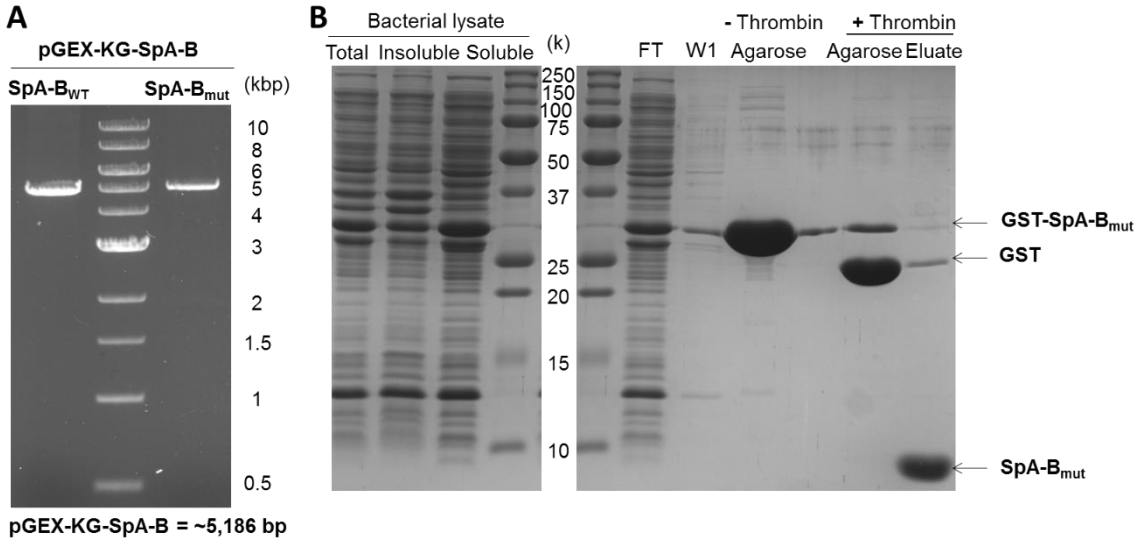

Figure 5. 3 Mutagenesis of SpA-B IgG Fab binding sites, expression and purification of the resultant SpA-B_{mut} protein

(A) pGEX-KG vectors containing genes encoding either SpA-B_{WT} or SpA-B_{mut} were subjected restriction digest linearization (BamHI enzyme), resolved by agarose gel electrophoresis and visualized by Trans-UV. (**B)** The bacterial lysate containing recombinantly-expressed GST-SpA-B_{mut} and the subsequent samples from the affinity-chromatography were subjected to SDS-PAGE followed by Coomassie staining. Cleavage with thrombin protease released SpA-B_{mut} from GST-tag which remained associated with the glutathione agarose.

5.2.2 Abolishment of IgG Fab interaction does not impact upon the binding of SpA-B_{mut} to IgG.

In order to confirm that SpA-B_{mut} was capable of coupling to rabbit IgG, GST-SpA-B_{mut} immobilized on glutathione agarose was incubated with rabbit serum for 1 hour at 4°C, washed extensively, prior to being subjected to SDS-PAGE both in the presence and absence of reductant. The subsequent Coomassie staining (Fig. 5.4 A) demonstrated that GST-SpA-B_{mut} retained a significant amount of bound protein with a M_r of ~250 k. In the presence of reductant this protein disassociated into ~50 k and ~25 k components, corresponding to the predicted molecular masses of the IgG heavy and light-chains, respectively. The parallel incubation of serum with a glutathione agarose only control established that the binding to the serum protein was being conferred by SpA-B_{mut}. The identity of this 250 k protein was confirmed as rabbit IgG by subsequent Western-blotting using an anti-rabbit IgG antibody (Fig. 5.4 B).

The consequence of limiting interaction to IgG Fc on the overall affinity for IgG was investigated by incubation of either agarose immobilized GST-SpA-B_{WT} or GST-SpA-B_{mut} with rabbit serum, with the relative levels of bound IgG assessed by dot-blot analysis using an anti-rabbit IgG antibody (Fig. 5.4 C). The comparable signal in the respective 10-fold dilutions confirmed no significant difference in the amount of IgG bound by either wild-type or mutated SpA-B.

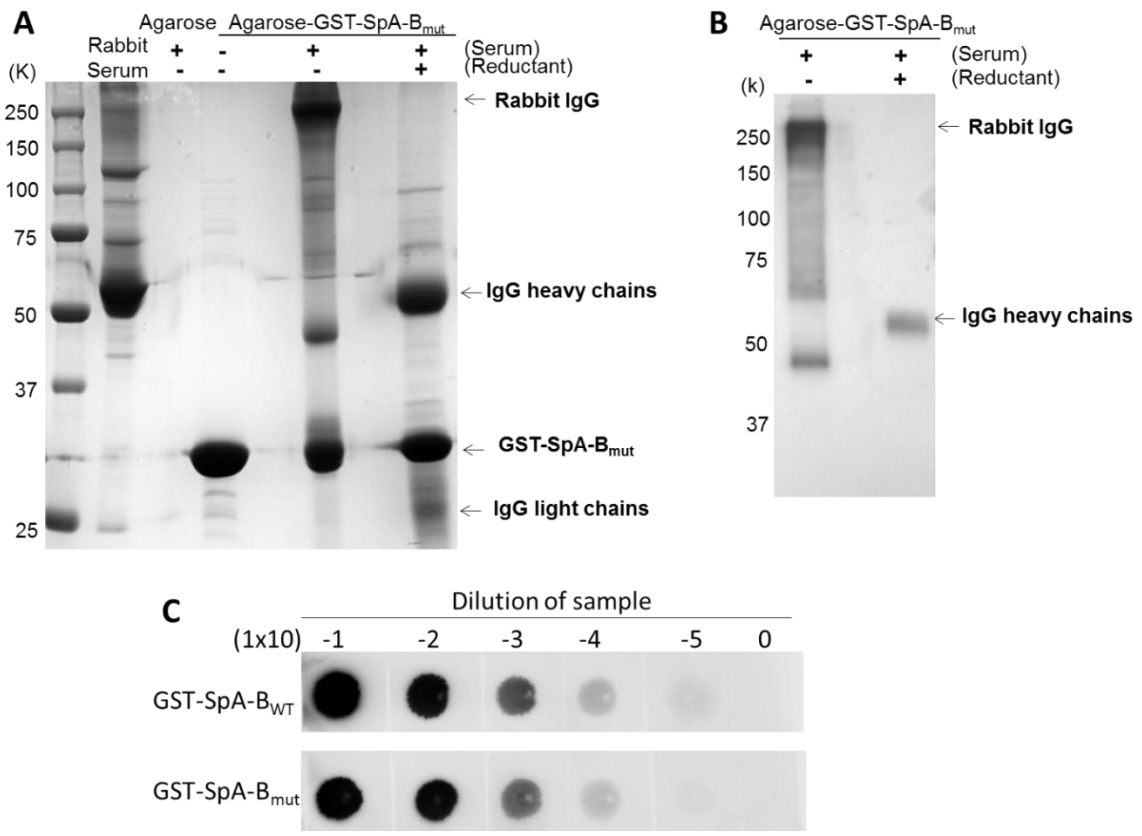

Figure 5. 4 Binding of SpA-B or SpA-B$_{mut}$ to rabbit IgG
(**A**) GST-SpA-B$_{mut}$ immobilized on glutathione agarose was incubated with rabbit serum for 1 hour at 4°C, washed extensively and subjected to SDS-PAGE followed by Coomassie staining. (**B**) Samples from (**A**) were analysed by Western-blotting using an anti-rabbit IgG antibody. (**C**). Either GST-SpA-B$_{WT}$ or GST-SpA-B$_{mut}$ immobilized on glutathione agarose was incubated with rabbit serum for 1 hour at 4°C, washed extensively, and released from the agarose by thrombin cleavage. Samples were then subjected to a series of 10-fold dilutions before being applied directly to nitrocellulose membrane and subjected to dot-blotting with an anti-rabbit IgG antibody.

5.2.3 Cloning, expression and purification of LC.H$_N$/A-SpA-B$_{mut}$.

The expression vector pGEX-KG-LC.H$_N$/A-SNAP-25 detailed in the Chapter 4 was subjected to restriction enzyme double digest by XbaI and XhoI to excise the DNA encoding the C-terminal SNAP-25. The DNA encoding SpA-B$_{mut}$ which had been amplified by PCR to incorporate consensus restriction sites, was digested in parallel. DNA ligation was subsequently performed to insert SpA-B$_{mut}$ into the position previously occupied by SNAP-25, resulting in pGEX-KG-LC.H$_N$/A- SpA-B$_{mut}$ (Fig. 5.5 A). The vector was transformed into BL21 (DE3) *E. coli* and the protein was recombinantly expressed by IPTG induction. Analysis of the resultant bacterial lysate by Coomassie staining of SDS-PAGE, confirmed successful expression of an appreciable yield of soluble product at the predicted M$_r$ of ~135 k, corresponding to single-chain GST-LC.H$_N$/A-SpA-B$_{mut}$ (Fig. 5.5 B). Subsequent affinity-chromatography purification on

glutathione agarose immobilized a significant quantity of the latter, although residual product could be detected in the flow-through and washes. Incubation with thrombin protease released LC.H_N/A-SpA-B_{mut} from the agarose-associated GST tag, producing the predicted ~ 25 k decrease in molecular mass corresponding to the removal of GST. Analysis of the separated eluate containing LC.H_N/A-SpA-B_{mut}, in both the absence and presence of reductant, confirmed that LC.H_N/A-SpA-B_{mut} had been predominantly converted to disulfide linked di-chain (Fig. 5.5 B). A final yield of ~1mg/L of bacterial culture was determined by BCA protein assay.

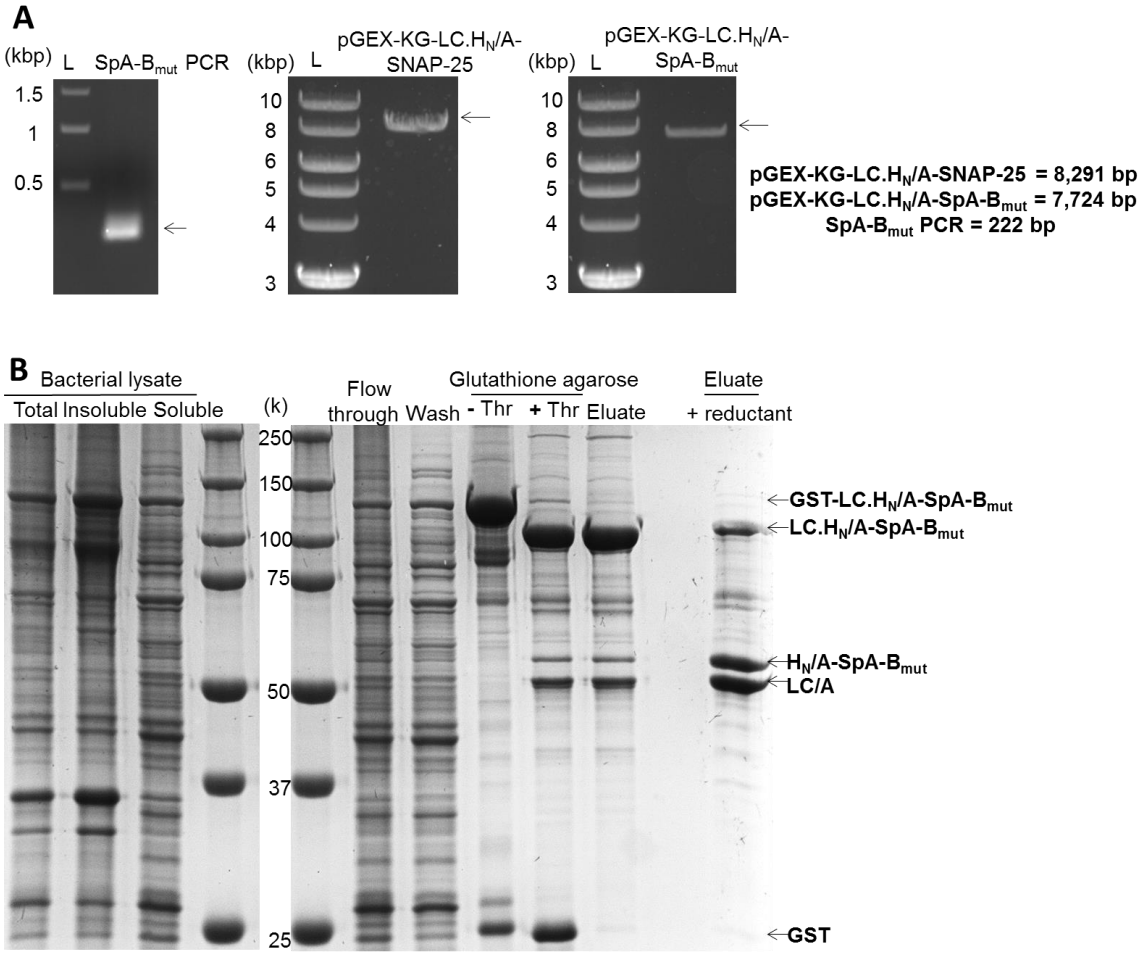

Figure 5. 5 Cloning, expression and purification of LC.H_N/A-SpA-B_{mut}
(A) PCR amplification of SpA-B_{mut} incorporated consensus restriction digest sites allowing its insertion into pGEX-KG-LC.H_N/A in exchange for SNAP-25. DNA samples from the principle cloning steps were subjected to agarose gel electrophoresis prior to visualization by Trans-UV. Arrows indicate the predicted DNA sizes as detailed to the left of the gels. (**B)** The bacterial lysate containing recombinantly-expressed GST-LC.H_N/A-SpA-B_{mut} and samples from the subsequent affinity-chromatography purification were subjected to SDS-PAGE (+/- ßME) followed by Coomassie staining. Cleavage with thrombin protease (Thr) released LC.H_N/A -SpA-B_{mut} from GST-tag, and arbitrated the conversion to disulfide linked di-chain.

5.2.4 LC.H_N/A-SpA-B_{mut} couples to rabbit IgG with high efficiency

Immobilization of GST-LC.H_N/A-SpA-B_{mut} on agarose before thrombin-mediated release proved convenient for the subsequent coupling to IgG. The latter could be incubated in molar excess to saturate the SpA-B_{mut} binding sites, prior to washing to remove both surplus unbound IgG and any contaminants present. As such, commercial rabbit IgG containing BSA stabilizer (included by the supplier) was incubated with agarose bound GST-LC.H_N/A-SpA-B_{mut} at ~3-fold molar excess, prior to washes. Ensuing analysis of the washes and the agarose resin by SDS-PAGE followed by Coomassie staining demonstrated a substantial amount of IgG remained coupled to GST-LC.H_N/A-SpA-B_{mut} (Fig. 5.6 A). Specificity of this interaction was unveiled by the contrasting presence of BSA only in the washes. Parallel analysis by Western-blotting using an anti-rabbit antibody substantiated the results from SDS-PAGE, and confirmed the identity of the rabbit IgG (Fig. 5.6 B).

Subsequent thrombin cleavage released LC.H_N/A-SpA-B_{mut}-IgG from the agarose-associated GST tag, reflected by the SDS-PAGE of the eluate which identified Coomassie stained protein bands corresponding to both IgG and LC.H_N/A-SpA-B_{mut} (Fig. 5.6 C). Analysis of the eluate was then performed by non-denaturing polyacrylamide gel electrophoresis (native-PAGE) to confirm the integrity of the coupled complex (Fig. 5.6 D).

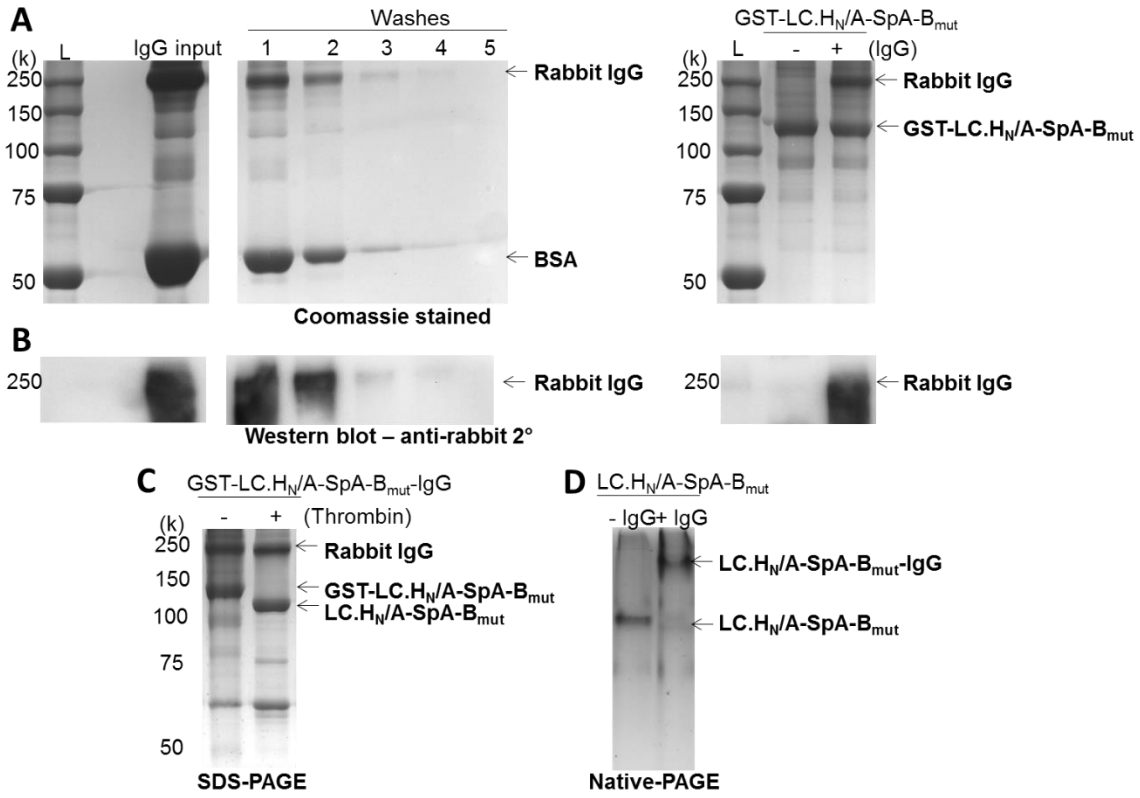

Figure 5. 6 Coupling of LC.H$_N$/A-SpA-B$_{mut}$ to IgG
(**A**) Glutathione-agarose immobilized GST-LC.H$_N$/A-SpA-B$_{mut}$ was incubated with 3-fold molar excess of rabbit IgG, followed by extensive washing with PBS. Coupling of IgG was demonstrated by SDS-PAGE followed by Coomassie staining. (**B**) Samples from (**A**) were subjected to Western-blotting with anti-rabbit secondary antibodies. (**C**) LC.H$_N$/A-SpA-B$_{mut}$ coupled to rabbit IgG was released from agarose bound GST by cleavage with thrombin protease. Samples of either the agarose prior to thrombin treatment or the eluate following treatment were subjected to SDS-PAGE followed by Coomassie staining. (**D**) Native-PAGE followed by Coomassie staining demonstrated a shift in mobility of LC.H$_N$/A -SpA-B$_{mut}$ due to binding of IgG.

5.2.5 IgG coupled to LC.H$_N$/A-SpA-B$_{mut}$ retains ability to bind its target antigen

Prior to assessment of cellular targeting of LC.H$_N$/A-SpA-B$_{mut}$ following coupling to anti-TrkA IgG, which was in limited supply, it was paramount to confirm that the associated IgG could bind its prescribed antigen. To this end, agarose-immobilized GST-LC.H$_N$/A-SpA-B$_{mut}$ was coupled to a rabbit antibody which binds to goat IgG, and incubated with the latter conjugated to alkaline phosphatase (AP). The presence of goat IgG following washing was confirmed by Western-blotting with an anti-goat antibody (Fig. 5.7 A) or by an enzyme-linked immunosorbent assay following addition of AP substrate (Fig. 5.7 B). SpA domains exhibit a species-specific affinity for IgG, having negligible affinity for that raised in goat (Iangone, 1982). Consequently, the presence of goat IgG can be directly attributed to the binding of the coupled rabbit anti-goat antibody. Interestingly, the SpA-

B_{mut} domain is capable of refolding sufficiently on the Western-blotting membrane to bind antibodies raised in rabbit during the second blotting incubation (Baum et al., 2009). Hence, GST-LC.H_N/A-SpA-B_{mut} can be detected at its predicted M_r of ~135 k (Fig. 5.7 A).

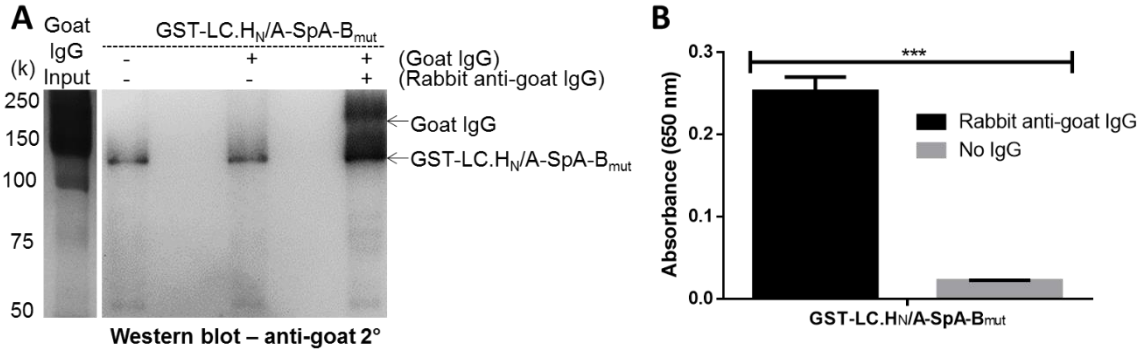

Figure 5. 7 IgG coupled to LC.H_N/A-SpA-B_{mut} can bind its target antigen
(**A**) Agarose-immobilized GST-LC.H_N/A-SpA-B_{mut} either uncoupled or coupled to an antibody which binds goat IgG was incubated with the latter for 1 hour at 4°C, washed extensively and subjected to Western-blotting with anti-goat secondary. (**B**) Experiment was performed as in (**A**), using goat IgG conjugated to alkaline phosphatase; binding of the latter was confirmed by colorimetric change (measured by absorbance at 650 nm) following addition of enzyme substrate. Data plotted are means ± S.E.M; n=3, statistical analysis performed by unpaired student t-test; *** $p < 0.001$.

5.2.6 LC.H_N/A-SpA-B_{mut} retains full protease activity following coupling to IgG

SNAP-25 protease activity of LC.H_N/A-SpA-B_{mut} (+/- coupled IgG), following release from glutathione agarose, was investigated by an established *in vitro* cleavage assay using a recombinant SNAP-25 fragment substrate (Wang et al., 2012) (Fig. 5.8 A and B). This established that LC.H_N/A-SpA-B_{mut} retained protease activity comparable to that of wild-type BoNT/A (Wang et al., 2012), which was not impeded by subsequent coupling to IgG.

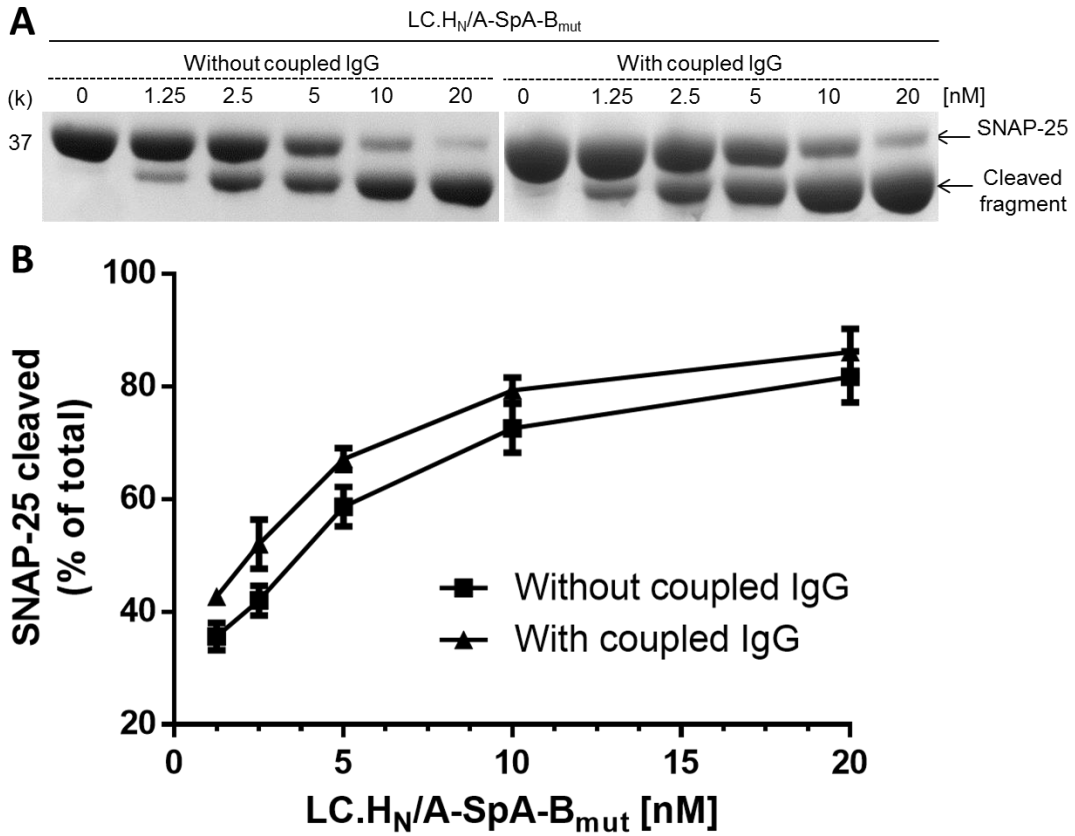

Figure 5. 8 *In vitro* cleavage of recombinant SNAP-25 fragment substrate by LC.H_N/A-SpA-B_{mut} with or without coupled IgG

(A) GFP-SNAP-$25_{(134-206)}$, incubated with 1.25 – 20 nM of LC.H_N/A-SpA-B_{mut} either uncoupled or coupled to rabbit IgG, was subjected to SDS-PAGE followed by Coomassie staining. (**B)** Densitometric analysis data from (**A**) was performed with ImageJ software to determine % cleavage at each concentration. Data plotted are means ± S.E.M; n=3.

5.2.7 Assessment of commercial IgG against TrkA

Having established the protocol for conjugating IgG to LC.H_N/A-SpA-B_{mut}, the next stage was to ascertain if coupling to an appropriate IgG raised against TrkA could deliver the SNARE protease into TrkA-expressing cells. Consequently, a commercial IgG against TrkA was selected based on its epitope (residues 342-356), coinciding with an IgG binding region previously shown to induce receptor internalization (Clary et al., 1994). To establish that the chosen IgG was capable of binding to TrkA and subsequently targeting LC.H_N/A-SpA-B_{mut}, an appropriate cell system was required. To this end, PC-12 cells, a clonal rat cell-line which express both TrkA and SNAP-25 (Tischler and Greene, 1975, Shone and Melling, 1992) were selected and cultured. PC-12 cells were chosen over cultured neurons, as the latter must be maintained in the presence of high concentrations of NGF to sustain viability (Malin et al., 2007) which, in theory, could compete with anti-TrkA targeted LC.H_N/A-SpA-B_{mut}. Significantly, PC-12 cells can be

grown in the absence of NGF, but following its addition to the culture medium, they adopt a neuronal phenotype, characterized by an outgrowth of neurites (Zhou et al., 1995) and an upregulation in TrkA expression (McKelvey et al., 2013).

An initial assessment of the IgG anti-TrkA IgG was performed by Western-blotting of PC-12 cell lysates from either undifferentiated or differentiated cells, with HEK-293 cell lysate functioning as a negative control (Fig. 5.9 A). The immunoblot confirmed binding to a protein at ~150 k in PC-12 lysate, the predicted molecular mass for glycosylated TrkA (Ehlers et al., 1995). In addition, the levels of TrkA were shown to increase following exposure to 2.5S NGF. The parallel Western-blotting with an anti-SNAP-25 antibody reaffirmed the presence of SNAP-25, endorsing PC-12 cells as an appropriate system in which to evaluate TrkA targeting of LC.H_N/A-SpA-B_{mut}. To confirm the ability of the IgG to bind to intact PC-12 cells, the latter were cultured and differentiated by treatment with 2.5S NGF, confirming functionality of the TrkA receptor present on the cell surface. The binding of the anti-TrkA IgG to both differentiated and undifferentiated PC-12 cells was demonstrated by ICC staining (Fig. 5.9 B).

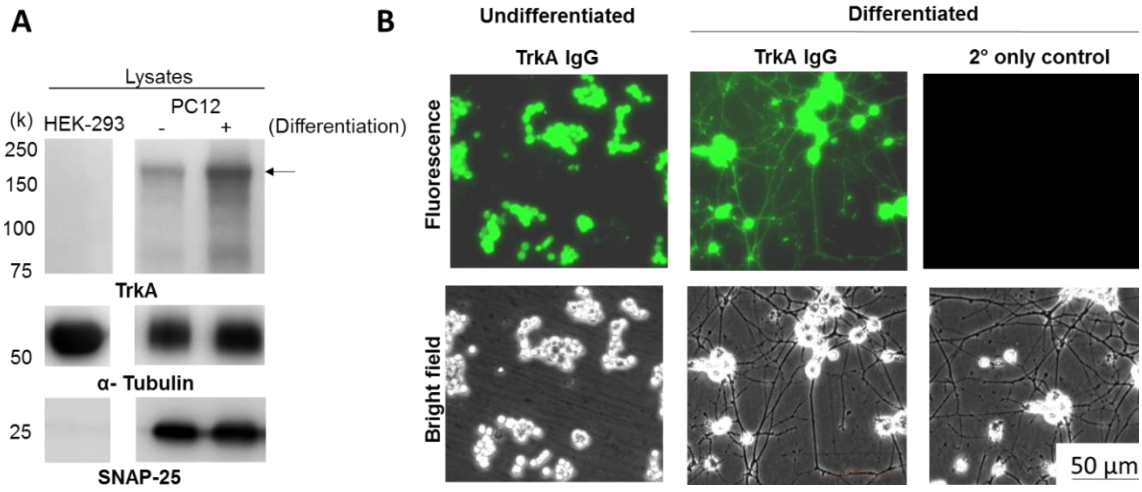

Figure 5. 9 Confirmation that IgG raised against TrkA binds to PC-12 lysate and intact cells
(A) HEK-293 or PC-12 cells lysates from either undifferentiated or differentiated cells were subjected to Western-blotting with antibodies against TrkA, α-Tubulin or SNAP-25. (**B**) PC-12 cells undifferentiated, or differentiated by 96 hours pre-treatment with 100 ng/ml 2.5S NGF, were subjected to ICC staining using the anti-TrkA antibody; a second antibody conjugated to Alexa-Fluor® 488 was used to detect binding. Image acquisition was performed by both fluorescence and bright-field microscopy; images chosen are representative (n=10 for each condition).

5.2.8 Coupling of anti-TrkA IgG to LC.H_N/A-SpA-B_{mut} increases binding to PC-12 cells and improves intracellular delivery of protease relative to the untargeted control

Coupling of anti-TrkA IgG to LC.H_N/A-SpA-B_{mut} significantly increased its binding to PC-12 lysate relative to uncoupled control, as determined by dot-blotting using an anti-LC/A antibody (Fig. 5.10 A). To investigate if this elevated binding correlated with the efficient delivery of the SNARE protease into cultured PC-12 cells, the latter were treated with 0.1-10 nM of untargeted control, or LC.H_N/A-SpA-B_{mut} coupled to anti-TrkA IgG. Western-blotting of the resultant cell lysates revealed increased SNAP-25 cleavage for the TrkA targeted toxin at 0.1 – 1 nM. However, equivalent SNAP-25 cleavage was detected for the untargeted control at 10 nM concentration (Fig. 5.10 B and C).

This initial dose-range finding indicated that anti-TrkA IgG was capable of mediating increased delivery of the SNARE protease at low nM concentrations, but with higher amounts the untargeted control bound non-specifically and was internalized into the PC-12 cells, such that the targeting effect of the IgG could no longer be discerned. To distinguish effective targeting, PC-12 cells were subsequently treated with lower concentrations of the toxins (1.2 – 0.15 nM) and the relative levels of SNAP-25 cleavage were determined by Western-blotting. The analysis confirmed anti-TrkA targeted toxin cleaved SNAP-25 at as low as 0.15 nM (Fig. 5.10 D and E), while negligible cleavage was detected for the untargeted control at any of the concentrations.

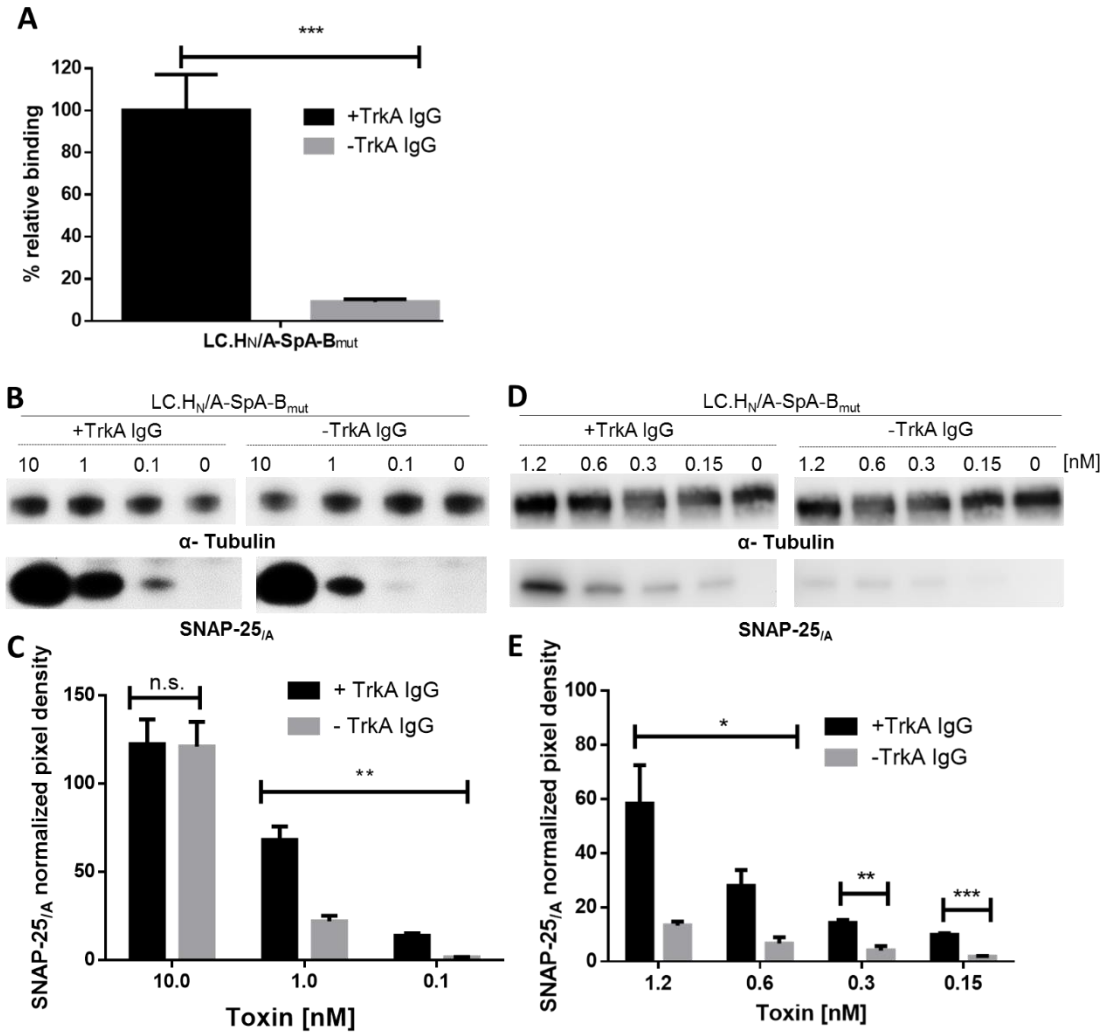

Figure 5. 10 Coupling of TrkA targeting IgG to LC.H$_N$/A-SpA-B$_{mut}$ increases binding and protease delivery into PC-12 cells

(**A**) PC-12 cell lysate (2 µg) was dot blotted onto nitrocellulose membrane, blocked with 5% BSA and incubated with 5 ng of LC.H$_N$/A-SpA-B$_{mut}$ (+/- coupled anti-TrkA IgG) for one hour. The membrane was washed extensively and the relative levels of binding were determined by dot-blotting using an anti-LC/A antibody. Densitometric analysis was performed with ImageJ software. Data plotted are means ± S.E.M, n=3, from independent experiments, normalized against the binding of anti-TrkA IgG. Statistical analysis performed by unpaired t-test: *** $p < 0.001$. (**B**) PC-12 cells were seeded at $4x10^5$ per well in a 24-well plate, and treated with indicated concentrations of LC.H$_N$/A-SpA-B$_{mut}$ (+/- coupled anti-TrkA IgG) for 48 hours prior to preparation of cell lysates; these were subjected to SDS-PAGE followed by Western-blotting with antibodies against α-Tubulin and SNAP-25$_{/A}$. (**C**) Densitometric analysis of data from (**B**). Data plotted are means ± S.E.M, normalized against the α-Tubulin loading control, statistical analysis performed by unpaired t-test: n.s. $p > 0.05$, * $p < 0.05$, ** $p < 0.01$, *** $p < 0.001$, n=3 from independent experiments. (**D-E**) Performed as for (**B**) and (**C**).

5.2.9 Design and cloning of recombinant baculovirus for expression of rFc-ßNGF-(His)$_6$ or ßNGF-(His)$_6$

To develop the additional approach of targeting LC.H$_N$/A-SpA-B$_{mut}$ via coupling to ßNGF, a recombinant baculovirus construct encoding Pre-proNGF-rFc-(His)$_6$ was generated for the subsequent expression of rFc-ßNGF-(His)$_6$ in Sf9 insect cells.

Additionally, a second baculovirus encoding Pre-proNGF-$(His)_6$ was generated as a positive control for baculovirus mediated Sf9 expression of functional homodimeric ßNGF-$(His)_6$ (Buxser et al., 1991).

The baculovirus constructs were generated using the Baculodirect™ system, in which the initial cloning is performed in a bacterial gateway vector (pENTER/D-TOPO), containing two recombination sites (*att*L1 and *att*L2) between which a gene of interest is inserted. Linearized Baculodirect™ DNA contains the corresponding recombination sites (*att*R1 and *att*R2), and site-specific recombination is catalysed by LR clonase™ II enzyme. This results in the insertion of the gene of interest into the baculovirus DNA backbone, in exchange for a gene which encodes herpes simplex virus type 1 thymidine kinase (TK). The DNA encoding Pre-proNGF-rFc-$(His)_6$ was designed and synthesised with codon optimization for insect cell expression, with subsequent PCR reactions performed to amplify the Pre-proNGF-rFc-$(His)_6$ or Pre-proNGF-$(His)_6$ genes (Fig. 5.11 A), with an additional 3' nucleotide sequence (CACC). The respective purified PCR reactions were subsequently incubated individually with linearized pENTER/D-TOPO vector conjugated to Topoisomerase I enzyme. The latter cleaves the PCR product producing an overhang of the inserted 3' sequence, and mediates its ligation with complementary bases in pENTER/D-TOPO. The pENTER/D-TOPO vectors containing Pre-proNGF-rFc-$(His)_6$ or Pre-proNGF-$(His)_6$ genes were then propagated in transformed *E. coli*, purified, linearized by single-site restriction digest; agarose gel electrophoresis followed by Trans-UV exposure (Fig. 5.11 B) confirmed that both vectors correspond to their respective predicted molecular sizes.

The gateway vectors were subsequently incubated, independently, with linearized Baculodirect™ DNA in the presence of LR clonase™ II. A sample from each reaction was subjected to PCR analysis, using primers with complement sequences in the Baculodirect™ DNA backbone. The ensuing agarose gel electrophoresis (Fig. 5.11 C) confirmed the presence of PCR products corresponding to the predicted sizes of the Pre-proNGF-rFc-$(His)_6$ or Pre-proNGF-$(His)_6$ genes in the respective PCR reactions. The heterogeneity of either sample reflects the poor purity of the respective baculovirus constructs following initial generation.

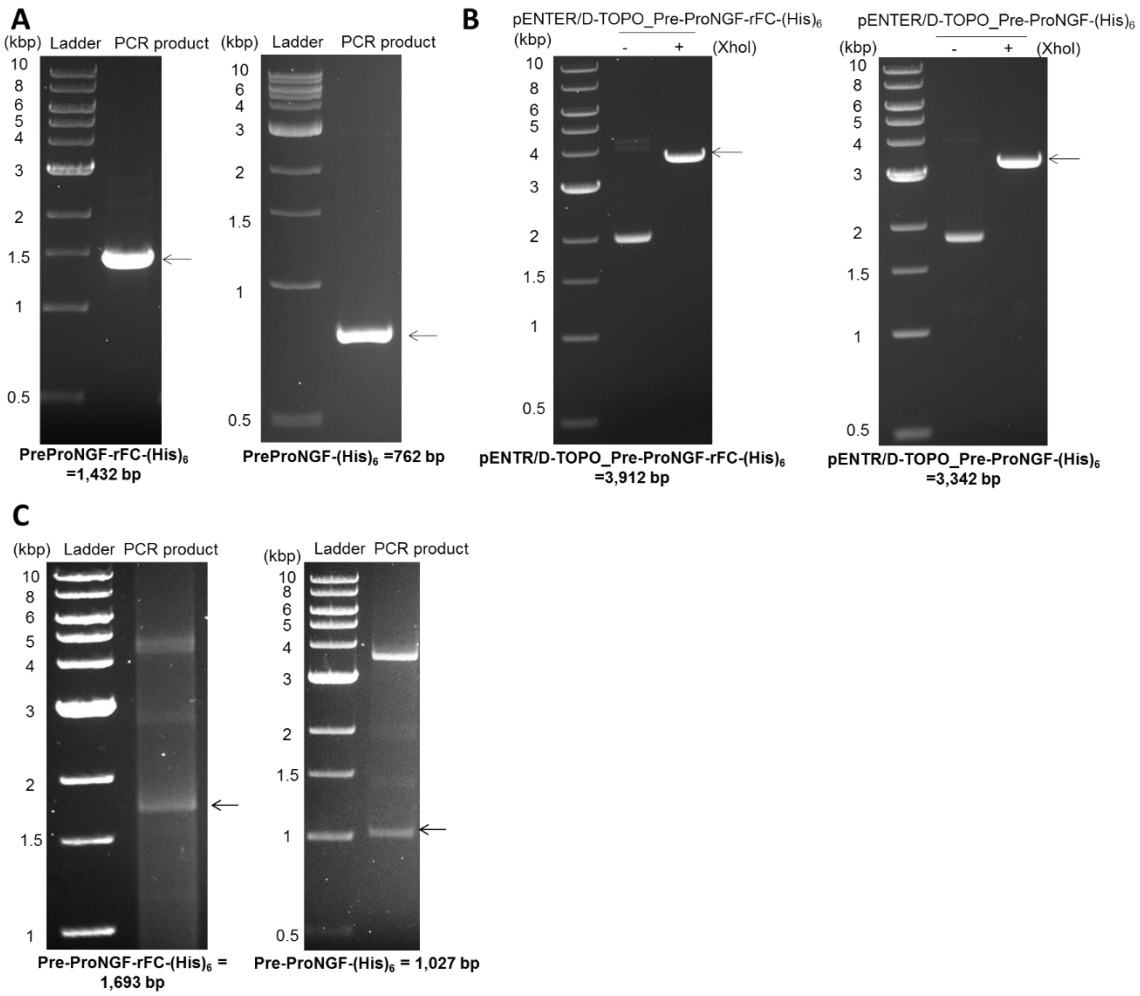

Figure 5. 11 Cloning of recombinant baculovirus constructs for expression of rFc-ßNGF-$(His)_6$ or ßNGF-$(His)_6$

(A) PCR reactions to amplify DNA encoding Pre-ProNGF-rFc-$(His)_6$ or Pre-ProNGF-$(His)_6$ with a 3' CACC nucleotide sequence, were subjected to agarose gel electrophoresis followed by Trans-UV imaging. Arrows indicate the predicted product sizes. (**B)** pENTER/D-TOPO vectors containing Pre-ProNGF-rFc-$(His)_6$ or Pre-ProNGF-$(His)_6$ were linearized with XhoI restriction enzyme, resolved by agarose gel electrophoresis and imaged by Trans-UV. Arrows indicate the predicted plasmid sizes. (**C)** The baculovirus recombination reactions for Pre-ProNGF-rFc-$(His)_6$ or Pre-ProNGF-$(His)_6$ were subjected to PCR using primers designed against consensus sequences within the Baculovirus backbone. The PCR products were subjected to agarose gel electrophoresis and imaged by Trans-UV. Arrows indicate the predicted product sizes.

5.2.10 Baculovirus generation and pilot expression of rFc-ßNGF-$(His)_6$ or ßNGF-$(His)_6$

The recombinant baculovirus encoding Pre-proNGF-rFc-$(His)_6$ or Pre-proNGF-$(His)_6$ were selected and amplified through successive rounds of Sf9 cell infection (Fig. 5.12 A). Initially, Sf9 insect cells cultured in a 6-well plate were transfected with either of the aforementioned constructs in the presence of 100 nM ganciclovir. The latter is a cell permeable nucleoside analogue, which upon phosphorylation by cytoplasmic TK,

incorporates into the genome of Sf9 cells and inhibits DNA replication (Rubsam et al., 1999). Consequently, Sf9 cells transfected with non-recombined baculovirus are negatively selected (Godeau et al., 1992), ensuring only cells transfected with a baculovirus in which TK has been excised following successful recombination of Pre-proNGF-rFc-$(His)_6$ or Pre-proNGF-$(His)_6$ were propagated (Fig. 5.11C). The respective cells were cultured until displaying morphology phenotypical of baculovirus infection (Fig. 5.12 B) (van Oers et al., 2015), at which point the supernatants were harvested, denoted as passage 1 (P1), and used to directly infect Sf9 cells in a higher volume flask format (P2). The recombinant baculovirus constructs were subjected to 3 such cycles of selection/amplification, following which the purity of the respective virus stocks was determined by PCR analysis as previously described (Fig. 5.12 C). Subsequent agarose gel electrophoresis of the PCR reactions confirmed the presence of homogenous DNA products corresponding to the predicted molecular size of either Pre-pro-ßNGF-rFc-$(His)_6$ or Pre-pro-ßNGF-$(His)_6$. The viral titre of each respective baculovirus was then determined by a series of plaque assays, which established that both baculovirus had been amplified successfully, with corresponding viral titres of ~2×10^9 pfu/ml.

To determine if the baculovirus constructs were capable of mediating recombinant expression of either ßNGF-$(His)_6$ or rFC-ßNGF-$(His)_6$, a pilot expression was performed. Sf9 insect cells were infected with either baculovirus at a multiplicity of infection (MOI) of 0.05 and cultured for 72 hours, following which the cell supernatants were harvested and subjected to Western-blotting using an anti-$(His)_6$ antibody (Fig. 5.12 D). The subsequent analysis confirmed the presence of $(His)_6$ containing proteins at the predicted molecular masses of ~28 k and ~80 k, corresponding to homodimeric ßNGF-$(His)_6$ or rFC-ßNGF-$(His)_6$, respectively; with no $(His)_6$ signal detected in the supernatant of the infected control.

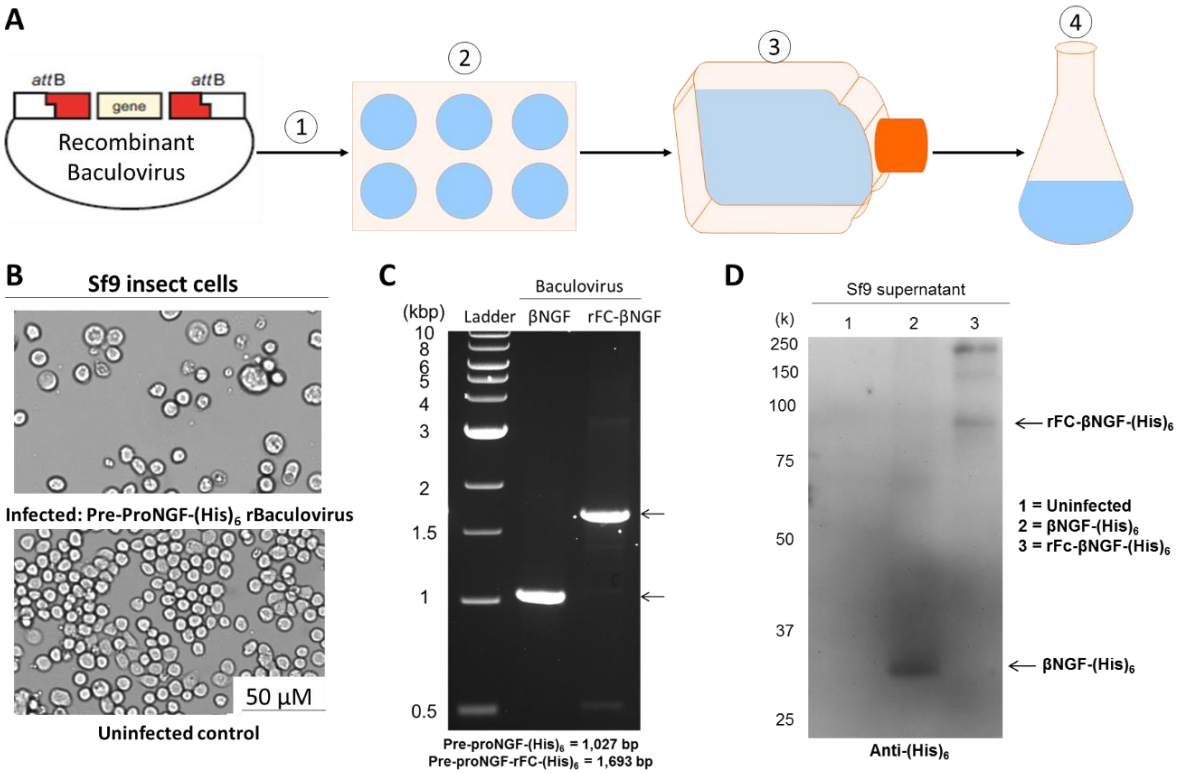

Figure 5. 12 Selection and amplification of baculovirus constructs, and pilot expression of ßNGF-$(His)_6$ or rFc-ßNGF-$(His)_6$

(**A**) 1. The recombinant baculovirus generated was transfected into Sf9 insect cells cultured in 6-well plates. 2. The cells were cultured until exhibiting morphology phenotypical of baculovirus infection (P1 virus). 3. The supernatant from infected cells was harvested, and used to directly infect Sf9 cells in a higher volume flask format (P2). The virus could be further amplified by successive cycles of infection to generate higher viral titre (P3+). 4. Once a high titre baculovirus was produced, parameters for optimal recombinant expression of target protein were established. (**B**) Sf9 cells seeded at $2x10^6$/well in a 6-well plate were transfected with recombinant baculovirus encoding pre-proNGF-$(His)_6$ and cultured for 72 hours prior to image acquisition. (**C**) DNA present in the supernatant of Sf9 cells following 72 hours infection with either Pre-ProNGF-rFc-$(His)_6$ or Pre-ProNGF-$(His)_6$ baculovirus, was precipitated and subjected to PCR amplification using primers designed against consensus sequences within the Baculovirus backbone. The resultant PCR products were subsequently resolved by agarose gel electrophoresis and imaged by Trans-UV. Arrow indicates the predicted product sizes. (**D**) The supernatants from uninfected Sf9 cells, or those infected with either Pre-ProNGF-rFc-$(His)_6$ or Pre-ProNGF-$(His)_6$ baculovirus for 72 hours, were subjected SDS-PAGE followed by Western-blotting with an anti-$(His)_6$ antibody.

5.2.11 Optimization of conditions for expressing and purifying rFc-ßNGF-$(His)_6$

The detection of ßNGF-$(His)_6$ in the supernatant of Sf9 cells following infection with Pre-proNGF-$(His)_6$ encoding baculovirus was a successful recapitulation of previous work (Buxser et al., 1991), validating Sf9 insect cells as a system for the secretion of processed ßNGF. Moreover, the detection of the novel rFC-ßNGF-$(His)_6$ protein from a parallel infection confirmed Sf9 cells remained capable of processing and secreting homodimerized ßNGF following its fusion to rFc. In order to maximise the recombinant yields of rFC-ßNGF-$(His)_6$ a series of expression parameters were assessed. The most commonly employed baculovirus expression protocols involve harvesting 72 hours post

infection, a sufficient time-frame for ample recombinant expression, while minimizing the risk of product degradation, exacerbated by protease release from lytic cells in late-stage (72+ hours) of infection (Gómez-Sebastián et al., 2014). To investigate the optimal duration of infection for expression of rFC-ßNGF-$(His)_6$, Sf9 cells were seeded at $2x10^6$ cells/ml, infected with an MOI of 0.05, and samples were taken of the supernatants at time of infection, and up to 96 hours post infection. Subsequent analysis by Western-blotting using an anti-$(His)_6$ antibody, detected a strong rFC-ßNGF-$(His)_6$ signal 72 hours post-infection, with increased signal detected following 96 hours infection (Fig. 5.13 A). Consequently, 96 hours post-infection was selected as the optimal infection time for expression of rFC-ßNGF-$(His)_6$.

The next parameter considered was MOI, the previous work on ßNGF expression in Sf9 cells utilized a MOI of 0.05 (Nguyen et al., 1993), comparatively low to the value of 10 used in the expression of other recombinant proteins (de Pinheiro et al., 2016). Low MOI infection affords the practical advantage of requiring less virus stock but, more significantly, high MOI infection can overload the production machinery of the cells resulting in poor recombinant yields. Furthermore, high MOI infection can induce over-emphasis on viral replication resulting in an accumulation of inhibitory defective interfering viral particles (Kool et al., 1991), a phenomenon known as the passage effect. Sf9 cells at $2x10^6$ cells/ml were infected with an MOI ranging from 0.05 -100, and supernatants harvested 96 hours post infection, prior to being subjected to SDS-PAGE followed either by Coomassie staining or Western-blotting as above (Fig. 5.13 B). Subsequent analysis confirmed an inverse relationship between MOI and rFC-ßNGF-$(His)_6$ expression/secretion. Furthermore, Coomassie staining revealed an MOI-dependent increase in the expression of a protein at the predicted molecular mass for glycoprotein 64 (Gp64), an endogenous baculovirus envelope protein and, thus, confirmed a shift to viral replication at higher MOIs.

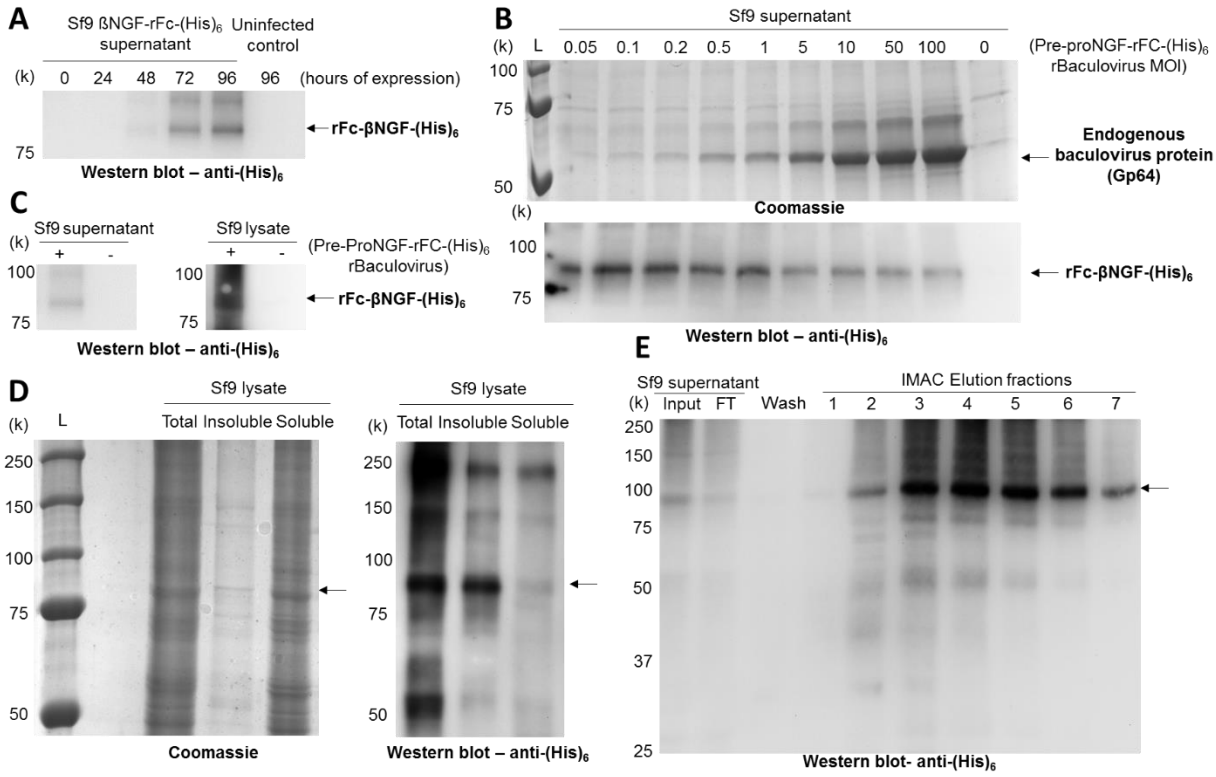

Figure 5. 13 Optimization of parameters for expression and purification of rFC-ßNGF-(His)$_6$
(A) Sf9 cells seeded at 2x10^6 cells/well in a 6-well plate were infected with Pre-ProNGF-rFc-(His)$_6$ baculovirus at an MOI of 0.05 and cultured for 96 hours at 27.5°C. Samples of the supernatant were collected every 24 hours and subjected to Western-blotting using an anti-(His)$_6$ antibody. (**B)** Sf9 cells seeded as above were infected with Pre-ProNGF-rFc-(His)$_6$ rBaculovirus with an MOI 0.05 – 100, cultured for 96 hours at 27.5°C, prior to harvesting of the supernatants. Samples of which were subjected to SDS-PAGE followed by either Coomassie staining or Western-blotting with an anti-(His)$_6$ antibody. **(C)** Sf9 cells seeded at 2x10^6 cells/well in a 6-well plate were either uninfected or infected with Pre-ProNGF-rFc-(His)$_6$ baculovirus at an MOI of 0.05. The cells were incubated for 96 hours, prior to harvesting of the supernatant, followed by preparation of cell lysates. Western-blotting of samples was performed with an anti-(His)$_6$ antibody. **(D)** Sf9 cells infected as in (**C**), were lysed with I-PER® insect cell protein extraction reagent 96 hours post-infection. The lysate was fractionated by centrifugation and samples were subjected to SDS-PAGE followed by Western-blotting with an anti-(His)$_6$ antibody. Arrow indicates the predicted size for rFc-ßNGF-(His)$_6$. (**E**) Sf9 cells seeded at 2x10^6/ml in a total volume of 500 ml were infected at an MOI of 0.05 and cultured for 96 hours, following which the cell supernatant was subjected to IMAC purification. Western-blotting of IMAC samples was performed with an anti-(His)$_6$ antibody. Arrow indicates the predicted size for rFc-ßNGF-(His)$_6$.

Although rFC-ßNGF-(His)$_6$ could be detected in the Sf9 supernatant following expression, the yields were lower than anticipated, particularly as baculovirus infection of Sf9 cells was shown to be capable of producing significant quantities of Gp64. To investigate if the deficiency was in the expression or the secretion of rFC-ßNGF-(His)$_6$, Sf9 cells were infected for 96 hours at an MOI of 0.05, following which the supernatant was harvested and the cells were lysed; both samples were subjected to Western-blotting with an anti-(His)$_6$ antibody (Fig. 5.13 C). Comparison of the signal corresponding to

rFC-ßNGF-$(His)_6$ between both the Sf9 lysate and supernatant, indicated that only a minute proportion of the protein was being secreted, with the majority remaining intracellular. To determine if intracellular rFC-ßNGF-$(His)_6$ could be released from Sf9 cells following lysis, the expression was repeated and cells were lysed using I-PER® insect cell protein extraction reagent, a proprietary reagent optimized for extraction of soluble proteins from insect cells. The resultant lysate was subsequently fractionated by centrifugation, and subjected to SDS-PAGE followed by either Coomassie staining or Western-blotting (Fig. 5.13 D); this determined that although I-PER® solubilized the majority of Sf9 proteins, intracellular rFC-ßNGF-$(His)_6$ was predominantly insoluble.

As the soluble and, thus, purifiable portion of rFC-ßNGF-$(His)_6$ was constrained to that which was secreted into the Sf9 supernatant, the expression scale was increased. Sf9 cells were seeded in 500 ml suspension culture at $2.5x10^6$ cells/ml, infected with an MOI of 0.05 and harvested 96 hours post-infection. The resultant supernatant was subjected to IMAC purification, with subsequent analysis of the IMAC samples performed by Western-blotting (Fig. 5.13 E); this confirmed that the majority of secreted rFc-ßNGF-$(His)_6$ could be purified and concentrated, although remaining detectable only by immuno-blotting.

5.2.12 Purified rFc-ßNGF-$(His)_6$ retains significant biological activity

Binding of ßNGF to TrkA induces intracellular transphosphorylation, with ERK 1/2 being major downstream effectors (Mitchell et al., 2012). Although the protein yield could not be determined, to ascertain whether the purified rFc-ßNGF-$(His)_6$ was functional and capable of activating TrkA, a qualitative but sensitive phosphorylation assay was performed (Fig. 5.14 A). PC-12 cells which had been serum-starved overnight to reduce background phosphorylation were treated for up to 1 hour with purified rFc-ßNGF-$(His)_6$, or a 2.5S NGF as a positive control. Lysates from untreated cells (0 minutes) and those treated for 15, 30 and 60 minutes were harvested and subjected to Western-blotting with antibodies against phosphorylated-ERK 1/2, unphosphorylated ERK 1/2 and SNAP-25 which functioned as a loading control. Analysis of the resultant blot confirmed that rFc-ßNGF-$(His)_6$ treatment induced phosphorylation of ERK 1/2, corresponding to a reduction in signal for the unphosphorylated isoform. The phosphorylated ERK 1/2 signal was found to decrease over time, corroborating the transient nature of ERK 1/2 phosphorylation (Adachi et al., 2002).

With a degree of rFc-ßNGF-$(His)_6$ functionality established, a more qualitative appraisal of its activity was performed using an established PC-12 survival assay (Gazzano-Santoro et al., 1999). In prolonged serum withdrawal PC-12 cells perish, but the presence of ßNGF dose-dependently promotes their survival. Treatment of serum-starved PC-12 cells with either increasing volumes of purified rFc-ßNGF-$(His)_6$, or concentrations of commercial 2.5S NGF, revealed that 10 µl rFc-ßNGF-$(His)_6$ retained functional activity equivalent to 10 ng/ml of commercial 2.5S NGF (Fig. 5.14 B). The potency of rFc-ßNGF-$(His)_6$ was further reflected by the degree of PC-12 neurite outgrowth induced by 1:100 dilution of purified sample being comparable to that induced by 50 ng/ml 2.5S NGF (Fig. 5.14 C). Together these results indicated that despite its low protein concentration, purified rFc-ßNGF-$(His)_6$ possessed significant biological activity.

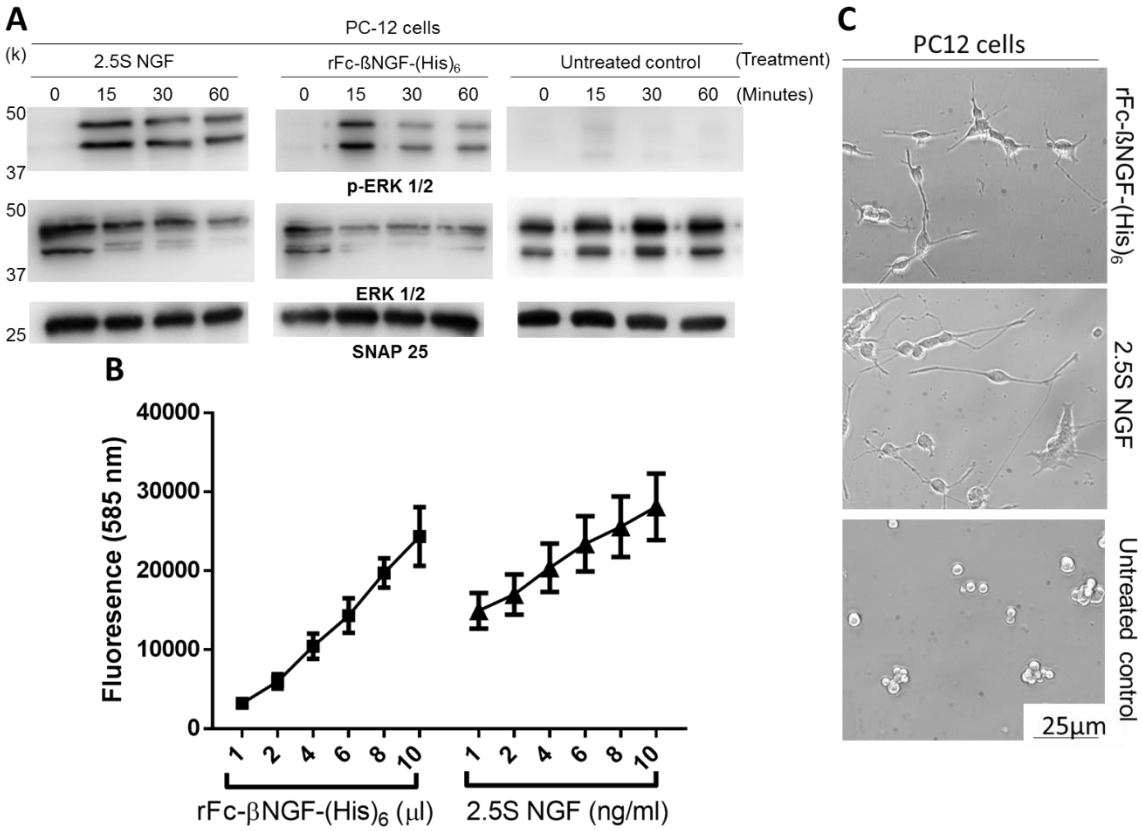

Figure 5. 14 Functional characterization of purified rFc-ßNGF-$(His)_6$

(**A**) PC-12 cells seeded at $4x10^4$ cells per well in a 12-well plate were cultured overnight at 37°C, 5% $C0_2$ in serum-free medium prior to treatment with 100 ng/ml 2.5S NGF or 100 µl of rFc-ßNGF-$(His)_6$. Cells were incubated for up to 60 minutes, washed once with ice-cold PBS, lysed and subjected to Western-blotting using antibodies against p-ERK1/2, ERK1/2 and SNAP-25. (**B**) PC-12 cells, seeded at $4x10^4$ per well in a 24-well plate in serum-free medium, were incubated with indicated dilution of either 2.5S NGF or purified rFc-ßNGF-$(His)_6$ in a final volume of 500 µl for 48 hours at 37°C, 5% $C0_2$. AlamarBLUE™ (50 µl) was added to each well and incubated for a further 24 hours prior to measurement of fluorescence (excitation 570 nm, emission 585 nm). Data plotted are means ± S.E.M, n=3. (**C**) PC-12 cells seeded at $1x10^4$ per well in a 12-well plate, were treated with 10 µl of purified rFc-ßNGF-$(His)_6$ or 50 ng/ml 2.5S NGF diluted directly into 1 ml of culture medium. Cells were incubated for 96 hours at 37°C, 5% $C0_2$, prior to image acquisition. Images chosen are representative (n=10 for each condition).

5.2.13 Coupling of LC.H_N/A-SpA-B_{mut} to rFc-ßNGF increases delivery of the SNARE protease into PC-12 cells

Purified rFc-ßNGF-$(His)_6$ efficiently coupled to agarose immobilized GST-LC.H_N/A-SpA-B_{mut}, as detected by Western-blotting using an anti-ßNGF antibody (Fig. 5.15 A). The resultant complex (LC.H_N/A-SpA-B_{mut}-rFc-ßNGF) was released from the agarose associated GST by thrombin cleavage, which also arbitrated removal of the $(His)_6$ tag. PC-12 cells treated with LC.H_N/A-SpA-B_{mut}-rFc-ßNGF or untargeted control were lysed and subjected to Western-blotting with antibodies against either α-Tubulin or SNAP-$25_{/A}$ (Fig. 5.15 B and C). Subsequent analysis confirmed that coupled rFc-ßNGF was able to productively target LC.H_N/A-SpA-B_{mut} despite the low incidence of complex, and produced a significant increase in SNAP-25 cleavage over that of the untargeted control.

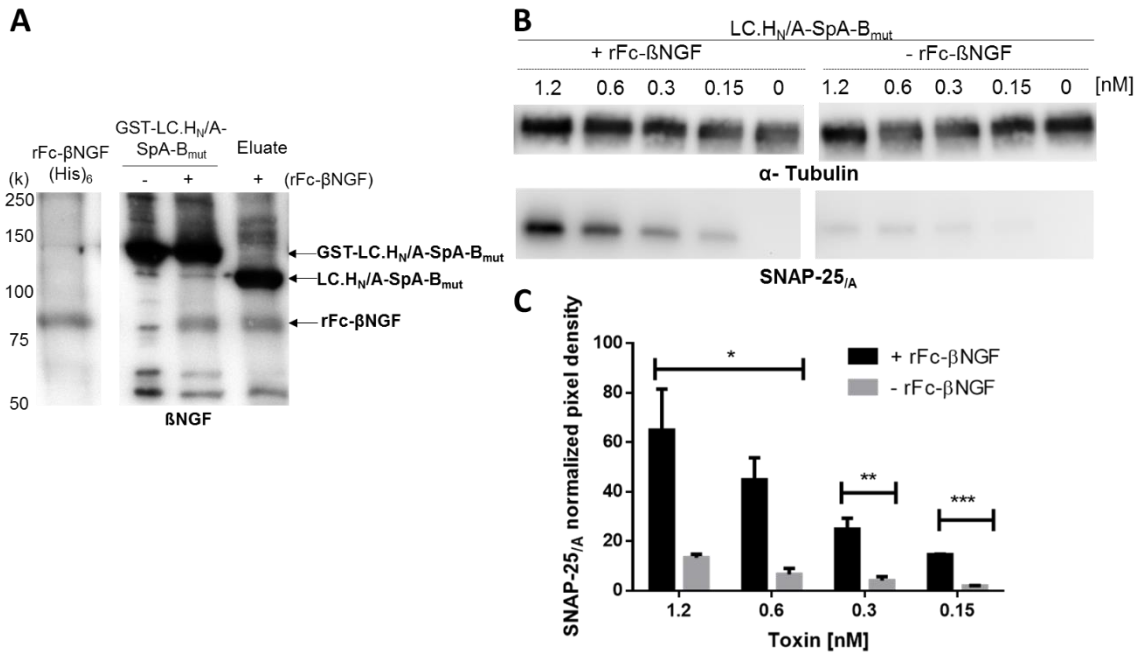

Figure 5. 15 LC.H_N/A-SpA-B_{mut} couples to rFc-ßNGF, which targets the SNARE protease into PC-12 cells

(**A**) Glutathione-agarose immobilized GST-LC.H_N/A-SpA-B_{mut} was incubated with 200 µl of purified rFc-ßNGF-$(His)_6$ for 2 hours at 4°C, followed by washing with PBS. LC.H_N/A-SpA-B_{mut} coupled to rFc-ßNGF was released from agarose-bound GST by cleavage with thrombin protease, which also removed the $(His)_6$ purification tag. Samples of the agarose before and after rFc-ßNGF-$(His)_6$ incubation, and the eluate following thrombin treatment, were subjected to SDS-PAGE followed by Western-blotting with an anti-ßNGF antibody. (**B**) PC-12 cells were seeded at $4x10^5$ per well in a 24-well plate, and treated with indicated concentration of LC.H_N/A-SpA-B_{mut} (+/- coupled rFc-βNGF) for 48 hours prior to preparation of cell lysates; these were subjected to Western-blotting with antibodies against α-Tubulin and SNAP-$25_{/A}$. (**C**) Densitometric analysis of data from (**B**). Data plotted are means ± S.E.M, normalized against α-Tubulin as a loading control; n=3 from independent experiments. Statistical analysis was carried out by unpaired t-test: * $p < 0.05$, ** $p < 0.01$, *** $p < 0.001$.

5.2.14 rFc-ßNGF and anti-TrkA IgG mediate comparable delivery of protease into PC-12 cells

To assess the relative abilities of rFc-ßNGF or anti-TrkA IgG to mediate protease delivery into PC-12 cells, the respective proteins were coupled to LC.H_N/A-SpA-B_{mut} as previously described, and PC-12 cells were treated in parallel with the resultant conjugates. Subsequent Western-blotting of the cell lysates revealed comparable levels of cleaved SNAP-25 for both targeting moieties (Fig. 5.16 A and B). When consideration is made for the proportion of IgG coupled to LC.H_N/A-SpA-B_{mut} relative to that coupled to rFc-ßNGF, it can be surmised that rFc-ßNGF mediated targeting is significantly more efficient than its IgG counterpart.

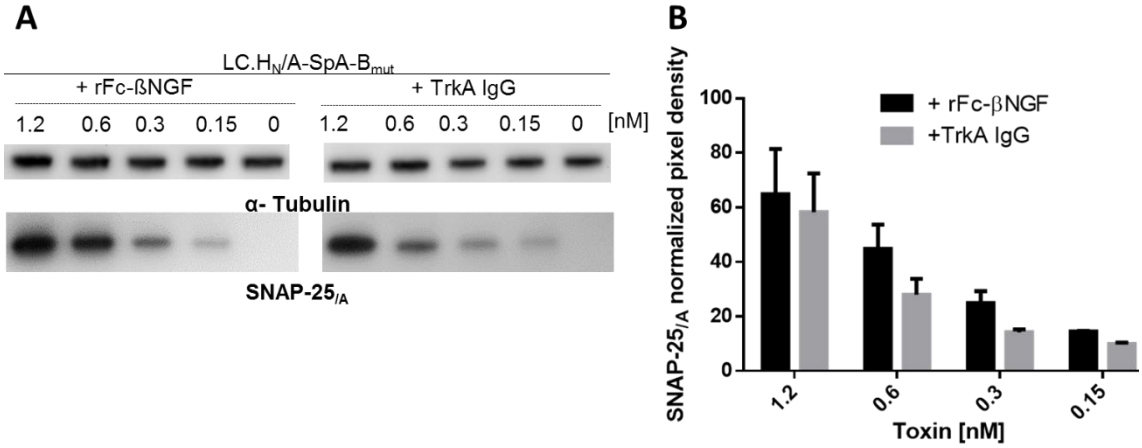

Figure 5. 16 rFc-ßNGF and anti-TrkA IgG mediate delivery of comparable levels of SNARE protease into PC-12 cells

(**A**) PC-12 cells seeded at $4x10^5$ per well in a 24-well plate were treated with the indicated concentrations of LC.H_N/A-SpA-B_{mut} coupled to either rFc-βNGF or anti-TrkA IgG. Cells were incubated for 48 hours prior to the preparation of cell lysates and Western-blotting subsequently performed with antibodies against α-Tubulin and SNAP-$25_{/A}$. (**C**) Densitometric analysis of data from (**B**). Data plotted are means ± S.E.M, normalized against α-Tubulin as a loading control; n=3 from independent experiments. Statistical analysis was carried out by unpaired t-test: * $p < 0.05$, ** $p < 0.01$, *** $p < 0.001$. (**B**) Densitometric analysis of data from (**A**). Data plotted are means ± S.E.M, normalized against α-Tubulin as a loading control; n=3 from independent experiments. n.s. $p > 0.05$.

5.3 Discussion

The SpA-B_{mut} strategy was conceived, and designed, to address the experienced short-comings of both the protein fusion and stapling conjugation methods. The delivery of the LC.H_N/A-SpA-B_{mut} into TrkA-expressing PC-12 cells, following coupling to either rFc-ßNGF or anti-TrkA IgG, demonstrates the success of the approach. Moreover, it highlights the versatility of the strategy, enabling rapid conjugation of the BoNT core-

therapeutic to diverse targeting ligands; this represents a major innovation as no other published protein conjugation strategy is applicable to the coupling of both IgG and recombinant ligands.

Significantly, rFc-ßNGF delivered LC.H_N/A-SpA-B_{mut} into PC-12 cells with efficiency comparable to considerably higher concentrations of coupled anti-TrkA IgG. As targeted therapeutics exhibit different internalization pathways, dependent upon their targeting ligand (Madshus et al., 1991, Fonfria et al., 2016), it can be concluded that the substantial biological activity of rFc-ßNGF negates the low occurrence of coupled complex. Although the concentration of rFc-ßNGF could not be determined, PC-12 cells were treated with a maximum of 1.2 nM of LC.H_N/A-SpA-B_{mut}, and of this only a proportion, likely corresponding to very low pM concentrations, was coupled to rFc-ßNGF. The considerable SNAP-25 cleavage achieved in spite of this demonstrates the significant targeting by rFc-ßNGF.

The pervasion of uncoupled LC.H_N/A-SpA-B_{mut} into cells at higher concentrations is consistent with the ability of both the fusion and stapling untargeted controls to intoxicate cells. This, consequently, suggests an inherent constraint in the development of retargeted BoNT/A-based therapeutics in the absence of sufficient yields of high-affinity agonistic ligands. Unfortunately, the difficulty encountered in purifying larger quantities of rFc-ßNGF-$(His)_6$, despite extensive optimization, prohibited higher-efficiency coupling to LC.H_N/A-SpA-B_{mut}. The low yields of soluble rFc-ßNGF-$(His)_6$ are likely a consequence of either the rFc fusion impairing post-translational modifications which the nascent protein undergoes intracellularly in Sf9 cells, or due to a subsequent over-burdening of the Sf9 secretory pathway. It can, however, be predicted that if higher yields were obtained, the delivery of the ßNGF-targeted therapeutic would have been increased considerably.

As exemplified by the multiple BoNT/A derivatives generated in this project, the development of targeted toxins is often constrained by both the availability and suitability of relevant targeting moieties and, thus, the identification, expression, purification and conjugation of the latter is often a rate-limiting step (Masuyer et al., 2014). The SpA-B_{mut} strategy was envisaged as a way in which to overcome this through expedient coupling to commercial IgG, vastly increasing the repertoire of readily available and validated targeting moieties. The feasibility of the approach is demonstrated by the increased

SNAP-25 cleavage detected in PC-12 cells following treatment with anti-TrkA coupled LC.H_N/A-SpA-B_{mut}. Consequently, in addition to its application in the targeting of BoNT/A to cells which express nociceptive transducers, the LC.H_N/A-SpA-B_{mut} core-therapeutic could, potentially, serve as a novel approach for evaluating the ability of targeting antibody candidates to mediate toxin internalization. Preceding techniques for such antibody assessment have involved microscopy (Rappoport, 2008), radiolabelling (Sun et al., 1996), thymidine incorporation (Kuo et al., 2009) or cell viability assays (Mazor et al., 2007). Use of LC.H_N/A-SpA-B_{mut} provides a simplified platform in which IgG can be coupled without requirement for chemical conjugation or cross-linking, and affords assessment of IgG-mediated internalization into an extensive range of target neurons or neuronal cell lines (Oyler et al., 1992, Némoz-Gaillard et al., 1998, Loranger and Linder, 2002) by Western-blotting detection of SNAP-25 cleavage product. This represents a major advance over prior techniques in terms of simplicity and reproducibility of IgG coupling, no compromise of cell-viability and a straightforward detection method.

As the ability of the untargeted LC.H_N/A-SpA-B_{mut} core-therapeutic to intoxicate cells at concentrations which exceed 10 nM is an obvious limitation, it is pertinent that the SpA-B_{mut} conjugation strategy also has potential in the development of targeted toxins supplementary to BoNT/A. The avidity of bacterial proteins for IgG has previously demonstrated potential in the conjugation of both diphtheria toxin and Pseudomonas exotoxin to antibodies (Mazor et al., 2007, Kuo et al., 2009). However, these earlier approaches were restricted to coupling to IgG, and either failed to obtain high-efficiency conjugation, or required chemical crosslinking to stabilize the resultant complex. Furthermore, former approaches made no provision to address binding to IgG Fab, and employed multiple IgG binding domains, which could induce potential for steric hindrance between coupled partners.

The comparable intoxication of PC-12 cells by LC.H_N/A-SpA-B_{mut} coupled to either rFc-ßNGF or anti-TrkA IgG highlights that for the development of targeted therapeutics the activity of the targeting ligand can in fact be more decisive than the proficiency of coupling; particular high-affinity recombinant ligands may serve as more efficient delivery agents than their IgG counterparts. Consequently, in addition to the coupling to IgG, it is significant that the SpA-B_{mut} is also applicable to the conjugation of recombinant ligands. The generation of such ligands is, however, a time-consuming and challenging

exercise, due both to the many steps involved in their generation and the frequent difficulty in retaining their biological activity. In most cases, as with DkTx, the original selection of a ligand is based on a supposition, influenced by information in the literature, that a particular cell-surface receptor represents a viable therapeutic target. The SpA-B_{mut} strategy affords a unique advantage, whereby, the initial utilization of appropriate IgG against a candidate receptor can be used to rapidly investigate its feasibility as a therapeutic target. This preliminary target evaluation can provide solid justification for embarking on recombinant ligand generation, potentially averting months of infertile investment.

The rFC fragment outlined incorporates the IgG hinge region, serving as an adept linker sequence between the targeting ligand and SpA-B_{mut} binding sites, previously exploited in the expression of complex mammalian protein fusions (Park et al., 1998). Furthermore, the expression of Fc-containing fusion proteins has been achieved in bacterial (Ying et al., 2012), mammalian (Czajkowsky et al., 2012), yeast (Higel et al., 2016) and insect cells as described in this Chapter. Moreover, fusion to IgG Fc has been shown to increase yields and solubility of difficult to express proteins in mammalian expression systems (Jue et al., 2010). However, as the binding of SpA to IgG Fc does not require Fc glycosylation (Jefferis et al., 1998), bacterial expression of Fc fusions with targeting ligands, which are more amenable to functional expression than ßNGF, is an attractive consideration.

Chapter 6. General discussion and recommendations for future work

6.1 SpA-B_{mut} strategy represents an advance on preceding approaches for the conjugation of BoNT/A to targeting ligands

Exploitation of BoNTs highly specific, potent and long-lasting inhibition of neurotransmitter release has demonstrated profound therapeutic success in the treatment of an ever-increasing number of pathological conditions (Münchau and Bhatia, 2000, Mahajan and Brubaker, 2007, Luvisetto et al., 2015). The same pharmacological properties which make BoNTs so efficacious, however, also make them the most potent acute lethal toxins known (Lebeda et al., 2008). Consequently, the development of retargeted BoNT-derived therapeutics (commonly termed targeted-secretion inhibitors) which seek to expand the toxins clinical utility while simultaneously reducing the prospect for motor-deficits, is the focus of intense academic and commercial investigation [reviewed by (Foster and Chaddock, 2010, Masuyer et al., 2014)]. Development of such retargeted BoNT/A-based therapeutics is, nevertheless, a complex and challenging endeavour, initially constrained by the identification of suitable cell-surface target receptors and appropriate targeting ligands. Following which, the functional expression, characterization and conjugating of the latter to a BoNT based core-therapeutic serves as a significant rate-limiting step.

The initial strategy of generating a core-therapeutic fusion with a spider-venom peptide (DkTx), was a novel approach which sought to exploit the bivalent and specific binding of the latter to the TRPV1 channel. A fusion approach was perceived as the most efficient means of ligand conjugation, particularly because the chemical coupling of ligands to BoNT domains has been previously demonstrated to reduce toxin activity (Band et al., 2010), or produce conjugation efficiency of only 12-16% (Chaddock et al., 2000a, Duggan et al., 2002). However, the difficulty in purifying and functionally characterizing the LC.H_N.H_{CN}/A-DkTx protein exemplifies the innate challenge in producing high-yields of soluble and biologically active chimeric fusion proteins, particularly those containing ICK motifs (Klint et al., 2013). Furthermore, the process of cloning, expressing, purifying and characterizing each fusion proved laborious and time-consuming and, thus, constrained the number of targeting ligands which could be generated and assessed. This limitation is highlighted by the previously published BoNT targeted fusions, based either on BoNT/C (Foster et al., 2006) or BoNT/A (Fonfria et al., 2016), both employing only EGF as a ligand.

The protein stapling was envisaged as a means to expedite the generation and assessment of targeting ligands, supported by its prior application in the conjugation of LC.H_N/A-SNAP-25 to a panel of 9 targeting ligands (Arsenault et al., 2013). The anticipated advantages of this coupling method were, notwithstanding the experienced issues with the synthetic syntaxin peptide, undermined by the problematic expression, purification and stability of the recombinant components. The supposed flexibility of the approach was further negated by an inability to obtain biologically-active VAMP 2-DkTx, with extensive trouble-shooting required to produce a protein which was ultimately non-functional. Conversely, in the absence of VAMP 2, DkTx expressed with a Trx tag was purified to an appreciable yield and purity, with confirmed biological activity. As the generation of chimeric protein fusions is so unpredictable, optimizing conditions for the production of even a single protein can represent a significant challenge. The protein fusion and protein stapling strategies were, consequently, both deemed inadequate for the development of a retargeted BoNT/A therapeutic, due to the innate difficulty in obtaining soluble, functional and high-proficiency targeting ligands through bacterial expression systems.

The SpA-B_{mut} conjugation strategy addressed this short-coming by its ability to mediate the rapid and high-efficiency coupling of the BoNT/A core-therapeutic to commercially available IgG antibodies, thereby, providing a repertoire of readily available and validated moieties with which to target. Significantly, although the strategy supports the coupling of recombinant ligands tagged with rFc, it does not compel the approach and, thus, confers unique and unrivalled flexibility. The therapeutic potential of targeting antibody-toxin molecules (termed immunotoxins) to pertinent cellular targets is widely investigated as a potential strategy for therapeutic intervention in cancer and other disorders (Antignani and FitzGerald, 2013). There has, however, been only one published example of such a strategy being employed for BoNT retargeting: conjugation of a BoNT/A-based core-therapeutic to an ScFv targeting $P2X_3$ (Ma et al., 2014). This previous approach, although somewhat successful at mediating toxin targeting to $P2X_3$ expressing DRGs, employed a single antibody chain and, thus, only a single epitope binding domain. A significant advantage of immunotoxins which employ whole antibodies, in addition to their high-specificity, is the bivalent nature of the targeting antibodies. The binding of an antibody to either dual epitopes on a distinct cell-surface receptor, or to adjacent receptors, can induce their crosslinking, which normally results in internalization of the antibody-toxin

complex (Schmidt et al., 2008). As the SpA-B_{mut} strategy enables coupling to whole IgG, it can exploit this advantageous attribute which, potentially, could facilitate the proficient targeting of BoNT/A to diverse membrane targets, including those for which there is no-known ligand. Although further comprehensive assessment of such targeting is required, the demonstrated coupling of LC.H_N/A-SpA-B_{mut} to commercial IgG, followed by the increased binding and detectable delivery of the TrkA-targeted toxin into PC-12 cells, establishes the proof of principle for this innovative and versatile approach.

6.2 Intoxication of cells by each of the untargeted BoNT/A core-therapeutics highlights an inherent flaw in their current design

The contribution of the H_{CN} sub-domain to neuronal binding, as outlined in Chapter 3, was initially perceived as a disadvantage for BoNT retargeting, promoting the association of the untargeted fusion control with cultured TGNs. However, as detailed in Chapters 4 and 5, the subsequent untargeted controls, containing only the LC.H_N/A domains, were also capable of intoxicating TGNs, SH-SY5Y and PC-12 cells. The significant finding that full-length BoNT/A containing a single mutation of W985L in the H_{CN} sub-domain retains high-affinity saturatable binding to cultured CGNs, but demonstrates reduced toxin internalization, suggests that this sub-domain is indispensable for the efficient delivery of the SNARE protease. Evidently, replacing the whole H_C domain of BoNT/A with exogenous binding moieties produces deficiencies in subsequent steps essential for cytosolic delivery of the LC protease. This necessitates higher concentrations of targeted toxins and longer cell treatments which, consequently, affords the untargeted controls increased opportunity to intoxicate cells. Future focus in the development of retargeted BoNT/A therapeutics should, therefore, be in maximising the efficiency of targeted delivery, and not in attempts to minimise the delivery of the untargeted control.

This implies that the LC.H_N domains utilized in all retargeted BoNTs published to-date are inadequate, and that future BoNT-based core-therapeutics must also incorporate the H_{CN}. Further to this, as the BoNT/A residues involved in binding to SV2 have been published (Benoit et al., 2014, Strotmeier et al., 2014), prospective BoNT/A therapeutics may prove even more effective if the core-therapeutic contains full-length toxin but with mutated SV2 binding sites. This progressive approach would afford the full advantage of the adeptly-evolved BoNT/A internalization and translocation mechanics, preserving native interactions between toxin domains and the neuronal membrane, without risk of

high-affinity binding to neuronal acceptors. The specificity of binding could then be conferred by the employed targeting ligand which, in tandem with H_{CC} ganglioside binding, the established contribution of the H_{CN} to binding/internalization and its suggested involvement to LC translocation (Muraro et al., 2009) could, potentially, prove a far more proficient means of delivering the SNARE protease into target cells.

A version of the described strategy was attempted in Chapter 3, in which a construct encoding a chimeric fusion of LC.H_N.H_{CN}/A and H_{CC}/B_{mut} was generated. The inability to purify the resultant protein following recombinant expression, or the cognate protein which additionally contained DkTx, reaffirms the inherent challenge in producing novel protein fusions. It is conceivable however, considering the expression and purification of LC.H_N/A-SNAP-25, that LC.H_N.H_{CN}/A-H_{CC}/B_{mut} may have been more amenable to recombinant expression if the pGEX-KG vector and associated GST tag had been employed.

Although LC.H_N/A-SpA-B_{mut} coupled to anti-TrkA IgG demonstrated a significant increase in binding to PC-12 cells relative to the untargeted control, this did not correlate with the proficient intracellular delivery of the SNARE protease. It can be surmised, therefore, that the comparatively low degree of SNAP-25 cleavage detected is due either to a deficit in the subsequent internalization of the complex, or inefficient cytoplasmic translocation of the LC. To this end, the generation of a novel full-length SV2 binding deficient core-therapeutic (BoNT/A_{mut}-SpA-B_{mut}) could, conceivably, rectify this significant limitation; this, in combination with the efficacy of IgG coupling, could establish the SpA-B_{mut} strategy as the preeminent method for developing future retargeted BoNT/A therapeutics.

6.3 ßNGF-mediated targeting of TrkA represents a viable potential strategy for delivery of retargeted BoNT/A-based pain therapeutics

The applicability of the SpA-B_{mut} approach to not only IgG coupling, but also to the conjugation of the core-therapeutic to recombinant ligands, is a significant advance on preceding techniques. This approach is, nonetheless, still constrained by the need to recombinantly express fusion proteins. Employment of baculovirus-mediated expression of rFc-ßNGF-$(His)_6$ in insect cells was envisaged as a way to circumvent the limitations of the bacterial expression systems. Significantly, despite the low protein yields, Sf9 cells were capable of producing biologically-active rFc-ßNGF-$(His)_6$, which could be coupled

to LC.H_N/A-SpA-B_{mut}. Although the conjugation of rFc-ßNGF to the core-therapeutic was only detectable by immuno-blotting, the considerable functional activity of ßNGF was sufficient to negate the low occurrence of coupled complex, delivering the SNARE protease into PC-12 cells equivalent to significantly higher concentrations of anti-TrkA IgG. This confirms that for retargeted BoNT core-therapeutics which employ the isolated LC.H_N domains, it is essential to employ a ligand that is not only specific and has high-affinity, but one which is also adept at inducing the internalization of its receptor.

The suggestion that a novel BoNT/A_{mut}-SpA-B_{mut} core-therapeutic may improve the IgG targeted delivery of the SNARE protease into cells is, at this stage, hypothetical. Accordingly, it is still necessary to consider utilization of other targeting ligands. The high-efficiency with which rFC-ßNGF was shown to deliver the SNARE protease into PC-12 cells establishes its suitability as an effective ligand for the targeting of LC.H_N/A-SpA-B_{mut} to TrkA-expressing cells. The NGF mediated delivery of SNAP-25 protease into PC-12 cells has also been achieved following its coupling to a BoNT/A derivative lacking the H_C (Chaddock et al., 2000a). In this instance, however, the removal of the H_C was achieved not by recombinant means as with LC.H_N/A-SpA-B_{mut}, but by trypsin protease digestion; which can produce a heterogeneous LC.H_N/A fragment (Shone et al., 1985). Furthermore, NGF was purchased commercially and subsequently conjugated via chemical cross-linking using Traut's reagent. This approach required an input of 2 mg of NGF to achieve ~250 µg of conjugated product, with higher efficiency linkage constrained by the susceptibility of LC to over derivatisation resulting in loss of enzymatic activity. Despite these limitations, chemical coupling of NGF targeted the SNAP-25 protease into PC-12 cells with an IC_{50} of 1.8 nM. This confirms, unequivocally, that for the development of targeted BoNT/A based therapeutics the affinity of the targeting ligand and the consequence of its receptor interaction, are absolutely paramount. Consequently, ßNGF-mediated targeting of TrkA represents a viable potential strategy for the future development of nociceptor retargeted BoNT/A-based pain therapeutics.

While the increased levels of SNAP-25 cleavage achieved by LC.H_N/A-SpA-B_{mut}-rFc-ßNGF over the untargeted control is encouraging, this serves only as an initial proof of principle. A considerable challenge remains in generating sufficient quantities of material for a comprehensive assessment of the consequences of SNAP-25 truncation on exocytosis and channel surface localization *in vitro* and, potentially, of the anti-nociceptive efficacy *in vivo*.

References

ABDULL RAZIS, A. F., ISMAIL, E. N., HAMBALI, Z., ABDULLAH, M. N. H., ALI, A. M. & MOHD LILA, M. A. 2008. Expression of Recombinant Human Epidermal Growth Factor in Escherichia coli and Characterization of its Biological Activity. *Applied Biochemistry and Biotechnology,* 144**,** 249-261.

ADACHI, T., KAR, S., WANG, M. & CARR, B. I. 2002. Transient and sustained ERK phosphorylation and nuclear translocation in growth control. *Journal of Cellular Physiology,* 192**,** 151-159.

ALOE, L., TUVERI, M. A., CARCASSI, U. & LEVI-MONTALCINI, R. 1992. Nerve growth factor in the synovial fluid of patients with chronic arthritis. *Arthritis & Rheumatism,* 35**,** 351-355.

ANTIGNANI, A. & FITZGERALD, D. 2013. Immunotoxins: The role of the toxin (†). *Toxins,* 5**,** 1486-1502.

AOKI, K. R. 2005. Review of a Proposed Mechanism for the Antinociceptive Action of Botulinum Toxin Type A. *NeuroToxicology,* 26**,** 785-793.

ARSENAULT, J., FERRARI, E., NIRANJAN, D., CUIJPERS, S. A. G., GU, C., VALLIS, Y., O'BRIEN, J. & DAVLETOV, B. 2013. Stapling of the botulinum type A protease to growth factors and neuropeptides allows selective targeting of neuroendocrine cells. *Journal of Neurochemistry,* 126**,** 223-233.

ATASSI, M. Z., TARUISHI, M., NAQVI, M., STEWARD, L. E. & AOKI, K. R. 2014. Synaptotagmin II and Gangliosides Bind Independently with Botulinum Neurotoxin B but Each Restrains the Other. *The Protein Journal,* 33**,** 278-288.

AVERILL, S., MCMAHON, S. B., CLARY, D. O., REICHARDT, L. F. & PRIESTLEY, J. V. 1995. Immunocytochemical localization of TrkA receptors in chemically identified subgroups of adult rat sensory neurons. *European Journal of Neuroscience,* 7**,** 1484-1494.

AYYAR, B. V., AOKI, K. R. & ATASSI, M. Z. 2015. The C-Terminal Heavy-Chain Domain of Botulinum Neurotoxin A Is Not the Only Site That Binds Neurons, as the N-Terminal Heavy-Chain Domain Also Plays a Very Active Role in Toxin-Cell Binding and Interactions. *Infection and Immunity,* 83**,** 1465-1476.

AYYAR, B. V. & ATASSI, M. Z. 2016. Effects of membrane properties on the binding activities of the HN and HC heavy-chain domains of botulinum neurotoxin A. *Biochimica et Biophysica Acta (BBA) - Proteins and Proteomics,* 1864**,** 1678-1685.

AZARNIA TEHRAN, D., ZANETTI, G., LEKA, O., LISTA, F., FILLO, S., BINZ, T., SHONE, C. C., ROSSETTO, O., MONTECUCCO, C., PARADISI, C., MATTAREI, A. & PIRAZZINI, M. 2015. A Novel Inhibitor Prevents the Peripheral Neuroparalysis of Botulinum Neurotoxins. *Scientific Reports,* 5**,** 17513.

BAE, C., KALIA, J., SONG, I., YU, J., KIM, H. H., SWARTZ, K. J. & KIM, J. I. 2012. High Yield Production and Refolding of the Double-Knot Toxin, an Activator of TRPV1 Channels. *PLoS ONE,* 7**,** e51516.

BAND, P. A., BLAIS, S., NEUBERT, T. A., CARDOZO, T. J. & ICHTCHENKO, K. 2010. Recombinant derivatives of botulinum neurotoxin A engineered for trafficking studies and neuronal delivery. *Protein Expression and Purification,* 71**,** 62-73.

BAUM, C., HASLINGER-LÖFFLER, B., WESTH, H., BOYE, K., PETERS, G., NEUMANN, C. & KAHL, B. C. 2009. Non-spa-typeable clinical Staphylococcus aureus strains are naturally occurring Protein A mutants. *Journal of Clinical Microbiology,* 47**,** 3624-3629.

BAUTISTA, D. M., SIEMENS, J., GLAZER, J. M., TSURUDA, P. R., BASBAUM, A. I., STUCKY, C. L., JORDT, S.-E. & JULIUS, D. 2007. The menthol receptor TRPM8 is the principal detector of environmental cold. *Nature,* 448**,** 204-208.

BENOIT, R. M., FREY, D., HILBERT, M., KEVENAAR, J. T., WIESER, M. M., STIRNIMANN, C. U., MCMILLAN, D., CESKA, T., LEBON, F., JAUSSI, R., STEINMETZ, M. O., SCHERTLER, G. F.

X., HOOGENRAAD, C. C., CAPITANI, G. & KAMMERER, R. A. 2014. Structural basis for recognition of synaptic vesicle protein 2C by botulinum neurotoxin A. *Nature,* 505**,** 108-111.

BERKMEN, M. 2012. Production of disulfide-bonded proteins in Escherichia coli. *Protein Expression and Purification,* 82**,** 240-251.

BERNTSSON, R. P. A., PENG, L., DONG, M. & STENMARK, P. 2013. Structure of dual receptor binding to botulinum neurotoxin B. *Nature Communications,* 4**,** 2058.

BIGALKE, H., DREYER, F. & BERGEY, G. 1985. Botulinum a neurotoxin inhibits non-cholinergic synaptic transmission in mouse spinal cord neurons in culture. *Brain Research,* 360**,** 318-324.

BLACKSHAW, L. A., PAGE, A. J. & YOUNG, R. L. 2011. Metabotropic Glutamate Receptors as Novel Therapeutic Targets on Visceral Sensory Pathways. *Frontiers in Neuroscience,* 5**,** 40.

BOHLEN, C. J., PRIEL, A., ZHOU, S., KING, D., SIEMENS, J. & JULIUS, D. 2010. A Bivalent Tarantula Toxin Activates the Capsaicin Receptor, TRPV1, by Targeting the Outer Pore Domain. *Cell,* 141**,** 834-845.

BONNINGTON, J. K. & MCNAUGHTON, P. A. 2003. Signalling pathways involved in the sensitisation of mouse nociceptive neurones by nerve growth factor. *The Journal of Physiology,* 551**,** 433-446.

BREIDENBACH, M. A. & BRUNGER, A. T. 2004. Substrate recognition strategy for botulinum neurotoxin serotype A. *Nature,* 432**,** 925-929.

BREIDENBACH, M. A. & BRUNGER, A. T. 2005. New insights into clostridial neurotoxin-SNARE interactions. *Trends in Molecular Medicine,* 11**,** 377-381.

BREIVIK, H., COLLETT, B., VENTAFRIDDA, V., COHEN, R. & GALLACHER, D. 2006. Survey of chronic pain in Europe: Prevalence, impact on daily life, and treatment. *European Journal of Pain,* 10**,** 287-287.

BRIDGES, D., THOMPSON, S. W. N. & RICE, A. S. C. 2001. Mechanisms of neuropathic pain. *British Journal of Anaesthesia,* 87**,** 12-26.

BRONFMAN, F. C., TCHERPAKOV, M., JOVIN, T. M. & FAINZILBER, M. 2003. Ligand-Induced Internalization of the p75 Neurotrophin Receptor: A Slow Route to the Signaling Endosome. *The Journal of Neuroscience,* 23**,** 3209-3220.

BURGESS-BROWN, N. A., SHARMA, S., SOBOTT, F., LOENARZ, C., OPPERMANN, U. & GILEADI, O. 2008. Codon optimization can improve expression of human genes in Escherichia coli: A multi-gene study. *Protein Expression and Purification,* 59**,** 94-102.

BUXSER, S., VROEGOP, S., DECKER, D., HINZMANN, J., POORMAN, R., THOMSEN, D. R., STIER, M., ABRAHAM, I., GREENBERG, B. D., HATZENBUHLER, N. T., SHEA, M., CURRY, K. A. & TOMICH, C.-S. C. 1991. Single-step purification and biological activity of human nerve growth factor produced from insect cells. *Journal of Neurochemistry,* 56**,** 1012-1018.

CARR, C. M. & MUNSON, M. 2007. Tag team action at the synapse. *EMBO Reports,* 8**,** 834-838.

CHADDOCK, J. A., PURKISS, J. R., DUGGAN, M. J., QUINN, C. P., SHONE, C. C. & FOSTER, K. A. 2000a. A Conjugate Composed of Nerve Growth Factor Coupled to a Non-toxic Derivative of Clostridium botulinum Neurotoxin Type A can Inhibit Neurotransmitter Release in Vitro. *Growth Factors,* 18**,** 147-155.

CHADDOCK, J. A., PURKISS, J. R., FRIIS, L. M., BROADBRIDGE, J. D., DUGGAN, M. J., FOOKS, S. J., SHONE, C. C., QUINN, C. P. & FOSTER, K. A. 2000b. Inhibition of Vesicular Secretion in Both Neuronal and Nonneuronal Cells by a Retargeted Endopeptidase Derivative of Clostridium botulinum Neurotoxin Type A. *Infection and Immunity,* 68**,** 2587-2593.

CHAHINE, M. & O'LEARY, M. E. 2014. Regulation/Modulation of Sensory Neuron Sodium Channels. *In:* RUBEN, P. C. (ed.) *Voltage Gated Sodium Channels.* Berlin, Heidelberg: Springer Berlin Heidelberg.

CHAPMAN, E. R. 2008. How Does Synaptotagmin Trigger Neurotransmitter Release? *Annual Review of Biochemistry,* 77**,** 615-641.

CLARY, D. O., WESKAMP, G., AUSTIN, L. R. & REICHARDT, L. F. 1994. TrkA cross-linking mimics neuronal responses to nerve growth factor. *Molecular Biology of the Cell,* 5**,** 549-563.
CONWAY, S. J. 2008. TRPing the switch on pain: an introduction to the chemistry and biology of capsaicin and TRPV1. *Chemical Society Reviews,* 37**,** 1530-1545.
COSTA, S., ALMEIDA, A., CASTRO, A. & DOMINGUES, L. 2014. Fusion tags for protein solubility, purification and immunogenicity in Escherichia coli: the novel Fh8 system. *Frontiers in Microbiology,* 5**,** 63.
CRAIK, D. J., DALY, N. L. & WAINE, C. 2001. The cystine knot motif in toxins and implications for drug design. *Toxicon,* 39**,** 43-60.
CUI, M., KHANIJOU, S., RUBINO, J. & AOKI, K. R. 2004. Subcutaneous administration of botulinum toxin A reduces formalin-induced pain. *Pain,* 107**,** 125-133.
CZAJKOWSKY, D. M., HU, J., SHAO, Z. & PLEASS, R. J. 2012. Fc-fusion proteins: new developments and future perspectives. *EMBO Molecular Medicine,* 4**,** 1015-1028.
DARIOS, F., NIRANJAN, D., FERRARI, E., ZHANG, F., SOLOVIEV, M., RUMMEL, A., BIGALKE, H., SUCKLING, J., USHKARYOV, Y., NAUMENKO, N., SHAKIRZYANOVA, A., GINIATULLIN, R., MAYWOOD, E., HASTINGS, M., BINZ, T. & DAVLETOV, B. 2010. SNARE tagging allows stepwise assembly of a multimodular medicinal toxin. *Proceedings of the National Academy of Sciences,* 107**,** 18197-18201.
DE LA PEÑA, E., MÄLKIÄ, A., CABEDO, H., BELMONTE, C. & VIANA, F. 2005. The contribution of TRPM8 channels to cold sensing in mammalian neurons. *The Journal of Physiology,* 567**,** 415-426.
DE PINHEIRO, C. G. M., PEDROSA, M. D. O., TEIXEIRA, N. C., ANO BOM, A. P. D., VAN OERS, M. M. & OLIVEIRA, G. G. D. S. 2016. Optimization of canine interleukin-12 production using a baculovirus insect cell expression system. *BMC Research Notes,* 9**,** 36.
DEIS, L. N., PEMBLE, C. W., QI, Y., HAGARMAN, A., RICHARDSON, D. C., RICHARDSON, J. S. & OAS, T. G. 2014. Multiscale conformational heterogeneity in the protein-binding domains of staphylococcal protein A: possible determinant of functional plasticity. *Structure (London, England : 1993),* 22**,** 1467-1477.
DEISENHOFER, J. 1981. Crystallographic refinement and atomic models of a human Fc fragment and its complex with fragment B of protein A from Staphylococcus aureus at 2.9- and 2.8-.ANG. resolution. *Biochemistry,* 20**,** 2361-2370.
DEVAL, E., NOËL, J., LAY, N., ALLOUI, A., DIOCHOT, S., FRIEND, V., JODAR, M., LAZDUNSKI, M. & LINGUEGLIA, E. 2008. ASIC3, a sensor of acidic and primary inflammatory pain. *The EMBO Journal,* 27**,** 3047-3055.
DIERING, G. H., NUMATA, Y., FAN, S., CHURCH, J. & NUMATA, M. 2013. Endosomal acidification by Na(+)/H(+) exchanger NHE5 regulates TrkA cell-surface targeting and NGF-induced PI3K signaling. *Molecular Biology of the Cell,* 24**,** 3435-3448.
DONG, M., YEH, F., TEPP, W. H., DEAN, C., JOHNSON, E. A., JANZ, R. & CHAPMAN, E. R. 2006. SV2 Is the Protein Receptor for Botulinum Neurotoxin A. *Science,* 312**,** 592.
DOVER, N., BARASH, J. R., HILL, K. K., XIE, G. & ARNON, S. S. 2013. Molecular Characterization of a Novel Botulinum Neurotoxin Type H Gene. *Journal of Infectious Diseases*.
DUBIN, A. E. & PATAPOUTIAN, A. 2010. Nociceptors: the sensors of the pain pathway. *The Journal of Clinical Investigation,* 120**,** 3760-3772.
DUGGAN, M. J., QUINN, C. P., CHADDOCK, J. A., PURKISS, J. R., ALEXANDER, F. C. G., DOWARD, S., FOOKS, S. J., FRIIS, L. M., HALL, Y. H. J., KIRBY, E. R., LEEDS, N., MOULSDALE, H. J., DICKENSON, A., GREEN, G. M., RAHMAN, W., SUZUKI, R., SHONE, C. C. & FOSTER, K. A. 2002. Inhibition of Release of Neurotransmitters from Rat Dorsal Root Ganglia by a Novel Conjugate of a Clostridium botulinum Toxin A Endopeptidase Fragment and Erythrina cristagalli Lectin. *Journal of Biological Chemistry,* 277**,** 34846-34852.
DURHAM, P. L., CADY, R. & CADY, R. 2004. Regulation of Calcitonin Gene-Related Peptide Secretion From Trigeminal Nerve Cells by Botulinum Toxin Type A: Implications for Migraine Therapy. *Headache: The Journal of Head and Face Pain,* 44**,** 35-43.

EHLERS, M. D., KAPLAN, D. R., PRICE, D. L. & KOLIATSOS, V. E. 1995. NGF-stimulated retrograde transport of trkA in the mammalian nervous system. *The Journal of Cell Biology,* 130**,** 149-156.

EID, S. R., CROWN, E. D., MOORE, E. L., LIANG, H. A., CHOONG, K.-C., DIMA, S., HENZE, D. A., KANE, S. A. & URBAN, M. O. 2008. HC-030031, a TRPA1 selective antagonist, attenuates inflammatory- and neuropathy-induced mechanical hypersensitivity. *Molecular Pain,* 4**,** 48-48.

ERBGUTH, F. J. 2004. Historical notes on botulism, Clostridium botulinum, botulinum toxin, and the idea of the therapeutic use of the toxin. *Movement Disorders,* 19**,** S2-S6.

ERHU, C., MAOFU, L., YIFAN, C. & DAVID, J. 2013. TRPV1 structures in distinct conformations reveal activation mechanisms. *Nature,* 504**,** 113-118.

FANG, X., DJOUHRI, L., MCMULLAN, S., BERRY, C., OKUSE, K., WAXMAN, S. G. & LAWSON, S. N. 2005. TrkA Is Expressed in Nociceptive Neurons and Influences Electrophysiological Properties via Nav1.8 Expression in Rapidly Conducting Nociceptors. *The Journal of Neuroscience,* 25**,** 4868-4878.

FERRARI, E., GU, C., NIRANJAN, D., RESTANI, L., RASETTI-ESCARGUEIL, C., OBARA, I., GERANTON, S. M., ARSENAULT, J., GOETZE, T. A., HARPER, C. B., NGUYEN, T. H., MAYWOOD, E., O'BRIEN, J., SCHIAVO, G., WHEELER, D. W., MEUNIER, F. A., HASTINGS, M., EDWARDSON, J. M., SESARDIC, D., CALEO, M., HUNT, S. P. & DAVLETOV, B. 2013. Synthetic Self-Assembling Clostridial Chimera for Modulation of Sensory Functions. *Bioconjugate Chemistry,* 24**,** 1750-1759.

FERRARI, E., SOLOVIEV, M., NIRANJAN, D., ARSENAULT, J., GU, C., VALLIS, Y., O'BRIEN, J. & DAVLETOV, B. 2012. Assembly of protein building blocks using a short synthetic peptide. *Bioconjug. Chem.,* 23**,** 479-484.

FISCHER, A., MUSHRUSH, D. J., LACY, D. B. & MONTAL, M. 2008. Botulinum Neurotoxin Devoid of Receptor Binding Domain Translocates Active Protease. *PLoS Pathog,* 4**,** e1000245.

FISCHER, A., SAMBASHIVAN, S., BRUNGER, A. T. & MONTAL, M. 2012. Beltless Translocation Domain of Botulinum Neurotoxin A Embodies a Minimum Ion-conductive Channel. *Journal of Biological Chemistry,* 287**,** 1657-1661.

FLYNN, T. 2010. Botulinum toxin: examining duration of effect in facial aesthetic applications. *American Journal of Clinical Dermatology,* 11**,** 183-199.

FONFRIA, E., DONALD, S. & CADD, V. A. 2016. Botulinum neurotoxin A and an engineered derivative targeted secretion inhibitor (TSI) enters cells via different vesicular compartments. *Journal of Receptors and Signal Transduction,* 36**,** 79-88.

FOSTER, K. & CHADDOCK, J. 2010. Targeted secretion inhibitors—innovative protein therapeutics. *Toxins,* 2**,** 2795-2815.

FOSTER, K. A., ADAMS, E. J., DUROSE, L., CRUTTWELL, C. J., MARKS, E., SHONE, C. C., CHADDOCK, J. A., COX, C. L., HEATON, C., SUTTON, J. M., WAYNE, J., ALEXANDER, F. C. G. & ROGERS, D. F. 2006. Re-engineering the target specificity of clostridial neurotoxins - a route to novel therapeutics. *Neurotoxicity Research,* 9**,** 101-107.

FROGER, A. & HALL, J. E. 2007. Transformation of Plasmid DNA into E. coli Using the Heat Shock Method. *Journal of Visualized Experiments : JoVE***,** 253.

GAZZANO-SANTORO, H., CHEN, A., CASTO, B., CHU, H., GILKERSON, E., MUKKU, V., CANOVA-DAVIS, E. & KOTTS, C. 1999. Validation of a rat pheochromocytoma (PC12)-based cell survival assay for determining biological potency of recombinant human nerve growth factor. *Journal of pharmaceutical and biomedical analysis,* 21**,** 945-959.

GODEAU, F., SAUCIER, C. & KOURILSKY, P. 1992. Replication inhibition by nucleoside analogues of a recombinant Autographa californica multicapsid nuclear polyhedrosis virus harboring the herpes thymidine kinase gene driven by the IE-1(0) promoter: a new way to select recombinant baculoviruses. *Nucleic Acids Research,* 20**,** 6239-6246.

GÓMEZ-SEBASTIÁN, S., LÓPEZ-VIDAL, J. & ESCRIBANO, J. M. 2014. Significant Productivity Improvement of the Baculovirus Expression Vector System by Engineering a Novel Expression Cassette. *PLOS ONE,* 9**,** e96562.

GOSWAMI, C., RADEMACHER, N., SMALLA, K.-H., KALSCHEUER, V., ROPERS, H.-H., GUNDELFINGER, E. D. & HUCHO, T. 2010. TRPV1 acts as a synaptic protein and regulates vesicle recycling. *Journal of Cell Science,* 123**,** 2045-2057.

GRIMES, M. L., ZHOU, J., BEATTIE, E. C., YUEN, E. C., HALL, D. E., VALLETTA, J. S., TOPP, K. S., LAVAIL, J. H., BUNNETT, N. W. & MOBLEY, W. C. 1996. Endocytosis of activated TrkA: evidence that nerve growth factor induces formation of signaling endosomes. *J. Neurosci.,* 16**,** 7950-7964.

GUILBERT, A., DHENNIN-DUTHILLE, I., HIANI, Y. E. L., HAREN, N., KHORSI, H., SEVESTRE, H., AHIDOUCH, A. & OUADID-AHIDOUCH, H. 2008. Expression of TRPC6 channels in human epithelial breast cancer cells. *BMC Cancer,* 8**,** 125-125.

HAKES, D. J. & DIXON, J. E. 1992. New vectors for high level expression of recombinant proteins in bacteria. *Analytical Biochemistry,* 202**,** 293-298.

HANAHAN, D., JESSEE, J. & BLOOM, F. R. 1991. Plasmid transformation of Escherichia coli and other bacteria. *Methods Enzymol.* Academic Press.

HERZIG, V. & KING, G. 2015. The Cystine Knot Is Responsible for the Exceptional Stability of the Insecticidal Spider Toxin ω-Hexatoxin-Hv1a. *Toxins,* 7**,** 4366.

HIGEL, F., SEIDL, A., SÖRGEL, F. & FRIESS, W. 2016. N-glycosylation heterogeneity and the influence on structure, function and pharmacokinetics of monoclonal antibodies and Fc fusion proteins. *European Journal of Pharmaceutics and Biopharmaceutics,* 100**,** 94-100.

HOLDENPAUL, H., ASOPA, V., ROBERTSON, A. G. S., CLARKE, A. R., TYLER, S., BENNETT, G. S., BRAIN, S. D., WILCOCK, G. K., ALLEN, S. J., SMITH, S. K. F. & DAWBARN, D. 1997. Immunoglobulin-like domains define the nerve growth factor binding site of the TrkA receptor. *Nat Biotech,* 15**,** 668-672.

HONDA, M., TAKENAKA, A., INOUE, S., CHANCELLOR, M. B. & YOSHIMURA, N. 2012. Sensory Neuron-Specific Receptor-Mediated Regulation of Micturition Reflex in Urethane-Anesthetized Rats. *Bju International,* 109**,** 628-633.

HUANG, J., ZHANG, X. & MCNAUGHTON, P. A. 2006. Inflammatory Pain: The Cellular Basis of Heat Hyperalgesia. *Current Neuropharmacology,* 4**,** 197-206.

HUR, C.-G., CHOE, C., KIM, G.-T., CHO, S.-K., PARK, J.-Y., HONG, S.-G., HAN, J. & KANG, D. 2009. Expression and localization of two-pore domain K+ channels in bovine germ cells. *Reproduction,* 137**,** 237-244.

IANGONE, J. J. 1982. Protein A of Staphylococcus aureus and Related Immunoglobulin Receptors Produced by Streptococci and Pneumonococci. *In:* FRANK, J. D. & HENRY, G. K. (eds.) *Advances in Immunology.* Academic Press.

ISHIKAWA, T., TERAI, H. & KITAJIMA, T. 2001. Production of a Biologically Active Epidermal Growth Factor Fusion Protein with High Collagen Affinity. *Journal of Biochemistry,* 129**,** 627-633.

JACKY, B. P. S., GARAY, P. E., DUPUY, J., NELSON, J. B., CAI, B., MOLINA, Y., WANG, J., STEWARD, L. E., BROIDE, R. S., FRANCIS, J., AOKI, K. R., STEVENS, R. C. & FERNÁNDEZ-SALAS, E. 2013. Identification of Fibroblast Growth Factor Receptor 3 (FGFR3) as a Protein Receptor for Botulinum Neurotoxin Serotype A (BoNT/A). *PLoS Pathog,* 9**,** e1003369.

JAGODIC, M. M., PATHIRATHNA, S., JOKSOVIC, P. M., LEE, W., NELSON, M. T., NAIK, A. K., SU, P., JEVTOVIC-TODOROVIC, V. & TODOROVIC, S. M. 2008. Up-regulation of the T-type calcium current in small rat sensory neurons after chronic constrictive injury of the sciatic nerve. *Journal of neurophysiology,* 99**,** 3151-3156.

JANSSON, B., UHLÉN, M. & NYGREN, P.-Å. 1998. All individual domains of staphylococcal protein A show Fab binding. *FEMS Immunology & Medical Microbiology,* 20**,** 69-78.

JEFFERIS, R., LUND, J. & POUND, J. D. 1998. IgG-Fc-mediated effector functions: molecular definition of interaction sites for effector ligands and the role of glycosylation. *Immunological Reviews,* 163**,** 59-76.

JUE, Z., JANE, C., SOPHIA, S., JASON, W. O. N., ANDREW, H. G., JOHN, D. & CHRISTOPHER, M. 2010. Fusion Partners as a Tool for the Expression of Difficult Proteins in Mammalian Cells. *Current Pharmaceutical Biotechnology,* 11**,** 241-245.

JULIUS, D. 2013. TRP Channels and Pain. *Annual Review of Cell and Developmental Biology,* 29**,** 355-384.

KAISHO, Y., WATANABE, T., NAKATA, M., YANO, T., YASUHARA, Y., SHIMAKAWA, K., MORI, I., SAKURA, Y., TERAO, Y., MATSUI, H. & TAKETOMI, S. 2005. Transgenic rats overexpressing the human MrgX3 gene show cataracts and an abnormal skin phenotype. *Biochemical and Biophysical Research Communications,* 330**,** 653-657.

KAN, S.-L., LI, Y., NING, G.-Z., YUAN, Z.-F., CHEN, L.-X., BI, M.-C., SUN, J.-C. & FENG, S.-Q. 2016. Tanezumab for patients with osteoarthritis of the knee: a meta-analysis. *PLoS ONE,* 11**,** e0157105.

KIM, H. K., CHENG, A. G., KIM, H.-Y., MISSIAKAS, D. M. & SCHNEEWIND, O. 2010. Nontoxigenic protein A vaccine for methicillin-resistant Staphylococcus aureus infections in mice. *J. Exp. Med.,* 207**,** 1863-1870.

KIM, YU S., CHU, Y., HAN, L., LI, M., LI, Z., LAVINKA, PAMELA C., SUN, S., TANG, Z., PARK, K., CATERINA, MICHAEL J., REN, K., DUBNER, R., WEI, F. & DONG, X. 2014. Central Terminal Sensitization of TRPV1 by Descending Serotonergic Facilitation Modulates Chronic Pain. *Neuron,* 81**,** 873-887.

KLINT, J. K., SENFF, S., SAEZ, N. J., SESHADRI, R., LAU, H. Y., BENDE, N. S., UNDHEIM, E. A. B., RASH, L. D., MOBLI, M. & KING, G. F. 2013. Production of recombinant disulfide-rich venom peptides for structural and functional analysis via expression in the periplasm of E. coli. *PLoS ONE,* 8**,** e63865.

KONG, B. & GUO, G. L. 2014. Soluble Expression of Disulfide Bond Containing Proteins FGF15 and FGF19 in the Cytoplasm of Escherichia coli. *PLoS ONE,* 9**,** e85890.

KOOL, M., VONCKEN, J. W., VAN LIER, F. L. J., TRAMPER, J. & VLAK, J. M. 1991. Detection and analysis of Autographa californica nuclear polyhedrosis virus mutants with defective interfering properties. *Virology,* 183**,** 739-746.

KUMAR, V. & MAHAL, B. A. 2012. NGF – the TrkA to successful pain treatment. *Journal of Pain Research,* 5**,** 279-287.

KUNERT-KEIL, C., BISPING, F., KRÜGER, J. & BRINKMEIER, H. 2006. Tissue-specific expression of TRP channel genes in the mouse and its variation in three different mouse strains. *BMC Genomics,* 7**,** 159-159.

KUO, S.-R., ALFANO, R. W., FRANKEL, A. E. & LIU, J.-S. 2009. Antibody internalization after cell surface antigen binding is critical for immunotoxin development. *Bioconjugate Chemistry,* 20**,** 1975-1982.

KUROKAWA, Y., YANAGI, H. & YURA, T. 2001. Overproduction of bacterial protein disulfide isomerase (DsbC) and its modulator (DsbD) markedly enhances periplasmic production of human nerve growth factor in Escherichia coli. *Journal of Biological Chemistry,* 276**,** 14393-14399.

LACY, D. B. & STEVENS, R. C. 1999. Sequence homology and structural analysis of the clostridial neurotoxins. *Journal of Molecular Biology,* 291**,** 1091-1104.

LAMPPA, J. W., TANYOS, S. A. & GRISWOLD, K. E. 2013. Engineering Escherichia coli for Soluble Expression and Single Step Purification of Active Human Lysozyme. *Journal of biotechnology,* 164**,** 1-8.

LEBEDA, F., ADLER, M., ERICKSON, K. & CHUSHAK, Y. 2008. Onset dynamics of type A botulinum neurotoxin-induced paralysis. *Journal of Pharmacokinetics and Pharmacodynamics,* 35**,** 251-267.

LINDBORG, M., DUBNOVITSKY, A., OLESEN, K., BJÖRKMAN, T., ABRAHMSÉN, L., FELDWISCH, J. & HÄRD, T. 2013. High-affinity binding to staphylococcal protein A by an engineered dimeric Affibody molecule. *Protein Engineering Design and Selection,* 26**,** 635-644.

LINDSAY, R. M. 1996. Role of neurotrophins and Trk receptors in the development and maintenance of sensory neurons: an overview. *Philosophical Transactions of the Royal Society of London. Series B: Biological Sciences,* 351**,** 365-373.

LINDSAY, R. M. & HARMAR, A. J. 1989. Nerve growth factor regulates expression of neuropeptide genes in adult sensory neurons. *Nature,* 337**,** 362-364.

LIU, Z.-Q. & YANG, P.-C. 2012. Construction of pET-32 α (+) vector for protein expression and purification. *North American Journal of Medical Sciences,* 4**,** 651-655.

LOBSTEIN, J., EMRICH, C. A., JEANS, C., FAULKNER, M., RIGGS, P. & BERKMEN, M. 2012. SHuffle, a novel Escherichia coli protein expression strain capable of correctly folding disulfide bonded proteins in its cytoplasm. *Microbial Cell Factories,* 11**,** 56-56.

LORANGER, S. S. & LINDER, M. E. 2002. SNAP-25 Traffics to the Plasma Membrane by a Syntaxin-independent Mechanism. *Journal of Biological Chemistry,* 277**,** 34303-34309.

LU, Z., YANG, Q., CUI, M., LIU, Y., WANG, T., ZHAO, H. & DONG, Q. 2014. Tissue kallikrein induces SH-SY5Y cell proliferation via epidermal growth factor receptor and extracellular signal-regulated kinase1/2 pathway. *Biochemical and Biophysical Research Communications,* 446**,** 25-29.

LUVISETTO, S., GAZERANI, P., CIANCHETTI, C. & PAVONE, F. 2015. Botulinum toxin type A as a therapeutic agent against headache and related disorders. *Toxins,* 7**,** 3818-3844.

MA, H., MENG, J., WANG, J., HEARTY, S., DOLLY, J. O. & O'KENNEDY, R. 2014. Targeted delivery of a SNARE protease to sensory neurons using a single chain antibody (scFv) against the extracellular domain of P2X3inhibits the release of a pain mediator. *Biochemical Journal,* 462**,** 247-256.

MADSHUS, I. H., STENMARK, H., SANDVIG, K. & OLSNES, S. 1991. Entry of diphtheria toxin-protein A chimeras into cells. *Journal of Biological Chemistry,* 266**,** 17446-17453.

MAHAJAN, S. T. & BRUBAKER, L. 2007. Botulinum toxin: From life-threatening disease to novel medical therapy. *American Journal of Obstetrics and Gynecology,* 196**,** 7-15.

MALIN, S. A., DAVIS, B. M. & MOLLIVER, D. C. 2007. Production of dissociated sensory neuron cultures and considerations for their use in studying neuronal function and plasticity. *Nat. Protocols,* 2**,** 152-160.

MAOFU, L., ERHU, C., DAVID, J. & YIFAN, C. 2013. Structure of the TRPV1 ion channel determined by electron cryo-microscopy. *Nature,* 504**,** 107-112.

MASUYER, G., CHADDOCK, J. A., FOSTER, K. A. & ACHARYA, K. R. 2014. Engineered botulinum neurotoxins as new therapeutics. *Annual Review of Pharmacology and Toxicology,* 54**,** 27-51.

MASUYER, G., DAVIES, J. R., MOORE, K., CHADDOCK, J. A. & RAVI ACHARYA, K. 2015. Structural analysis of Clostridium botulinum neurotoxin type D as a platform for the development of targeted secretion inhibitors. *Scientific Reports,* 5**,** 13397.

MAZOR, Y., BARNEA, I., KEYDAR, I. & BENHAR, I. 2007. Antibody internalization studied using a novel IgG binding toxin fusion. *Journal of Immunological Methods,* 321**,** 41-59.

MCKELVEY, L., SHORTEN, G. D. & O'KEEFFE, G. W. 2013. Nerve growth factor-mediated regulation of pain signalling and proposed new intervention strategies in clinical pain management. *Journal of Neurochemistry,* 124**,** 276-289.

MEENTS, J. E., NEEB, L. & REUTER, U. 2010. TRPV1 in migraine pathophysiology. *Trends in Molecular Medicine,* 16**,** 153-159.

MEHTA, H. M., WOO, S. B. & NEET, K. E. 2012. Comparison of Nerve Growth Factor Receptor Binding Models Using Heterodimeric Muteins. *Journal of neuroscience research,* 90**,** 2259-2271.

MENG, J., DOLLY, J. O. & WANG, J. 2014. Selective Cleavage of SNAREs in Sensory Neurons Unveils Protein Complexes Mediating Peptide Exocytosis Triggered by Different Stimuli. *Molecular Neurobiology*, 1-15.

MENG, J., OVSEPIAN, S. V., WANG, J., PICKERING, M., SASSE, A., AOKI, K. R., LAWRENCE, G. W. & DOLLY, J. O. 2009. Activation of TRPV1 mediates calcitonin gene-related peptide release, which excites trigeminal sensory neurons and is attenuated by a retargeted botulinum toxin with anti-nociceptive potential. *J. Neurosci.,* 29**,** 4981-4992.

MENG, J., WANG, J., LAWRENCE, G. & DOLLY, J. O. 2007. Synaptobrevin I mediates exocytosis of CGRP from sensory neurons and inhibition by botulinum toxins reflects their anti-nociceptive potential. *Journal of Cell Science,* 120**,** 2864.

MENG, J., WANG, J., STEINHOFF, M. & DOLLY, J. O. 2016. TNFα induces co-trafficking of TRPV1/TRPA1 in VAMP1-containing vesicles to the plasmalemma via Munc18–1/syntaxin1/SNAP-25 mediated fusion. *Scientific Reports,* 6**,** 21226.

MICHAEL, J. C., MARK, A. S., MAKOTO, T., TOBIAS, A. R., JON, D. L. & DAVID, J. 1997. The capsaicin receptor: a heat-activated ion channel in the pain pathway. *Nature,* 389**,** 816-824.

MITCHELL, D. J., BLASIER, K. R., JEFFERY, E. D., ROSS, M. W., PULLIKUTH, A. K., SUO, D., PARK, J., SMILEY, W. R., LO, K. W.-H., SHABANOWITZ, J., DEPPMANN, C. D., TRINIDAD, J. C., HUNT, D. F., CATLING, A. D. & PFISTER, K. K. 2012. Trk Activation of the ERK1/2 Kinase Pathway Stimulates Intermediate Chain Phosphorylation and Recruits Cytoplasmic Dynein to Signaling Endosomes for Retrograde Axonal Transport. *The Journal of Neuroscience,* 32**,** 15495-15510.

MITCHELL, K., BATES, B., KELLER, J., LOPEZ, M., SCHOLL, L., NAVARRO, J., MADIAN, N., HASPEL, G., NEMENOV, M. & IADAROLA, M. 2010. Ablation of rat TRPV1-expressing Adelta/C-fibers with resiniferatoxin: analysis of withdrawal behaviors, recovery of function and molecular correlates. *Molecular Pain,* 6**,** 94.

MOISEENKOVA-BELL, V. Y. & WENSEL, T. G. 2009. Hot on the Trail of TRP Channel Structure. *The Journal of General Physiology,* 133**,** 239-244.

MOKS, T., ABRAHMSÉN, L., NILSSON, B., HELLMAN, U., SJÖQUIST, J. & UHLÉN, M. 1986. Staphylococcal protein A consists of five IgG-binding domains. *European Journal of Biochemistry,* 156**,** 637-643.

MORENILLA-PALAO, C., PLANELLS-CASES, R., GARCÍA-SANZ, N. & FERRER-MONTIEL, A. 2004. Regulated Exocytosis Contributes to Protein Kinase C Potentiation of Vanilloid Receptor Activity. *Journal of Biological Chemistry,* 279**,** 25665-25672.

MÜNCHAU, A. & BHATIA, K. P. 2000. Uses of botulinum toxin injection in medicine today. *British Medical Journal,* 320**,** 161-165.

MURARO, L., TOSATTO, S., MOTTERLINI, L., ROSSETTO, O. & MONTECUCCO, C. 2009. The N-terminal half of the receptor domain of botulinum neurotoxin A binds to microdomains of the plasma membrane. *Biochemical and Biophysical Research Communications,* 380**,** 76-80.

MUSTAFA, G., ANDERSON, E. M., BOKRAND-DONATELLI, Y., NEUBERT, J. K. & CAUDLE, R. M. 2013. Anti-nociceptive effect of a conjugate of substance P and light chain of botulinum neurotoxin type A. *Pain,* 154**,** 2547–2453.

NEELAM, B., RICHTER, A., CHAMBERLIN, S. G., PUDDICOMBE, S. M., WOOD, L., MURRAY, M. B., NANDAGOPAL, K., NIYOGI, S. K. & DAVIES, D. E. 1998. Structure−Function Studies of Ligand-Induced Epidermal Growth Factor Receptor Dimerization. *Biochemistry,* 37**,** 4884-4891.

NEELANDS, T., JARVIS, M., HAN, P., FALTYNEK, C. & SUROWY, C. 2005. Acidification of rat TRPV1 alters the kinetics of capsaicin responses. *Molecular Pain,* 1**,** 28.

NÉMOZ-GAILLARD, E., BOSSHARD, A., REGAZZI, R., BERNARD, C., CUBER, J.-C., TAKAHASHI, M., CATSICAS, S., CHAYVIALLE, J.-A. & ABELLO, J. 1998. Expression of SNARE proteins in

enteroendocrine cell lines and functional role of tetanus toxin-sensitive proteins in cholecystokinin release. *FEBS Letters,* 425**,** 66-70.

NGUYEN, B., JARNAGIN, K., WILLIAMS, S., CHAN, H. & BARNETT, J. 1993. Fed-batch culture of insect cells: a method to increase the yield of recombinant human nerve growth factor (rhNGF) in the baculovirus expression system. *Journal of Biotechnology,* 31**,** 205-217.

NOËL, J., ZIMMERMANN, K., BUSSEROLLES, J., DEVAL, E., ALLOUI, A., DIOCHOT, S., GUY, N., BORSOTTO, M., REEH, P., ESCHALIER, A. & LAZDUNSKI, M. 2009. The mechano-activated K(+) channels TRAAK and TREK-1 control both warm and cold perception. *The EMBO Journal,* 28**,** 1308-1318.

NOORBAKHSH, F., VERGNOLLE, N., HOLLENBERG, M. D. & POWER, C. 2003. Proteinase-activated receptors in the nervous system. *Nat Rev Neurosci,* 4**,** 981-990.

OYLER, G. A., POLLI, J. W., HIGGINS, G. A., WILSON, M. C. & BILLINGSLEY, M. L. 1992. Distribution and expression of SNAP-25 immunoreactivity in rat brain, rat PC-12 cells and human SMS-KCNR neuroblastoma cells. *Developmental Brain Research,* 65**,** 133-146.

PAPPERT, E. J. & GERMANSON, T. 2008. Botulinum toxin type B vs. type A in toxin-naïve patients with cervical dystonia: Randomized, double-blind, noninferiority trial. *Movement Disorders,* 23**,** 510-517.

PARK, E., STARZYK, R. M., MCGRATH, J. P., LEE, T., GEORGE, J., SCHUTZ, A. J., LYNCH, P. & PUTNEY, S. D. 1998. Production and Characterization of Fusion Proteins Containing Transferrin and Nerve Growth Factor. *Journal of Drug Targeting,* 6**,** 53-64.

PASSMORE, G. M., SELYANKO, A. A., MISTRY, M., AL-QATARI, M., MARSH, S. J., MATTHEWS, E. A., DICKENSON, A. H., BROWN, T. A., BURBIDGE, S. A., MAIN, M. & BROWN, D. A. 2003. KCNQ/M Currents in Sensory Neurons: Significance for Pain Therapy. *The Journal of Neuroscience,* 23**,** 7227-7236.

PIRAZZINI, M., HENKE, T., ROSSETTO, O., MAHRHOLD, S., KREZ, N., RUMMEL, A., MONTECUCCO, C. & BINZ, T. 2013. Neutralisation of specific surface carboxylates speeds up translocation of botulinum neurotoxin type B enzymatic domain. *FEBS Letters,* 587**,** 3831-3836.

PIRAZZINI, M., TEHRAN, D. A., LEKA, O., ZANETTI, G., ROSSETTO, O. & MONTECUCCO, C. 2016. On the translocation of botulinum and tetanus neurotoxins across the membrane of acidic intracellular compartments. *Biochimica et Biophysica Acta* 1858**,** 467-474.

PRESCOTT, M., NOWAKOWSKI, S., NAGLEY, P. & DEVENISH, R. J. 1999. The Length of Polypeptide Linker Affects the Stability of Green Fluorescent Protein Fusion Proteins. *Analytical Biochemistry,* 273**,** 305-307.

PUNTAMBEKAR, P., VAN BUREN, J., RAISINGHANI, M., PREMKUMAR, L. S. & RAMKUMAR, V. 2004. Direct Interaction of Adenosine with the TRPV1 Channel Protein. *The Journal of Neuroscience,* 24**,** 3663-3671.

RAFTERY, M. N., RYAN, P., NORMAND, C., MURPHY, A. W., DE LA HARPE, D. & MCGUIRE, B. E. 2012. The Economic Cost of Chronic Noncancer Pain in Ireland: Results From the PRIME Study, Part 2. *The Journal of Pain,* 13**,** 139-145.

RAFTERY, M. N., SARMA, K., MURPHY, A. W., DE LA HARPE, D., NORMAND, C. & MCGUIRE, B. E. 2011. Chronic pain in the Republic of Ireland—Community prevalence, psychosocial profile and predictors of pain-related disability: Results from the Prevalence, Impact and Cost of Chronic Pain (PRIME) study, Part 1. *PAIN,* 152**,** 1096-1103.

RAPPOPORT, JOSHUA Z. 2008. Focusing on clathrin-mediated endocytosis. *Biochemical Journal,* 412**,** 415.

RAU, K. K., MCILWRATH, S. L., WANG, H., LAWSON, J. J., JANKOWSKI, M. P., ZYLKA, M. J., ANDERSON, D. J. & KOERBER, H. R. 2009. Mrgprd Enhances Excitability in Specific Populations of Cutaneous Murine Polymodal Nociceptors. *The Journal of Neuroscience,* 29**,** 8612-8619.

REMILLARD, C. V. & YUAN, J. X. J. 2006. Transient receptor potential channels and caveolin-1: good friends in tight spaces. *Molecular pharmacology,* 70**,** 1151-1154.
ROSENBLATT, R. A. & CATLIN, M. 2012. Opioids for Chronic Pain: First Do No Harm. *The Annals of Family Medicine,* 10**,** 300-301.
ROSSETTO, O., PIRAZZINI, M. & MONTECUCCO, C. 2014. Botulinum neurotoxins: genetic, structural and mechanistic insights. *Nat Rev Micro,* 12**,** 535-549.
RUBSAM, L. Z., BOUCHER, P. D., MURPHY, P. J., KUKURUGA, M. & SHEWACH, D. S. 1999. Cytotoxicity and Accumulation of Ganciclovir Triphosphate in Bystander Cells Cocultured with Herpes Simplex Virus Type 1 Thymidine Kinase-expressing Human Glioblastoma Cells. *Cancer Research,* 59**,** 669-675.
RUMMEL, A., EICHNER, T., WEIL, T., KARNATH, T., GUTCAITS, A., MAHRHOLD, S., SANDHOFF, K., PROIA, R. L., ACHARYA, K. R., BIGALKE, H. & BINZ, T. 2007. Identification of the protein receptor binding site of botulinum neurotoxins B and G proves the double-receptor concept. *Proceedings of the National Academy of Sciences,* 104**,** 359-364.
SAEGUSA, H., KURIHARA, T., ZONG, S., KAZUNO, A.-A., MATSUDA, Y., NONAKA, T., HAN, W., TORIYAMA, H. & TANABE, T. 2001. Suppression of inflammatory and neuropathic pain symptoms in mice lacking the N-type Ca(2+) channel. *The EMBO Journal,* 20**,** 2349-2356.
SANZ-SALVADOR, L., ANDRÉS-BORDERIA, A., FERRER-MONTIEL, A. & PLANELLS-CASES, R. 2012. Agonist- and Ca2+-dependent Desensitization of TRPV1 Channel Targets the Receptor to Lysosomes for Degradation. *Journal of Biological Chemistry,* 287**,** 19462-19471.
SATO, S., RELIGA, T. L., DAGGETT, V. & FERSHT, A. R. 2004. Testing protein-folding simulations by experiment: B domain of protein A. *Proceedings of the National Academy of Sciences of the United States of America,* 101**,** 6952-6956.
SCHMIDT, M., DUBIN, A. E., PETRUS, M. J., EARLEY, T. J. & PATAPOUTIAN, A. 2009. Various signals involved in nociception regulate TRPA1 levels at the plasma membrane. *Neuron,* 64**,** 498-509.
SCHMIDT, M. M., THURBER, G. M. & WITTRUP, K. D. 2008. Kinetics of anti-carcinoembryonic antigen antibody internalization: effects of affinity, bivalency, and stability. *Cancer immunology, immunotherapy : CII,* 57**,** 1879-1890.
SCHMOLDT, H.-U., WENTZEL, A., BECKER, S. & KOLMAR, H. 2005. A fusion protein system for the recombinant production of short disulfide bond rich cystine knot peptides using barnase as a purification handle. *Protein Expression and Purification,* 39**,** 82-89.
SCHUMACHER, M. A. 2010. Transient Receptor Potential Channels in Pain and Inflammation: Therapeutic Opportunities. *Pain Practice,* 10**,** 185-200.
SEIDAH, N. G., BENJANNET, S., PAREEK, S., SAVARIA, D., HAMELIN, J., GOULET, B., LALIBERTE, J., LAZURE, C., CHRÉTIEN, M. & MURPHY, R. A. 1996. Cellular processing of the nerve growth factor precursor by the mammalian pro-protein convertases. *Biochemical Journal,* 314**,** 951-960.
SERAS-FRANZOSO, J., AFFENTRANGER, R., FERRER-NAVARRO, M., DAURA, X., VILLAVERDE, A. & GARCÍA-FRUITÓS, E. 2012. Disulfide Bond Formation and Activation of Escherichia coli β-Galactosidase under Oxidizing Conditions. *Applied and Environmental Microbiology,* 78**,** 2376-2385.
SERMADIRAS, I., REVELL, J., LINLEY, J. E., SANDERCOCK, A. & RAVN, P. 2013. Recombinant Expression and In Vitro Characterisation of Active Huwentoxin-IV. *PLoS ONE,* 8**,** e83202.
SHEN, J., TARESTE, D. C., PAUMET, F., ROTHMAN, J. E. & MELIA, T. J. 2007. Selective Activation of Cognate SNAREpins by Sec1/Munc18 Proteins. *Cell,* 128**,** 183-195.
SHONE, C. C., HAMBLETON, P. & MELLING, J. 1985. Inactivation of Clostridium botulinum type A neurotoxin by trypsin and purification of two tryptic fragments. *European Journal of Biochemistry,* 151**,** 75-82.

SHONE, C. C. & MELLING, J. 1992. Inhibition of calcium-dependent release of noradrenaline from PC12 cells by botulinum type-A neurotoxin. Long-term effects of the neurotoxin on intact cells. *Eur J Biochem,* 207**,** 1009-1016.

SIKAND, P., DONG, X. & LAMOTTE, R. H. 2011. BAM8–22 peptide produces itch and nociceptive sensations in humans independent of histamine release. *The Journal of neuroscience,* 31**,** 7563-7567.

SILBERSTEIN, S., MATHEW, N., SAPER, J., JENKINS, S. & FOR THE, B. M. C. R. G. 2000. Botulinum Toxin Type A as a Migraine Preventive Treatment. *Headache: The Journal of Head and Face Pain,* 40**,** 445-450.

SOLINSKI, H. J., BOEKHOFF, I., BOUVIER, M., GUDERMANN, T. & BREIT, A. 2010. Sensory Neuron-Specific Mas-Related Gene-X1 Receptors Resist Agonist-Promoted Endocytosis. *Molecular Pharmacology,* 78**,** 249-259.

SÖLLNER, T., BENNETT, M. K., WHITEHEART, S. W., SCHELLER, R. H. & ROTHMAN, J. E. 1993. A protein assembly-disassembly pathway in vitro that may correspond to sequential steps of synaptic vesicle docking, activation, and fusion. *Cell,* 75**,** 409-418.

SOMM, E., BONNET, N., MARTINEZ, A., MARKS, P. M. H., CADD, V. A., ELLIOTT, M., TOULOTTE, A., FERRARI, S. L., RIZZOLI, R., HÜPPI, P. S., HARPER, E., MELMED, S., JONES, R. & AUBERT, M. L. 2012. A botulinum toxin–derived targeted secretion inhibitor downregulates the GH/IGF1 axis. *The Journal of Clinical Investigation,* 122**,** 3295-3306.

STAIKOPOULOS, V., SESSLE, B. J., FURNESS, J. B. & JENNINGS, E. A. 2007. Localisation of P2X2 and P2X3 Receptors in Rat Trigeminal Ganglion Neurons. *Neuroscience,* 144**,** 208-216.

STANCHEV, D., BLOSA, M., MILIUS, D., GEREVICH, Z., RUBINI, P., SCHMALZING, G., ESCHRICH, K., SCHAEFER, M., WIRKNER, K. & ILLES, P. 2009. Cross-inhibition between native and recombinant TRPV1 and P2X3 receptors. *PAIN,* 143**,** 26-36.

STENMARK, P., DUPUY, J., IMAMURA, A., KISO, M. & STEVENS, R. C. 2008. Crystal Structure of Botulinum Neurotoxin Type A in Complex with the Cell Surface Co-Receptor GT1b—Insight into the Toxin–Neuron Interaction. *PLoS Pathog,* 4**,** e1000129.

STEWART, E. J., ASLUND, F. & BECKWITH, J. 1998. Disulfide bond formation in the Escherichia coli cytoplasm: an in vivo role reversal for the thioredoxins. *The EMBO Journal,* 17**,** 5543-5550.

STROBER, W. 2001. Trypan Blue Exclusion Test of Cell Viability. *Current Protocols in Immunology.* John Wiley & Sons, Inc.

STROTMEIER, J., MAHRHOLD, S., KREZ, N., JANZEN, C., LOU, J., MARKS, J. D., BINZ, T. & RUMMEL, A. 2014. Identification of the synaptic vesicle glycoprotein 2 receptor binding site in botulinum neurotoxin A. *FEBS Letters,* 588**,** 1087-1093.

STUDIER, F. W. 2005. Protein production by auto-induction in high-density shaking cultures. *Protein Expression and Purification,* 41**,** 207-234.

SÜDHOF, T. C. & RIZO, J. 2011. Synaptic vesicle exocytosis. *Cold Spring Harbor perspectives in biology,* 3**,** a005637.

SUN, Q., WOODCOCK, J. M., RAPOPORT, A., STOMSKI, F. C., KORPELAINEN, E. I., BAGLEY, C. J., GOODALL, G. J., SMITH, W. B., GAMBLE, J. R., VADAS, M. A. & LOPEZ, A. F. 1996. Monoclonal antibody 7G3 recognizes the N-terminal domain of the human interleukin-3 (IL-3) receptor alpha-chain and functions as a specific IL-3 receptor antagonist. *Blood,* 87**,** 83.

SUTTON, R. B., FASSHAUER, D., JAHN, R. & BRUNGER, A. T. 1998. Crystal structure of a SNARE complex involved in synaptic exocytosis at 2.4 Å resolution. *Nature,* 395**,** 347-353.

TAKAYAMA, Y., UTA, D., FURUE, H. & TOMINAGA, M. 2015. Pain-enhancing mechanism through interaction between TRPV1 and anoctamin 1 in sensory neurons. *Proceedings of the National Academy of Sciences of the United States of America,* 112**,** 5213-5218.

TAMURA, S., MORIKAWA, Y. & SENBA, E. 2005. TRPV2, a capsaicin receptor homologue, is expressed predominantly in the neurotrophin-3-dependent subpopulation of primary sensory neurons. *Neuroscience,* 130**,** 223-228.

TERMAN, G. 2003. Spinal mechanisms and their modulation. *Bonica's Management of Pain, Third Edition,* 21**,** 527-528.

THOMAS, K. C., SABNIS, A. S., JOHANSEN, M. E., LANZA, D. L., MOOS, P. J., YOST, G. S. & REILLY, C. A. 2007. Transient Receptor Potential Vanilloid 1 Agonists Cause Endoplasmic Reticulum Stress and Cell Death in Human Lung Cells. *Journal of Pharmacology and Experimental Therapeutics,* 321**,** 830-838.

TISCHLER, A. S. & GREENE, L. A. 1975. Nerve growth factor-induced process formation by cultured rat pheochromocytoma cells. *Nature,* 258**,** 341-342.

TÓTH, A., BLUMBERG, P. M., CHEN, Z. & KOZIKOWSKI, A. P. 2004. Design of a High-Affinity Competitive Antagonist of the Vanilloid Receptor Selective for the Calcium Entry-Linked Receptor Population. *Molecular Pharmacology,* 65**,** 282-291.

TREEDE, R.-D., RIEF, W., BARKE, A., AZIZ, Q., BENNETT, M. I., BENOLIEL, R., COHEN, M., EVERS, S., FINNERUP, N. B., FIRST, M. B., GIAMBERARDINO, M. A., KAASA, S., KOSEK, E., LAVAND'HOMME, P., NICHOLAS, M., PERROT, S., SCHOLZ, J., SCHUG, S., SMITH, B. H., SVENSSON, P., VLAEYEN, J. W. S. & WANG, S.-J. 2015. A classification of chronic pain for ICD-11. *Pain,* 156**,** 1003-1007.

TSUKAMOTO, M., WATANABE, H., OOISHI, A. & HONDA, S. 2014. Engineered protein A ligands, derived from a histidine-scanning library, facilitate the affinity purification of IgG under mild acidic conditions. *Journal of Biological Engineering,* 8**,** 15-15.

TYSON, D. R., LARKIN, S., HAMAI, Y. & BRADSHAW, R. A. 2003. PC12 cell activation by epidermal growth factor receptor: role of autophosphorylation sites. *International Journal of Developmental Neuroscience,* 21**,** 63-74.

VAN OERS, M. M., PIJLMAN, G. P. & VLAK, J. M. 2015. Thirty years of baculovirus–insect cell protein expression: from dark horse to mainstream technology. *Journal of General Virology,* 96**,** 6-23.

WALKER, M., EWALD, D., PERNEY, T. & MILLER, R. 1988. Neuropeptide Y modulates neurotransmitter release and Ca2+ currents in rat sensory neurons. *The Journal of Neuroscience,* 8**,** 2438-2446.

WANG, H. & WOOLF, C. J. 2005. Pain TRPs. *Neuron,* 46**,** 9-12.

WANG, J., CASALS-DIAZ, L., ZURAWSKI, T., MENG, J., MORIARTY, O., NEALON, J., EDUPUGANTI, O. P. & DOLLY, O. 2017a. A novel therapeutic with two SNAP-25 inactivating proteases shows long-lasting anti-hyperalgesic activity in a rat model of neuropathic pain. *Neuropharmacology,* 118**,** 223-232.

WANG, J., MENG, J., LAWRENCE, G. W., ZURAWSKI, T. H., SASSE, A., BODEKER, M. O., GILMORE, M. A., FERNÁNDEZ-SALAS, E., FRANCIS, J., STEWARD, L. E., AOKI, K. R. & DOLLY, J. O. 2008. Novel Chimeras of Botulinum Neurotoxins A and E Unveil Contributions from the Binding, Translocation, and Protease Domains to Their Functional Characteristics. *Journal of Biological Chemistry,* 283**,** 16993-17002.

WANG, J., MENG, J., NUGENT, M., TANG, M. & DOLLY, J. O. 2017b. Neuronal entry and high neurotoxicity of botulinum neurotoxin A require its N-terminal binding sub-domain. *Scientific Reports,* 7**,** 44474.

WANG, J., ZURAWSKI, T. H., MENG, J., LAWRENCE, G., OLANGO, W. M., FINN, D. P., WHEELER, L. & DOLLY, J. O. 2011. A dileucine in the protease of botulinum toxin A underlies its long-lived neuroparalysis: transfer of longevity to a novel pain therapeutic. *Journal of Biological Chemistry,* 286**,** 6375-6385.

WANG, J., ZURAWSKI, T. H., MENG, J., LAWRENCE, G. W., AOKI, K. R., WHEELER, L. & DOLLY, J. O. 2012. Novel chimeras of botulinum and tetanus neurotoxins yield insights into their distinct sites of neuroparalysis. *FASEB J.,* 26**,** 5035-5048.

WATSON, J. J., ALLEN, S. J. & DAWBARN, D. 2008. Targeting nerve growth factor in pain. *BioDrugs,* 22**,** 349-359.

WEGIERSKI, T., HILL, K., SCHAEFER, M. & WALZ, G. 2006. The HECT ubiquitin ligase AIP4 regulates the cell surface expression of select TRP channels. *The EMBO Journal,* 25**,** 5659-5669.

WIESMANN, C., ULTSCH, M. H., BASS, S. H. & DE VOS, A. M. 1999. Crystal structure of nerve growth factor in complex with the ligand-binding domain of the TrkA receptor. *Nature,* 401**,** 184-188.

WILLIAMS, R. S., TSE, C. K., DOLLY, J. O., HAMBLETON, P. & MELLING, J. 1983. Radioiodination of botulinum neurotoxin type A with retention of biological activity and its binding to brain synaptosomes. *Eur J Biochem,* 131**,** 437-45.

WINTER, J. 2005. TRPV1 distribution and regulation. *In:* MALMBERG, A. B. & BLEY, K. R. (eds.) *Turning up the Heat on Pain: TRPV1 Receptors in Pain and Inflammation.* Basel: Birkhäuser Basel.

WINTER, Z., BUHALA, A., OTVOS, F., JOSVAY, K., VIZLER, C., DOMBI, G., SZAKONYI, G. & OLAH, Z. 2013. Functionally important amino acid residues in the transient receptor potential vanilloid 1 (TRPV1) ion channel - an overview of the current mutational data. *Molecular Pain,* 9**,** 30.

WOOD, H. 2010. Migraine: Familial migraine with aura is associated with a mutation in the TRESK potassium channel. *Nat Rev Neurol,* 6**,** 643-643.

XIE, Z.-L., SHAO, S.-L., LV, J.-W., WANG, C.-H., YUAN, C.-Z., ZHANG, W.-W. & XU, X.-J. 2011. Co-transfection and tandem transfection of HEK293A cells for overexpression and RNAi experiments. *Cell Biology International,* 35**,** 187-192.

XU, Q. & YAKSH, T. L. 2011. A brief comparison of the pathophysiology of inflammatory versus neuropathic pain. *Current Opinion in Anesthesiology,* 24**,** 400-407 10.1097/ACO.0b013e32834871df.

YANG, S., LIU, Y., LIN, A. A., CAVALLI-SFORZA, L. L., ZHAO, Z. & SU, B. 2005. Adaptive evolution of MRGX2, a human sensory neuron specific gene involved in nociception. *Gene,* 352**,** 30-35.

YASUKAWA, T., KANEI-ISHII, C., MAEKAWA, T., FUJIMOTO, J., YAMAMOTO, T. & ISHII, S. 1995. Increase of Solubility of Foreign Proteins in Escherichia coli by Coproduction of the Bacterial Thioredoxin. *Journal of Biological Chemistry,* 270**,** 25328-25331.

YE, Y., DANG, D., ZHANG, J., VIET, C. T., LAM, D. K., DOLAN, J. C., GIBBS, J. L. & SCHMIDT, B. L. 2011. Nerve Growth Factor Links Oral Cancer Progression, Pain, and Cachexia. *Molecular Cancer Therapeutics,* 10**,** 1667-1676.

YEH, F. L., ZHU, Y., TEPP, W. H., JOHNSON, E. A., BERTICS, P. J. & CHAPMAN, E. R. 2011. Retargeted Clostridial Neurotoxins as Novel Agents for Treating Chronic Diseases. *Biochemistry,* 50**,** 10419-10421.

YING, T., CHEN, W., GONG, R., FENG, Y. & DIMITROV, D. S. 2012. Soluble Monomeric IgG1 Fc. *The Journal of Biological Chemistry,* 287**,** 19399-19408.

YOGEESWARI, P., SEMWAL, A., MISHRA, R. & SRIRAM, D. 2009. Current approaches with the glutamatergic system as targets in the treatment of neuropathic pain. *Expert Opinion on Therapeutic Targets,* 13**,** 925-943.

YOUNG, C. L., BRITTON, Z. T. & ROBINSON, A. S. 2012. Recombinant protein expression and purification: A comprehensive review of affinity tags and microbial applications. *Biotechnology Journal,* 7**,** 620-634.

ZHANG, Y., GARDBERG, A. S., EDWARDS, T. E., SANKARAN, B., ROBINSON, H., VARNUM, S. M. & BUCHKO, G. W. 2013. Structural insights into the functional role of the Hcn sub-domain of the receptor-binding domain of the botulinum neurotoxin mosaic serotype C/D. *Biochimie,* 95**,** 1379-85.

ZHOU, J., VALLETTA, J. S., GRIMES, M. L. & MOBLEY, W. C. 1995. Multiple Levels for Regulation of TrkA in PC12 Cells by Nerve Growth Factor. *Journal of Neurochemistry,* 65**,** 1146-1156.

ZIMMERMANN, K., LENNERZ, J. K., HEIN, A., LINK, A. S., KACZMAREK, J. S., DELLING, M., UYSAL, S., PFEIFER, J. D., RICCIO, A. & CLAPHAM, D. E. 2011. Transient receptor potential cation channel, subfamily C, member 5 (TRPC5) is a cold-transducer in the peripheral nervous system. *Proceedings of the National Academy of Sciences of the United States of America,* 108**,** 18114-18119.

Appendix

List of suppliers

Company	Country	Web address
Alomone	Israel	www.alomone.com
ATCC (Ordered through LGC standard)	UK	www.lgcstandards-atcc.org
Bio-rad (Ordered through Fannin)	Ireland	www.fannin.eu
Biomatik	USA	www.biomatik.com
Eurofins Genomics	Germany	www.eurofinsgenomics.eu
Jackson Immuno-research	UK	www.jireurope.com
Envigo (formerly Harlan labs)	UK	www.envigo.com
Life Technologies (Ordered through Biosciences)	Ireland	www.biosciences.ie
Merck Millipore	UK	www.merckmillipore.com/IE
Mirus Bio (Ordered through Medical Supply Company)	Ireland	www.medical-supply.ie
New England Biolabs (Ordered through Brennan & Company)	Ireland	www.brennanco.ie

Perkin Elmer	UK	www.perkinelmer.com
Peptide Synthetics	UK	www.peptidesynthetics.co.uk
Qiagen	UK	www.qiagen.com
Sarstedt	Ireland	www.sarstedt.com
Sigma Aldrich (Additionally a supplier of GE Healthcare products)	Ireland	www.sigmaaldrich.com/ireland
Vector Laboratories	UK	www.vectorlabs.com